

3-D Jetting for Enhanced Functionality of Thermoset Elastomeric Materials

By

Marija Lukic

A doctoral thesis submitted in partial fulfilment of the requirements for the
award of Doctor of Philosophy of Loughborough University

June 2017

Supervisors: Dr. Jane Clarke

Dr. Will Whittow

Professor Christopher Tuck

© by Marija Lukic

Acknowledgements

I would like to express my deepest appreciation and gratitude to my supervisors for their unconditional support, guidance, and for giving me that extra nudge when they saw I needed it most.

I am very grateful to my family, who have given me so much love and support during my work and who have encouraged me to give my best in everything I do. A very special thanks to my fiancé, soon to be husband, Nicholas Mann, who has stuck with me through it all.

I would like to thank my project sponsors, the National PhD Programme and DSTL, for giving me the opportunity to work on this project.

My sincerest gratitude goes to all the technicians at Loughborough University, particularly Mr. Keith Yendall, Mr. Andy Wooley, Mr. Ray Owens, Dr. Zhaoxia Zhou, Mr. Giuseppe Forte, Mr. Scott Doak, and Mr. Shaun Fowler. I am greatly appreciative of their aid, advice, and endless patience which has immeasurably helped me during my research.

And finally, I would like to thank all my friends and colleagues at Loughborough University as well for being so kind and amazing. Their names include, but aren't limited to, Sebnem Pehlivan-Davis, Sian Higlett, and James West.

Abstract

The aim of this work was to assess the feasibility of 3-D inkjet printing of elastomers in latex form to create a novel material that would offer shielding against electromagnetic interference (EMI).

To achieve this aim it was necessary to characterise and select suitable materials, carry out ink jetting trials, modify the materials accordingly to improve the printability and assess post jetting conditions including drying and curing behaviour. Particle size, surface tension, and viscosity measurements were made for a series of elastomer latex materials and carboxylated styrene butadiene rubber (XSBR) latex was identified as the most suitable. Latex ink optimisation included dilution with water and the addition of a humectant, triethylene glycol monomethyl ether (TGME), which delayed drying and reduced nozzle blocking. The surface energy was measured for a range of potential substrates and PET was identified as the most suitable, due to its relatively high surface energy which allowed for an ideal level of wetting and spreading. Analysis of the cross-sectional profiles of the printed samples by white light interferometry showed that drying during printing was an important issue for the latex ink. Ink jetting of a composite material with control of filler distribution was shown to be feasible when ten layers of conductive carbon black ink were deposited alternately between ten layers of XSBR ink. Printing was successfully carried out with a latex combined with a resorcinol resin which was subsequently cured, indicating that it should be possible to 3D print a thermoset elastomer in this way. Conductive carbon black was printed in various patterns onto PET sheet and the dielectric properties measured. Results indicated that at very low carbon contents, the printed patterns could provide EMI shielding.

The research has shown that it is feasible to create a cured 3D elastomeric object containing filler with a controlled distribution that is capable of providing EMI shielding.

Contents

Chapter 1 Introduction	1
1.1 General Background.....	1
1.2 3-D Printing Technology.....	1
1.3 3D printing of elastomeric materials	2
1.3.1 3-D Printing Techniques for Thermoplastic Elastomers	3
1.3.2 3-D Printing Techniques for Thermoset Elastomers	4
1.4 Aims and Objectives	7
Chapter 2 Principles and Review of 3D Ink Jetting.....	9
2.1 Introduction.....	9
2.2 The Effect of Ink Properties: Viscosity, Surface Tension and Particle Size	9
2.3 Inkjet Printing Parameters	14
2.3.1 Type of Printers and Print Heads	14
2.3.2 Effect of nozzle geometry and jetting parameters	16
2.4 Droplet Deposition.....	20
2.4.1 Characterisation Techniques.....	20
2.4.2 Viscoelasticity and the Role of Humectants	20
2.4.3 Effect of the Substrate Surface Energy, Drop Impact, and Substrate Topography	22
2.4.4 Drying Behaviour: Marangoni Effect and the Coffee Ring Effect	27
2.5 3D Ink Jetting Elastomeric Ink	29
2.6 Conclusion	31
Chapter 3 EMI Shielding Polymers	37
3.1 Introduction.....	37
3.2 Concept of shielding	37
3.3 The theory and principles of dielectric materials.....	38
3.3.1 Material properties	38
3.3.2 Permittivity	38
3.3.3 Dielectric mechanisms	39
3.4 Polymer composites with conductive fillers.....	42
3.5 EMI shielding	43

3.5.1 Carbon black, carbon nanotube and carbon fibre filled composites.....	46
3.5.2 Temperature, material thickness, and frequency effects on EMI shielding.....	53
3.5.3 Polymers with conductive metallic fillers	55
3.6 Conclusion	60
Chapter 4: Experimental	65
4.1 Materials	65
4.2 Liquid Latex Property Measurement	67
4.2.1 Surface Tension	67
4.2.2 Viscosity	67
4.2.3 Particle Size	68
4.3 Preliminary printing trials	69
4.4 Development of a latex ink.....	69
4.5 Jetting Trials	71
4.6 Surface Energy Measurement of Substrates	71
4.7 Droplet Analysis	72
4.8 Single Layer Printing Trials.....	72
4.9 Multilayer Printing Trials	73
4.9.1 Printing Rectangle Patterns and Logos.....	73
4.9.2 3-D Pattern Printing with XSBR Ink	74
4.9.3 Introducing Time Delay between Layers.....	75
4.9.4 Printing onto a Heated Bed	76
4.9.5 Printing onto Different Substrates	76
4.10 Multilayer Printing with XSBR and Carbon Black Ink	77
4.11 Curing, Solvent Swelling and Tensile Testing of XSBR combined with Resorcinol resin.....	78
4.12 Multilayer Printing with XSBR Ink Combined with Resorcinol Resin.....	80
4.13 Characterisation of Printed Latex	80
4.14 Electromagnetic Characterisation of Latex and Carbon Black.....	81
4.14.1 Combining Carbon Black with Latexes.....	81
4.14.2 Printing patterns with carbon black on PET and latex.....	83
4.14.3 Thermogravimetric Analysis (TGA) of carbon black concentrations	85
4.14.4 Dielectric measurements.....	85

4.15 Conclusion	87
Chapter 5: Results and Discussion.....	89
5.1 Liquid Latex Properties	89
5.1.1 Surface Tension	89
5.1.2 Viscosity	90
5.1.3 Particle Size	91
5.2 Preliminary Printing Trials	93
5.3 Development of a Latex Ink	96
5.3.1 Effect of TGME on drying time of XSBR latex	96
5.3.2 Surface Tension	99
5.3.3 Viscosity	101
5.3.4 Particle size	104
5.3.5 Z number.....	105
5.4 Jetting Trials	108
5.5 Droplet Deposition.....	114
5.5.1 Substrate surface energy	114
5.5.2 Droplet Analysis	116
5.6 Single Layer Latex Ink Deposition.....	120
5.7 Multilayer printing.....	125
5.7.1 Effect of substrate on multilayer printing	125
5.7.2 Multilayer complex 2D Patterns	129
5.7.3 3-D Pattern Printing	131
5.7.4 Effect of Time Delay between Layers	132
5.7.5 Effect of Heated Bed.....	137
5.7.6 Depositing onto Different Substrates.....	139
5.7.7 3-D Jetting to Create a Latex and Carbon Black Composite.....	142
5.7.8 3-D Jetting with XSBR Combination with Resorcinol Curing Resin	146
5.7.9 Crosslinking and Tensile Properties of XSBR latex cured with Resorcinol Resin.	148
5.8 Combining carbon black with latex	152
5.8.1 TGA Results for Carbon Black Content in XSBR	156
5.9 Conclusion	159

Chapter 6: EMC Results	161
6.1 Introduction.....	161
6.2 Electromagnetic Simulations	161
6.3 Electromagnetic Characterisation of Latex and Conductive Carbon Black Utilising Monopole Antennas	164
6.3.1 Latex samples with Carbon Black	164
6.3.2 SPDR Results for Carbon Black Patterns Printed on Cast Latex and PET	169
6.3.3 SPDR Results for Cast Latexes	174
6.3.4 Shielding Effectiveness of 1, 5, and 10 Layers of Inkjet Printed Carbon Black	175
6.4 Conclusion	179
7. Conclusions and Recommendations	181
7.1 Conclusions.....	181
7.2 Recommendations for Future Work	184
Appendix.....	186

Table of Figures

Figure 1.1 Forms of current thermoplastic and thermoset methods of 3-D printing elastomers	2
Figure 1.2 An illustration of FDM 3-D printing	3
Figure 1.3 An illustration of the SLS 3-D printing process	4
Figure 1.4 Stereolithography 3D printing process	5
Figure 1.5 Extrusion 3-D printing process	5
Figure 1.6 Inkjet printing AM process with UV curing	6
Figure 2.1 A coordinate system used to plot the Reynolds, Weber, and Ohnesorg equations	12
Figure 2.2 Droplet formation process from initiation of pulse to the breakoff of the droplet [47]	13
Figure 2.3 the effect of the Z number on the printability of a liquid material	14
Figure 2.4 Thermal ink jetting process inside the print head [63]	15
Figure 2.5 Simulation results produced by Chen et al illustrating the effect of the driving volume change vs nozzle diameter	17
Figure 2.6 Simulation results by Chen et al comparing the driving time with the velocity of the droplet	18
Figure 2.7 Effect of orifice diameter of the nozzles of PZT print heads jetting an unfilled paraffin wax ink, where the y-axis is the volume response of the droplet based on the driving signal	19
Figure 2.8 Shore and Harrison experiments carried out on a Newtonian fluid to determine the effects of changes to the pulse amplitude and how this affects the tail ligament before the drop breakoff point	19
Figure 2.9 Successive images taken using a high speed camera of a droplet of ink being jetted from a 50 um diameter nozzle	20
Figure 2.10 An SEM image of silica microspheres that were deposited onto hydrophilic Si wafer. A 4 vol% concentration of (a) water-based ink, (b) a combination of water and diethylene glycol ink, (c) water and formamide ink was deposited onto the same substrate and the results of the dried drops and spread of particles were analysed	21
Figure 2.11 A simple schematic illustrating the impact and spreading of a droplet of ink on a solid surface	22
Figure 2.12 A droplet deposited onto a hydrophilic substrate that has a groove or channel will spread/wet the groove	23
Figure 2.13 An experimental example produced to illustrate the effects of droplets moving away from hydrophobic areas of the substrate to more hydrophilic [59]	24

Figure 2.14 Treated polyimide substrate to produce a higher contact angle. Hydrophilic untreated polyimide had a contact angle of about 30°, while the treated substrate had an increase in contact angle to 109° [59].....	24
Figure 2.15 Droplets of ink deposited onto a treated hydrophobic and non-treated hydrophilic substrate [59].....	25
Figure 2.16 Dots of ink printed onto three different types of substrates showing the effect of substrate porosity on the resolution of the print.....	26
Figure 2.17 Microscope images and interferometric data gathered on printing PEG onto epoxy resin substrate (left) and a substrate with a pre-printed layer (right)	26
Figure 2.18 An image obtained using interferometric microscope of the zirconia ink printed onto a glass substrate at temperatures (a) 25°C, (b) 35°C, (c) 50°C, (d) 100°C.....	28
Figure 2.19 Illustrated image showing droplets of ink printed onto solid and porous substrates. The white arrows show the internal radial flow, the grey arrows represent the fluxes from evaporation, and the black arrows the Marangoni flow.....	29
Figure 2.20 The Autodrop™ printer from Microdrop Technologies GmbH.....	29
Figure 2.21 Profiles of the 40 wt% and 20 wt% printed polyurethane.....	30
Figure 2.22 Profile image of 3-D printed 40 wt% polyurethane material using white-light interferometry.....	31
Figure 2.23 3-D images obtained using white-light interferometry of 5 layers of 3-D printed polyurethane in pyramid shape.....	31
Figure 3.1 A comparison between the frequency and reflection loss for steel, aluminium, and copper.....	41
Figure 3.2 Magnetic field (illustrated as yellow lines) propagating around the shielding material	41
Figure 3.3 A diagram illustrating the Band Theory for metallic materials, semiconductors and insulators.....	42
Figure 3.4 Simple representation of the EM spectrum.....	44
Figure 3.5 Shielding can be used to prevent (a) EM waves interfering with another object and (b) be harmed by another object.	45
Figure 3.6 Electrical conductivity based on the type of materials and the electrical conductivity range that can be covered by conductive fillers.....	46
Figure 3.7 Filler volume fraction effect on the electrical conductivity of a material.....	49
Figure 3.8 Graphs illustrating the shielding effectiveness at 1 GHz, with comparison between (a) VGCNF/HDPE processes at 20rpm and 100rpm at 7.5 wt% and (b) VGCNF/HDPE processed at 50rpm at 7.5 wt% with different processing temperatures.....	50
Figure 3.9 TEM images of 5 wt.% (a) carbon black particles, (b) carbon nano fibers, (c) carbon nano tubes dispersed in ABS material.....	51

Figure 3.10 A compilation with standard deviation of electrical volume resistivity of varying concentrations of conductive carbon black, carbon nano fibers, and carbon nano tubes dispersed in ABS plastic.....	52
Figure 3.11 Shielding effectiveness of carbon black powder, nano-fibre and nano-tubes tested at 8.2 GHz with standard deviation bars.....	52
Figure 3.12 Shielding effectiveness of MWCNT/PS composites with varying plate thickness.....	53
Figure 3.13 Comparison between (a) the real permittivity and (b) imaginary permittivity...	54
Figure 3.14 Comparison between reflection loss and frequency (a) and reflection loss and temperature (b) using 5mm thick sample of carbon fibers dispersed in silica.....	54
Figure 3.15 The shielding effectiveness of a 0.5mm sheet of copper.....	55
Figure 3.16 Dielectric permittivity measurements for MWCNT composites (left) and PVDF composites (right).....	57
Figure 3.17 Dielectric loss tangent results for MWCNT composites (left) and PVDF copper nanowire composites (right).....	57
Figure 3.18 EMI SE of 210mm thick CCP/PS composite samples with varying concentrations of copper nanowire filler.....	59
Figure 3.19 the absorption, reflection, and overall EMI shielding provided by copper nanowire filler as a function of filler loading.....	59
Figure 4.1 An illustrated example of the pendant drop measuring method.....	67
Figure 4.2 A basic cross sectional illustration of the 3-D wave pattern that was used to test 3-D jetting with XSBR ink.....	74
Figure 4.3 Patterns utilized for printing conductive carbon black onto PET substrates. These include (a) dot pattern, (b) octo grid, (c) parallel lines, (d) alternating chevron, (e) dot grid, and (f) continuous rectangle.....	84
Figure 4.4 A simplified schematic of the SPDR that was used to carry out dielectric tests on the latex materials.....	86
Figure 4.5 Monopole antenna design and measurements.....	87
Figure 5.1 Surface tension of the latex.....	89
Figure 5.2 Brookfield viscosity for latexes.....	90
Figure 5.3 Shear viscosity of latex measured using the parallel plate rheometer.....	91
Figure 5.4 Particle size distribution results for latex.....	92
Figure 5.5 Particle size analysis of latex with 60 second ultrasonic treatment.....	93
Figure 5.6 Photograph of 10 layers of diluted XSBR printed using a 2cm x 2cm square pattern onto silicone coated paper	94

Figure 5.7 Thickness measurement and topography analysis using the Alicona white light interferometer	95
Figure 5.8 A 3-D image of the printed XSBR generated by the Alicona white light interferometer	96
Figure 5.9 Effect of TGME on drying of XSBR latex at 60°C.....	97
Figure 5.10. Effect of TGME on water content after drying at 60°C for 180 min.....	98
Figure 5.11 Effect of TGME concentrations on remaining liquid after drying at 60°C for 24h.....	99
Figure 5.12 Shear viscosity measurements for original and diluted latex.....	101
Figure 5.13 Shear viscosity measurements for original latex and latex ink.....	102
Figure 5.14 Particle size distributions for CR, XSBR, XNBR, and HNBR inks	104
Figure 5.15 Jetting waveform split into 3 phases or stages	109
Figure 5.16 Waveform for first jetting trial.....	109
Figure 5.17 Ink jetting resulting from the waveform as shown in Figure 5.16.....	110
Figure 5.18 Waveform for second jetting trial	111
Figure 5.19 Waveform for third jetting trial	112
Figure 5.20 Ink jetting resulting from the third waveform shown in Figure 5.24.....	112
Figure 5.21 Fourth waveform used for ink jetting	112
Figure 5.22 Formation of droplets from 4 nozzles as they are ejected utilising the fourth waveform.....	114
Figure 5.23 Captured image of a droplet of de-ionised water on PET substrate	116
Figure 5.24 SEM image of droplets printed onto PET substrate for droplet analysis	117
Figure 5.25 Droplet analysis of XSBR droplet printed onto a glass microscope substrate.	118
Figure 5.26 SEM image of droplets printed onto PTFE tape	119
Figure 5.27 Effect of substrate surface energy on printed dot size	120
Figure 5.28 Image captured of the PTFE coated fabric using the Dimatix fiducial camera	121
Figure 5.29 Single layer of XSBR deposited onto PTFE coated fabric	121
Figure 5.30 XSBR single layer deposited onto PTFE tape	122
Figure 5.31 Single layer XSBR ink deposition onto PET substrate to test the wettability of the substrate.....	122

Figure 5.32 Single layer of XSBR on a glass microscope slide	123
Figure 5.33 SEM image of XSBR lines printed onto glass slide	124
Figure 5.34 10 layers of XSBR ink printed onto PET substrate	124
Figure 5.35 10 layers of XSBR ink printed onto PTFE coated fabric substrate.....	126
Figure 5.36 10 layers of XSBR ink printed onto a glass microscope slide.....	127
Figure 5.37 10 layers of XSBR ink printed onto PET substrate.....	128
Figure 5.38 10 layers of XSBR ink printed onto PTFE tape.....	128
Figure 5.39 Loughborough University logo printed with XSBR ink (approximately 5cm long and 1 cm high).....	130
Figure 5.40 ZEON logo printed using HNBR liquid latex provided by Zeon Chemicals (approximately 4cm long and 1.5cm wide pattern).....	130
Figure 5.41 Cross sectional profile of 30 layers of XSBR ink printed using a 3D wave pattern.....	131
Figure 5.42 Cross sectional profile of 30 layers of XSBR ink printed using a 3D wave pattern	131
Figure 5.43 10 layers of XSBR ink printed onto PET without time delay.....	133
Figure 5.44 10 layers of XSBR ink printed onto PET substrate with a 30 second time delay between layers.....	133
Figure 5.45 10 layers of XSBR ink printed onto PET substrate with a 60 second time delay between layers	134
Figure 5.46 20 layers of XSBR printed without time delay.....	134
Figure 5.47 20 layer of XSBR printed with a 30 second time delay between layers	135
Figure 5.48 20 layers of XSBR printed with a 60 second time delay between layers	135
Figure 5.49 30 layers of XSBR printed without time delay	136
Figure 5.50 30 layers of XSBR printed with a 30-second delay.....	136
Figure 5.51 30 layers of XSBR printed with a 60 second time delay between layers.....	136
Figure 5.52 A scatter graph illustrating the effect the number of printed layers have on the individual layer height when introducing a 30 second time delay between printing of layers and a bed temperature of 60°C.....	139
Figure 5.53 SEM image of XSBR latex ink printed onto a PET substrate.....	140
Figure 5.54 XSBR ink printed onto Teflon coated fabric.....	141
Figure 5.55 XSBR ink printed onto cast sheet of XSBR.....	142

Figure 5.56 XSBR and conductive carbon black 3-D jetted composite material.....	143
Figure 5.57 The 5x4mm XSBR carbon black composite with a top layer of XSBR latex ink.....	144
Figure 5.58 Thickness measurement of one layer of conductive carbon black ink printed onto PET substrate.....	145
Figure 5.59 Thickness measurement for five layers of conductive carbon black printed onto PET substrate.....	145
Figure 5.60 Ten layers of XSBR Resorcinol ink printed onto a PET substrate.....	146
Figure 5.61 Fifty layers of XSBR ink combined with Resorcinol resin printed onto PET substrate.....	147
Figure 5.62 One hundred layers of XSBR ink with Resorcinol resin printed onto PET...	147
Figure 5.63 % Weight gain results for swell tests on cured XSBR samples, as well as a control test of uncured sample with resin.....	148
Figure 5.64 Tensile test results for cured and control XSBR samples.....	149
Figure 5.65 Second tensile test results for cured and control XSBR samples.....	150
Figure 5.66 Conductive carbon black powder mixed with diluted XSBR latex.....	153
Figure 5.67 Diluted conductive carbon black powder on left and diluted conductive carbon black paste on right. Samples were left stagnant for three hours	154
Figure 5.68 Carbon black paste combined with XSBR latex.....	154
Figure 5.69 XSBR combined with carbon black in a petri dish to be dried.....	155
Figure 5.70 Colour changes were observed during the drying process.....	155
Figure 5.71 Dried sample of XSBR combined with carbon black paste produced for dielectric measurements.....	156
Figure 5.72 TGA results for printed XSBR ink.....	157
Figure 5.73 TGA results for NR with 55% phr carbon black.....	158
Figure 6.1 Monopole antenna simulation.....	162
Figure 6.2 Monopole design (Figure not to scale).....	163
Figure 6.3 Horizontal lines of conductive carbon black printed onto cast sheet of XNBR. Lines are approximately 1mm thick with 1mm gap between lines. Thickness of printed carbon black was measured at 1.2 μ	165
Figure 6.4 A crosshatch pattern (3 layers) printed onto cast sheet of XSBR latex.....	165
Figure 6.5 10 layers of conductive carbon black printed onto XNBR.....	166
Figure 6.6 Measured results for the transmission between two monopoles with different printed shields for cast samples with printed conductive carbon black patterns.....	168

Figure 6.7 Octogrid pattern that was used to print conductive carbon black ink onto PET substrates.	170
Figure 6.8 S.E. of single layer of carbon black with thickness of 1 μm	177
Figure 6.9 S.E. of five layers of carbon black with thickness of 1.2 μm	178

Table of Tables

Table 3.1 Properties of some common dielectric materials.....	40
Table 3.2 A comparison of EMI shielding effectiveness (SE) for a polyethersulfone matrix composite with different fillers between 1 and 2 GHz frequency.....	56
Table 4.1 Ink trade names and manufacturers used for printing.....	65
Table 4.2 Substrates used for printing.....	65
Table 4.3 Ink trade names and manufacturers used for printing.....	65
Table 4.4 Substrates used for printing.....	66
Table 4.5 Concentrations of TGME in XSBR latex.....	70
Table 4.6 XSBR and resorcinol curing resin mixture	79
Table 5.1 Surface tension of latexes in their original form	99
Table 5.2 Surface tension of latexes diluted with de-ionised water to 33 % solids content	100
Table 5.3 Surface tension of latex inks, diluted with deionised water and with 10 wet wt.% TGME (solid content = 33 wet. wt.%)......	100
Table 5.4 Properties of the inks related to their printability (Z).....	106
Table 5.5 Surface energies of substrates.....	115
Table 5.6 Comparison of individual layer thickness for 10, 20, and 30 layers of XSBR with varying time delays.....	137
Table 5.7 Effect of number of layers on layer thickness with a 30 second time delay (bed temperature 50°C).....	138
Table 5.8 Recorded values of tensile strength and % elongation.....	151
Table 5.9 TGA carbon content results for all samples.....	160
Table 6.1 Measured relative permittivity and dielectric loss tangent results for single and 5 layers of conductive carbon black printed onto PET sheets in various patterns	171
Table 6.2 Measured relative permittivity results for hot press moulded rubber and conductive carbon black printed onto PET.....	172
Table 6.3 Measured dielectric loss tangent results for hot press moulded rubber with 25 % and 40% carbon black concentration and conductive carbon black printed onto PET, NR, and XSBR.....	172
Table 6.4 Permittivity and dielectric loss measurements of samples.....	173
Table 6.5 Permittivity and dielectric loss tangent results for XSBR with varying concentrations of conductive carbon black.....	174

Table 6.6 S.E. (dB) comparison for 1, 5, and 10 layers of conductive carbon black printed onto PET substrate.....179

Chapter 1 Introduction

1.1 General Background

Additive manufacturing (AM), also known as 3-D printing, is receiving more attention and consideration from researchers and engineering companies with every passing year due to the adaptability and efficiency of the technology. 3-D printing is a process of creating a physical object using computer aided design (CAD) to model a component and 3-D printing technology which deposits multiple numbers of layers of a material onto a substrate. Until recently, 3-D printing was a niche and expensive method of creating solid parts from modelling software but is becoming a valuable method of creating precision parts for the engineering industry and is becoming a more readily available form of manufacturing.

The current project examines the possibilities and outcomes of inkjet printing with elastomeric compounds in the form of a latex ink. An investigation is also carried out into the potential for using inkjet technology to create elastomeric components with novel internal structure or composition by controlling the distribution of filler. Such a material has great potential in many areas of engineering, one example being electromagnetic interference (EMI) shielding.

1.2 3-D Printing Technology

There are certain advantages and limitations to current 3-D printing processes and technology. The main advantage of utilising 3-D printing is the ability to create prototypes with relative ease and speed compared to more conventional manufacturing methods. One-off or small numbers of parts can be created, which has the potential to save on tooling costs as well as time. With 3-D printing, complex geometries can be produced, including intricate internal structures that can be made in one go. The final advantage is customisation, particularly in biomedical applications, which offers the potential for bespoke manufacturing [1].

There are, however, certain limitations to 3-D printing. Because this technology is still under development, it is not yet generally suitable for mass production as it is slow and expensive compared to conventional manufacturing techniques. The second limitation is the materials that can be used as they are generally:

- Expensive
- Limited in number and range of properties
- Specially developed for 3-D printing, so there is no option for utilising those materials outside of their original design
- Material functional properties are often inferior when compared to materials used in mass production, e.g. injection moulding
- Components are usually made from only one material, therefore there is limited compatibility between different printing methods for different materials.

1.3 3D printing of elastomeric materials

There are two types of elastomers that can be used in 3-D printing, thermoplastic and thermoset. Thermoplastic elastomers soften on heating and can be processed using conventional thermoplastic processing equipment. Thermoset elastomers require a curing stage to bring about crosslinking [2]. The specific technologies that can be used are illustrated in Figure 1.1.

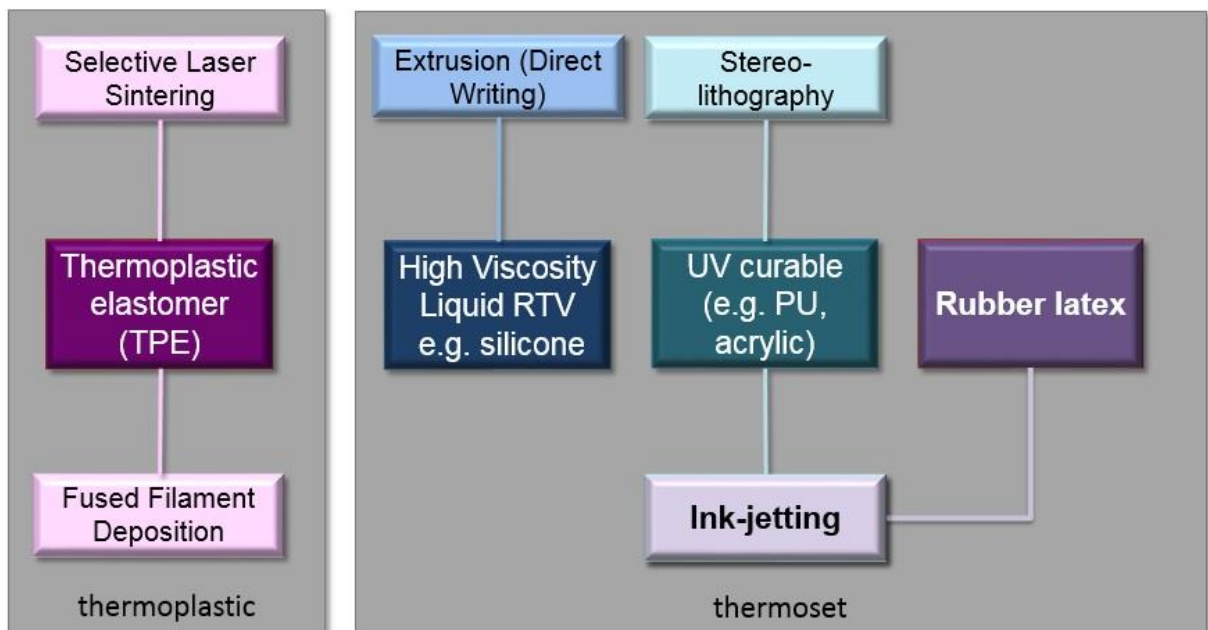


Figure 0.1.1 Forms of current thermoplastic and thermoset methods of 3-D printing elastomers

This section provides a brief overview of the types of 3-D printing methods that fall into the thermoplastic and thermoset categories, and will conclude with the method of 3-D printing that was selected for this project: ink-jetting.

1.3.1 3-D Printing Techniques for Thermoplastic Elastomers

Fused Deposition Modelling

Fused deposition modelling (FDM) produces 3-D objects by melting and extruding thin thermoplastic filaments. The filaments are mechanically fed through a heated nozzle that melts the elastomer and deposits it onto a bed. Figure 1.2 provides a basic illustration of FDM.

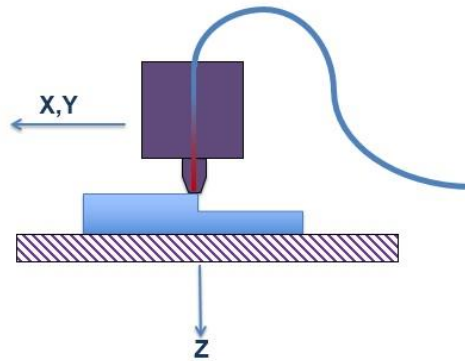


Figure 1.0.2 An illustration of FDM 3-D printing

The benefits of this type of 3-D printing:

- No curing of the final print necessary
- No post-processing
- No drying
- Materials are cost effective and the equipment for printing is less expensive than other 3-D printing technologies

These materials are utilised in FDM printing and are plastic or polymer materials that are melted during printing. These thermoplastics can have high melting temperatures up to 230°C.

Selective Laser Sintering

This method of 3-D printing uses a powder and a high-power laser to melt the powder according to the CAD pattern and design. However, unlike stereolithography, selective laser sintering (SLS) can be utilised to print with a variety of materials, which include various metal and ceramic powders, as well as polymers, plastics, and a combination of metals and polymers [3, 4]. Composite materials can also be created using metals or polymers in combination with specific fillers such as fibre glass, copper, and polyamide [5, 6, 7, 8]. Figure 1.3 provides an illustration of the SLS process.

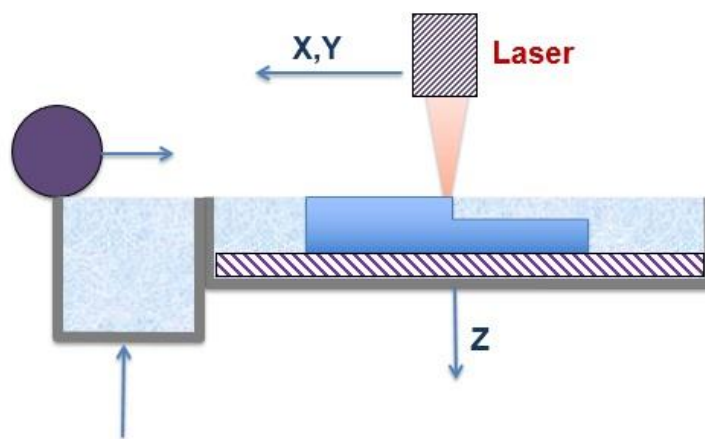


Figure 1.0.3 An illustration of the SLS 3-D printing process

1.3.2 3-D Printing Techniques for Thermoset Elastomers

Stereolithography

This method of 3-D printing was developed to create objects by curing a photosensitive liquid polymer material using a UV laser. A laser is passed over a container of the photosensitive liquid polymer, curing the material in specific areas according to the pattern created in CAD software. During printing, a supporting structure is printed along with the model. Once the printing is complete the supporting structure can be removed and the remaining liquid that was not used during printing is drained and can be used for another printing session [8]. Figure 1.4 provides an illustration of the stereolithography process.

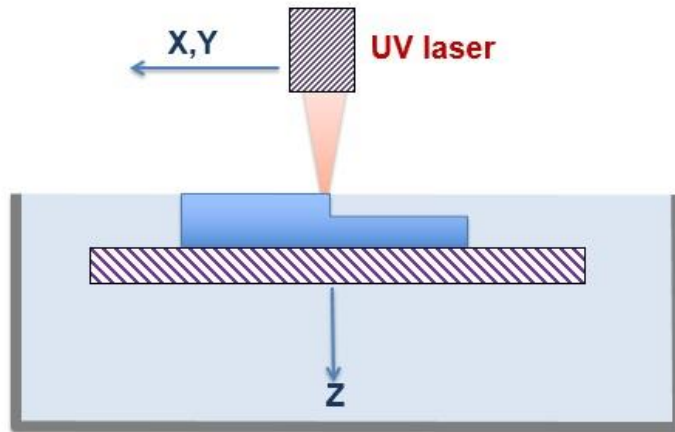


Figure 1.0.4 Stereolithography 3D printing process

Extrusion (Direct writing)

This method of 3-D printing utilises highly viscous materials to deposit. A variety of materials are available for direct writing, including ceramic paste and highly viscous polymer and are capable of printing single or multilayer materials. Silicone rubber is commonly utilised for extrusion 3-D printing [9]. Figure 1.5 provides a simplified illustration of extrusion 3-D printing.

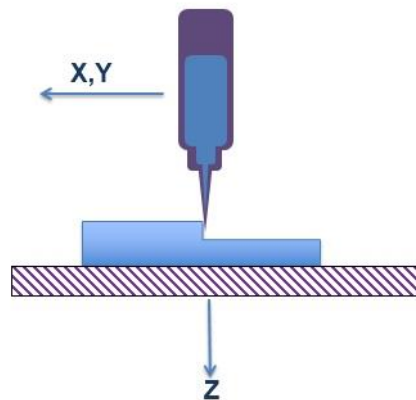


Figure 1.0.5 Extrusion 3-D printing process

Inkjet Printing

Inkjet printing technology has been widely available to the public since the 1970s. Currently there are a number of methods inkjet printing is carried out, including continuous jet printing, drop-on-demand, and laser inkjet printing. Recently inkjet printing has become

an interesting method of 3-D printing, providing the ability to print with a wide variety of materials and with different methods of deposition. This method utilises a liquid material contained in a cartridge, which is ejected out of nozzles that are tens of micrometres in diameter. Figure 1.6 provides an illustration of the inkjet printing process. This method of 3-D printing is ideal for creating thin layers of material and for printing flexible circuitry [10].

In this project, the potential of creating elastomeric articles by inkjet printing with latex is investigated. The potential benefits of this technique lie with the characteristics of the elastomer latex materials themselves. The elastomers within the latex have a high molecular weight, which provide good mechanical properties. Typically, materials that have a high molecular weight have a high viscosity, which is not ideal for ink jetting. However, a latex comprises a nano-scale suspension of the solid rubber in water and has a relatively low viscosity. Hence, it is possible to achieve ink jetting of a material that would normally be highly viscous in its solid form while maintaining its beneficial properties. Furthermore, there is the possibility of introducing a filler, and controlling its distribution in the elastomer article.

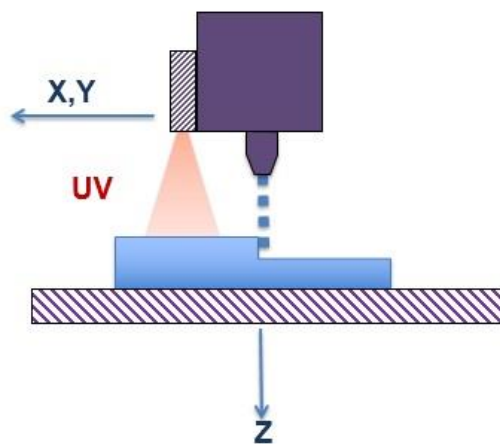


Figure 1.0.6 Inkjet printing AM process with UV curing

1.4 Aims and Objectives

The overall aim of this Thesis is to present the investigation carried out into 3-D printing of thermoset elastomeric materials from liquid latex using inkjet technology. A further aim was to assess the feasibility of printing a micro-composite composite material by depositing elastomer and a filler to obtain special functionality, such as novel electromagnetic shielding performance.

The specific objectives of the project regarding inkjet printing of elastomeric latex materials include the determination of:

- The optimum latex properties for inkjet printing, including determining the effects of viscosity, surface tension, and particle size on the inkjet process.
- The best substrate for elastomeric ink, by investigating the effect of surface energy and topography on the final print quality.
- The optimum parameters to for multilayer inkjet printing of liquid latex, to create 3Dobjects.
- The effect that conductive carbon black has on electromagnetic properties, by using a split-post dielectric resonator.
- The effect that different inkjet printed conductive carbon black patterns have on electromagnetic properties.
- The feasibility of using inkjet technology to create a composite material from liquid latex ink and conductive carbon black ink.
- The feasibility of creating a cross-linked elastomer using inkjet technology combined with a post-curing process.

References for Chapter 1

- [1] Guo, N., Leu, C. M. *Additive Manufacturing: Technology, Applications and Research Needs*. (2013). *Frontiers of Mechanical Engineering*, vol. 8, no. 3, pp. 215-243.
- [2] Automated Dynamics – Composite Structures, Automation Equipment, and Engineering Service. (2017). Thermoset vs thermoplastic composites | Automated Dynamics – Composite Structures, Automation Equipment, and Engineering Services. [online] Available at: <http://www.automateddynamics.com/article/composite-basics/thermoset-vs-thermoplastic-composites> [Accessed 22 April 2017].
- [3] S. Ashley. *Rapid prototyping systems*. (1991). *Mechanical Engineering*, vol. 113, no. 4, p. 34.
- [4] J. W. Halloran, V. Tomeckova, S. Gentry et al. *Photopolymerization of powder suspensions for shaping ceramics*. (2011). *Journal of the European Ceramic Society*, vol. 31, no. 14, pp. 2613–2619.
- [5] T. Hwa-Hsing, C. Ming-Lu, Y. Hsiao-Chuan. *Slurrybased selective laser sintering of polymer-coated ceramic powders to fabricate high strength alumina parts*. (2011). *Journal of the European Ceramic Society*, vol. 31, no. 8, pp. 1383–1388.
- [6] G. V. Salmoria, R. A. Paggi, A. Lago, V. E. Beal. *Microstructural and mechanical characterization of PA12/ MWCNTs nanocomposite manufactured by selective laser sintering*. (2011). *Polymer Testing*, vol. 30, no. 6, pp. 611–615.
- [7] Stampfl, J., Baudis, S., Heller, C., Liska, R., Neumeister, A., Kling, R., Ostendorf, A., and Spitzbart, M. Photopolymers with tunable mechanical properties processed by laser-based high-resolution stereolithography. *Journal of Micromechanics and Microengineering*, vol. 18, no. 12, pp. 125014.
- [8] Neumeister A, Himmelhuber R, Materlik C, Temme T, Pape F, Gatzen H-H and Ostendorf A. (2008). *Properties of three-dimensional precision objects fabricated by using laser based micro stereolithography*. *J. Laser Micro/Nano Eng.* vol. 3, no. 2, pp. 67-72.
- [9] Polmanteer, K. *Silicone Rubber, Its Development and Technological Progress*. (2008). *Rubber Chemistry and Technology*, vol. 61, no. 3, pp. 470-502.
- [10] de Gans B.-J., Duineveld P. C. & Schubert U. S. Inkjet printing of polymers: State of the art and future developments. (2004). *Advanced Materials*, vol. 16, pp. 203–213.

Chapter 2 Principles and Review of 3D Ink Jetting

2.1 Introduction

3-D printing using ink jetting technology involves the creation of a solid object, with the aid of computer aided design (CAD), by depositing many successive layers of liquid droplets. Since Lord Rayleigh's studies of droplet formations in the late 1800s, inkjet printing has progressed significantly and has become a fundamental and practical technology that is used globally for various needs and purposes. Inkjet printing technology is intricate and is the result of significant advances in material science, engineering and research over many decades. This section analyses the various parameters that must be considered in order to achieve ideal jetting results that provide the desired physical geometries of the printed material and the many factors that can influence the resolution and jetting behaviour of inkjet inks.

2.2 The Effect of Ink Properties: Viscosity, Surface Tension and Particle Size

The study of droplet formation and behaviour was first examined by Lord Rayleigh in 1878 [1]. His findings published in the London Mathematical Society titled "On the instability of jets" made it possible for the first commercially available inkjet devices to be patented and created in 1948 by Siemens [2]. This was the first push into inkjet printing technology that galvanized further research into the study of printing parameters and how they may be adapted to be used for 3-D printing processes.

Inkjet printing is dependent on a variety of factors, which include material properties of the inks and substrates. The purpose of this section is to analyse and discuss these parameters in detail to better understand the requirements for ideal jetting results.

Three ink material properties are crucial for successful ink jetting of colloidal materials. These include the viscosity of the liquid, surface tension, and density [3]. Viscosity is represented by the η symbol in equations, and it is defined by shear stress divided by shear rate:

$$\eta = \text{Viscosity} = \frac{F'}{S} = \frac{\text{Shear stress}}{\text{Shear rate}} \quad \text{Eq. 2.1}$$

The units of measurement for viscosity usually used for inkjet inks are centipoise (cps), or mPa.s, which are numerically equivalent measures of dynamic viscosity. Generally

fluid materials are classified as Newtonian or Non-Newtonian, where Newtonian fluids exhibit a straight line relationship between shear stress and shear rate and the viscosity of non-Newtonian fluids changes as the shear rate alters.

With ink jet 3-D printing devices, viscosity values are required to be low and there are various types of inks that satisfy this criterion, which include solvents, UV-curable inks, and dye sublimation inks. Depending on the type of print head used, the viscosities of the inks can vary between 8 and 45 mPa.s for piezoelectric and thermal print heads.

The viscosity for drop on demand (DoD) piezoelectric ink jet printer heads is required to be ideally below 20 mPa.s for aqueous ink jetting [4] and should be less than 30 mPa.s for ceramic based suspended inks [5]. The ideal viscosity enables an ink to be pulled into and ejected out of the nozzle chamber. In comparison, water has a viscosity of 1 mPa.s. Factors that can affect an ink's viscosity include environmental conditions (temperature), solid content of the ink, and the addition of fillers and or solvents. Increasing the temperature of the ink decreases the viscosity of the ink [6, 7]. However, the majority of inkjet printing systems have a viscosity range that the equipment can jet, this range being stated by the manufacturer.

Although ink viscosity is a key property for ink jetting, it is important in combination with other material properties and externally determined conditions, such as velocity. With ink jetting, the behaviour of the ink droplets can be characterised by considering Reynolds (Re), Weber (We), and Ohnesorge (Oh) numbers. The equations that define them are as follows:

$$Re = \frac{v\rho\alpha}{\eta} \quad \text{Eq. 2.2}$$

$$We = \frac{v^2\rho\alpha}{\gamma} \quad \text{Eq. 2.3}$$

$$Oh = \frac{\sqrt{We}}{Re} = \frac{\eta}{(\gamma\rho\alpha)^{1/2}} \quad \text{Eq. 2.4}$$

Where η , ρ , and γ are dynamic viscosity, density, and surface tension respectively, v is the velocity of the droplet, and α is the characteristic length of the droplet [8]. The three main significant printing fluid properties are surface tension, density and viscosity as these are the properties that affect the formation of the droplets once they are ejected [1].

The Ohnesorge number was first identified by Fromm in relation to inkjet printing [10]. The Z value is the dimensionless inverse of the Ohnesorge number and is defined by the ratio between Reynolds number and square root of Weber number in the following equation:

$$Z = \frac{(\rho\gamma)^{1/2}}{\eta} \quad \text{Eq. 2.5}$$

Fromm originally proposed that the ideal Z value for generating stable droplets was greater than 2. However, Reis and Derby [11] created a simulation of droplet generation and proposed that the range for stable formation is $10 > Z > 1$. Their research led to the determination that drop ejection was prevented for low Z values, due to viscous dissipation. On the other hand, high Z values created a significant amount of satellite droplets that accompanied the main droplet. According to the research carried out by Jang and Kim, attempts to print with a material that has a Z number less than 4 produces a droplet with a long tail and increases the time taken to eject a single droplet. For inks with Z values greater than 14, the printing resulted in minimal satellite droplet creation [1]. The satellite droplets were created due to the high surface tension and low viscosity of the inks that caused the retreating tail of the main droplet to detach at or before the nozzle exit point. With inkjet inks that are particularly viscous, the droplets can experience non-linear instability in the tail, as was observed with ink mixtures of glycerol and water [12, 13]. All this is due to the necking formation that occurs during the jetting process. Resistance towards the necking forces is dependent on the viscosity of the ink as well as the elastic stresses, the surface tension, and inertia; all of which has a significant influence on the final form of the droplet once it is ejected [14, 15, 16]. This evidence is supported by Hoath et al [18], who studied the effects of fluid viscosity on ink jet break off with the aid of computer simulations. Their simulations were carried out to determine the changes in viscosity of Newtonian fluids during jetting, and it was determined that more viscous inks have the possibility of creating ligaments that rupture before the ink exits the nozzle. Therefore, most inks used for inkjet printing have a low viscosity around 20 mPa.s. This reduces the pressure drop that is present in the nozzles during jetting and ensures that the print head does not clog and that the size and shape of each droplet that is ejected is reproducible [14]. A graph created by Derby [19] on how the Z number affects ink jetting is illustrated in Figure 2.1.

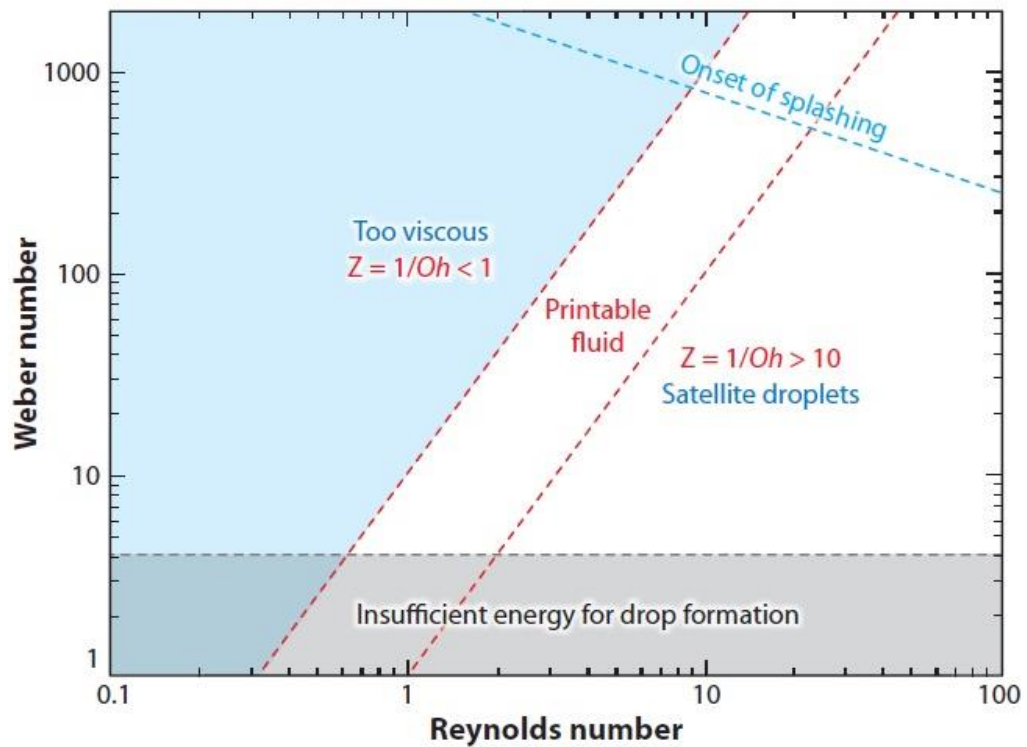


Figure 2.1 A coordinate system used to plot the Reynolds, Weber, and Ohnesorg equations [19]

Satellite droplet formations are a direct result of the tail ligament of the droplet breaking off and forming two different droplets due to instability during ejection. This instability is caused by slight incompatibilities between the materials properties of the ink, such as viscosity and surface tension, being too low [45]. With ink materials that are quite viscous on the other hand, the radial collapse of the droplet's tail is delayed due to viscous dissipation [46], therefore eliminating the creation of satellite droplets. Figure 2.2 illustrates the process of droplet formation during inkjet printing.

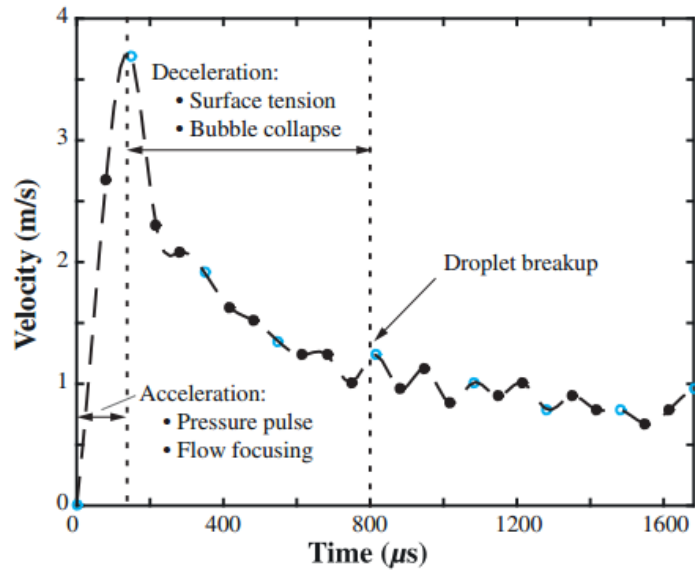


Figure 2.2 Droplet formation process from initiation of pulse to the breakoff of the droplet [47]

The particle size of any dispersed colloidal particle inks or suspensions is another significant material property that requires attention. The particles in the ink or suspension are required to be less than 5% of the total diameter of the print head nozzle [17]. This is to ensure that there is no instability created during droplet ejection as large particles can agglomerate and create blockages inside the nozzles, preventing the print head from ejecting the ink.

Figure 2.3 illustrates the limits of printability for a liquid material extrapolated from Fromm’s parameters by Derby. There is a clear indication that for any Z values over 10, the formation of satellite droplets becomes inescapable, and no droplet formations for Z values less than 1. Therefore, this mathematical method could be utilised during initial ink formulation to determine the effective printability of the prototype ink. It is important to note that this should not be considered the defining method of establishing how successful the ink jetting process will be for an ink, as jetting is also dependent on the type of equipment used and the parameters of the print heads.

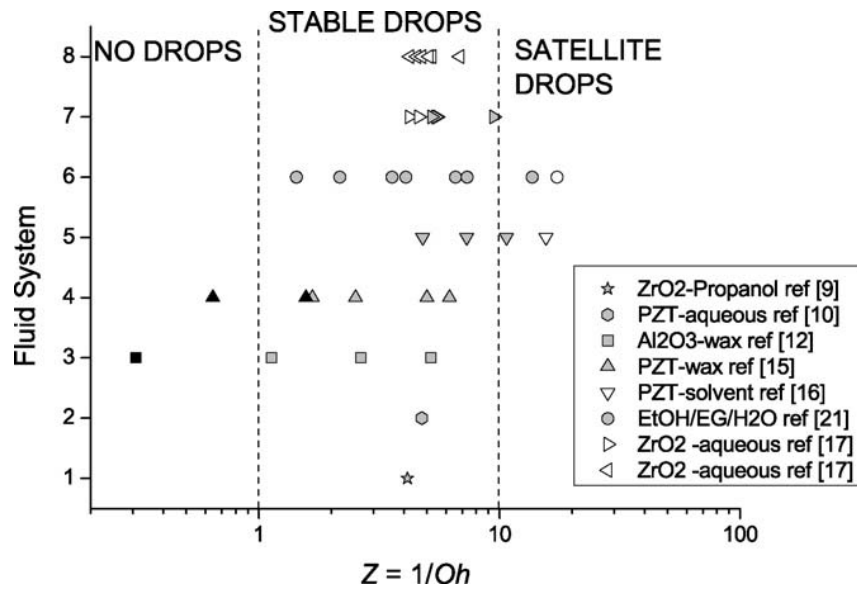


Figure 2.3 the effect of the Z number on the printability of a liquid material [19]

2.3 Inkjet Printing Parameters

Along with the material properties of the ink, the type of print head and operating parameters are the next consideration in the ink jetting process. Today there is a wide variety of inkjet printing systems that are designed for use in the commercial or research sector. This section explores the various types of inkjet printing systems, methods, and what effect the print heads and their operation have on jetting capabilities.

2.3.1 Type of Printers and Print Heads

Inkjet printing is a form of non-contact material deposition and the printing process is entirely controlled by computer [20]. There are currently two different types of inkjet printers, continuous and Drop on Demand (DoD). There are two types of DoD printer heads, thermal and piezoelectric.

Continuous inkjet printing

With continuous inkjet printing, the ink is ejected continuously with the use of a piezoelectric transducer. Depending on the type and make of the print head, the nozzles are between 50 and 80 μ m in diameter and deposit a continuous stream of ink droplets. These droplets are formed by Rayleigh instability, where the liquid column of ink is expelled through the nozzles with high pressure. The droplets are directed to the substrate by using charging electrodes which create an electrostatic deflection at the field plates. A positive

voltage is applied to the charging electrode and the field plates, which guides and directs the droplets to the desired area of the substrate [19, 20].

Drop on Demand (DoD) inkjet printing

With inkjet printing technology, thermal and piezoelectric print head systems usually fall under the Drop on Demand inkjet printing category, also known as DoD printing. DoD technology is novel and has emerged in the printing industry quite recently compared to the other methods of ink jetting discussed in this section. The difference between DoD and continuous ink jetting is that DoD involves non-contact printing of separate droplets that are jetted with precise control and are deposited only when needed. This yields a final print which has a very high resolution, between 600 and 2400 dpi and higher [20].

Drop on Demand Thermal inkjet printing

A thermal inkjet printer uses high temperature inside the print head to eject the ink. A thermal inkjet print head consists of hundreds of nozzles, each having a separate firing chamber inside the nozzles which is responsible for ejecting ink. This type of print head consists of a thin film heating resistor and an ink barrier channel leading into the nozzle. A current is passed through the thin film resistor to increase the temperature rapidly and create a vapour bubble in the ink. The pressure from the expanding gas causes the ink to be ejected in uniform droplet formations [21]. A simple diagram in Figure 2.4 illustrates how this process takes place.

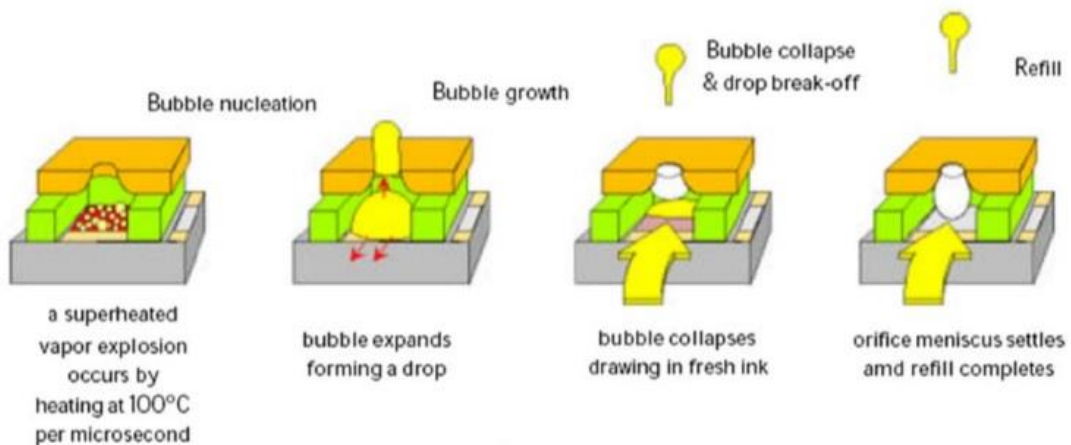


Figure 2.4 Thermal ink jetting process inside the print head [63]

Drop-on-Demand Piezoelectric inkjet printing

Piezoelectric ink jetting printing is currently the world leading method of ink jetting. This method of ink jetting is able to dispense ink by utilising a piezoelectric material inside the nozzles that, when an electric current is applied, deforms the material. This deformation creates a pressure that ultimately ejects the ink out of the nozzles.

There are four different types of piezoelectric print heads which work using similar principles but are classified according to their modes. These four types include:

- Squeeze mode
- Bend mode
- Push mode
- Shear mode

With the squeeze mode, ink is passed through a chamber with piezoelectric walls which are connected to electrodes. When an electric current is passed through these walls, they contract inwards. It is this sudden displacement that forces the ink out of the nozzle to eject a droplet. Once a droplet is ejected and the piezoelectric walls return to their original state, it creates a negative pressure that causes more ink from the cartridge to be pulled into the nozzle ready to be ejected [22].

The shear mode method of ink jetting utilises shear mode actuation using the piezoelectric walls in a similar manner to that of the squeeze mode. However, with the shear mode ink jetting system, typically more than one nozzle is used.

The bend mode normally utilises a piezoelectric ceramic material diaphragm that, when the driving voltage is applied, creates a bend in the diaphragm which forces the ink to be expelled out of the nozzle.

Push mode works in a similar manner to the bend mode. There is a piezoelectric diaphragm that is situated directly behind the nozzle and pushes the ink out.

2.3.2 Effect of nozzle geometry and jetting parameters

With inkjet printing, the jetting performance of the printer is dependent on certain parameters which include (a) type of print head used. (b) size, or diameter, of the nozzle, and (c) the jetting parameters [23]. This section analyses and discusses these three points

with regard to drop-on-demand (DoD) ink jet printers that have nozzles driven by piezoelectric actuators.

The driving waveforms, the configuration of the print head and the nozzle geometry all have a great influence on the droplet generation and ejection of drop on demand inkjet printers [23]. At the exit of the nozzle the surface tension of the ink helps to retain the material inside the print head until a waveform is generated that changes the volume of the chamber (driving volume change), leading ultimately to the ejection of an ink droplet. Driving volume change and driving time is used to describe the chamber volume change that occurs in piezoelectric (PZT) driven nozzles due to the ejection motion, and the time that is taken for a single droplet to be ejected. Minimum driving volume refers to the change required to achieve droplet ejection. Highest or maximum driving volume refers to the printing properties that are observed when the PZT nozzles begin ejecting columns of ink instead of droplets. DOD inkjet printers normally operate between 0.1-10 kHz for droplet generation [24].

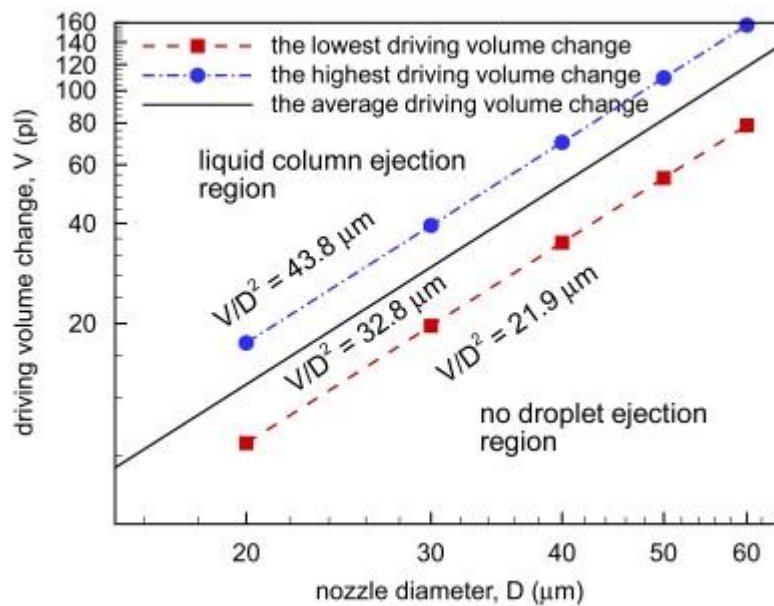


Figure 2.5 Simulation results produced by Chen et al illustrating the effect of the driving volume change vs nozzle diameter [23]

Chen et al conducted an analysis of the influence of droplet generation waveforms and nozzle geometry on the printing process. Figure 2.5 illustrates the effects of altering the driving waveform and nozzle diameter on the jetting performance. The volume factor, or V/D^2 , illustrated by the dotted red line in Figure 2.5 is used to define the region beyond which droplet ejection is halted.

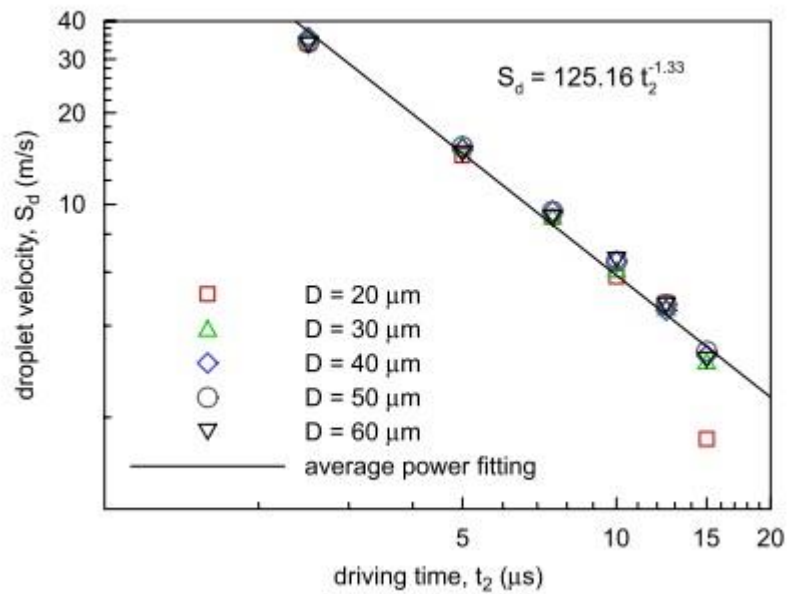


Figure 2.6 Simulation results by Chen et al comparing the driving time with the velocity of the droplet [23]

Figure 2.6 illustrates the simulation results of a comparative study on the driving time and the velocity of the droplet. The shorter driving time t_2 , which is the time taken for a droplet to be ejected from the moment of jetting initiation to completion, increased the velocity of the droplet.

Reis and Derby [25] carried out research to determine the effects that nozzle parameters have on the jetting process of paraffin wax ink combined with fine alumina powder. The results in Figure 2.7 illustrate the effect of the diameter of the nozzle on the droplet volume in response to the actuator driving signal. The error bars in the graph represent the uncertainty with regards to the maxima interpolated from the discrete data points.

Experiments carried out by Shore and Harrison [24] indicate that the act of altering the pulse amplitude (voltage) of the driving function has an impact on the ejected droplet. The results from these experiments are displayed in Figure 2.8 and it is evident that increasing the pulse amplitude significantly increases the length of the trailing tail of the droplet before it breaks off from the nozzle to impact the substrate. According to Cooper-White et al [26], the increased molecular weight of a liquid can also cause an increase in the thread length.

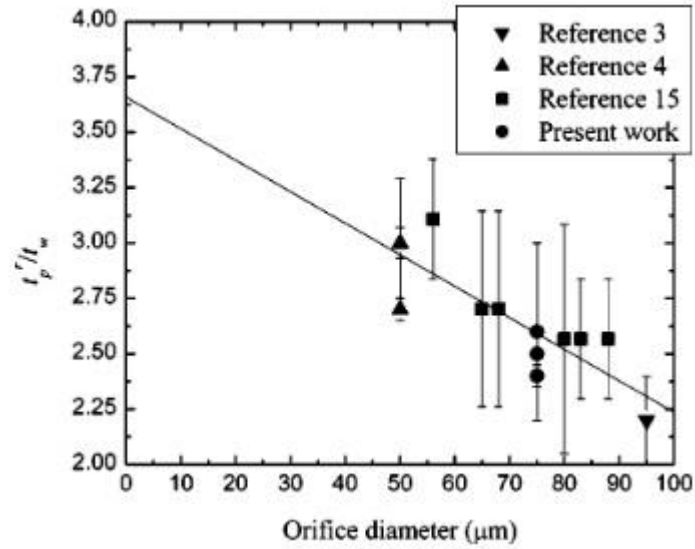


Figure 2.7 Effect of orifice diameter of the nozzles of PZT print heads jetting an unfilled paraffin wax ink, where the y-axis is the volume response of the droplet based on the driving signal [25]

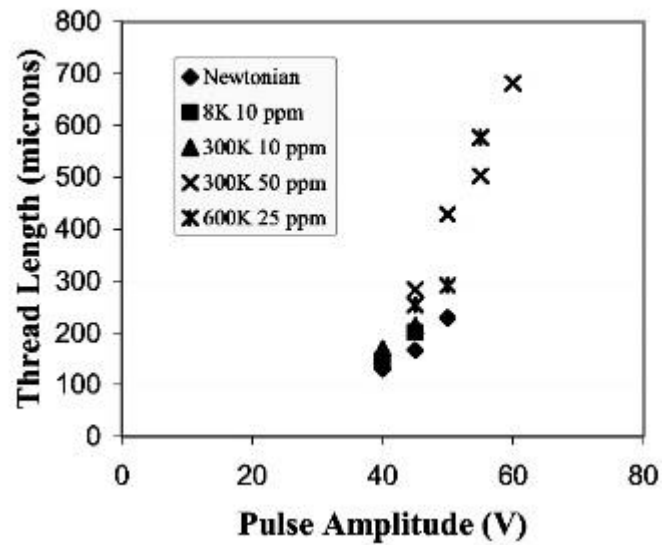


Figure 2.8 Shore and Harrison experiments carried out on a Newtonian fluid to determine the effects of changes to the pulse amplitude and how this affects the tail ligament before the drop breakoff point [24]

2.4 Droplet Deposition

The focal point of this section is the analysis of droplet behaviour following ejection from the print head and its behaviour once it lands and dries onto a substrate.

2.4.1 Characterisation Techniques

Current characterisation techniques for inkjet droplet flight and deposition include the use of high speed cameras to track the droplets and using microscopes or white light interferometry to analyse the ink materials deposited onto substrates. Inkjet 3-D printers that have a high-speed camera are very useful as they can be used to monitor the effects of fluid oscillations, droplet break off points, droplet size and even to determine if the printing system will generate debris or satellite droplets. Figure 2.9 shows an example of such capability.

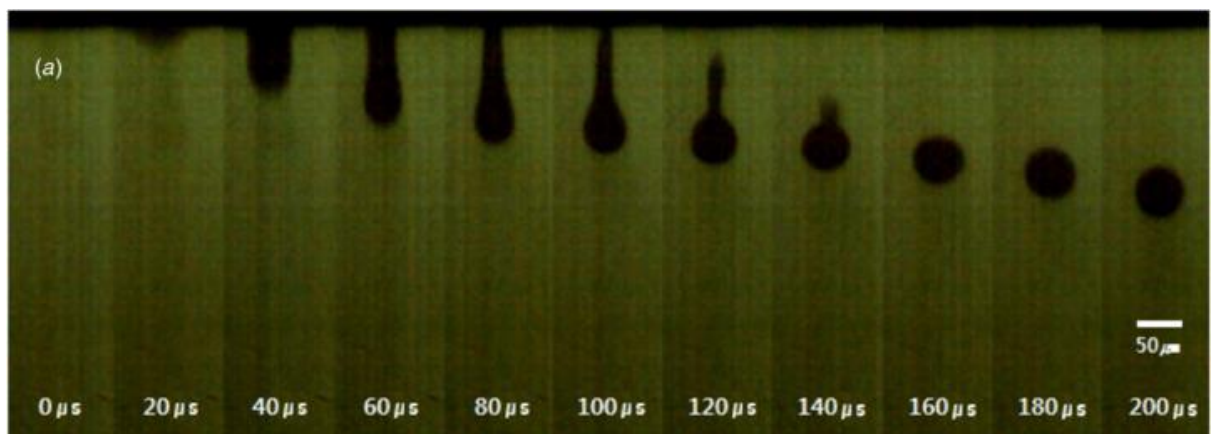


Figure 2.9 Successive images taken using a high speed camera of a droplet of ink being jetted from a 50 μm diameter nozzle [50]

2.4.2 Viscoelasticity and the Role of Humectants

Viscoelasticity of a liquid refers to its viscous and elastic traits when the liquid is exposed to stresses and deformation. Viscoelastic liquids have a tendency of returning back to their original shape after deformation, and in inkjet printing this is a common occurrence. With inkjet printing of polymeric materials, or inks that contain concentrations of polymers, the behaviour of the droplet's break-up is partly caused by the strain softening caused by high strain rates during jetting [27-29, 30]. This behaviour is a result of the polymer chains transitioning from their natural coiled state to a stretched state.

Humectants are chemicals that are typically used in the formulation of ink jetting inks in order to inhibit the evaporation of the inks. This aids in the prevention of clogging print heads, especially with inks that contain particles. Humectants also reduce the rate of drying of the deposited ink. Rapid drying of droplets leads to a ring formation due to convections that are created inside the liquid, which push the particles to the edges of the droplet. This phenomenon is observable when a droplet of water is heated very quickly on a hot substrate and the liquid begins to boil off from the centre, pushing the mineral particles inside the droplet to the edges of the droplet to create a ring once dried. The use of humectants can thus reduce the rate of drying and result in a more even deposition of the ink solids.

Wilhelm [62] estimated that approximately 8 hours is required for the solvents and water in a deposited ink to evaporate, leaving dry solid ink particles to be left on the substrate. This is due to the high water content the majority of inkjet inks contain. Approximately 95% of the composition of a typical ink is water combined with solvents, while the remaining 5% accounts for particles, surfactants and humectants and any other materials that are needed to maintain the integrity of the ink.

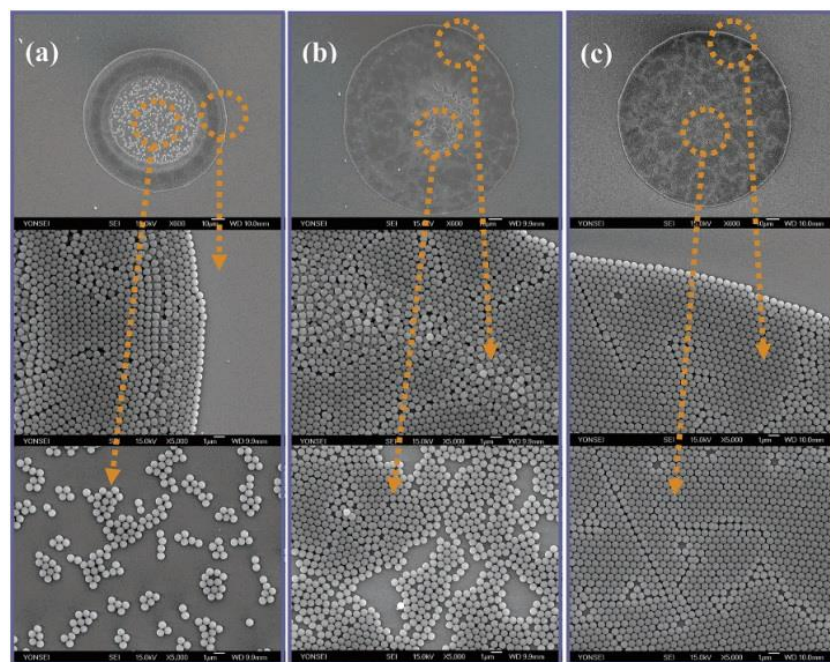


Figure 2.10 An SEM image of silica microspheres that were deposited onto hydrophilic Si wafer. A 4 vol% concentration of (a) water-based ink, (b) a combination of water and diethylene glycol ink, (c) water and formamide ink was deposited onto the same substrate and the results of the dried drops and spread of particles were analysed [62]

Figure 2.10 is an example of what effect varying the solvents and humectants in an ink can have on the behaviour of the particles once the ink is deposited onto a substrate. The addition of humectants in the ink resulted in longer drying period compared to the particles dispersed in water. Therefore, the results for the fast drying water based ink resulted in a ring like formation with most of the particles concentrated in the centre of the droplet; whereas the drying of the inks (b) and (c) resulted in the spread of the silica particles throughout the surface area of the droplet.

2.4.3 Effect of the Substrate Surface Energy, Drop Impact, and Substrate Topography

Much research is currently being conducted into the effect substrates with different surface energies and textures have on the final print of the ink material. This section analyses the various physical properties of substrates used for inkjet printing and the influence of these properties on the ink that is deposited onto them.

The substrate that the ink is deposited onto has a significant impact on the morphology of the ink and how it dries. Inks have been printed onto various substrates, including paper, powder solid glass and metal, all with varying surface energies and chemical composition.

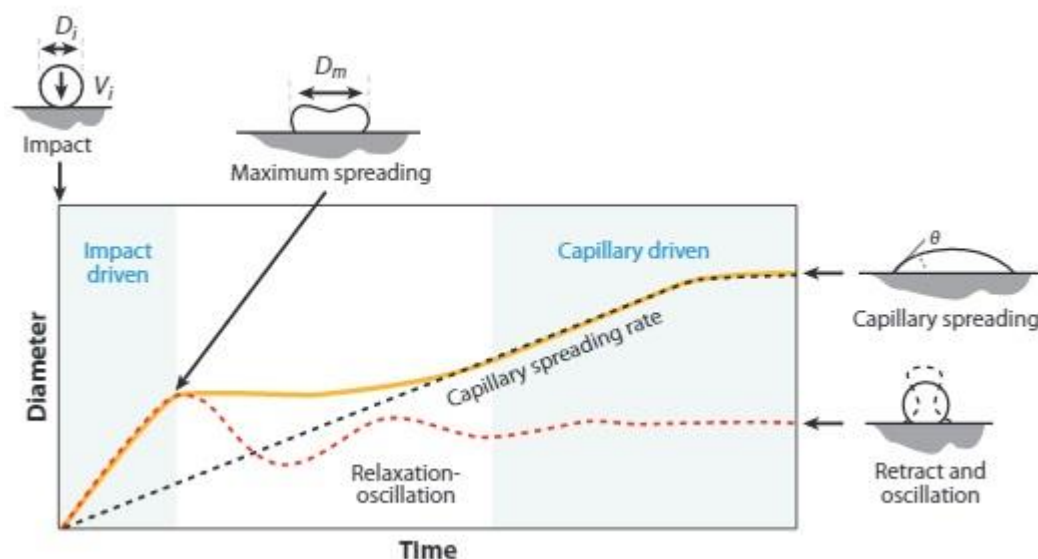


Figure 2.11 A simple schematic illustrating the impact and spreading of a droplet of ink on a solid surface [19]

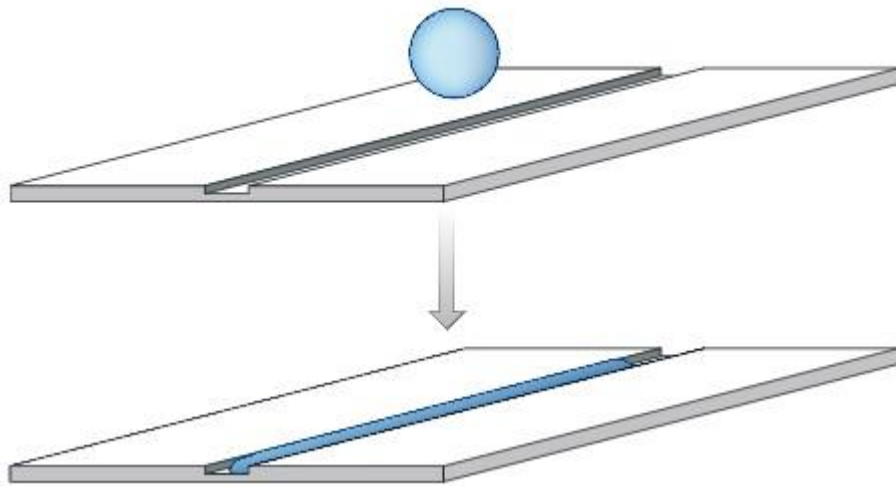


Figure 2.12 A droplet deposited onto a hydrophilic substrate that has a groove or channel will spread/wet the groove [19]

Figure 2.11 illustrates the behaviour of the droplet after it is ejected and deposited onto a solid substrate. The graph shows the initial drop impact, which induces maximum spreading due to the impact oscillations, followed by the capillary-driven flow.

Water based inks deposited onto extremely hydrophobic or hydrophilic surfaces could lead to too little wetting, or too much. An issue with too little wetting is that it can prevent droplets that are deposited onto the hydrophobic substrate from merging to form a continuous line. Instead, what would be observed is a series of droplets in linear formation. Another issue that could occur, as explained by Chaudhury and Whitesides, is that ink droplets deposited onto a hydrophobic substrate can migrate to more hydrophilic areas of the substrate [58]. The issue with too much wetting is that it can cause the ink to wet the substrate almost completely, therefore losing the resolution and accuracy of the print [59]. Other factors that can influence spreading include the temperature of the substrate, condensation, the properties of the ink itself, surface roughness of the substrate, and the gas-liquid interaction between the ink and the substrate [52-57]. The temperature of the substrate can influence droplet spreading, but is dependent on the type of ink used. If the ink particles are dispersed in a solution with a high concentration of water, droplet spreading can occur if the temperature of the substrate is low, therefore preventing thermo-capillary convection to occur.

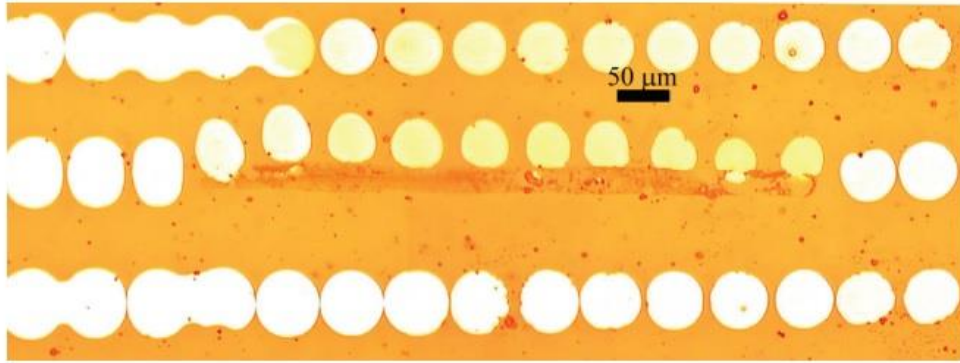


Figure 2.13 An experimental example produced to illustrate the effects of droplets moving away from hydrophobic areas of the substrate to more hydrophilic [59]

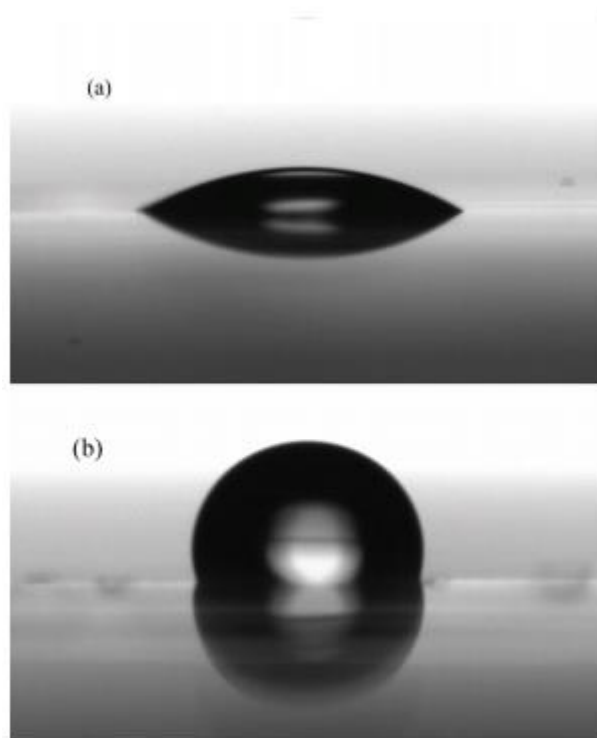


Figure 2.14 Treated polyimide substrate to produce a higher contact angle. Hydrophilic untreated polyimide had a contact angle of about 30° , while the treated substrate had an increase in contact angle to 109° [59]

An example from the experiments carried out by Lin *et al* of how the surface energy of a substrate can affect the print quality and resolution is illustrated in Figures 2.13, 2.14 and 2.15. Figure 2.13 illustrates the effect that printing onto hydrophobic substrates has on the accuracy of the print. Many of the droplets do not stay in the position they were printed and have shifted from their deposited origin to more hydrophilic areas and some have

merged with their neighbour droplets. In Figure 2.14 the treated substrate shown on the right contains deposited droplets of silver ink retaining their high contact angle and maintaining a droplet shape, while the droplets deposited onto the untreated left side of the substrate appears to be non-existent due to complete wetting that caused the droplets to disperse and spread, the particles creating a uniform layer of silver.

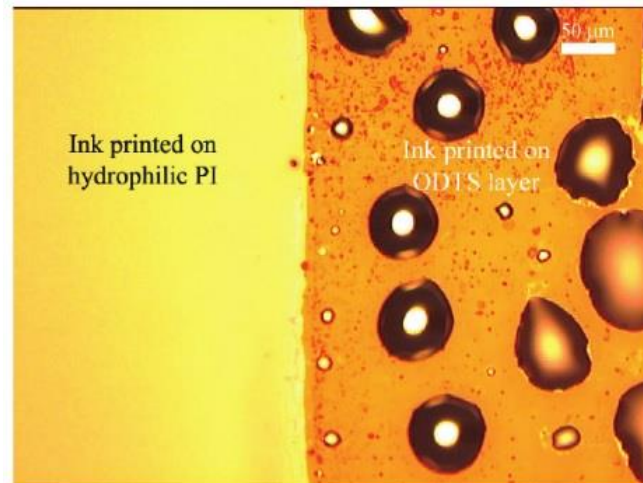


Figure 2.15 Droplets of ink deposited onto a treated hydrophobic and non-treated hydrophilic substrate [59]

An example of how inkjet inks react when deposited onto various substrates is shown in Figure 2.16, where droplets of ink were deposited onto three different substrates. Due to the porosity of the plain paper and the cast coated paper, the definition of the droplets was lost as the substrate absorbed the moisture of the ink and caused spreading [60]. Cast coating refers to porous substrate materials, such as paper, that are coated or treated with a protective layer of hydrophobic material to prevent the ink from spreading through the paper.

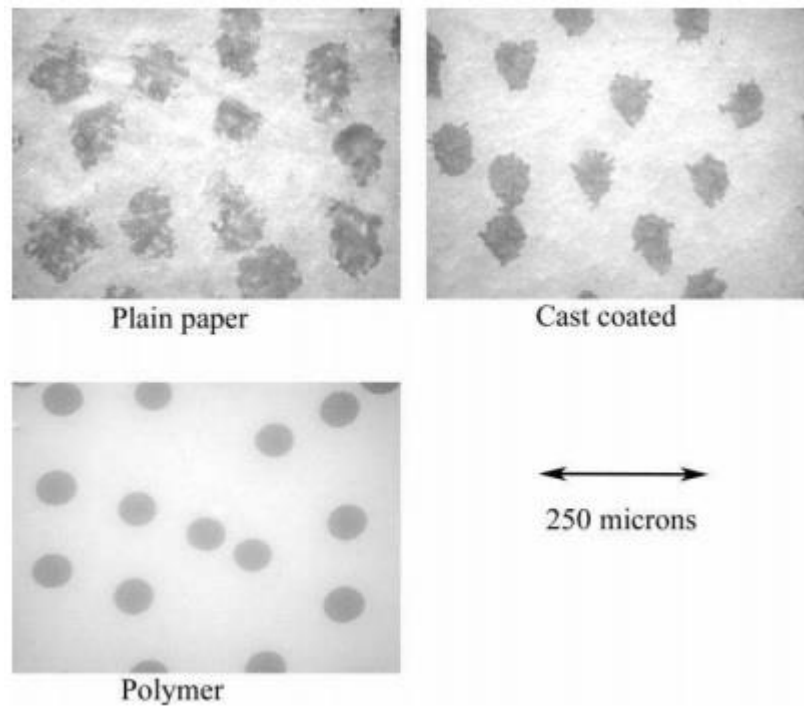


Figure 2.16 Dots of ink printed onto three different types of substrates showing the effect of substrate porosity on the resolution of the print (36)

The fibrous nature and unevenness of the paper was responsible for diffusing the droplets, while the micro cracks in the cast coated substrate are responsible for allowing some ink to leak into the crevices and spread on the substrate. Printing droplets onto the polymer coated substrate however has much improved results and well defined isotropic droplets.

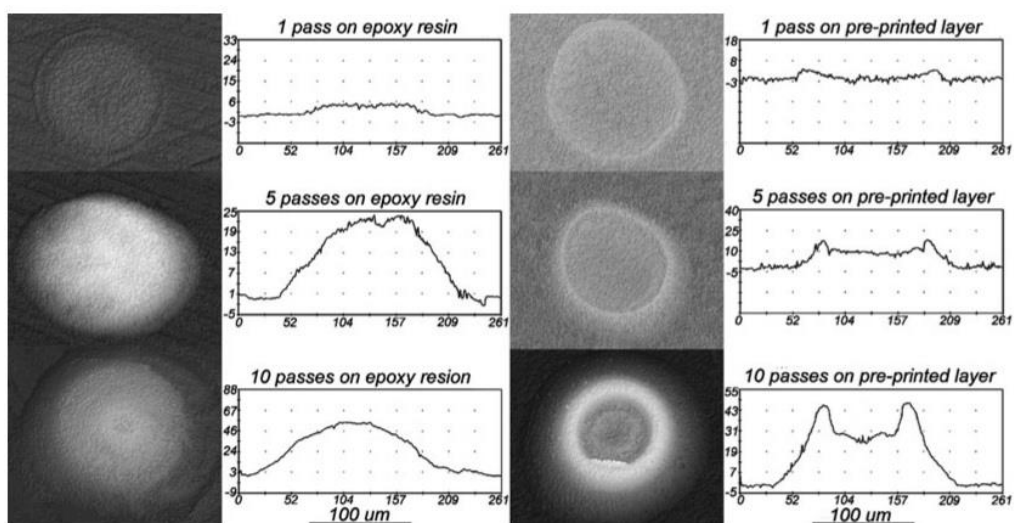


Figure 2.17 Microscope images and interferometric data gathered on printing PEG onto epoxy resin substrate (left) and a substrate with a pre-printed layer (right) (27)

Figure 2.17 provides inkjet printing results from Dou and Derby [27] of their 10 vol% zirconium oxide ink deposited onto an epoxy substrate and on a substrate with a pre-printed layer of zirconium oxide. We can observe a considerable difference between printing on epoxy and the pre-printed substrate. The coffee ring effect is present on the pre-printed substrate because the pre-printed substrate had dried and the zirconium particles had resulted in a powdery substrate surface, which allowed for some of the liquid from the ink droplets to be absorbed and spread through the pre-printed substrate, therefore resulting in a noticeable coffee ring. This phenomenon is discussed in the following 2.4.4 section.

2.4.4 Drying Behaviour: Marangoni Effect and the Coffee Ring Effect

The drying process and behaviour of ink jetted materials and substrate topography are important factors to consider as they can affect the final result.

Dou and Derby conducted research into inkjet printing of zirconia onto glass substrates at varying temperatures to study the Marangoni effect [27]. The solvent evaporation creates a surface tension gradient that initiates a flow inside the liquid, which is known as the Marangoni effect. The results of the printing can be observed in Figure 2.18. Coffee staining, or the coffee ring effect, occurs during the drying process of the ink when the particles that are suspended in the liquid ink flow to the edges of the droplet, thus creating a concentration of particles at the edges rather than having homogeneously dispersed particles inside the droplet. Deegan *et al* attributed the coffee staining to contact line pinning of a droplet once it is deposited onto a substrate and begins to dry [28, 29], however the droplet radius on the substrate does not change. Due to this, during evaporation the liquid flows outward from the centre of the droplet to the edges, where it begins to form the coffee ring. However, as a phenomenon that can sometimes impair the quality and properties of the final print, the coffee ring effect can also be useful in aiding the coalescence of droplets. It is also significant to note that the coffee ring effect is prominent in non-absorbent substrates and the root cause is the evaporation time and behaviour of the particles inside the droplet [61].

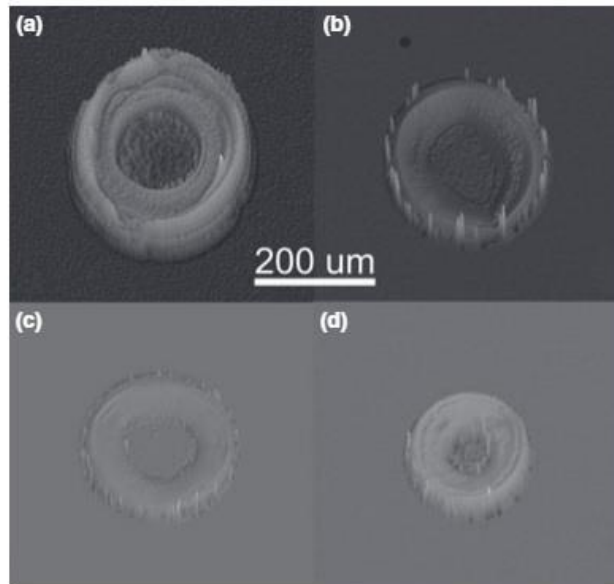


Figure 2.18 An image obtained using interferometric microscope of the zirconia ink printed onto a glass substrate at temperatures (a) 25°C, (b) 35°C, (c) 50°C, (d) 100°C [27]

From Dou and Derby's results presented in Figure 2.18, it is evident that for all temperatures there is coffee staining. The diameter of the droplets printed at higher temperatures (35°C and above) decreases, however the higher temperature did not solve the issue of coffee staining. However, it has been observed from other research carried out [30, 31] that an increase in temperature does reduce the coffee staining phenomenon. According to Soltman and Subramaian [32] and Ozawa [33] the explanation for Dou and Derby's results is that the heating of the liquid inks initiates drying at the edges or the contact lines.

Dou and Derby studied the effects of printing onto porous substrates as well and the impact that the porous structure of the substrate has on the coffee ring effect. The work was carried out by printing onto a metal titanium alloy sheet, photographic paper, filter paper, and dried powder beds with Tosoh-Zirconia powder and alumina powders, with the particle size of the Zirconia at 140 nm and the alumina between 35 and 300 nm [34]. Figure 17 is an illustration of the droplet experiment that was carried out on various substrates. Printing onto a porous substrate has the effect of removing the moisture by absorbing the liquid matter and leaving the solid particles to rest on the surface of the substrate. However, according to Holman [48] and Wang [49], the porosity of the substrate could be the cause that influences coffee rings to appear.

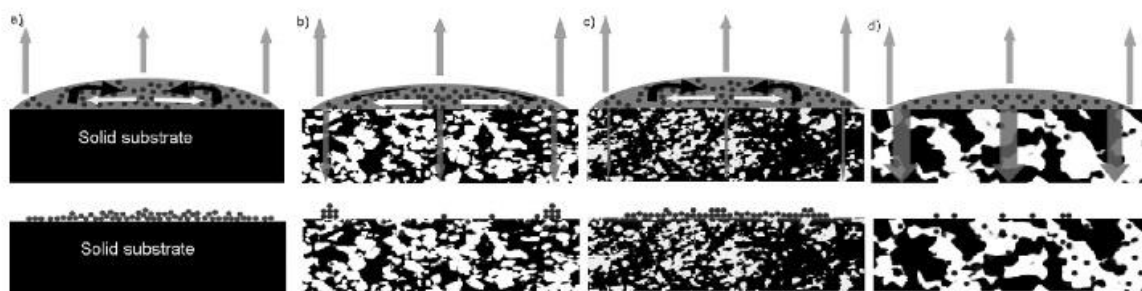


Figure 2.19 Illustrated image showing droplets of ink printed onto solid and porous substrates. The white arrows show the internal radial flow, the grey arrows represent the fluxes from evaporation, and the black arrows the Marangoni flow [27]

In order to prevent the formation of coffee rings, Shen et al [35] proposed that the solvent in the ink should be allowed ample time to evaporate in order for the particles in the ink to arrange in a uniform manner and produce a flat layer of material.

2.5 3D Ink Jetting Elastomeric Ink

Elastomeric inks in the 3-D printing community are becoming more popular as research into 3-D printing for polymers is ever expanding. Being able to inkjet polymer materials to create 3-D objects can have great benefits for the polymer industry as it would create a new branch for manufacturing polymeric materials and objects. Some industries use inkjet printing to create flexible electronic circuits [39] and flexible organic LED displays [40]. One such research, carried out by van den Berg [41], has proven to be successful with a diluted 20 wt% and 40 wt% colloidal dispersion of polyurethane. The successful 3-D print was carried out using the Autodrop™ printer displayed in Figure 2.20.

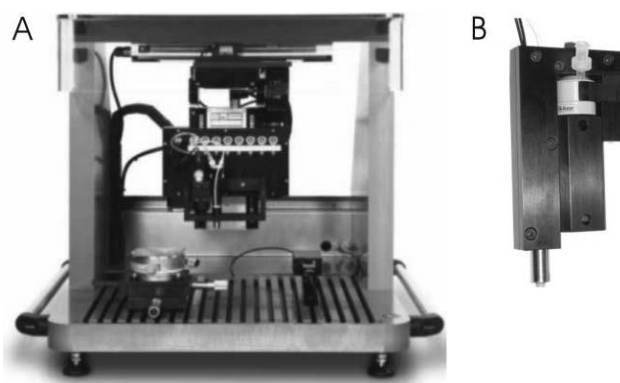


Figure 2.20 The Autodrop™ printer from Microdrop Technologies GmbH

Van den Berg ink jetted with 40 wt% and diluted 20 wt% polyurethane ink to determine the effects that dilution has on the printed material, and the results proved to be intriguing. Figure 2.21 is a profile of single layers of the printed samples obtained using white-light interferometry.

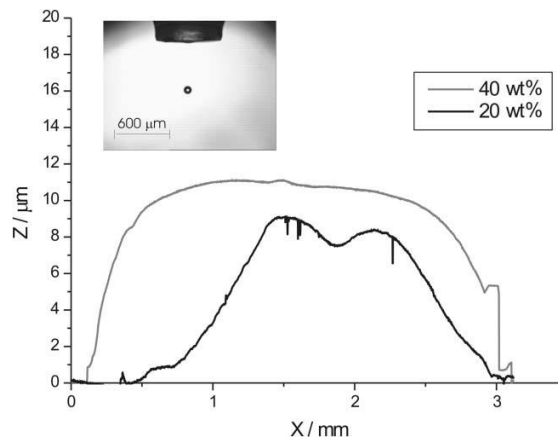


Figure 2.21 Profiles of the 40 wt% and 20 wt% printed polyurethane [42]

The inset profile outline is that of the diluted sample, whereas the outer outline is that of the 40 wt%. The result for the outline of the printed diluted sample is explained by Deegan *et al* [42] where the particles of a dilute solution are spread in the deposited droplet and the arrangement of the particles is based on the drying boundaries. As the droplet dries, the particles inside the droplet migrate to the centre or the edges of the droplet, which is dependent on the drying environment: temperature, humidity and air currents. Van den Berg also determined that diluting the polyurethane ink resulted in a decrease in the thickness of the printed sample, which is due to the particles becoming more dispersed throughout the liquid. Increasing the solids content, or particle loading, of an ink is known to increase the overall viscosity of the ink [43], therefore an ink with a 40 wt% particle concentration requires an increase in the jetting voltage. Seerden *et al.* [44] determined that inks with 30 wt% particle loading required 70 V and 80 V was required for 40 wt% inks.

Van den Berg also attempted to use the polyurethane ink to create a small 3-D sample, illustrated in Figures 2.22 and 2.23. Van den Berg determined that a single printed layer of 40 wt% polyurethane ink was approximately 10 μ m thick.

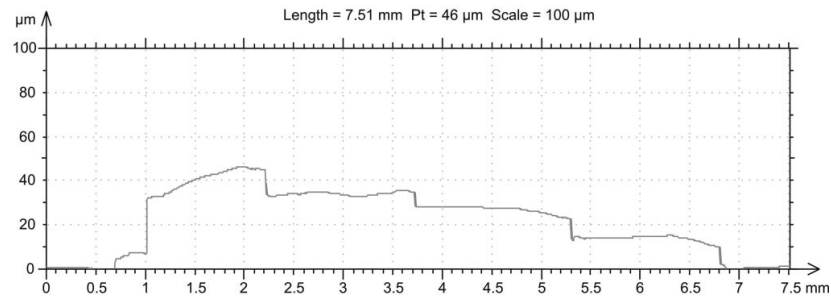


Figure 2.22 Profile image of 3-D printed 40 wt% polyurethane material using white-light interferometry [51]

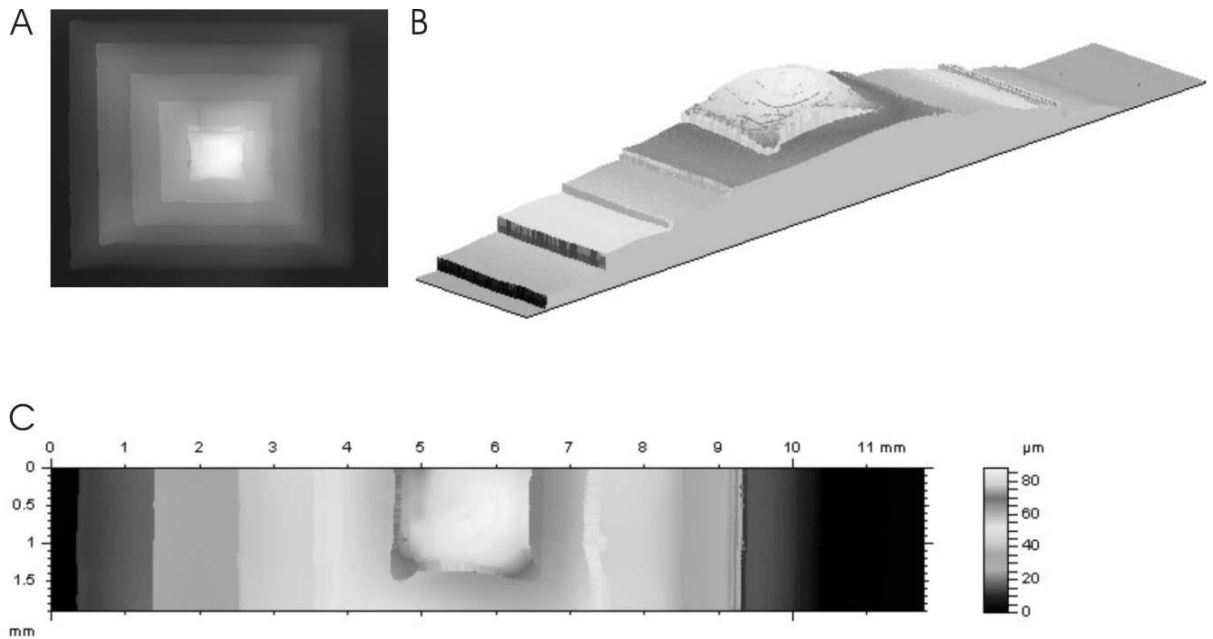


Figure 2.23 3-D images obtained using white-light interferometry of 5 layers of 3-D printed polyurethane in pyramid shape [51]

There are other examples of 3-D printing with polymers, however the majority of these inks employ phase changing ingredients which are added directly into the ink in order to solidify the material either upon impact [44] or cross-linking induced using UV light during printing [45]. However, van den Berg's research is one that is of significance for this project as the main objective is to utilise ink jetting technology to create flexible elastomeric materials.

2.6 Conclusion

Inkjet printing is a relatively well studied and researched area of material deposition, although it is only recently that its potential in 3-D printing is being given serious consideration, especially in terms of its use for inkjet printing elastomeric materials. In this chapter, the key characteristics for inkjet printing a material have been identified, and it has been determined that this method has the potential to be utilised for a variety of liquid

materials, so long as all the property requirements of viscosity, surface tension, and particle size are met according to the standards used by the inkjet printer. Other factors that could impact the results of printing include the properties of the substrate used to deposit the ink onto, such as surface energy and topography.

References for Chapter 2:

- [1] Brünahl, J., Grishin, A.M. *Piezoelectric-shear-mode-drop-on-demand-inkjet-actuator*. (2002). *Sensors and Actuators A: Physical*, vol. 101, no. 3, pp. 371-382.
- [2] R. Elmqvist. *Measuring instrument of the recording type*, US Patent no. 2,566,443 (1948).
- [3] Jang, D., Kim, D., Moon, J., Jang, D., Kim, D., & Moon, J. *Influence of Fluid Physical Properties on Ink-Jet Printability*. (2009). *American Chemical Society*, vol. 25, no. 5 pp. 2629–2635.
- [4] Korvink, J., Smith, P., Shin, D. *Inkjet-based micromanufacturing*. (2012). Weinheim: Wiley-VCH.
- [5] Lee, D. H., Derby, B. *Preparation of PZT suspensions for direct ink jet printing*. (2004). *Journal of the European Ceramic Society*, vol. 24, no. 6, pp. 1069-1072.
- [6] Vitz, J., Erdmenger, T., Haensch, C., Schubert, U.S. *Extended Dissolution Studies of Cellulose in Imidazolium Based Ionic Liquids*. (2009). *Green Chem.*, vol. 11, pp. 417-424.
- [7] O. A. El Seoud, V. C. da Silva, S. Possidonio, T. Casarano, E. P. G. Areas, P. Gimenes, *Macromol. Microwave-assisted Derivatization of Cellulose – The Surprising Effect of The Structure of Ionic Liquids on The Dissolution and Acylation of The Biopolymer*. (2011). *Chem. Phys.*, vol. 23, no. 212, pp. 2541-2550.
- [8] Martin GD, Hoath SD, Hutchings IM. *Inkjet printing: the physics of manipulating liquid jets and drops*. (2008). *J. Phys. Conf. Ser.* vol. 105, pp. 012001
- [10] Fromm JE. *Numerical-calculation of the fluid-dynamics of drop-on-demand jets*. (1984). *IBM J. Res. Dev.* vol. 28, no. 3, pp. 322–33
- [11] Reis N, Derby B. *Ink jet deposition of ceramic suspensions: modelling and experiments of droplet formation*. (2000). *MRS Symp. Proc.* Vol. 624, pp. 65–70
- [12] T.A. Kowalewski. *On the Separation of Droplets*. (1996). *Fluid Dyn. Res.* vol. 17, pp. 121–145.
- [13] X.D. Shi, M.P. Brenner, and S.R. Nagel. *A Cascade of Structure in a Drop Falling from a Faucet*. (1994). *Science*, vol. 265, pp. 219-222.
- [14] de Gans, B.J., Duineveld, P.C., Schubert, U.S. *Inkjet printing of polymers: state of the art and future developments*. (2004). *Adv. Mater.* vol. 16, no. 3, pp. 203-213.

- [15] McKinley, G.H. *Recent developments in shear and extensional micro-rheometry of complex fluids*. (2004). Proc. XIVth International Congress on Rheology, Seoul, Korea, pp. 22-27.
- [16] G.H. McKinley, in: D.M. Bindings, K. Walters (Eds.). *Visco-Elastic Capillary Thinning and Break-up of Complex Fluids*. (2005). Rheology Reviews, The British Society of Rheology, pp. 1-49.
- [17] Rachel, E.S., Gough, J.E., and Derby, B. *Delivery of human fibroblast cells by piezoelectric drop-on-demand inkjet printing*. (2008). Biomaterials, vol. 29, pp. 193-203.
- [18] D. Hoath, S., Martin, G. D., & Hutchings, I. M. *Effects of fluid viscosity on drop-on-demand ink-jet break-off*. (2010). NIP26 and Digital Fabrication, pp. 10–13.
- [19] Derby, B. *Inkjet printing of functional and structural materials*. (2010). Annual Review of Materials Research, vol. 40, pp. 395–414.
- [20] Cooley, P., Wallace, D., Antohe, B. *Applications of Ink-Jet Printing Technology to BioMEMS and Microfluidic Systems*. (2001). Journal of the Association for Laboratory Automation, vol. 7, no. 5, pp. 33-39.
- [21] Beeson, R. *Thermal (TIJ) or Piezo? Who Cares?*. (1998). IMI 7th Annual Inkjet Printing Conference.
- [22] Wijshoff, H. *The dynamics of the piezo inkjet printhead operation*. (June 2010). Physics Reports, vol. 491, no. 4-5, pp. 77-177.
- [23] Chen, Y. S., Huang, Y. L., Kuo, C. H., & Chang, S. H. *Investigation of design parameters for droplet generators driven by piezoelectric actuators*. (2007). International Journal of Mechanical Sciences, vol. 49, no. 6, pp. 733–740.
- [24] Shore, H.J. and Harrison, G.M. The effect of added polymers on the formation of drops ejected from a nozzle. (2005). *Physics of Fluids*, Volume 17(3), pp. 033104.
- [25] Reis, N., Ainsley, C., & Derby, B. *Ink-jet delivery of particle suspensions by piezoelectric droplet ejectors*. (2005). Journal of Applied Physics, vol. 97, no. 9.
- [26] Cooper-White, J.J., Fana, J.E., Tirtaatmadja, V., Lester, D.R., Boger, D.V. *Drop formation dynamics of constant low-viscosity, elastic liquids*. (2002). J. Non-Newtonian Fluid Mech. Vol. 106, pp. 25.
- [27] Dou, R., Wang, T., Guo, Y., & Derby, B. *Ink-jet printing of zirconia: Coffee staining and line stability*. (2011). Journal of the American Ceramic Society, vol. 91, no. 11, pp. 3787-3792.
- [28] Deegan, R.D., Bakajin, O., Dupont, T.F., Huber, G., Nagel, S.R., Witten, T.A. *Capillary Flow as the Cause of Ring Stains from Dried Liquid Drops*. (1997). Nature, vol. 389, pp. 827–9.
- [29] Deegan, R. D., Bakajin, O., Dupont, T. F., Huber, G., Nagel, S. R., Witten, T. A. *Contact Line Deposits in an Evaporating Drop*. (2000). Phys. Rev. E, vol. 62, no. 1, pp. 756–65.

- [30] J. W. Song, J. Kim, Y. H. Yoon, B. S. Choi, J. H. Kim, and C. S. Han. *Inkjet Printing of Single-Walled Carbon Nanotubes and Electrical Characterization of the Line Pattern*. (2008). *Nanotechnology*, vol. 19, no. 9, pp. 095702.
- [31] T. Wang, M. A. Roberts, I. A. Kinloch, and B. Derby. *Inkjet Printed Carbon Nanotube Networks: The Influence of Drop Spacing and Drying on Electrical Properties*. (2011). *Journal of Physics D: Applied Physics*, vol. 45, no. 31, pp. 315304.
- [32] D. Soltman and V. Subramanian. *Inkjet-Printed Line Morphologies and Temperature Control of the Coffee Ring Effect*. (2008). *Langmuir*, vol. 24, no. 5, pp. 2224–31.
- [33] K. Ozawa, E. Nishitani, and M. Doi, *Modelling of the Drying Process of Liquid Droplet to Form Thin Film*. (2005). *Jap. J. Appl. Phys. Part 1*, vol. 44, no. 6A, pp. 4229–34.
- [34] Dou, R., Derby, B. *Formation of coffee stains on porous surfaces*. (2012). *Langmuir*, Volume 28(12), pp. 5331–5338.
- [35] Shen, X.; Ho, C. M.; Wong, T. S. *Minimal Size of Coffee Ring Structure*. (2010). *J. Phys. Chem. B* 2010, vol. 114, pp. 5269–5274.
- [36] Fricker, A., Hodgson, A. and Sandy, M. *An investigation into the effects of solvent content on the image quality and stability of ink jet digital prints under varied storage conditions*. (2010). *Journal of Physics: Conference Series*, vol. 231, pp. 012017.
- [37] Hoath, D., S. *Fundamentals of Inkjet Printing*. (2016). Wiley-VCH Verlag GmbH & Co. KGaA, Boschstr. 12, 69469 Weinheim, Germany.
- [38] Park, J., Moon, J. *Control of Colloidal Particle Deposit Patterns within Picoliter Droplets Ejected by Ink-Jet Printing*. (2016). *Langmuir*, vol. 22, no. 8, pp. 3506-3513.
- [39] de Gans, B. J., Duineveld, P. C., Schubert, U. S. *Inkjet Printing of Polymers: State of the Art and Future Developments*. (2004). *Adv. Mater.*, Volume 16, pp. 203.
- [40] Holdcroft, S. *Patterning π -Conjugated Polymers*. (2001). *Advanced Materials*, vol. 13, pp. 1753.
- [41] van den Berg, A.M.J., Smith, P.J., Perelaer, J., Schrof, W., Koltzenburg, S. and Schubert, U.S. *Inkjet printing of polyurethane colloidal suspensions*. (2007). *Soft Matter*, vol. 3, no. 2, pp. 238–243.
- [42] Deegan, R. D., Bakajin, O., Dupont, T. F., Huber, G., Nagel, S. R., Witten, T. A. *Capillary Flow as the Cause of Ring Stains from Dried Liquid Drops*. (1997). *Witten, Nature*, vol. 389, pp. 827.
- [43] http://www.microdrop.com/wDeutsch/products/md_series.shtml (Accessed 4th May 2016)
- [44] K. A. M. Seerden, N. Reis, J. R. G. Evans, P. S. Grant, J. W. Holloran and B. Derby, J. *Ink-Jet Printing of Wax-Based Alumina Suspensions*. (2001). *Am. Ceram. Soc.*, vol. 84, pp. 2514-20.
- [45] J. Stampfl and R. Liska, *Macromol. New Materials for Rapid Prototyping Applications*. (2005). *Chem. Phys.*, Volume 206, pp. 1253.

- [46] S. D. Hoath, S. Jung, and I. M. Hutchings, *A simple criterion for filament break-up in drop-on-demand inkjet printing*. (2013). *Phys. Fluids*, vol. 25, pp. 021701-1 – 021701-4.
- [47] Delrot, P., Modestino, M.A., Gallaire, F., Psaltis, D. and Moser, C. *Inkjet printing of viscous monodisperse Microdroplets by laser-induced flow focusing*. (2016). *Physical Review Applied*, Volume 6(2), pp. 024003-1 – 024003-8.
- [48] Holman, R. K.; Cima, M. J.; Uhland, S. A.; Sachs, E. J. *Spreading and Infiltration of Inkjet-Printed polymer solution droplets on a Porous Substrate*. (2002). *Colloid Interface Sci.*, vol. 249, pp. 432–440.
- [49] Wang, T. M.; Patel, R.; Derby, B. *Formation of Coffee Stains on Porous Surfaces*. (2008). *Soft Matter*, vol. 4, pp. 2513– 2518.
- [50] Kim, Y.-J., Kim, S. and Hwang, J. *Drop-on-demand hybrid printing using a piezoelectric MEMS printhead at various waveforms, high voltages and jetting frequencies*. (2013). *Journal of Micromechanics and Microengineering*, vol. 23, no. 6, pp. 065011.
- [51] van den Berg, A.M.J., Smith, P.J., Perelaer, J., Schrof, W., Koltzenburg, S., Schubert, U.S. *Inkjet printing of polyurethane colloidal suspensions*. (2007). *Soft Matter*, vol. 3, no. 2, pp. 238–243.
- [52] Carey, V. P. *Liquid-vapor phase-change phenomena*. (2008) 2nd ed., Hemisphere Publishing Corporation, New York.
- [53] Gennes, P. G. *Wetting: Statics and Dynamics*. (1985). *Review of Modern Physics*, vol. 57, pp. 827.
- [54] Bonn, D., Eggers, J., Indekeu, J., Meunier, J., Rolley, E. *Wetting and Spreading*. (2009). *Review of Modern Physics*. 81, 739.
- [55] Neumann, A. W., Spelt, J. K. *Applied Surface Thermodynamics*. (1996). Marcel Dekker: New York.
- [56] Wenzel, R. N. *Resistance of Solid Surfaces to Wetting by Water*. (1936). *Industrial and Engineering Chemistry*, vol. 28, pp. 988-994.
- [57] Sefiane, K., Skilling, J., MacGillivray, J. *Contact Line Motion and Dynamic Wetting of Nanofluid Solutions*. (2008). *Adv. Colloid Interface Sci.*, vol. 138, pp. 101-120.
- [58] Chaudhury, M. K. and Whitesides, G. M. *How to Make Water Run Uphill*. (1992). *Science*, vol. 256 (5063), pp. 1539-1541.
- [59] Lin, J., Dahlsten, Pekkanen, J., Österbacka, R., Lindén, M., Mäntysalo, M. *Surface energy patterning for inkjet printing in device fabrication*. (2009). *Proceedings of SPIE - The International Society for Optical Engineering*, vol. 7417, pp. 74171.
- [60] Hodgson, A., Jackson, A. M. *The light fading of dye based inkjet images - a multidimensional issue*. (2004). *Society for Imaging Science and Technology*. pp 43-48(6).
- [61] Steiger, J., Heun, S., Tallant, N. *Polymer Light Emitting Diodes Made by Ink Jet Printing*. (2003). *J. Imaging Science and Technology*, vol. 47, no. 6, pp. 473 – 478.

[62] McCormack-Goodhart, M, Wilhelm, H. *New test methods for evaluating the humidity fastness of inkjet prints*. (2005). Proc. The Annual Conf. of the Imaging Society of Japan, pp. 95-98

[63] Nigro, Stephen, and Evan Smouse. "Hewlett-Packard Inkjet Printing Technology: the state of the art HP Inkjet Printing Technology." HP Techpress (http://h10088.www1.hp.com/gap/download/oeminkjet/techpress_11_2.pdf) (1999).

Chapter 3 EMI Shielding Polymers

3.1 Introduction

This chapter analyses the research that has been carried out on polymers with electromagnetic interference (EMI) shielding capabilities. It considers the different aspects of shielding, such as the concept and theory behind EMI shielding, with an emphasis on the material properties such as thickness, different types of fillers, variation on frequencies, and the processing method the materials were put through, as well as the effects that would have on the shielding capabilities.

3.2 Concept of shielding

Materials research and manufacture is ever adapting in order to accommodate the development in electronics technology, more specifically to provide shielding against electromagnetic and radio frequency radiation that is emitted by all electrical devices. EMI shielding was developed to protect electronic equipment by means of absorption or reflection of the radiated interference. These shields are physical objects which can envelope all or part of sensitive electronic devices that are susceptible to electric fields. However, due to heat that is generated from electronically operated devices, apertures for heat dissipation must be present. Apertures for openings for cables or doors, and seams created during manufacturing, are also present in all devices. Electromagnetic waves can pass through these apertures, and the purpose of developing and utilising EMI shielding polymers is to provide shielding for these apertures [67]. The effectiveness of a material's ability to shield against EMI is referred to as electromagnetic interference shielding effectiveness, or EMI SE, and is identified by the formula:

$$EMI SE = 10 \log \frac{1}{|S_{12}|^2} = 10 \log \frac{1}{|S_{21}|^2} \quad [67] \quad \text{Eq. 3.1}$$

Where $|S_{12}|^2$ is the power transmitted from port 1 to port 2, and

$|S_{21}|^2$ is the power transmitted from port 2 to port 1.

Port 1 and port 2 refer to the connecting cables of the network analyser, however in real devices there is no network analyser. Therefore, this means the electric fields transmitted through the shield are compared to incident electric fields before the shield.

Electromagnetic waves consist of electric and magnetic waves, and the electric to magnetic field ratio of propagation through a homogeneous material is known as the intrinsic impedance [1], as defined by the 3-2 formula:

$$\eta = \sqrt{\frac{j\omega\mu}{\sigma + j\omega\epsilon}} \quad \text{Eq. 3.2}$$

Where η is the intrinsic impedance, j is the imaginary unit, ω is the angular frequency, μ is permeability, ϵ is permittivity, and σ is the electrical conductivity.

3.3 The theory and principles of dielectric materials

3.3.1 Material properties

An electrically insulating material that is capable of storing an applied external charge is known as a dielectric. These materials are able to enhance capacitor energy storage by neutralising the charges of the electrodes in an electronic device [2]. Dielectric materials can be in solid, liquid, or gaseous form, and include typical materials such as glass, elastomers, porcelain, transformer oil, certain silicon liquid, nitrogen and hydrogen gas. The inorganic material mica is also used as a dielectric, especially for applications which involve high frequencies. Air is one of the most common and abundant dielectrics available and is used in condensers as the dielectric loss is practically zero. However, air can only be utilised as a dielectric for low voltage applications.

3.3.2 Permittivity

Permittivity, or dielectric permittivity as it is also known, is a material's ability to physically resist an applied electric field [68]. An electric field is defined as the electric force per unit charge. High permittivity values denote that a material is better able to reduce electric fields. Permittivity is defined by the equation:

$$\epsilon = \epsilon' - i\epsilon'' \quad [68] \quad \text{Eq. 3.3}$$

Where ϵ' and $i\epsilon''$ are real and imaginary permittivity

An electric field is defined by the equation:

$$E = \frac{F}{q} \quad [68] \quad \text{Eq. 3.4}$$

Where E is the electric field, F is the electric force in Newtons, and q is the charge in Coulombs.

3.3.3 Dielectric mechanisms

Dielectric mechanisms refer to the polarization, capacitance, and dielectric constant of a material. Polarization is achieved by re-arranging the electric charge carriers that are present in a dielectric material. This is achieved by exposing the material to an electric field, which causes the charge carriers present in the dielectric to re-arrange themselves [69].

Capacitance refers to the electric charge capacity storage and the relationship between the dielectric constant and capacitance is summarised in the formula:

$$C = \frac{\epsilon_0 \epsilon_r A}{t} \quad \text{Eq.3.5}$$

Where ϵ_0 is 8.854×10^{-12} F/m, dielectric constant of free space, ϵ_r is the dielectric constant of the material, A is the area of the electrical conductor, and t is the thickness of the material. A greater capacitance value indicates a higher dielectric constant. Table 3.1 details some of the more common dielectric materials that are used for shielding against EMI.

Table 3.1 Properties of some common dielectric materials [3]

Dielectric	Dielectric Constant	Dissipation factor (%)	Thickness (μm)	Specific Capacitance (nF/cm^2)	Energy Density at 5 V ($\mu\text{J}/\text{cm}^2$)
Unfilled laminated polymer	4	0.1-1.5	25	0.14	0.002
Ferroelectric-filled polymer	50	<3	25	1.8	0.023
Spin-on BCB	2.7	0.1	2.0	1.2	0.015
SiO ₂	3.7	0.03	0.2	16	0.20
SiO	6	0.01	0.2	27	0.34
Al ₂ O ₃	9	0.4-1	0.2	40	0.50
Ta ₂ O ₅	24	0.2-1	0.2	110	1.40
TiO ₂	40	2-5	0.2	180	2.30
BaTiO ₃	~ 2000	5	1.0	1800	22

Dielectric materials that have a ϵ constant value, or relative permittivity, greater than 7, such as silicon nitride, it is classified as high. If the ϵ constant is less than 3.9 then the material is classified as having a low dielectric constant [4]. Other materials that are commonly used for high frequency EMI shielding are copper and aluminium. Figure 3.1 illustrates the frequency versus reflection of some of the common metals used for shielding against EMI.

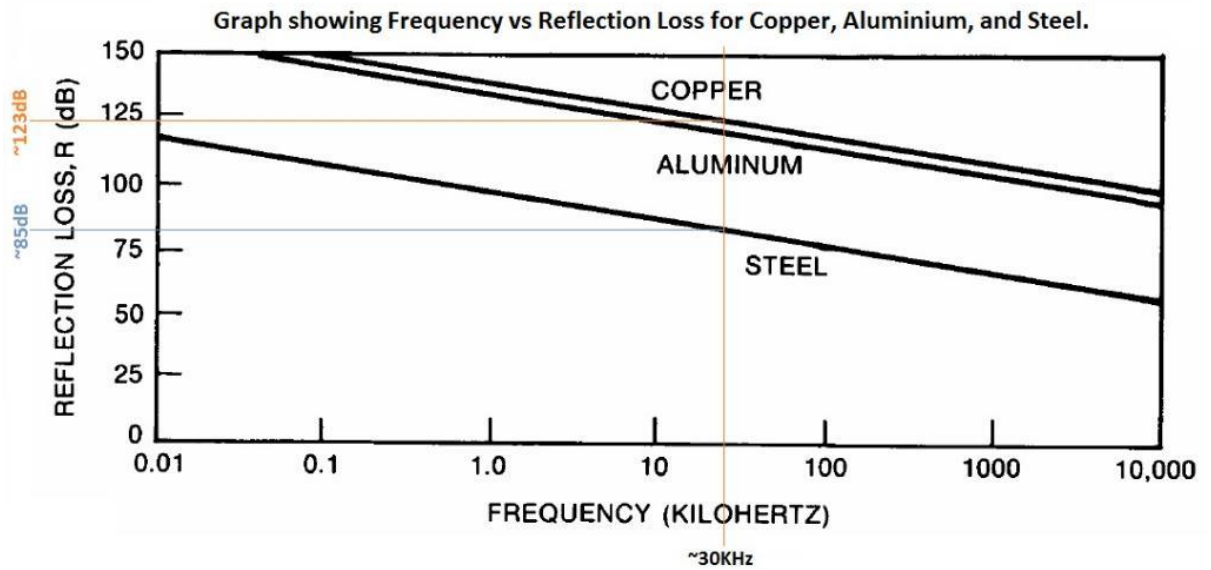


Figure 3.1 A comparison between the frequency and reflection loss for steel, aluminium, and copper [5]

Due to the high conductivity of copper and aluminium, these two metals have a higher electric reflection loss than steel. Compared to steel, both copper and aluminium have approximately five times the amount of conductivity, which makes them ideal materials to use for stopping electric fields. However, the chemical and material composition of steel can be altered to produce varying grades with increased conductive properties, such as stainless steel, which can affect its ability to stop electric fields.

Figure 3.2 illustrates a simulated model of a copper container 5cm in thickness being exposed to magnetic waves. The lighter colours signify the propagating interference waves while the dark colour indicates areas where the waves cannot penetrate. Both Figures 3.1 and 3.2 illustrate the inherently good properties of metals to shield against electric and magnetic fields.

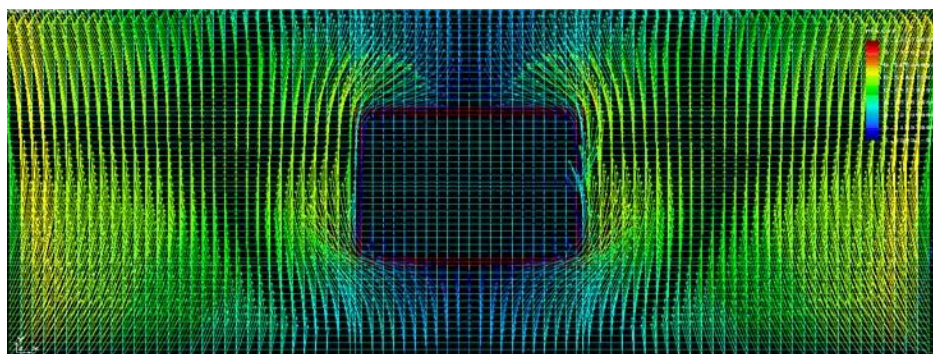


Figure 3.2 Magnetic field (illustrated as yellow lines) propagating around the shielding material [6]

3.4 Polymer composites with conductive fillers

This section addresses the polymer materials that are utilised for EMI shielding, the methods of manufacture both in industrial scale and research, and the multitude of conductive and non-conductive fillers that are utilised to either reflect or absorb interference radiation.

To provide a high level of shielding against EMI interference, a conductive material must be utilised. The Band Theory [7] is used to explain the conductivity of materials, which states that every energy state forms bands that they traverse through free space, and the energy levels or band of electrons are considered as travelling in a horizontal line. All solid materials have different electrical properties with varying energy levels that form two bands: valence and conduction bands. For polymer materials, there is an energy drop, or gap, between these two bands where electrons do not pass through. In the valence band electrons are restricted to individual atoms. However, with metallic materials the valence and conduction bands overlap, which explains the high conductivity of metal materials. Figure 3.3 illustrates a diagram used to describe the Band Theory.

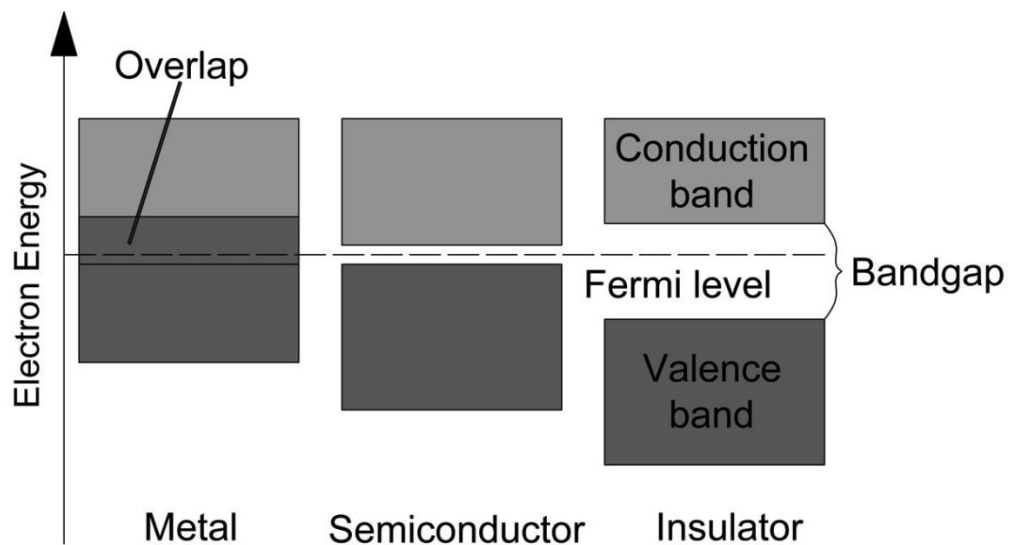


Figure 3.3 A diagram illustrating the Band Theory for metallic materials, semiconductors and insulators [8]

The gap between semiconductors is not as significant as for insulators, which enables them to transfer some electrons between the gaps. Insulators have a more prominent gap between the bands, which does not allow electrons to be conducted through the material when an electric field is applied. Dielectric materials are poor conductors of electric currents

and are classified as insulating materials. These materials are not good at conducting because they do not have free electrons present, and when dielectric materials are exposed to an electric field polarization occurs as positive charges in the material get displaced in the electric field direction and negative charges are displaced in the opposite direction of the electric field. This charge displacement (polarization) is the cause for the reduction of any electric field that a dielectric material becomes exposed to.

3.5 EMI shielding

The effectiveness of a material as a shield against EMI depends on the conductivity of the material as well as allowing the frequencies that are desired and blocking the ones that are not. All electronic devices radiate electromagnetic signals, and this can cause interference with signal processing in the components, which can interrupt the electronic signals in the device and cause malfunctions to occur [9]. This is especially hazardous for sensitive equipment, such as pacemakers in patients and on board navigation equipment in aircraft as any electromagnetic waves could interfere with normal operation of the electronic devices. As the electromagnetic pollution from increasingly densely packed electronic devices increases, the EMI shielding technology must be able to provide sufficient control. Therefore, every device must pass EMI tests where the amount of EM fields they emit is limited and they cannot be sensitive to EM fields to the point of allowing that interference to obstruct operating function.

Electromagnetic shielding material selection is dependent on the wavelength of the EM fields. As illustrated in Figure 3.4, low frequency EM has a long wavelength with low quantum energy. Long wavelengths are emitted by radio stations, which is ideal as the frequency has a better chance of being received over large distances. Higher frequencies produce shorter wavelengths with a higher quantum energy than long wavelengths.

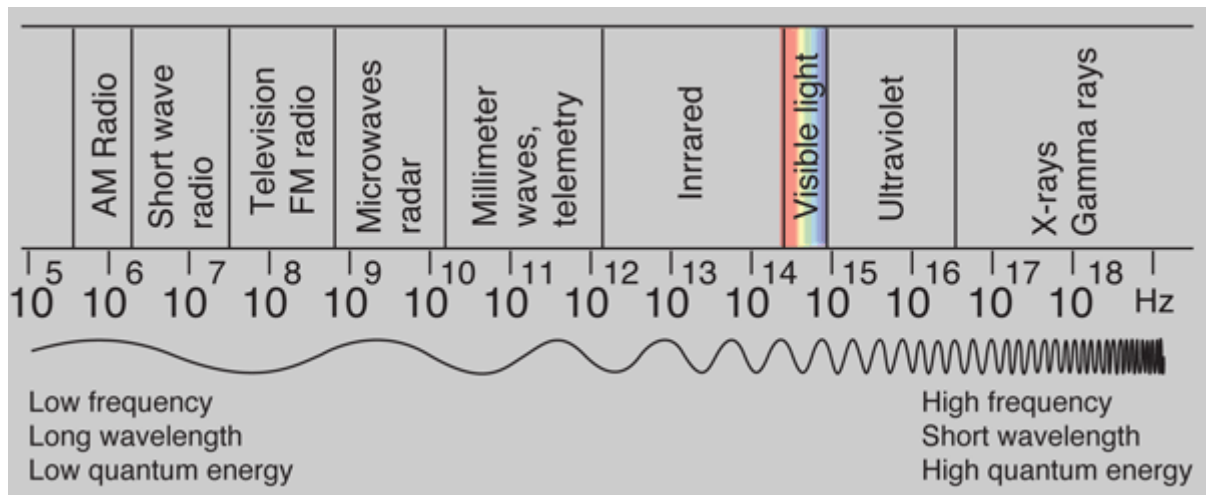


Figure 3.4 Simple representation of the EM spectrum [10]

Wavelength is determined by dividing the velocity, or speed, of the wave by the frequency, as presented in formula:

$$\lambda = \frac{v}{f} \quad \text{Eq. 3.6}$$

Velocity, v , is the speed of light (299,792,458 m/s) and frequency f is the number of waves that is produced for every second, measured in Hertz where one Hertz equals one wavelength per second. Devices inadvertently emit EM waves at all frequencies, and wireless equipment typically use low Hertz frequencies where the wavelength is approximately 10-30 cm.

A simplified example of a method of EMI and RFI shielding is presented in Figure 3.5, where an electrical component able to emit and receive frequencies is placed in a containment chamber that prevents EMI and RFI from being transmitted and received. A practical example of this method of shielding is a Faraday cage. This type of shielding employs a screen enclosure made from conductive metal material, such as copper or aluminium, which prevents EMI from reaching a device by distributing the electric charges to cancel the EM field.

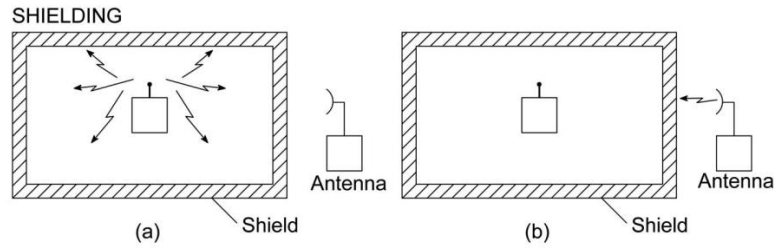


Figure 3.5 Shielding can be used to prevent (a) EM waves interfering with another object and (b) be harmed by another object [11]

EMI SE refers to the ability of a conductive material to block EM radiation. This is expressed in dB and the formula is:

$$EMI SE = 10 * \log_{10}\left(\frac{P_I}{P_T}\right) \quad \text{Eq. 3.7}$$

Where *EMI SE* is the shielding effectiveness

P_I is the incident power

P_T is the transmitted power

And

$$EMI SE = 20 * \log_{10}\left(\frac{E_I}{E_T}\right) = 20 * \log_{10}\left(\frac{H_I}{H_T}\right) \quad \text{Eq. 3.8}$$

Where E_I and E_T are the root mean square of incident and transmitted electric fields

H_I and H_T are the root mean square of incident and transmitted magnetic fields.

These formulas can be used to calculate the SE of conductive materials.

Metallic materials are most commonly used for EMI shielding applications due to the good reflective properties exhibited that are caused by the free electrons. However, metals can be heavy and bulky, especially if shielding is to be provided for a small device. Metallic coatings or electroless plating of polymers can be carried out and is a common and cost effective method of shielding [11-26]. Coatings can however suffer degradation from physical damage such as abrasion, and environmental factors. For this reason, conductive polymers or polymer composites have been used and continue to be developed. Conductive polymers are materials that are inherently conducting, however, these polymers often possess relatively poor mechanical properties [27-46].

Conductive polymer composites refer to a branch of polymer materials that have been combined with conductive filler materials to increase their overall conductivity. There are a variety of conductive filler options that can be utilised with polymers, which includes conductive carbon black powder, carbon nanotubes, graphene, and metal powders such as copper and silver. Composite polymers with an added conductive filler have the advantage that they possess good shielding properties while maintaining good mechanical properties. However, high filler content can negatively affect the mechanical properties of the polymer, making it brittle. Figure 3.6 offers a useful illustration on the range that the conductive fillers that can be utilised. Section 3.5.1 focuses on carbon based fillers, while Section 3.5.2 discusses the properties of polymers filled with metallic particles.

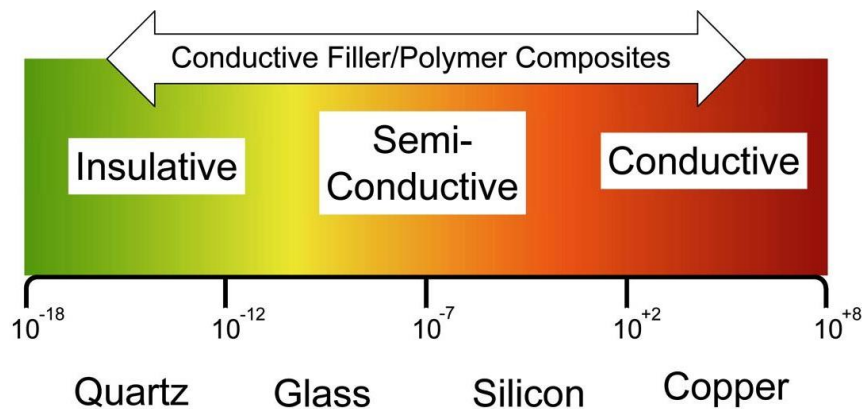


Figure 3.6 Electrical conductivity based on the type of materials and the electrical conductivity range that can be covered by conductive fillers [47]

Conductive filler polymer composites are able to shield against EMI interference due to the heterogeneous structure between the polymer materials and the fillers. The shielding effectiveness is dependent on many factors, some of which include the thickness of the overall material, the filler concentration, and the shielding frequency range. For polymer matrix composite materials the dominant mechanism of shielding against EMI is reflection [48].

3.5.1 Carbon black, carbon nanotube and carbon fibre filled composites

The percolation theory describes that a composite material's electrical conductivity is dependent on the filler volume fraction, where an increase in the filler concentration leads to a contact being established between the particles to create a continuous path, thus enabling electrons to travel through the composite if it is conductive [49].

Research into various types of fillers used for manufacturing EMI shielding polymers, including carbon fibres, carbon black powder, metal particles and metal coated glass fibres have been carried out by Bigg [50]. Research carried out by Lou and Chung [34] into composite carbon materials with continuous carbon fibres revealed that the shielding effectiveness of such a material was 124 dB, while having a low surface impedance and high reflectivity in the 0.3 MHz to 1.5 GHz frequency range. Lou and Chung determined that the shielding effectiveness was less for polymer composites with discontinuous fillers than for those with continuous fillers. If fillers in a material are discontinuous, they create a dielectric material. If the fillers are continuous however, then the material possibly behaves as a conductor. It was also determined that a 2.9 vol. % introduction of discontinuous filler with carbon filaments of 0.1mm diameter between 7mm layers of continuous carbon fibres proved detrimental to overall shielding effectiveness. The detriment of utilising a carbon-carbon composite, as opposed to a polymer-carbon matrix, include brittleness of the material, reliance on moulds, lack of flexibility, and the need to replace an entire carbon-carbon component if it is damaged.

Composite polymer matrix materials that are created using appropriate polymers or elastomers, combined with continuous or discontinuous conductive fillers are widely utilised for the purposes of shielding against EMI [35, 36]. Non-metallic conductive fillers that have been utilised in creating polymers capable of shielding against EMI and RFI include conductive carbon black particles, carbon nanotubes and graphite. Carbon black is especially effective and widely used in EMI shielding applications due to its ease of processing, effective mixing with a wide variety of polymers, as well as being cost effective. Due to the flexibility and mouldability of carbon black polymer matrix materials, they are especially attractive for EMI shielding by helping to eliminate seams or gaps in components. Research into the effectiveness of EMI shielding using polymer matrix materials combined with continuous carbon fibre showed that the shielding efficiency can block out almost all of the interference between 1 to 12 GHz frequencies [37-39], depending on the type of materials used for the measurements. Greater shielding effectiveness is also achieved by thicker materials due to the increased losses as the EM wave passes through the material in the medium. Other research carried out into effective shielding materials included continuous glass fibre combined with carbon microballoons in a polymer matrix [40]. As carbon glass is not a conductive but an insulating material, the microballoons greatly improved the shielding effectiveness of the matrix.

With the addition of a conductive filler into a polymer or elastomer, the insulating properties of the material are changed towards a conductive property. However the concentration of filler determines the effectiveness of electromagnetic shielding. It was determined from previous research that a 40 vol% concentration of isotropic conductive filler was necessary in order to produce a conductive elastomeric material [41]. The high concentration of conductive filler aids in the percolation threshold that aids in creating a physical connection between filler particles, thus creating an almost continuous layer of conductive material embedded in the elastomer. This high concentration of conductive filler is detrimental to the flexibility and density of the elastomer, therefore high concentrations of fillers are not ideal. Malliaris and Turner [42] demonstrated that if a conductive filler is distributed as a segregated network within the material in low concentrations, then it is possible to create a matrix material with conductive properties.

Conductive carbon black is able to transmit an electric current due to the high graphitic structure content. Matrix materials with carbon black have been created using ethylene propylene diene monomer (EPDM) rubber [43], as well as SBR [44], ethylene acrylic [45], siloxane [46], and EVA/NBR [50] combinations. The research conducted by Mohanraj et al [44] determined that a matrix of SBR elastomer with carbon black was not effective in producing sufficient EMI shielding of approximately 20dB, unless a higher concentration of over 35 wt% of carbon black was mixed into the SBR or the thickness of the sample with 15 wt% concentration was increased to approximately 7 cm. Whereas it has been shown that when vulcanising EPDM and carbon black matrix it is possible to obtain 20dB shielding with only a 5.5 mm matrix thickness [43].

Figure 3.7 illustrates how the volume fraction of conductive carbon black filler can affect the electrical conductivity of a material.

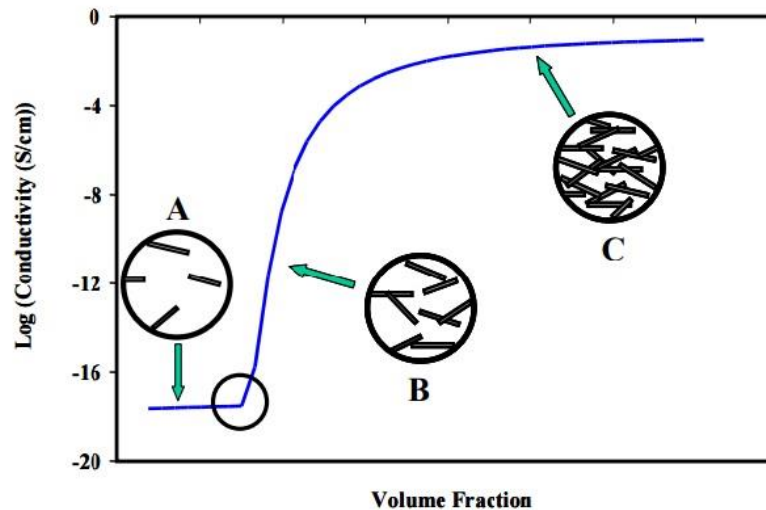


Figure 3.7 Filler volume fraction effect on the electrical conductivity of a material [51]

It is evident that with low filler content (up to 5 wt %) the polymer does not alter its electrical conductivity and still has results that are comparable with a polymer without filler. However, once critical loading is achieved, percolation threshold is attained. This result indicates that a sufficient amount of filler was added to create conductive pathways through the polymer matrix. As the carbon black concentration is increased within the matrix, there is also an increase in the material conductivity. In order to create a network with dispersed carbon black particles, there must be no more than a 10 nm space between particles, and a minimum of two connections for one particle [52]. Percolation generally occurs with 10 wt % concentration of carbon black particles [50], and a conductive network is established. However the concentration of carbon black particles to achieve percolation threshold is dependent on the shape and size of the particles, as well as the properties of the electrical properties of the material they are dispersed in. There is also evidence from research that illustrates how processing and temperature can affect the shielding effectiveness of the matrix material, as shown in Figure 3.8 [53].

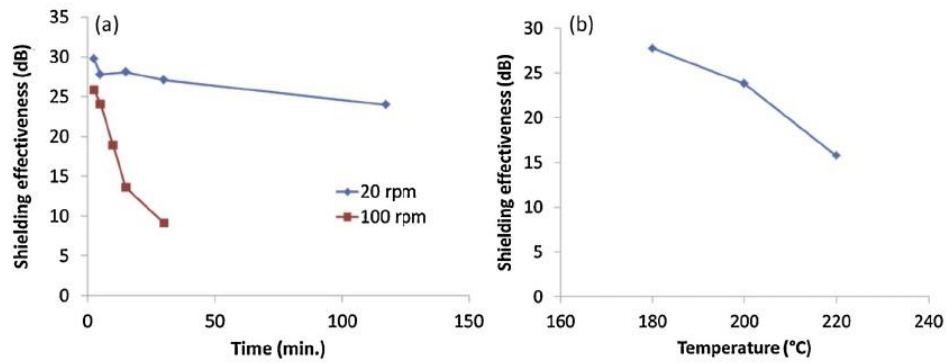


Figure 3.8 Graphs illustrating the shielding effectiveness at 1 GHz, with comparison between (a) vapour grown carbon nanofibers (VGCNF)/HDPE processes at 20rpm and 100rpm at 7.5 wt% and (b) VGCNF/HDPE processed at 50rpm at 7.5 wt% with different processing temperatures [54]

In Figure 3.8 (a) there is clear indication that the processing speed and time affect the shielding properties of matrix polymers. Processing the materials at a lower rpm speed appears to have a beneficial effect and creates a material that is capable of shielding between 25 and 30 dB. This effect is not observed with the matrix processed at 100 rpm speed, where the shielding effectiveness is seen to decrease significantly and continues to do so with prolonged processing time at this speed. It can be concluded that a prolonged processing duration has a detrimental effect on the shielding effectiveness of a polymer matrix. This could be due to loss of conductive carbon black filler during roll milling. It is possible that during the milling process some of the filler is lost, and it is possible that with prolonged mixing that filler agglomerates may form, therefore creating a non-homogenous dispersion of carbon black with agglomerates that are isolated, or not in physical contact, with other particles. In Figure 3.8 (b) a study of the effects of temperature variations during processing illustrates that temperature increase past 180°C have adverse effects on shielding effectiveness.

Figure 3.9 illustrates the various fillers that were mixed in ABS material. Considering filler type is significant when attempting to create an elastomer with EMI shielding capabilities as this dictates how effective the filler will be in conducting a current. It is immediately apparent that at 5 wt% concentration, the carbon black powder particles in Figure 3.9 (a) would not be enough to provide sufficient shielding against EMI as the particles are very widely dispersed and the network is too discontinuous to effectively transfer a current, therefore a much higher concentration would be required. The carbon nano-fibres in (b), although still at the same concentration of 5 wt%, appear to create a better

network for conducting a current, while the carbon nano-tubes in (c) appear to create a good network for conduction, however it appears that the carbon nano-tubes are prone to agglomeration in ABS polymer. Studying the images in Figure 3.9, it is evident that the nano-tubes and the nano-fibres would be ideal for use as fillers for EMI shielding. However, these materials are more expensive to produce and purchase than conventional conductive carbon black powder.

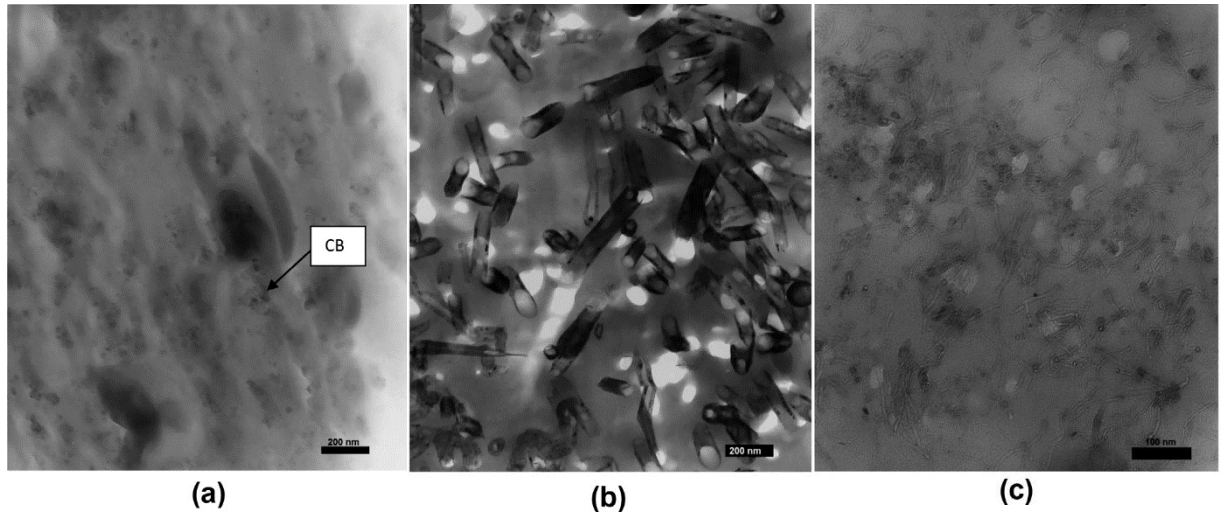


Figure 3.9 TEM images of 5 wt.% (a) carbon black particles, (b) carbon nano fibers, (c) carbon nano tubes dispersed in ABS material [55]

Figure 3.10 provides data results from Al-Saleh's comparative findings for all three filler materials: carbon black, carbon nano-fibre, and carbon nano-tube. It is evident that an increase in the filler content within the naturally insulating ABS polymer increases the electrical conductivity of the material. The percolation threshold is reached at the lowest concentration for the nano tubes and at the highest concentration for the carbon black. This confirms that the nanotubes are most effective and carbon black least effective at establishing a conductive network. The consequent effect on shielding is shown in Figure 3.11. An increase in the filler loading of the carbon nano-tubes resulted in higher shielding effectiveness compared to the carbon powder and fibres. Shielding effectiveness of approximately 20dB is considered ideal for real world applications [1, 2]. This EMI SE value is attained with only 2 wt% of carbon nano-tubes compared to 15 wt% for powder.

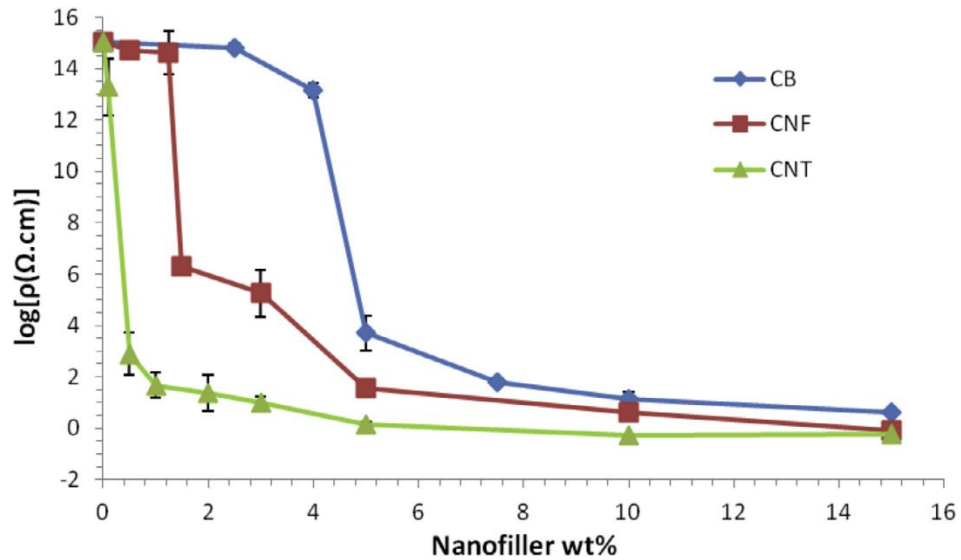


Figure 3.10 A compilation with standard deviation of electrical volume resistivity of varying concentrations of conductive carbon black, carbon nano fibers, and carbon nano tubes dispersed in ABS plastic [55]

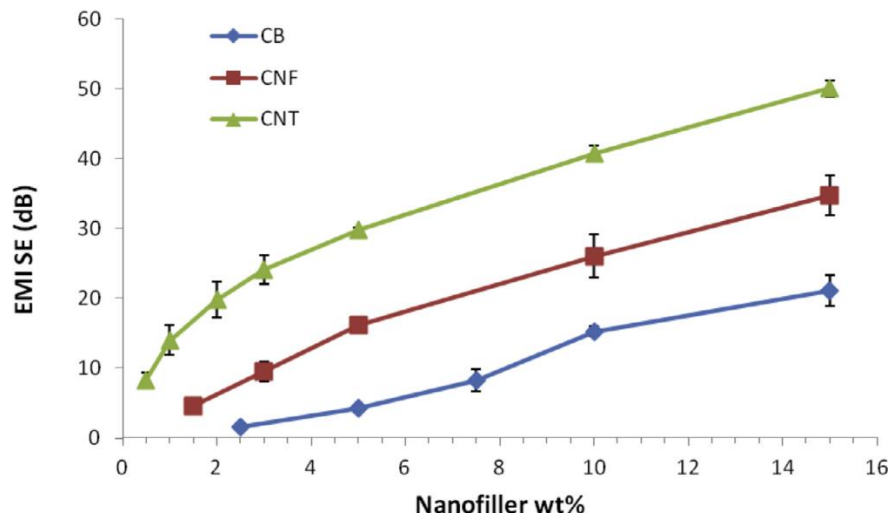


Figure 3.11 Shielding effectiveness of carbon black powder, nano-fibre and nano-tubes tested at 8.2 GHz with standard deviation bars [55]

As filler concentrations have an effect on the EMI SE of a medium, so too does the thickness of that medium as shown in Figure 3.12 comparing the thicknesses of the composites.

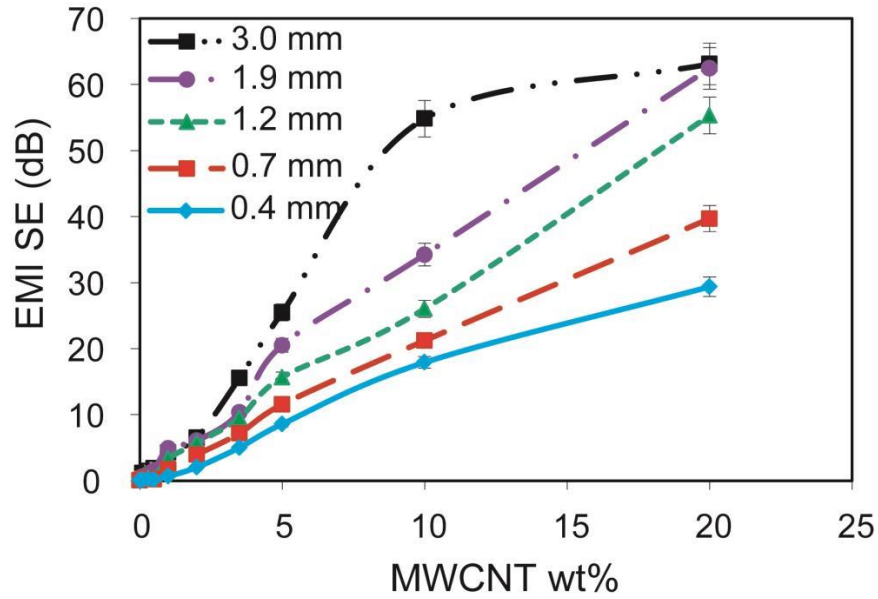


Figure 3.12 Shielding effectiveness of MWCNT/PS composites with varying plate thickness [56]

3.5.2 Temperature, material thickness, and frequency effects on EMI shielding

The temperature that an EMI shielding material is exposed to, as well as the EM frequencies, has a substantial impact on shielding effectiveness. A study carried out by Cao *et al* [57] to determine what the effects of temperature and EMI frequency have on carbon fibre and silica ceramic composites provided interesting results that are presented in Figures 3.11 and 3.12. The EMI shielding materials were exposed to frequencies between 8.2 and 12.4 GHz and temperatures between 30°C and 600°C. Figure 3.13 illustrates how temperature affects imaginary and real permittivity. It is evident that the permittivity increases with increase in temperature. This is caused by a shortening in the electron relaxation time. It is also observed that polarization plays a key role in this due to the inherently good electrical conductivity of carbon fibres [58,59]. It is also known that with an increase in temperature, the conductivity of carbon fibre is enhanced, as the increase in heat helps electrons to “hop” or migrate between the conductive fibres.

In Figure 3.14 (a) the results show that the absorption of the EMI frequencies at 600°C is in the lower spectrum, which indicates that as the temperature increases the material’s maximum absorption frequency is in the lower hertz values. In Figure 3.14 (b) the results implicate that the ideal absorption of the carbon fibre silica material is at low temperatures.

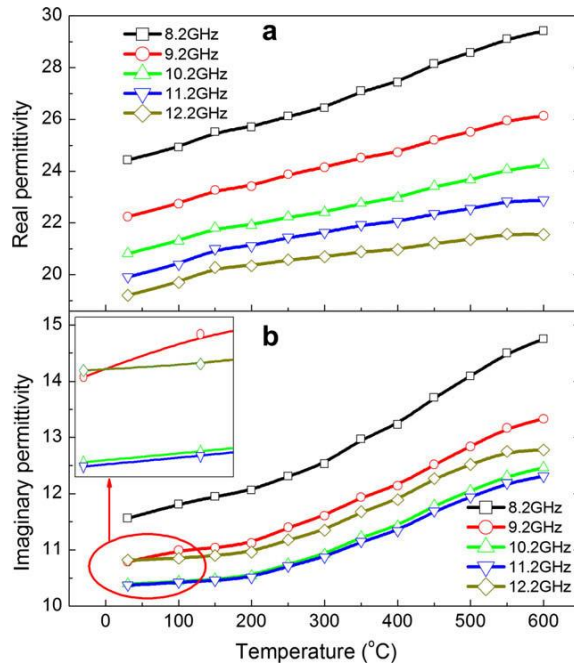


Figure 3.13 Comparison between (a) the real permittivity and (b) imaginary permittivity [60]

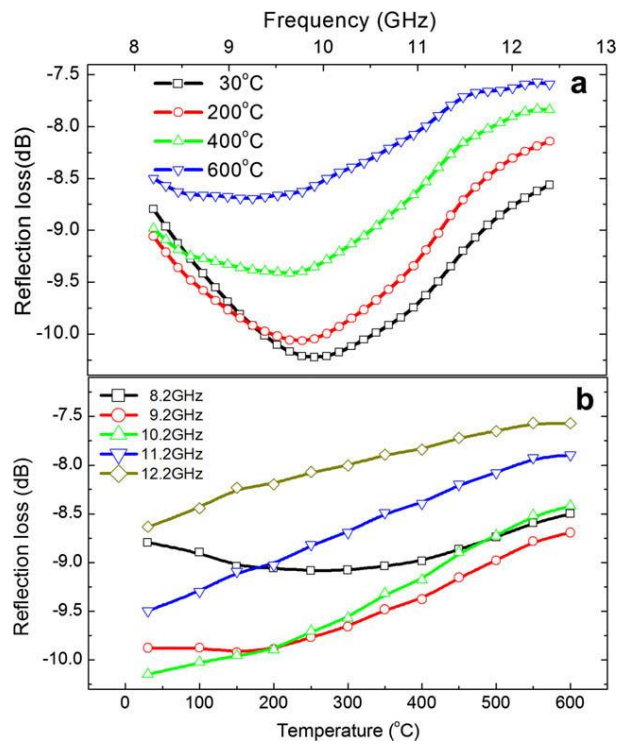


Figure 3.14 Comparison between reflection loss and frequency (a) and reflection loss and temperature (b) using 5mm thick sample of carbon fibers dispersed in silica [60]

Cao *et al* [57] have demonstrated that, for a composite material with conductive carbon fibre filler, the absorption coefficient increases as reflection decreases with increase in EM frequencies. However, exposing EMI shielding polymers to such high temperatures would cause degradation to a polymer-carbon matrix material.

Material thickness of shielding materials is also a significant property to consider when consideration is placed on the design of the shielding device. Figure 3.15 illustrates the total shielding effect of a 0.5 mm sheet of copper when exposed to a 30 kHz frequency.

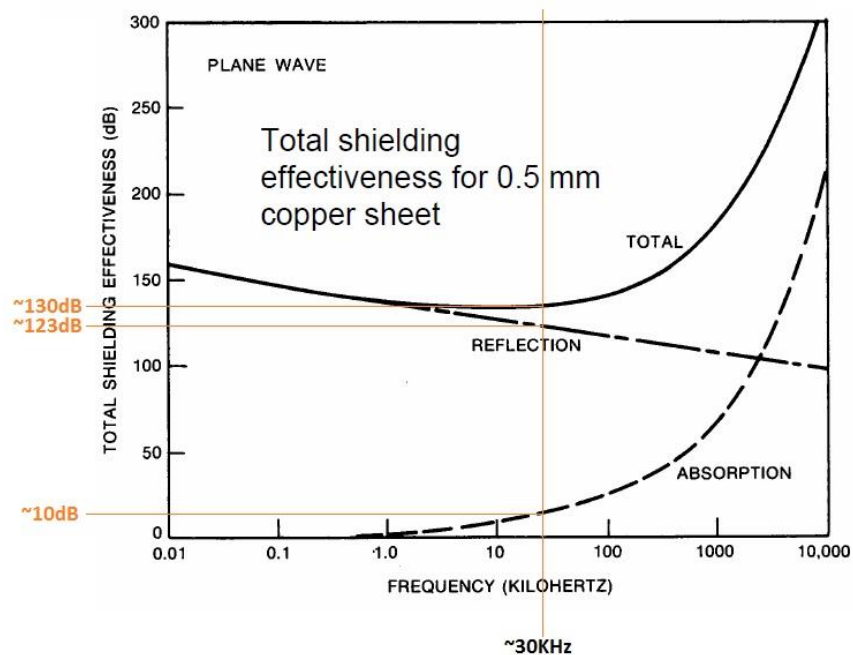


Figure 3.15 The shielding effectiveness of a 0.5mm sheet of copper [13]

The thickness of a shielding material can also have an impact on its ability to reflect or absorb interference. Generally, the absorption abilities of a material are greatly improved by increasing thickness or choosing to utilise a metal material that has a high permeability.

3.5.3 Polymers with conductive metallic fillers

Polymers with metallic particles are sought after materials for EMI shielding due to the higher conductivity that the metals possess. Metallic fibres with 2 μ m thicknesses are also viable conductive fillers for polymers. Table 3.2 compares the various types of conductive fillers, both metal and carbon, for shielding between 1-2 GHz frequency range.

Table 3.2 A comparison of EMI shielding effectiveness (SE) for a polyethersulfone matrix composite with different fillers between 1 and 2 GHz frequency [58]

Filler	Vol. %	EMI shielding effectiveness (dB)
Al flakes (15x15x0.5µm)	20	26
Steel fibres (1.6 µm diam. x 30~56 µm)	20	42
Carbon fibres (10 µm diam. x 400 µm)	20	19
Ni particles (1~5 µm diam.)	9.4	23
Ni fibres (20 µm diam. x 1 mm)	19	5
Ni fibres (2 µm diam. x 2mm)	7	58
Carbon filaments (0.1 µm diam. x >100 µm)	7	32
Ni filaments (0.4 µm diam. x >100 µm)	7	87

Studying the materials listed in Table 3.2, it is evident that Ni filaments (0.4µm dia x > 100µm) provide the best EMI shielding effectiveness with a small volume % concentration compared to the other materials. As mentioned in Section 3.5.1, percolation plays a vital role for effective shielding, and it is desirable to achieve percolation with a low concentration of filler for polymers to maintain the physical properties of the polymer. It is also important in keeping the cost of the material low, [61] as these filler materials are costlier than polymer materials. Percolation with low filler concentration can be achieved if the filler has a high aspect ratio, therefore there is an increased chance of the fillers making contact with one another and therefore creating a conductive network [62, 63].

Some metal materials that are utilised for employing absorption EMI shielding include copper, aluminium, gold, and silver. Super permalloys are also utilised for EMI shielding of more sensitive equipment due to their excellent absorption of interference signals. A factor that distinguishes absorption and reflection methods of shielding is that with increasing frequency absorption loss increases as well, whereas with reflection loss decreases with increasing frequency.

Attempts to create a composite material with conductive copper nanowire filler were conducted by Arjmand [64]. The results of the copper nanowire composite were compared

with multi-walled carbon nano-tube (MWCNT) composites as illustrated in Figures 3.16 and 3.17.

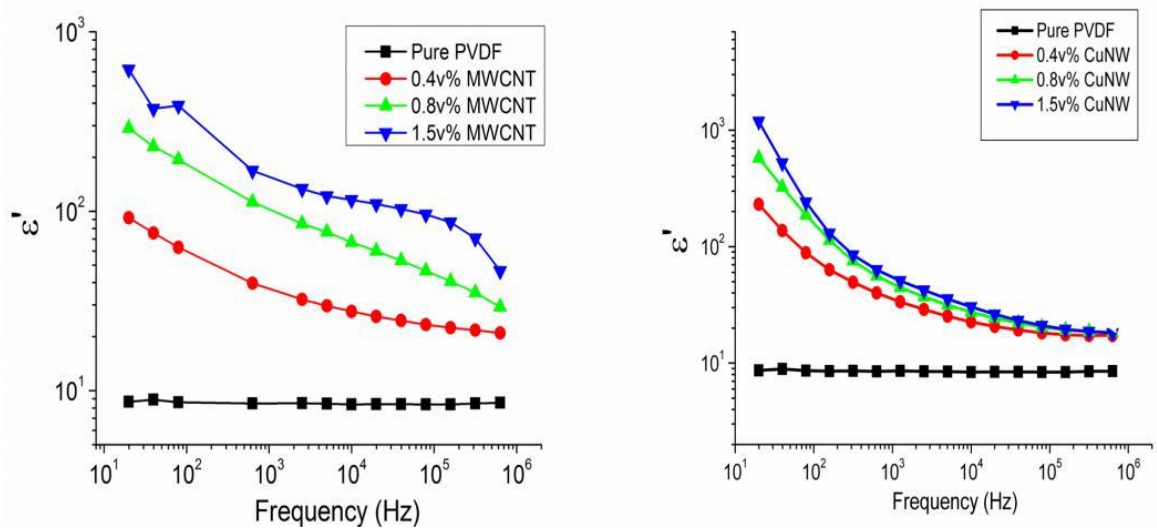


Figure 3.16 Dielectric permittivity measurements for MWCNT composites (left) and PVDF composites (right) [64]

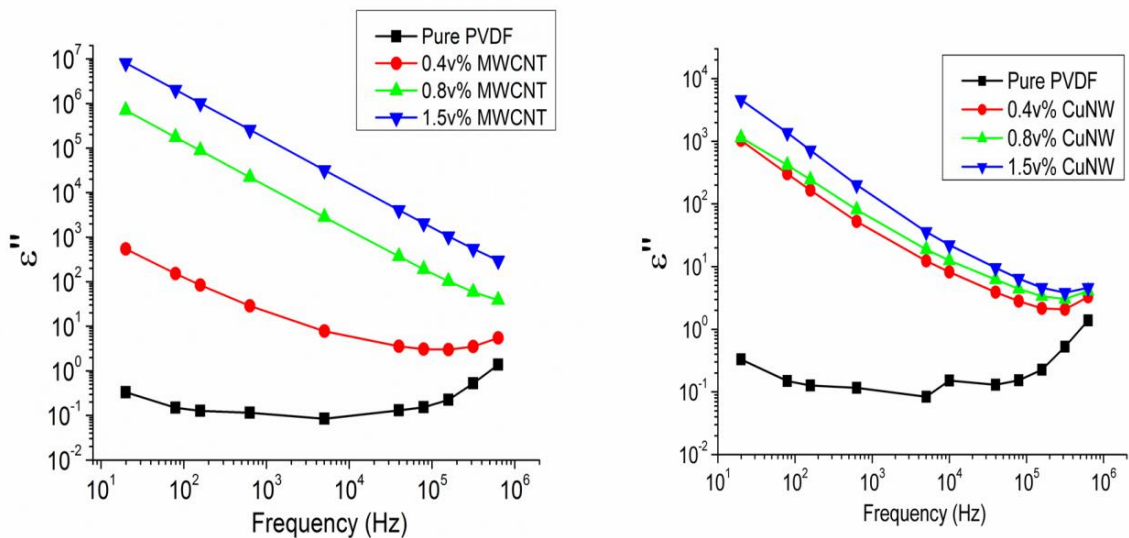


Figure 3.17 Dielectric loss tangent results for PVDF/MWCNT composites (left) and PVDF copper nanowire composites (right) [64]

The dielectric permittivity values displayed in Figure 3.16 increased for both MWCNT and copper as the filler content increased. This is due to the creation of nanocapacitors with an increase in the amount of conductive filler, where the nanodielectric polymer and the nanoelectrode conductive fillers create interfacial polarization [65].

However, the copper filler produced higher dielectric permittivity results compared to MWCNT filler. This is attributed to the higher conductive properties of the copper filler material.

Dielectric loss tangent results displayed in Figure 3.17 show an increase as the filler content rises for both copper and MWCNT materials. This is a result of Ohmic loss, where the electric charges are dissipated due to high conductive material content. The conductive path that is created within a matrix with high filler loadings enables improved dissipation of electrical energy due to electrons having a greater free path in the electric alternating field. Comparing the dielectric loss tangent results for MWCNT and copper nanowire filler, it is evident that the copper filler provided lower dielectric loss. This result is due to the oxidation of the copper filler that is exposed to outside elements, which consequently reduced the Ohmic loss of the matrix and decreased the free path for electron charges (due to the decayed conductive network). The creation of this novel composite with high dielectric permittivity and low dielectric loss due to surface oxidised copper nanowire displayed ideal dielectric properties which made the copper nanowire a superior filler compared to the MWCNT filler.

Another metal filler test conducted by Al-Saleh [66], with results illustrated in Figure 3.18, demonstrates the advantages of utilising highly conductive copper nanowire filler for creating EMI shielding polymers. This material was created by combining a conductive copper nanowire powder with a polymer powder, and the process of mixing created an ideal dielectric material capable of providing effective shielding at very low filler content. The EMI SE increases with an increase in copper nanowire concentration, as higher concentration creates percolation and the creation of a viable conductive network within a polymer matrix. A very low concentration of copper nanowire is needed to provide enough EMI shielding against most every day interference signals generated by electronic equipment. The sample with 1.3 vol% provided shielding for 27dB, which corresponds to blocking 99.8% of the EMI wave generated.

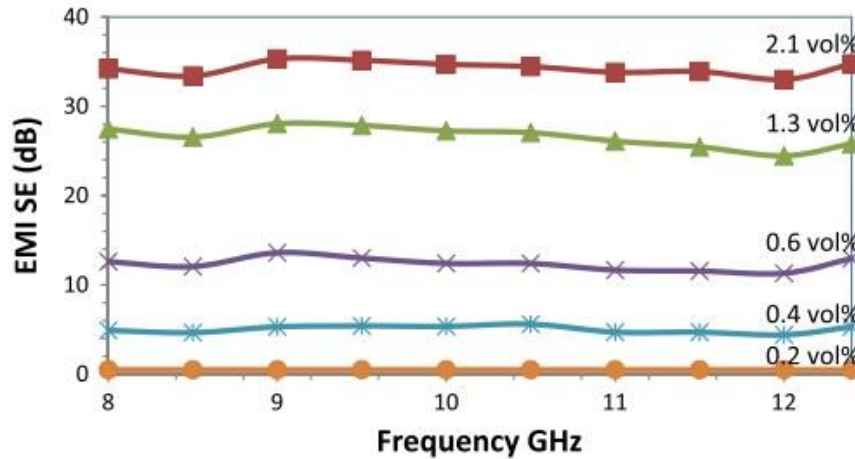


Figure 3.18 EMI SE of 210mm thick CCP/PS composite samples with varying concentrations of copper nanowire filler [66]

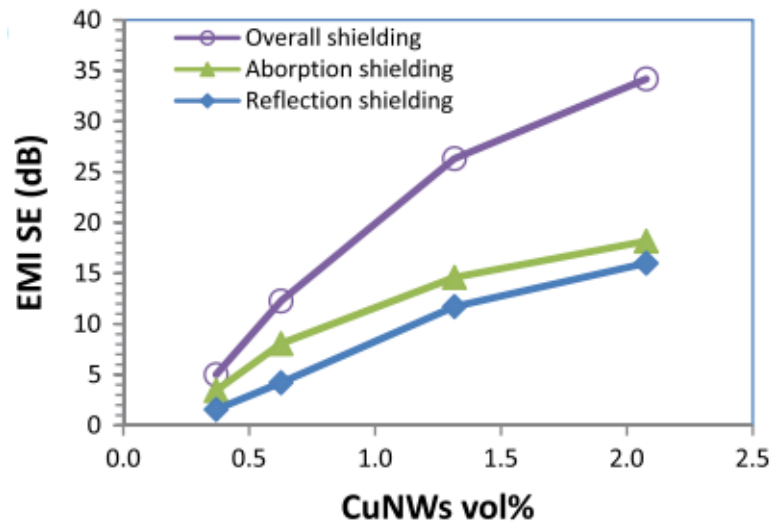


Figure 3.19 the absorption, reflection, and overall EMI shielding provided by copper nanowire filler as a function of filler loading [66]

In Figure 3.19, we can observe that, as with previous EMI shielding results illustrated in this section, the amount of shielding is dependent on the filler content. As the volume of the filler increases, absorption increases as well. We can also observe that with regards to the copper filler, reflection of the EM waves increases with an increase in metal filler. This result is expected as metal materials are highly reflective of EM waves.

3.6 Conclusion

Interference waves generated by devices that are powered by electricity have the potential to interfere with other surrounding devices. This causes a concern especially if the electronic components are particularly sensitive to these emissions, as this could cause disruptions in their operation. With the advancement of modern technology, there is an ever growing need to improve and create new methods of shielding against electric emissions released by operating devices, especially in and around seals and openings of metal covers where EM waves can penetrate.

This chapter has discussed the various types of shielding materials that can be utilised to shield against unwanted EM waves, including metal sheets, and polymers with metallic and non-metallic fillers, as well as the impact the physical characteristics (thickness, shape, conductive or insulating) may have on shielding effectiveness.

References for Chapter 3:

- [1] Kiser kl. *Electromagnetic Shielding*. (2006). Boca Raton: CRC Press, pp. 1-52.
- [2] G.A. Gelves, M.H. Al-Saleh, U. Sundararaj. *Copper nanowire/polystyrene nanocomposites: Lower percolation threshold and higher EMI shielding*. (2011). *Composites Part A* 42, pp. 92-97.
- [3] R. K. Ulrich, L.W. Schaper. *Integrated Passive Component Technology*. (2003). Hoboken, NJ: IEEE Press, Wiley-Interscience.
- [4] Singh, R. *Electrochem*. (1999). Available at: <https://www.electrochem.org/dl/interface/sum/sum99/IF6-99-Pages26-30.pdf> (Accessed: 24 August 2016).
- [5] Tong, X.C. and Tong, C. *Advanced materials and design for electromagnetic interference shielding*. (2008). Boca Raton: Taylor & Francis.
- [6] Keshtkar, A., Maghoul, A. and Kalantarnia, A. *Magnetic Shield Effectiveness in Low Frequency*. (2011). *International Journal of Computer and Electrical Engineering*, vol. 3, pp. 507–513.
- [7] Blythe T, Bloor D. *Electrical Properties of Polymers*. 2nd ed. New York: Cambridge University Press; 2005.
- [8] Isolator-Metal. Available from: <http://commons.wikimedia.org/wiki/File:Isolator-metal.svg> [cited June 2016].
- [9] Yang SY, Lozano K, Lomeli A, Foltz HD, Jones R. *Electromagnetic interference shielding effectiveness of carbon nanofiber/LCP composites*. (2005). *Composites Part A-Applied Science and Manufacturing*, vol. 36, no. 5, pp. 691-7.

- [10] *Photoelectric effect*. Available at: <http://hyperphysics.phy-astr.gsu.edu/hbase/mod2.html> (Accessed: 24 August 2016).
- [11] Sadchikov VV, Prudnikova ZG. *Amorphous materials in electromagnetic shields*. (1997). *Stal'*, vol. 4, pp. 66-9.
- [12] Shinagawa S, Kumagai Y, Urabe K. *Conductive papers containing metallized polyester fibers for electromagnetic interference shielding*. (1999). *Journal of Porous Materials*, vol. 6, no. 3, pp. 185-90.
- [13] Jackson BC, Shawhan G. *Electromagnetic Compatibility, Current review of the performance characteristics of conductive coatings for EMI control*. (1998). In: *IEEE Int. Symp Vol. 1*, Piscataway, New Jersey, USA: IEEE, pp. 567-72.
- [14] Kumar R, Kumar A, Kumar D. *Electromagnetic Interference and Compatibility*. (1997). In: *Proc. Int. Conf. IEEE, Piscataway, RFI/EMI/microwave shielding behaviour of metallized fabric – a theoretical approach*, New Jersey, USA: IEEE, pp. 447-50.
- [15] Bhatgadde LG, Joseph S. *Electromagnetic Interference and Compatibility*. (1997). In: *Proc. Int. Conf. IEEE, Piscataway, New Jersey, USA: IEEE*, pp. 443-5
- [16] Sidhu A, Reike J, Michelsen U, Messinger R, Habiger E, Wolf J. *Metallization of plastics for shielding*. (1997). *IEEE, Piscataway New Jersey, USA: IEEE*, pp. 102-5
- [17] Hajdu J. *New challenges for electroless plating technologies*. (1997). *Trans. Inst. Metal Finish*; vol. 75(pt. 1): pp. B7-B10
- [18] Klemmer G. *Shielding approaches*. (1996). In: *Special Areas, 54th Annual Technical Conf. – ANTEC, Conf. Proc, vol. 3, Brookfield, Connecticut, USA: Society of Plastics Engineers*, p. 336.
- [19] Gwinner D, Scheyrer P, Fernandez W. *Selective deposition of aluminium on plastic parts for EMI shielding*. (1996). In: *Proc. 39th Annual Technical Conf. – Soc. Vacuum Coaters, Albuquerque, New Mexico, USA: Society of Vacuum Coaters*, p. 336.
- [20] Bhatia MS. *Technique for depositing metal layers over large areas for EMI shielding*. (1995). In: *Proc. 1995 4th Int. Conf. Electromagnetic Interference and Compatibility, Madras, India: IEEE*, pp. 321-4
- [21] Zhang L, Li W, Liu J, Ren B. *Process and performance of electroless Cu/Ni-P double film*. (1995). *Cailiao Gongcheng/Journal of Materials Eng.*; Vol. 7, pp. 38-41.
- [22] Mandich NV. *EMI shielding by electroless plating of ABS plastics*. (1994). *Plating & Surface Finish*, vol. 81, no. 10, pp. 60-3.
- [23] Jackson BC, Kuzyk P. *Practical guide on the use of electroless coatings for EMI shielding*. In: *IEEE, Conf. Publications, No. 396, Stevenage, UK: IEEE, 1994*, pp. 119-24.
- [24] Nagasawa C, Kumagai Y, Urabe K, Shinagawa S. *Electromagnetic shielding particle board with nickel-plated wood particles*. (1999). *J Porous Mater*, vol. 6, no. 3, pp. 247-54

- [25] Dixon DS, Masi J. *Thin coatings can provide significant shielding against low frequency EMF/magnetic fields.* (1998). In: IEEE Int. Symp. Electromagnetic Compatibility, Vol. 2, Piscataway, New Jersey, USA: IEEE, pp. 1035-40.
- [26] Mason PJD. *Technologies and markets for thin film EMI/RFI shielding materials.* (1994). In: Proc. 37th Annual Technical Conf. – Soc. Vacuum Coaters, Albuquerque, New Mexico, USA: Society of Vacuum Coaters, pp. 192-7.
- [27] Pomposo JA, Rodriguez J, Grande H. *Polypyrrol-based conducting hot melt adhesives for EMI shielding applications.* (1999). Synth Met, vol. 104, no. 2, pp. 107-11.
- [28] Park J-S, Ryn S-H, Chung O-H. *Preparation of conducting composites and studies on some physical properties.* (1998). In: 56th Annual Technical Conf. – ANTEC, Conf. Proc, Vol. 2, Brookfield, Connecticut, USA: Society of Plastics Engineers, pp. 2410-4
- [29] Courric S, Tran VH. *Electromagnetic properties of poly(p-phenylene-vinylene) derivatives.* (1998). Polymer, vol. 39, no. 12, pp. 2399-408.
- [30] Angelopoulos M. *Conducting polyanilines: properties and applications in microelectronics.* (1997). In: Proc. 3rd Annual Conf. Plastics for Portable and Wireless Electromagnetics Brookfield, Connecticut, USA: Society of Plastics Engineers, pp 66.
- [31] Makela T, Pienimaa S, Taka T, Jussila S, Isotalo H. *Thin polyaniline films in EMI shielding.* (1997). Synth Met, vol. 85, no. 1-3, pp. 1335-6.
- [32] Kohlman RS, Min YG, MacDiarmid AG, Epstein AJ. *Tunability of high frequency shielding in electronic polymers.* (1996). Journal of Engineer Applied Sci., vol. 2: pp. 1412-6.
- [33] Naishadham K. *Microwave characterization of polymeric materials with potential applications in electromagnetic interference (EMI) shielding.* (1994). In: 7th Int. SAMPE Electronics Conf, Vol. 7, Covina, California, USA: SAMPE, pp. 252-65.
- [34] Luo, X. and Chung, D.D.L. *Electromagnetic interference shielding using continuous carbon-fiber carbon-matrix and polymer-matrix composites.* (1999). Composites Part B: Engineering, vol. 30, no. 3, pp. 227–231.
- [35] Murthy M. 4th Int. SAMPE Electronics Conference. *Electronic Materials-Our Future.* (1990). edited by Allred RW, Marinez RJ, Wischmann KB, vol. 4, pp. 806–818.
- [36] Jana PB, Mallick AK, De K. *Effects of sample thickness and fiber aspect ratio on EMI shielding effectiveness of carbon fiber filled polychloroprene composites in the X-band frequency range.* (1992). IEEE Trans Electromagnetic Compatibility; vol. 34, no. 4, pp. 478–481.
- [37] Jana PB, Mallick AK. *Studies on effectiveness of electromagnetic interference shielding in carbon fiber filled polychloroprene composites.* (1994). Journal of Elastomers and Plastics. vol. 26, no. 1, pp. 58– 73.
- [38] Atkins DJ, Miller JA, Sanders JD. 8th Int. Conf. Electromagnetic Compatibility, Electronics Division, Institution of Electrical Engineering, London, (1992), pp. 100–107.

- [39] Jaworske DA, Gaier JR, Hung CC, Banks BA. *SAMPE Q.* (1986). Vol. 18, no. 1, pp. 9–14.
- [40] Olivero DA, Radford DW. *SAMPE Q.* (1997). Vol. 33, no. 1, pp. 51 – 57.
- [41] J. Gurland, *Truns. Met. Soc. AIME*, 236, 642 (1966).
- [42] A. Malliaris and D. T. Turner]. *Appl. Phys*, 42,614 (1971)
- [43] P. Ghosh, A. Chakrabarati. (2000). *Eur. Polym. J.* vol. 36, pp. 1043-1054.
- [44] G.T. Mohanraj, T.K. Chaki, A. Chakraborty, D. Khastgir, *Polym. Eng. Sci.* 46 (2006), pp. 1342-1349
- [45] B.P. Sahoo, K. Naskar, D.K. Tripathy, *J. Mater. Sci.* 47 (2012), pp. 2421-2433.
- [46] O.A. Al-Hartomy, F. Al-Solamy, A. Al-Ghamdi, N. Dishovsky, V. Iliev, F. El-Tantawy, *Int. J. Polym. Sci.* (2011), pp. 837803-07.
- [47] Chung DDL. *Electromagnetic interference shielding effectiveness of carbon materials.* *Carbon.* 2001; vol. 39, no. 2, pp. 279-85.
- [48] Chung, D.D.L. *Materials for Electromagnetic interference shielding.* (2000). *Journal of Materials Engineering and Performance*, vol. 9, no. 3, pp. 350–354.
- [49] Broadbent, S. R. and Hammersley, J. M. (1957). *Proc.Camb.Phil.Soc.*, vol. 53, no. 3, pp.629.
- [50] M. Rahaman, T.K. Chaki, D.J. Khastgir. *Mater. Sci.* Vol. 46 (2011), pp. 3989-3999.
- [51] Weber, Erik PhD Dissertation. *Development and Modelling of Thermally Conductive Polymer/Carbon Composites.* (2001).
- [52] C. Pecharroman, J. S. Moya. *Experimental evidence of a giant capacitance in insulator-conductor composites at the percolation threshold.* (2000). *Advanced Materials*, vol. 12, pp. 294-297.
- [53] M.H. Al-Saleh, U. Sundararaj, *Polym. Adv. Technol.* Vol. 22 (2011), pp. 246.
- [54] Thomassin, J.-M., Jérôme, C., Pardoën, T., Bailly, C., Huynen, I. and Detrembleur, C. *Polymer/carbon based composites as electromagnetic interference (EMI) shielding materials.* (2013). *Materials Science and Engineering: R: Reports*, Vol. 74, no. 7, pp. 211–232.
- [55] Al-Saleh, M.H., Saadeh, W.H. and Sundararaj, U. *EMI shielding effectiveness of carbon based nanostructured polymeric materials: A comparative study.* (2013). *Carbon*, vol. 60, pp. 146–156.
- [56] Arjmand, M. (2014). *Electrical Conductivity, Electromagnetic Interference Shielding and Dielectric Properties of Multi-Walled Carbon Nanotube/Polymer Composites* (Doctoral thesis, University of Calgary, Alberta, Canada). Retrieved from <http://theses.ucalgary.ca/handle/11023/1379>
- [57] Cao, M.-S., Song, W.-L., Hou, Z.-L., Wen, B., Yuan, J. *The effects of temperature and frequency on the dielectric properties, electromagnetic interference shielding and*

microwave-absorption of short carbon fiber/silica composites. (2010). Carbon, Vol. 48, no. 3, pp. 788–796.

[58] Chung DDL. *Electromagnetic interference shielding effectiveness of carbon materials.* Carbon. (2001). Vol. 39, no. 2, pp. 279-285.

[59] Wu JH, Chung DDL. *Increasing the electromagnetic interference shielding effectiveness of carbon fiber polymer-matrix composite by using activated carbon fibers.* (2002). Carbon, vol. 39, no. 2, pp. 445-467.

[60] Cao, M.-S., Song, W.-L., Hou, Z.-L., Wen, B. and Yuan, J. *The effects of temperature and frequency on the dielectric properties, electromagnetic interference shielding and microwave-absorption of short carbon fiber/silica composites.* (2010). Carbon, vol. 48, no. 3, pp. 788–796.

[61] Shenoy AV. *Rheology of filled polymer systems.* (1999). Pune, India, Springer-Science.

[62] Li J, Ma PC, Chow WS, To CK, Tang BZ, Kim JK. *Correlations between percolation threshold, dispersion state, and aspect ratio of carbon nanotubes.* (2007). Advanced Functional Materials, vol. 17, no. 16, pp. 3207-15.

[63] Bauhofer W, Kovacs JZ. *A review and analysis of electrical percolation in carbon nanotube polymer composites.* (2009). Composites Science and Technology; vol. 69, no. 10, pp. 1486-98.

[64] Arjmand, Mohammad. (2014). *Electrical Conductivity, Electromagnetic Interference Shielding and Dielectric Properties of Multi-walled Carbon Nanotube/Polymer Composites.* PhD thesis. University of Calgary.

[65] Z.M. Dang, J.K. Yuan, J.W. Zha, T.Z. Zhou, S.T. Li, G.H. Hu. *Fundamentals, processes and applications of high-permittivity polymer–matrix composites.* (2012). Prog. Mater. Sci. Vol. 57, pp. 660–723.

[66] Al-Saleh, M.H., Gelves, G.A. and Sundararaj, U. *Copper nanowire/polystyrene nanocomposites: Lower percolation threshold and higher EMI shielding.* (2011). Composites Part A: Applied Science and Manufacturing, Vol. 42, no. 1, pp. 92–97.

[67] X. Colin Tong, *Advanced Materials and Design for Electromagnetic Interference Shielding*, Taylor & Francis Group, 2009.

[68] *ASTM Standard Designation: D 4935-99*, “Standard test method for measuring the electromagnetic shielding effectiveness of planar materials,” 1999.

[69] M.S. Sarto and A. Tamburrano, “Innovative test method for the shielding effectiveness measurement of conductive thin films in a wide frequency range,” *IEEE Transactions on Electromagnetic Compatibility*, vol. 48, no. 2, pp. 331–341, 2006.

Chapter 4: Experimental

4.1 Materials

Tables 4.1 - 4.4 present the information that was gathered from the manufacturers on the various materials that were used.

Table 4.1 Ink trade names and manufacturers used for printing

Name	Manufacturer/Supplier	Trade Name
Conductive carbon black powder	Columbian Chemicals Company	Conductex 7055 Ultra
Conductive carbon black ink	Methode Development Co.	3804 Carbon Ink 0601-61
Conductive carbon black paste	Bare Conductive	Electric Paint 50ML

Table 4.2 Substrates used for printing

Substrates	Manufacturer/Supplier	Trade Name
Glass slides	Fisher Scientific	Standard glass microscope slide
PET	Printed Electronics LTD	
PTFE fabric		
Silicone coated paper	Tesco Supermarket	Silicone coated baking paper

Table 4.3 Ink used and TGME added to XSBR ink.

Ink	Manufacturer/Supplier	Trade Name	Viscosity (cp)
Carbon black ink	Methode Development co	3804 Carbon Ink 0601-61	12
TGME	Sigma Aldrich	Triethylene Glycol Monomethyl Ether 95%	N/A

Table 4.4 Latex property information obtained from manufacturers

Elastomer	Name	Manufacturer	Trade name/grade	Solids Content	Ammonia Content (%)	Surface Tension (mN/m)	Viscosity (mPa s)
XNBR	Carboxylated butadiene-acrylonitrile	Synthomer	Synthomer X426C	39	n/a	n/a	14
XSBR	Carboxylated styrene-butadiene copolymer	Synthomer	Litex T 71S20	50	n/a	47	<500
CR	2-Chlorobutadiene	Synthomer	Lipren T	58	n/a	37	100
NR	Natural rubber latex	Synthomer	HCE68	68.5	0.62	n/a	1600
PVNR	Pre-vulcanised natural rubber latex	Synthomer	VRB884	60.25	0.7	n/a	66
HNBR	Hydrogenated Nitrile Butadiene Rubber	Zeon Chemicals	Zetpol HNBR		n/a		

4.2 Liquid Latex Property Measurement

4.2.1 Surface Tension

To determine the surface tension of the latex, a Kruss DSA100 contact angle device was used with the appropriate pendant drop measuring method selected. A contact angle device can measure surface tension and surface energy of materials. In order to carry out measurements of surface tension of liquid materials, a separate syringe was utilised to avoid cross-contamination. Approximately 2mL of liquid was loaded into the syringe and attached to the contact angle's deposition section. A pendant drop needle's width was measured with a micrometer, the value recorded and entered into the software before attaching the needle onto the syringe. The dosing was set to 1 μ L. The liquid was slowly dispensed until it reached a point where the droplet formed a pear like shape and was on the point of detaching from the needle, as demonstrated in Figure 4.1.

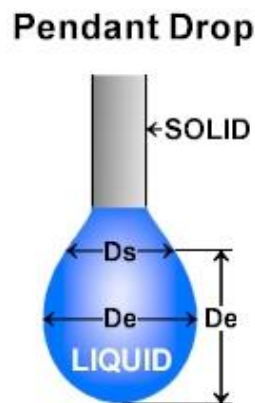


Figure 4.1 An illustrated example of the pendant drop measuring method [2]

An image was captured and the software on the computer was used to measure the surface tension of the liquid based on the diameter of the droplet at its widest point, the diameter of the droplet close to the tip of the needle, and the height of the droplet.

4.2.2 Viscosity

A Brookfield viscometer was initially used to determine the viscosity of the latex materials. To determine the viscosities using the Brookfield viscometer, 100ml of liquid latex samples were placed into respective beakers so that the spindle on the viscometer could record the values. The viscometer operates with the use of an electric motor which rotates a spindle attached at the bottom of the device. The spindle is a rod of metal with saucer shaped planes, which lie perpendicular to the rod, with varying sizes and thicknesses. On the front

of the viscometer is a scale that records the value of the friction between the saucer plane and the liquid, which was used with the Brookfield Factor Finder to calculate the value of the viscosity.

However, due to the fact that a significant amount of liquid is required to measure the viscosity of the latexes, a parallel plate shear rheometer was used in further tests as it only requires approximately 1 ml of liquid and provides information on how the viscosity changes with shear rate and temperature. A Kinexus Rheometer was used with parallel plates attached to determine shear viscosity of the latex materials using 0.75 ml of liquid latex. Minimum and maximum shear rates were set to 10 and 1000 1/s respectively, and the temperature set to 25°C. The duration for each test required approximately 15 minutes to complete. The Kinexus Rheometer records a maximum strain rate at the plate edge.

4.2.3 Particle Size

Determining particle size of the latex materials is vital as it can determine whether the liquid latex materials in question can be ink-jetted or not.

Initially SEM was utilised to attempt to determine the particle size of the latexes. XSBR latex was diluted to 1% wet weight solids content, a single droplet was deposited onto a conductive copper grid and was allowed to dry before sputter coating the sample with silver and placing it into the SEM. However, it was determined early on that this method of particle size analysis was ineffective, therefore a different method of analysis was utilised.

A Mastersizer 2000 from Malvern was used to measure the size of liquid latex particles. The Mastersizer uses laser diffraction to analyse the size of particles (0.02 to 2000µm) that are dispersed in de-ionized water.

The Mastersizer comprises three elements: the optical bench, a sample dispersion unit, and the software that enables the user to carry out the desired experiments on the computer. To find the particle size of the liquid latex, a few drops of the selected material were dispersed in de-ionized water, approximately 0.5 – 1 ml of material in 600 ml of de-ionised water, and exposed to sonication for approximately 60 seconds to disperse any particles that may have agglomerated. Once sonication was complete, a dispersed sample passed through a silicone tube for measurement in the optical bench. It was exposed to a laser beam which illuminated the particles in that sample.

Particle sizes of all the latex materials detailed in Table 4.1, the carbon black ink from Methode Development Co, and latex ink that was developed by diluting latex with de-ionized water and TGME, were measured using the Mastersizer to determine if their particle sizes would be suitable for inkjet printing.

4.3 Preliminary printing trials

The printer used for the development and printing of latex inks for this project was the Dimatix Materials Printer DMP-2831 by Fujifilm. Initial attempts to jet the latex ink involved filling the printer cartridge with 2ml of unmodified XNBR and XSBR. The process involved passing the latex through a 5 μ m filter attached to a syringe, to ensure that there were no agglomerates, into the MEMS-based cartridge. The print heads were then attached to the cartridge and a manual purge using a syringe was carried out by creating positive pressure around the ink bag inside the cartridge. The first single layer of XSBR ink was printed onto silicon coated paper. This paper was chosen due to its hydrophobic silicone coating and so that multilayer printed samples could be easily removed from the substrate.

After the test print was carried out with the XSBR and XNBR, it was determined that the latex required modification due to clogging.

4.4 Development of a latex ink

Both the XSBR and XNBR were diluted using de-ionized water to reduce the solids content from 52% for XNBR and 50% for XSBR to 34.6% and 33.3% respectively.

Once diluted, the process of filtering and purging were repeated before attempting a second print trial. Diluting the latex did aid in the jetting process, and it was possible to print a layer of XNBR onto a silicone coated paper substrate. Nevertheless, the process resulted in another clogged print head which stopped the jetting of the ink.

After determining that the issue would only be solved by decreasing the evaporation rate of the latex, a humectant was incorporated into the diluted latex. Triethylene glycol monomethyl ether (TGME) was selected as it has a proven and successful record of being the humectant of choice for developing and existing inks. In order to determine how much TGME was required for successful printing, a series of experiments were carried out by varying the concentrations of TGME in latexes.

The first experiment that was carried out was used to determine how the latexes reacted to the addition of TGME. This involved combining 1 g of TGME with 10 g of XSBR, XNBR, CR, and HNBR. Once combined, the latexes were passed through a 5µm filter with a syringe. It was determined that the addition of TGME to the XNBR, CR, and HNBR latexes had caused some agglomeration, with the XSBR experiencing no agglomeration. Therefore, the XSBR was the only material that was suitable to use for the following tests.

The second experiment involved determining the effects TGME had on the drying time of XSBR. Table 4.5 details the wet weight percentages of TGME used.

Table 4.5 Concentrations of TGME in XSBR latex

TGME, g	XSBR, g	De-ionised Water, g	TGME wet wt %
0	10	5	N/A
0.25	10	N/A	2.43
0.5	10	N/A	4.76
1	10	N/A	9.09
1.5	10	N/A	13
2	10	N/A	16.6

1g of each of the mixtures stated in Table 4.5 was placed in labelled aluminium dishes and put in a pre-heated oven at 60°C to determine how each factor affected the drying time of the XSBR. The samples were weighed at 30 minute intervals and left to dry overnight. From the results of these experiments the concentration of TGME that would be used for printing trials was determined.

1g of TGME was introduced to 15 ml diluted samples of XNBR and XSBR. Filtering and purging some of the latex ink was repeated and jetting was carried out successfully. All 16 nozzles were operating efficiently and the latex was jetted in a controlled manner with droplets following a straight line down with the droplet tails intact and with minimal to no satellite droplet formations.

After modifications to the latexes were carried out to ensure better printability, another set of measurements were carried out to determine the effects of these modifications

on the viscosity, particle size, and surface tension. Measurements were obtained for diluted latex samples, as well as diluted latexes containing TGME humectant. The same equipment mentioned in section 4.2 was utilised for measuring these properties.

4.5 Jetting Trials

Ink jetting trials were carried out to determine how the newly developed ink behaved and to determine how the droplets formed once ejected out of the nozzles. The printability indicator, also referred to as the Z number, has been determined and is listed for all latex samples that were used in Chapter 5 section 5.3.5.

Jetting and printing properties that were used:

- Drop spacing: 30 μm
- Nozzle jetting voltages set to 26V
- Maximum jetting frequency: 20kHz
- Nozzle temperature settings: off
- Cleaning cycles: 0.3 second blot

The jetting trials involved observing the jetting process of latex inks using the drop-watch camera that is installed in the Dimatix Material Printer. Nozzles are numbered 1 to 16, and once a nozzle was selected, the jetting process began instantly. The dispensed ink was collected in a small container directly underneath the print head. A grid overlay with vertical and horizontal lines was used to assess the descent of the droplets. All nozzles were tested and the shape and formation of the droplets and tail were analysed using this method. Nozzles that were jetting correctly, with the droplet tail remaining intact and no sputtering of the ink from the nozzle, were selected to be used for the droplet analysis.

4.6 Surface Energy Measurement of Substrates

The most efficient method of determining the surface energy of a solid material is to perform contact angle tests. These tests were carried out with the Contact Angle System OCA equipment manufactured by Dataphysics.

The sessile drop contact angle method was used to measure the surface energy. A 1 μL drop of de-ionized water or diiodomethane was dispensed and deposited through a needle onto the surface of the substrates. An image of the droplet resting on the substrate was

captured, and the contact angle was calculated with the aid of the software on the Dataphysics equipment.

Surface energies were measured for the glass slides, PET, PTFE coated fabric, and silicone coated paper. Square samples roughly 10 cm x 10 cm were cut for the PET, PTFE fabric, and silicone coated paper and handled using latex gloves to avoid contaminating the surfaces. The glass slides measured 2.6 cm x 7.6 cm and were standard microscope slides. Lint free paper and some compressed air was used to clear any debris or impurities that may have fallen onto the surfaces of the substrates. Once prepared, the substrates were secured onto the base of the contact angle device, the focus of the camera was adjusted to display a clear image of the surface of the substrate, and the light settings behind the sample were adjusted to give the right contrast for the software to register.

4.7 Droplet Analysis

Droplet analysis is a method of determining how well the ink behaves during the jetting process, if the nozzles that have been selected for printing are functioning optimally, and it can also be used to observe how the ink behaves when deposited on various substrates.

A droplet analysis of ink involved printing a line pattern with a series of droplets that were deposited on a suitable substrate by an optimally functioning nozzle and observing the size and shape of the droplets under SEM or optical microscopy. The droplet analysis pattern used for printing was created using the pre-installed computer software for the Dimatix printer. The specifications of the pattern include:

- 100 μm drop spacing
- X-width: 50.15mm
- Y-height: 2.15mm
- Print head angle: 36.2°

Using this pattern, a single layer of droplets was deposited onto a PET substrate. The sample was then sputter coated in gold palladium and the droplet patterns observed under SEM.

4.8 Single Layer Printing Trials

Single layers of XSBR ink were deposited on PET, glass, cast sheet of XSBR, silicone coated paper, and PTFE coated fabric to determine what effects the various

substrates have on the overall sample. A 1 x 1 cm square pattern was used to print the XSBR on the various substrates and the same printing parameters were used in each case. The printing height remained the same at 1 mm for the PET, silicone coated paper, and the PTFE coated fabric, however the height required adjustment to 2000 μ m for the glass substrate and 2700 μ m for the cast sheet of XSBR due to the greater thicknesses of the substrates used to deposit ink onto and to keep the printing height, which is the distance from the upper substrate surface to the print head, at 1000 μ m.

4.9 Multilayer Printing Trials

Multilayer printing involved printing successive layers of latex ink, or a combination of other inks such as conductive carbon black. This section provides details of the parameters used to deposit multiple layers of XSBR onto substrates.

4.9.1 Printing Rectangle Patterns and Logos

Rectangle patterns that were 3x2mm, 5x4mm, and a 10x10mm square were created. These patterns were used to determine how accurate the finished printed product was compared to the pattern created on the computer and to determine if there was any spreading of the ink. A droplet spacing of 20 μ m was used during these experiments.

The 3x2mm patterns were created using 26V jetting voltage, a print height of 1000 μ m, and a cleaning cycle of 0.3 second blot was used after every layer. The blot cleaning cycles involve expelling some ink from the cartridge for 0.3 seconds, then lowering the print head down to the porous cleaning pad to absorb the ink. Samples with 10-120 layers were printed using the 3x2mm pattern.

The 5x4mm pattern used the same printing parameters in terms of the jetting voltage and printing height, with a 0.5 second blot cleaning cycle used instead of the 0.3 second. Samples with 10-100 layers were printed using the 5x4mm pattern. These patterns were printed onto PET, glass microscope slide, and PTFE coated fabric substrates.

The Loughborough University logo was printed using the XSBR ink as was the logo for ZEON Chemicals Company using their HNBR latex that was diluted and combined with TGME to create a latex ink.

The printing process for the logo involved setting the print head to an angle of 6.8°, setting the jetting voltages to 26V, a printing height of 1000 μ m, and a cleaning cycle to run

after every 30 passes/lines deposited with a 0.3 second blot purge on the cleaning pad. A total of 60 layers of XSBR ink was printed to create the Loughborough University shield logo and name.

The HNBR from ZEON Chemicals was diluted to 34.6% solids content by combining 5ml of de-ionised water in 10ml of HNBR latex, and 1ml of TGME was combined with the diluted latex. The latex ink was then passed several times through a 5 μ m filter to ensure a homogeneous mixture was obtained and that no agglomerates would form. The printing process for the ZEON logo included the same printing parameters as were used for printing the University's logo, however the cleaning cycles was changed to a 1 second blot purge on the cleaning pad after 30 passes, and a total of 70 layers was printed.

4.9.2 3-D Pattern Printing with XSBR Ink

A pre-designed 1x1cm 3-D pattern on the Dimatix computer was used to attempt to print a 3-D pattern to observe how the ink behaves when deposited in this manner. This pattern featured a wave cross-sectional profile, as illustrated in Figure 4.2.



Figure 4.2 A basic cross sectional illustration of the 3-D wave pattern that was used to test 3-D jetting with XSBR ink

With the XSBR ink, 10 layers were printed to create a 3-D sample. The printing parameters included:

- Print head angle: 6.8°
- Printing height: 1000 μ m
- Thickness of substrate: 200 μ m
- Substrate: PET
- 0 Second time delay
- Cleaning cycle: 1 second purge
- Jetting voltage: 25V

4.9.3 Introducing Time Delay between Layers

The benefit of introducing a time delay before a successive layer of ink was deposited was that it allowed for the previously deposited layer time to partially dry, which could prevent the ink from spreading. The purpose of introducing a time delay during the printing process was to determine if the time delay affected the thickness of each layer of printed latex compared to layers printed without time delay.

Time delays of 30 and 60 seconds were included in printing trials. Rectangular samples measuring 3x2mm in size were printed onto a PET substrate. 10, 20, and 30 layers of XSBR ink were printed using a time delay of 0, 30 and 60 seconds that was scheduled after each layer was deposited. The heated bed option was not utilised and the bed temperature was recorded at 22.3°C.

Two 50 layer samples of XSBR were also printed one with and one without a time delay. The printer settings for the 50 layers included:

- 26V jetting voltage
- 6.8° print-head angle
- No set temperature on the cartridge
- Printing height: 1000µm
- 3x2mm rectangle patterns
- Meniscus set point: 4.0
- Number of nozzles used: 16
- Time to print 1 layer: 18.6 seconds
- Bed at room temperature: 24.5°C
- Time delay: 0 seconds for 1st sample, 20 seconds for 2nd sample

All 16 nozzles on the print-head were performing optimally and were used to print 50 layers of XSBR with and without time delay. Printing time can be reduced by using all or most of the working nozzles, as it decreases the time taken to print a single layer. However, in order to use most or all of the nozzles, it is necessary for all of the nozzles to be jetting properly.

A final sample of 100 layers of XSBR was printed onto a PET substrate using 3x2mm pattern, a total of 8 nozzles, and a time delay of 30 seconds between layers.

4.9.4 Printing onto a Heated Bed

Printing of 3x2 mm and 5x4 mm rectangle samples was carried out to determine what the effects of printing onto a heated bed are compared to printing the same size samples onto a non-heated bed at room temperature. The purpose of printing onto a heated bed was to determine whether the higher temperature would aid drying of the printed XSBR enough to counteract ink spreading and aid in creating a smoother surface.

The first printing trials involved printing a 3x2 mm sample on a PET substrate at room temperature (approximately 21°C) without the use of a time delay. 10, 20, and 30 layers of XSBR ink were printed onto a sheet of PET that was secured to the bed using the vacuum function of the bed, without a time delay with the bed at room temperature. The printing parameters included:

- Jetting voltage: 25V
- Cleaning cycle: 0.3second blot
- Printing height: 1000µm
- Nozzle temperature: off
- Meniscus set point: 4.0

Once printing was complete, the samples were carefully removed from the bed and placed in a sample petri dish. Using the Dimatix printing software, the bed temperature was changed to 60°C, another sheet of PET was secured to the bed using the vacuum function, and once the printer reached the desired temperature the printing was initiated to print another set of 10, 20, and 30 layers of XSBR ink using the same printing parameters.

4.9.5 Printing onto Different Substrates

During experimentation, it was necessary to print samples of latex ink onto various substrates to determine how the latex reacts when exposed to the different surface energies. The types of substrates that were used for printing onto included:

- PET
- Untreated glass microscope slides
- PTFE coated fabric
- PTFE tape
- Photographic paper

- Silicone coated baking paper

The silicone coated paper was the first substrate that the XSBR latex was deposited onto. The intention was to be able to remove or peel the printed sample off the substrate.

A 1cmx1cm square pattern was printed onto an untreated Fisher brand glass microscope. 5 layers of XSBR were printed onto the glass slide.

A substrate of weaved PTFE coated fabric was used to print 70 layers of XSBR onto. This substrate was chosen for its hydrophobicity in the hopes that this material property would facilitate the creation of samples with straight edges and to maintain pattern resolution by preventing the ink from spreading.

4.10 Multilayer Printing with XSBR and Carbon Black Ink

Printing trials were conducted with XSBR and conductive carbon black latex to create a multilayer printed material. There are many benefits to having a multilayer printed material, with the fundamental benefit being the control over the distribution of fillers. Similar printing jetting parameters that were detailed in section 4.9 were used to print both the XSBR latex ink and the conductive carbon black ink.

Two cartridges were used, one which contained the latex ink and the other the conductive carbon black ink. 2mL of the XSBR ink was filtered through a 5 μ m filter through a syringe and into the cartridge. With the cartridge filled the print head was attached and a purge was completed by hand. The same procedure was followed for the carbon black ink.

With the cartridge holding the latex ink installed in the printer and the jetting parameters entered, a 3x2mm rectangular pattern was selected for printing. The printing parameters included:

- 1 layer
- Bed temperature: 21°C (room temperature)
- 0 second delay between layers
- Printing height 1000 μ m
- 26V jetting frequency
- 6.8° print-head angle

Once a single layer of XSBR was deposited onto the PET substrate, the cartridge was removed and a cartridge filled with conductive carbon black ink was installed. The same

printing parameters that were used for the XSBR were also used for the carbon black ink. 3 optimally performing nozzles were selected and used to deposit a layer of carbon ink. This process was repeated until there was a total of 10 layers of carbon black sandwiched alternately between 10 layers of XSBR.

Another sample of a multilayer print with carbon black and XSBR ink was created using the same ink cartridges with print-heads, PET substrate, and the same overall process. However, for the second sample a first layer of conductive carbon black ink was deposited onto the PET, followed by a layer of XSBR, until there were 10 layers of carbon black and 10 layers of XSBR.

Multilayer printing was also carried out just with the carbon black ink. Several patterns were selected, ranging from a rectangle with small dots, to mesh or grid like patterns, and a rectangle pattern 7.5x6.5cm in size. The carbon black ink was loaded into a cartridge and the print-head was attached. Each pattern was printed onto PET with the bed temperature at 21°C. Single and 5 layer samples were printed without the addition of a time delay.

4.11 Curing, Solvent Swelling and Tensile Testing of XSBR combined with Resorcinol resin

Crosslinking, or curing, elastomers greatly improves their mechanical properties, which also results in a material that is less flexible than the pre-cured sample. The XSBR that was used for 3-D jetting did not have any pre-curing chemicals or treatment, hence the dried samples remained very elastic with some adhesive properties. Better mechanical properties are required for in-service use to equal the properties of existing conventional rubber components. Therefore, a resorcinol-formaldehyde resin from INDSPEC Chemical Corporation was combined with diluted latex. The complete mix is detailed in Table 4.6.

Table 4.6 XSBR and resorcinol curing resin mixture

Weight, g	
Water	29.1
NaOH	0.0455
Penacolite resin (50%)	4.58
XSBR latex (50% solids)	48.8
Water	17.5
Total weight %	100

The NaOH was combined with water and resin in a separate container, then mixed with the diluted XSBR latex. Once combined, approximately 3 g of the material was poured into 43x12mm diameter x height aluminium weighing boats and placed in a pre-heated oven at 60°C to dry overnight. The dried samples were then cured at high temperatures. A total of 5 samples were placed in an oven pre-heated to 180, 190, 200, 210, and 220°C for 30 minutes to determine the best curing temperature. 5 test tube containers were prepared with 10ml of toluene. Once the latex samples were cured, strips of each sample were cut and weighed before being placed into the test tubes for a 30-minute swell test. After the allotted time was complete, the samples were removed from their containers, weighed and the values recorded.

With the addition of the curing resin to the XSBR latex, it was necessary to cure the samples and to carry out a tensile test to observe what effect the curing resin had on the sample's properties. Four sets of samples were created, each with three dog bones of the same material. Temperatures that the samples were cured at were 190°, 200°, 210°, and 220°. A set of control samples with unmodified XSBR dog bones was utilised as a method of comparison.

A Ray-Ran RR/PCP pneumatically operated sample cutting press was used to cut cured and uncured samples of XSBR latex. The gauge length and width for the dogbone samples was 30 mm and 4 mm respectively. The Lloyd Instruments 10000 bench-top computer controlled dual column tensometer was operated to determine the tensile strength of the samples. A 1kN load cell was fitted to the machine and properly secured. Grips were attached to the central straining axis of the machine. Samples of XSBR dog bones were

secured in the grips and a 500mm/min test speed was specified in the computer system with a break detector set to 10N. This procedure was repeated for a total of 25 samples.

4.12 Multilayer Printing with XSBR Ink Combined with Resorcinol Resin

Multilayer printing was carried out with the XSBR ink combined with the resorcinol-formaldehyde curing resin to determine how well the mix can jet and whether the introduction of the resin would have an impact on clogging of the nozzles.

A 3x2mm rectangle pattern was used for printing with the same printing parameters utilised as detailed in section 4.9.3. Samples with 10, 20, 30, 40, 50, and 100 layers were printed to determine the impact of layer thickness when printing multiple layers with and without a time delay. A droplet analysis pattern as detailed in section 4.7 was also used to analyse the shape and size of the droplets.

4.13 Characterisation of Printed Latex

Various methods and equipment was used to determine the surface characteristics of the printed latex samples. As the latex samples that were printed were not cured and therefore retained their soft and pliable properties, it was necessary to carry out non-contact characterisation. These included:

- White light interferometry using the Taylor Hobson Talysurf CLI 2000, the Zygo Newview 5000, and Alicona InfiniteFocus
- Field emission gun scanning electron microscope (FEGSEM) by Carl Zeiss (Leo), model number 1530 VP
- Benchtop Scanning Electron Microscope by Hitachi, model number TM3030
- Polaron Emitech SC7640 Sputter Coater

The Talysurf CLI 2000 is a surface profiling system, capable of 2 dimensional or 3 dimensional analysis using either chromatic length aberration or laser triangulation. The Talysurf was used to determine the cross-sectional profiles of the printed samples by manually selecting an area of interest, positioning the white light beam at the centre of the sample, entering in the known dimensions of the sample and calibrating the measurement to begin 2mm in front and after the sample's surface footprint. Once the measurements were complete, the data was processed by the computer's software.

The Zygo uses white light interferometry for non-contact, 3-dimensional surface texture measurements and the user can also carry out an analysis on a variety of opaque or transparent surfaces. Quantitative results for the topographic features as well as surface properties can be gathered using the Zygo. This equipment was initially used to determine the thickness of the printed samples as well as the surface topography. However, the equipment can only be used to measure a small square-shaped section of a sample, making it difficult to obtain a definite thickness measurement; therefore the Zygo was used mainly to analyse the topography of the printed samples.

The FEGSEM was used to determine the finer features of the printed samples, such as satellite droplets, printing direction, to determine if the sample has spread or shrunk, and to determine the layer distribution. The Polaron Emitech SC7640 was used to sputter coat the samples with silver particles. Samples were mounted on steel stubs, a drop of diluted silver particles was placed on the corner of each samples, and they were loaded onto the specimen stage and the coating time set to 90 seconds. Initially the FEGSEM was used to attempt to determine the thickness of the printed samples, however the images were difficult to capture and it was not possible to obtain an exact measurement. The EHT of the equipment was set to 5kV and a working distance of 15mm was used.

The Hitachi benchtop scanning electron microscope was used to observe the multilayer printed samples with carbon black and XSBR latex ink. As with the FEGSEM, the equipment was set to 5kV with working distance at 15mm.

4.14 Electromagnetic Characterisation of Latex and Carbon Black

4.14.1 Combining Carbon Black with Latexes

The intention of combining carbon black with latexes is to determine how effective conductive carbon black is at shielding against EMI in a well dispersed form, compared to printed patterns and layers. The objective was to produce a solid latex sheet containing uniformly dispersed carbon black.

Initial trials to incorporate carbon black involved combining Conductex carbon black powder with liquid latex. The combination involved using 10mL of XSBR and CR latex, adding 1% concentration or 0.1g of sodium dodecyl sulphate (SDS) surfactant to both latexes. Once the surfactant was incorporated into the latexes, 10% concentration or 1g of carbon black powder was mixed in the liquids. This was followed by placing the containers

of XSBR and CR mixed with carbon black into an ultrasonic bath for half an hour to ensure a homogeneous mixture was obtained. This process yielded a more even mixture than attempting to incorporate the powder in the latex by hand. After the materials were combined, they were poured into 10cm diameter glass petri dishes and placed in an oven to dry overnight at 40°C. This low temperature was used to ensure that no cracks or deformations formed while the sample was drying.

Once the materials had dried and were removed from their petri dish containers, the samples were cut into squares and a hot-pressed sample was prepared with a 12x12 cm mould at 2mm thickness. Two sheets of Teflon were used between to prevent the latex from sticking to the steel mould. The moulding of the dried latex samples was carried out to ensure an even and flat surface for use in future dielectric measurements. The latexes were placed in their moulds in the hot press at 60°C for a total of 30 minutes per sample. However, once the latexes were removed from their containers, it was determined that some of the particles of carbon black had agglomerated during the period that they were drying in the oven.

Another conductive carbon black material to be used instead of the carbon black powder was procured from Bare Conductive, a company that specialises in creating a carbon black paste which can be used for drawing or painting fully functional circuits that can carry an electric current. The paste was used in a similar manner as the carbon black powder. 1, 2, 5, and 10 weight percentage carbon black concentration XSBR samples were prepared by diluting 0.3 g, 0.6 g, 1.5 g, and 3 g of the carbon black paste in 20mL of water before combining with 30g of XSBR latex. The samples were then placed in petri dishes in the oven at 65°C to dry overnight. Once dry, the samples were taken out of the petri dishes and two sides were cut to make a straight edge and the thicker lip that formed around the edges was removed in order to ensure the samples would be able to fit through the split post dielectric resonator (SPDR).

Using the carbon black paste instead of the powder facilitated the creation of a sample with homogeneously dispersed carbon black powder with no formation of carbon black agglomerates after drying.

4.14.2 Printing patterns with carbon black on PET and latex

Conductive carbon black ink was printed onto sheets of PET to determine its electromagnetic properties in different patterns and amounts. Although the patterns varied in shape and number of layers, the printing process remained the same for each one. The parameters that were utilised for printing included:

- Single layers and 5 layers printed for every pattern
- Bed temperature: 20°C (room temperature)
- 0 second delay between layers
- Bed vacuum function on
- Nozzle temperature off
- Cleaning cycle: 0.3 second blot
- Printing height 1000µm
- 26V jetting frequency
- 6.8° print-head angle

The patterns that were used included a large dot pattern, an octo grid, parallel lines, continuous rectangle, and dot grid. The patterns are illustrated in Figure 4.3. Multiple prints were made for each pattern (1 layer and 5 layers) in order to determine the effects of number of layers on the shielding properties. The size of the patterns was kept as similar as possible, with minimum measurements of 7cm for length and 6cm for width.

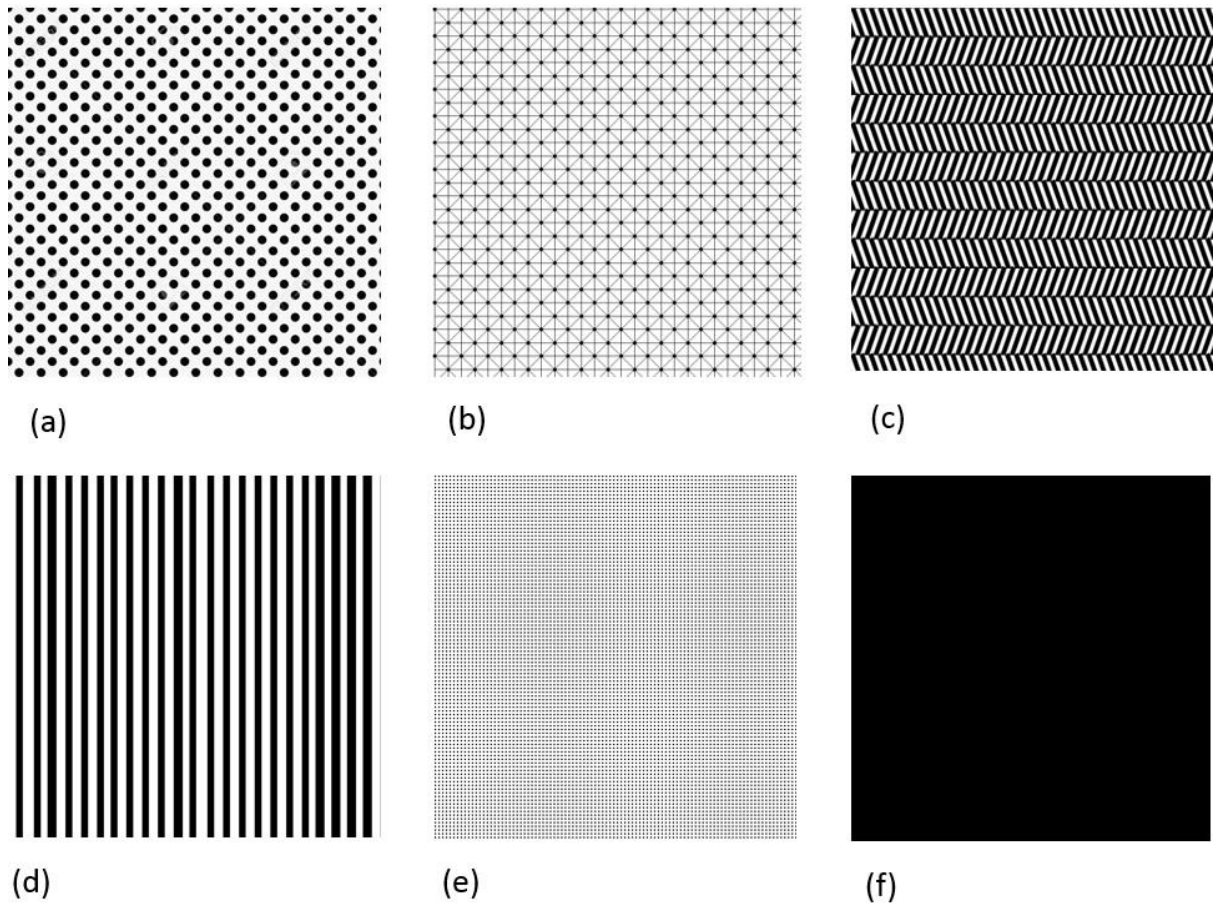


Figure 4.3 Patterns utilized for printing conductive carbon black onto PET substrates. These include (a) dot pattern, (b) octo grid, (c) parallel lines, (d) alternating chevron, (e) dot grid, and (f) continuous rectangle

The dielectric properties of these printed samples were measured in the SPDR (illustrated in Figure 4.4). This process is detailed in section 4.14.4.

4.14.3 Thermogravimetric Analysis (TGA) of carbon black concentrations

Thermogravimetric analysis was utilised to determine the carbon black concentrations in the XSBR samples. A TA Instruments Q5000IR was loaded with 7 samples into individual sample pans. The samples were cut into small pieces ranging in weight between 14mg and 18mg. Three samples were XSBR with different carbon black concentrations. These samples were made by combining 30ml of XSBR with 0.3g, 0.6g, and 1.5g of conductive carbon black paste from Bare Conductive diluted in 10ml of de-ionised water. This diluted carbon black paste was combined with the 30ml XSBR, then cast in a glass petri dish with a diameter of 5cm until dry. One sample was 100 layers of XSBR ink that was ink jetted onto PET without carbon black and was used as a control sample. It was removed from the PET substrate before the TGA tests was conducted. Two samples were nitrile rubber with varying concentrations of carbon black powder that were pre-made in a rubber internal mixer and moulded using a hydraulic hot press. One of these samples was nitrile rubber with a 55 parts per hundred rubber (phr) concentration of carbon black, and the second contained 25% phr carbon black. Pre-cut squares of these materials were placed in the centre of a 12 cm by 12 cm steel mould with 3 mm thickness. The mould was sandwiched between two sheets of high temperature resistant PTFE coated fabric to prevent the polymer from adhering to the hot press plates. Temperature of the hot press was set to 200°C and the materials were pressed by applying approximately 5 tonnes of pressure.

In the TGA test the samples were in a containment unit filled with nitrogen gas for the first half of the test. The samples were heated to 700°C. Upon the completion of the analysis, the furnace was allowed to cool to 350°C. Once at 350°C, oxygen was introduced into the oven and the temperature gradually increased to 700°C to burn off the remaining carbon residue of the samples.

4.14.4 Dielectric measurements

The electromagnetic characteristics of the latex and carbon black was measured using a split post dielectric resonator (SPDR) at 2.4GHz. The equipment that was used to calibrate the frequencies for the SPDR is the Anritsu 37397D Vector Network Analyzer. Each material that was used for analysing was placed in the metal enclosure of the SPDR. A simplified schematic of the SPDR is illustrated in Figure 4.4.

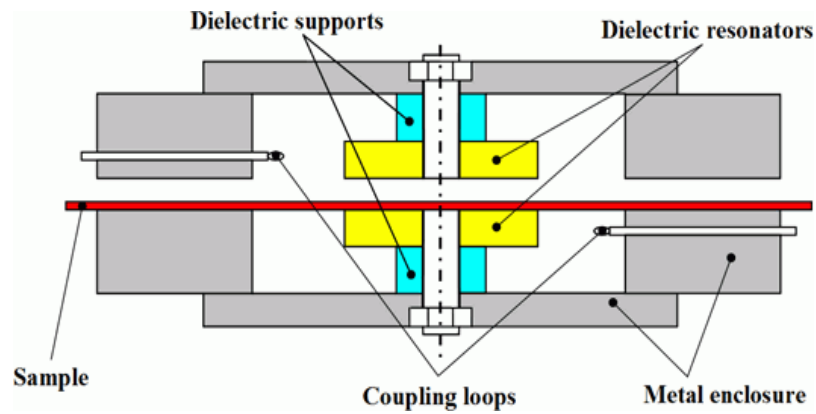


Figure 4.4 A simplified schematic of the SPDR that was used to carry out dielectric tests on the latex materials [1]

In the schematic, the red line labelled “Sample” is where the materials were placed for measuring. These measurements were obtained to measure the permittivity as well as the loss tangent values of the latex materials in order to observe what the effects of the addition of conductive carbon black have on the ability of the materials to provide shielding against EMI and RFI.

The conductive carbon black samples printed onto PET were measured using the SPDR. Despite PET not being a material that exhibits significant dielectric properties, an 8x7cm rectangle of PET was placed inside the gap between the dielectric resonators and the machine was calibrated to read the PET as “empty”, which therefore made it possible to measure the properties of the carbon black patterns exclusively. Before the measurements could be carried out, it was necessary to enter in the thickness values for each sample measured. White light interferometry was used to determine the thickness of the printed carbon black patterns beforehand, which was approximately 0.1 μ m for the single layer carbon black, and 0.2 μ m for 5 layers of carbon black patterns. Approximately 10 readings were carried out for each sample measured to ensure that the variations are minimal and that the results are reproducible. The computer software installed on the laptop that was used for carrying out the SPDR measurements recorded the values for the dielectric loss tangent, permittivity, +3dB and -3dB, and the Q value. When the measurements were completed, the results were copied and saved onto an Excel spreadsheet for study.

The same process was repeated for other samples used to measure the dielectric properties. Sheets of plain XSBR, XNBR, CR, and HNBR were cast in large 15cm diameter petri dishes and cut into rectangles with a minimum length of 8cm and width of 7cm. The

thickness of each samples were measured with a micrometer and an average thickness value was entered into the computer software before the dielectric measurements were taken for each cast sheet.

To carry out simulations for this experiment to observe the effects of propagation of interference signals through shielding material, EMPIRE XCcel V6 software was used. Two monopole antennas were modelled in the software, one antenna to emit the interference frequencies and the second placed behind a simulated shielding material (RF-45-0620 Taconic). The monopoles were spaced 30cm from each other, with the shielding material in the centre (15cm distance between both antennas). Figure 4.7 illustrates the monopole design measures that were used. Frequencies of 3.25 and 3.6 GHz were entered into the simulation software for modelling the wave propagation through the substrate.

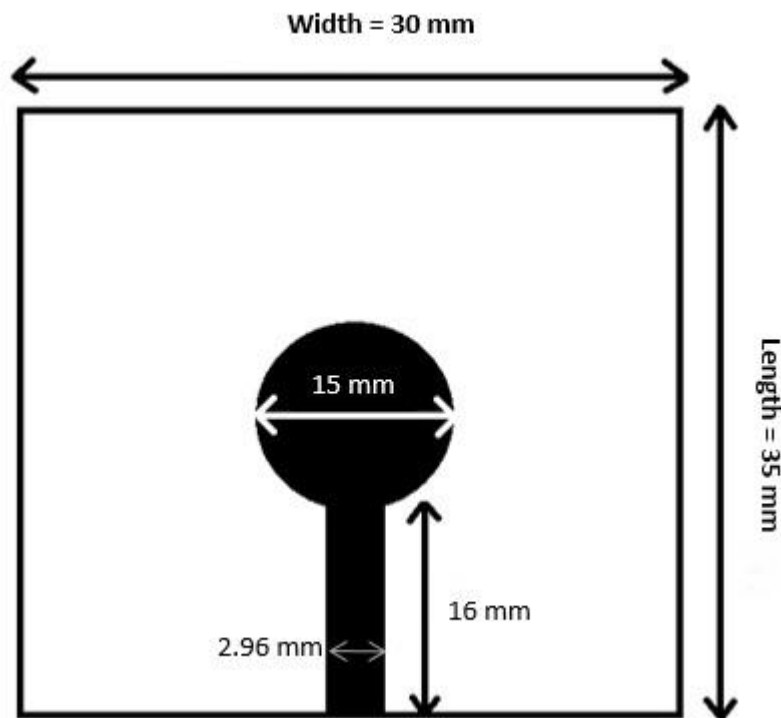


Figure 4.5 Monopole antenna design and measurements

4.15 Conclusion

This chapter has detailed the experimental methods used to carry out research into inkjet printing and determining dielectric properties of the tested materials to calculate the shielding effectiveness. Listed properties of the elastomers materials obtained from the manufacturers were detailed so that a comparison and verification of the values could be

made in the following chapter, and details of the measurements, printing processes carried out for elastomeric and carbon black inks specified, as well as the patterns utilised.

References:

- [1] Rudnicki, J. *Software for Electromagnetic design*. (2016). Available at: http://www.qwed.com.pl/resonators_spdr.html (Accessed: 22 February 2017).
- [2] Ramehart.com. (2017). Surface Tension. [online] Available at: http://www.ramehart.com/surface_tension.htm (Accessed: 20 December 2017).

Chapter 5: Results and Discussion

5.1 Liquid Latex Properties

This section details the measured properties of the latexes, which include surface tension, viscosity, and particle size. These are the three main properties which can determine whether latex has the potential for ink jetting.

5.1.1 Surface Tension

Initial surface tension tests were carried out to determine the inkjet printing viability of the original latexes. The results of these measurements are illustrated in Figure 5.1.

Initial contact angle measurements, show that the highest average surface tension value is 48.9 mN/m for the XSBR and the lowest average at 30.8 mN/m for HNBR, with a standard deviation of 0.4 and 0.2 respectively. Previous research suggests that inks with high surface tension used with inkjet printing technology would not be jettable due to the creation of unstable droplets and satellite droplets [1-3]. The creation of unstable droplets results in no control over the printing resolution. Although conventional methods recommend the ideal surface tension values for inkjet inks to be between 20 and 30 mN/m, this does not automatically disqualify materials with higher values from ink jetting consideration. For example, the high surface tension of the XSBR and CR latexes, could possibly be reduced by introducing surfactants if required.

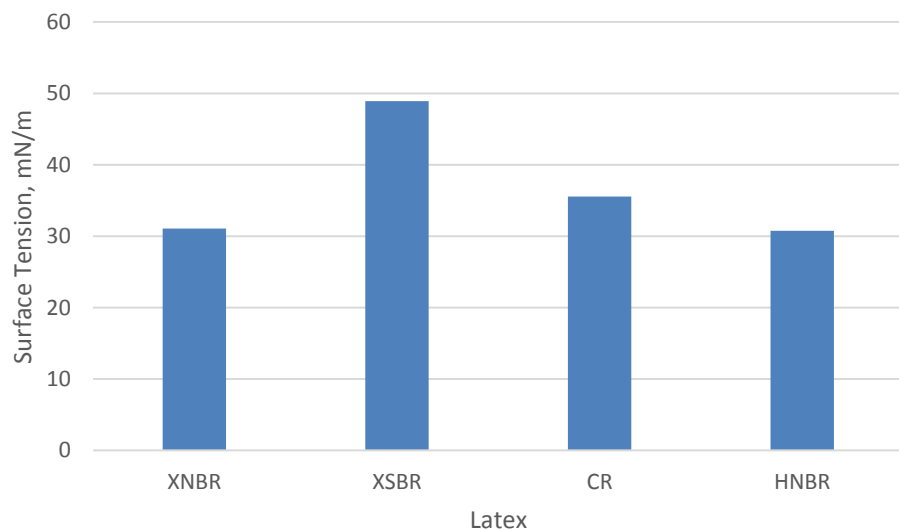


Figure 5.1 Surface tension of the latex

5.1.2 Viscosity

Viscosity was initially measured using a Brookfield viscometer (Figure 5.2). Ideal viscosity levels for inkjet inks are between 10-20 cp [4]. According to these results the most suitable latexes for inkjet printing are the XSBR and the CR. However, the Brookfield viscometer does not provide enough information about the effect of strain rate on the dynamic viscosity of the latex. This is important to consider since it is likely that the latexes may have strain rate dependent viscosity and the strain rate during ink jetting can exceed 1000 s^{-1} [9]. High strain rates can cause a reduction in viscosity during printing, which is caused by stretching the natural coil shape of the polymer [5] and it is possible that this will also apply to a polymer latex. Therefore, a parallel plate rheometer was used to determine the shear viscosity, of the latexes over a range of strain rates. The shear viscosity results obtained from the parallel plate rheometer are illustrated in Figure 5.3. The test subjected the latex materials from low shear rates to very high shear rates of up to 1000 s^{-1} . As is the case with most elastomers, in these results we can observe that shear thinning is occurring, where the shear viscosity of the latexes decreases as the shear rate increases. The viscosity values at low strain rates are 11 mPa s for XSBR, 7.5 for CR, 2.8 mPa s for XNBR and 3.3 mPa s for HNBR. These values are similar to the Brookfield viscosity measurements, which were 12 mPa s for XSBR, 12 mPa s for CR, and 4 mPa s for XNBR. The slight discrepancies between the 2 sets of values can be attributed to the less accurate manual operation of the Brookfield viscometer. Viscosity at high strain rates, up to 1000 s^{-1} , which may be more relevant to the ink jetting process, are lower than 5mPa s [2].

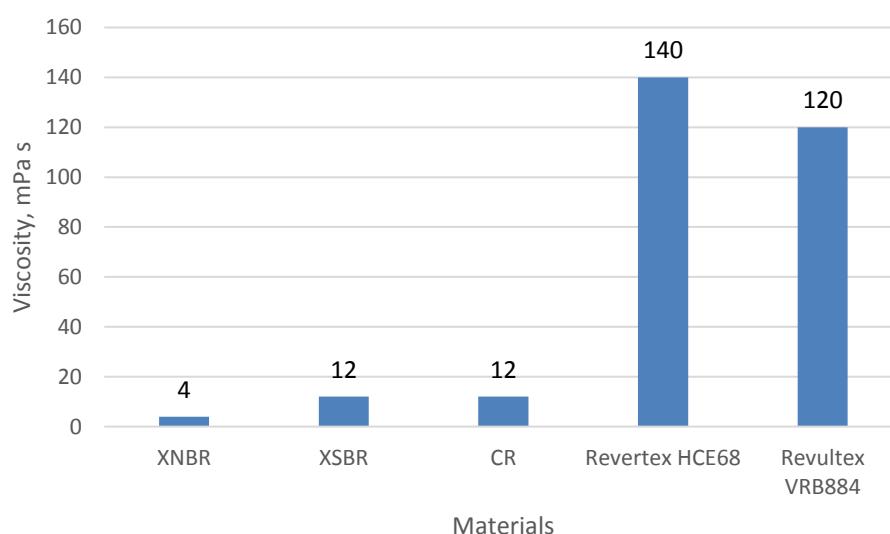


Figure 5.2 Brookfield viscosity for latexes

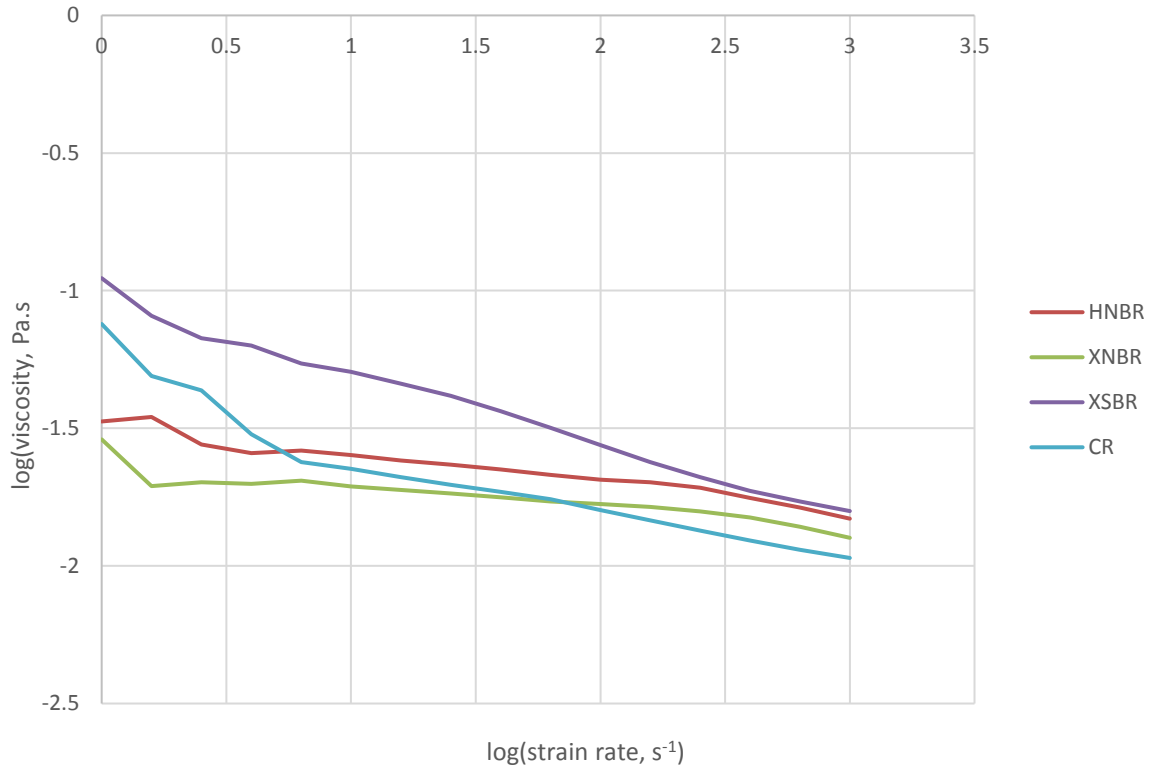


Figure 5.3 Shear viscosity of latex measured using the parallel plate rheometer

During the test the latex materials have remained stable with no agglomeration and there were no unexpected complications. These results suggest that even when exposed to high shear stresses that could be produced inside the printer, the latex will remain stable. The strain rate measurements obtained for XSBR and CR show the viscosities are within an acceptable range for good printing. Values for XNBR and HNBR are too low for ideal printing, which indicates that obtaining stable jetting and droplets as a potential problem.

5.1.3 Particle Size

One of the key factors when creating a novel colloidal suspension ink for additive manufacturing is the particle size of the material. 3-D jetting print heads have small nozzle diameters and it is imperative that the size of the particles does not exceed 10% of the size of the nozzle to avoid damaging or clogging the print head. The 10 picolitre print heads that were used for the Fujifilm Dimatix printer have a nozzle diameter of 21 μ m, therefore the ideal particle size of the latex ink should be less than approximately 2 μ m.

A Malvern Mastersizer was used to determine the size of the latex particles for XNBR, XSBR, CR, HNBR, Revultex and Revertex latex. The averages of 10 measurements are shown in Figure 5.4 with the size values represented on a logarithmic scale. The latexes that appear to have particle sizes ideal for ink jetting, because they contain no particles greater than 2 μm , are XSBR and CR. By contrast, the HNBR, XNBR, Revultex and Revertex latexes also have larger particle sizes present that may cause clogging problems. The expected particle size for latexes vary between 0.085 to 0.330 μm [9], depending on the type of latex and the manufacturing process. Therefore, the considerably higher particle sizes observed for some of the latexes indicate that some agglomeration may be taking place.

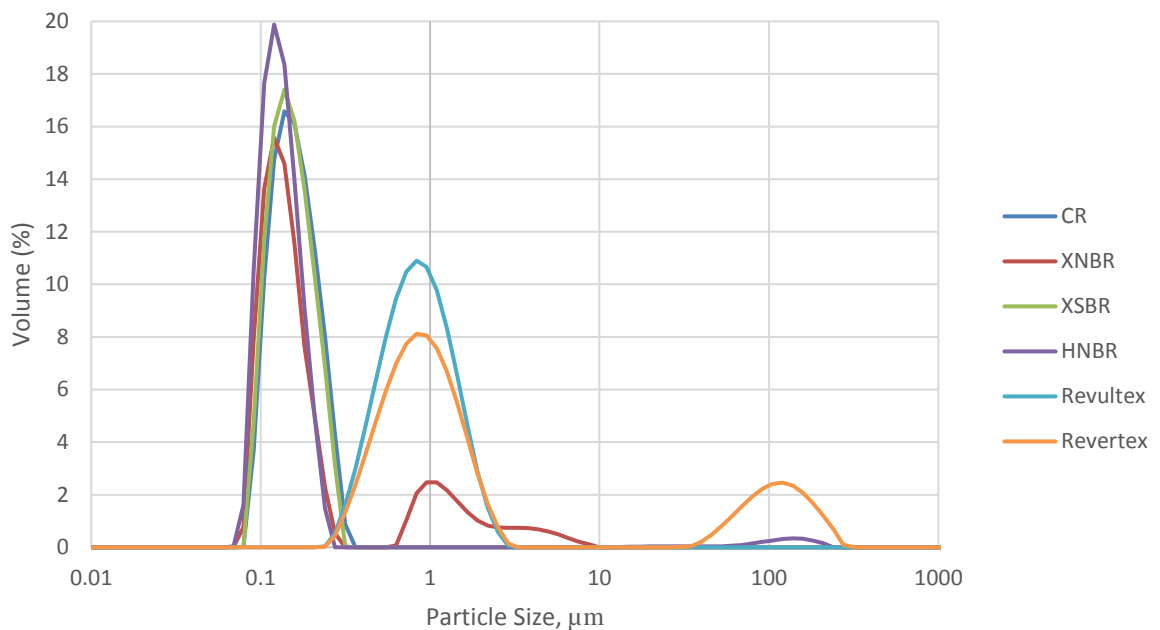


Figure 5.4 Particle size distribution results for latex

One of the issues with colloidal inks that can arise is agglomeration of particles. In Figure 5.4 we can see that the XNBR, HNBR, Revultex and Revertex appear to have some particle agglomeration, due to the secondary peaks that are observed at large sizes, particularly at 1 and 100 μm . This agglomeration is possibly due to a slightly unstable colloidal suspension being left in their containers for extended periods without undergoing ultrasonication or mixing. A possible solution for this was to carry out an ultrasonic treatment of the latex that would break the agglomerated particles apart. This does involve exposing the liquid and particles to very high vibrations, which can cause the liquid itself to

heat up due to intense friction if the ultrasonic treatment is performed for a long duration. Due to this reason, the ultrasonic treatment was limited to 60 seconds.

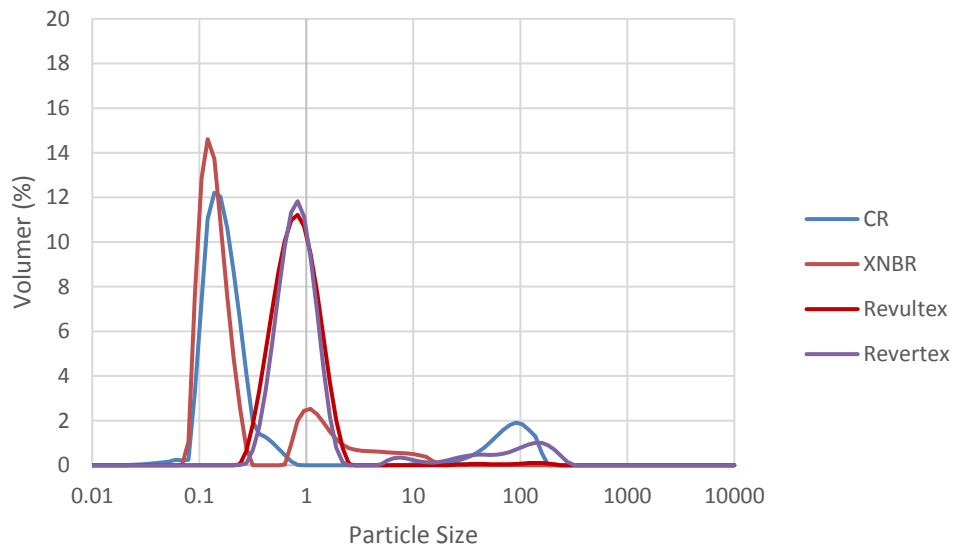


Figure 5.5 Particle size analysis of latex with 60 second ultrasonic treatment

Particle size distributions of four of the ultrasonically treated latexes are shown in Figure 5.5. The results indicate that an ultrasonic treatment of the latex inks exacerbated the problem of agglomeration. The aggravated agglomeration is likely caused by the vigorous sonication process, where the colloidal latex particles near the sonication probe forcefully collide with surrounding particles, causing larger agglomerates to form. The results indicate that, unfortunately, sonication cannot be used to solve the latex agglomeration problem and therefore, that a latex showing no agglomeration, such as XSBR, should be used in the initial printing trials.

5.2 Preliminary Printing Trials

The first printing trial involved printing a layer of unmodified XSBR liquid latex in a 2 cm by 2 cm square pattern onto silicone coated paper substrate. The XSBR was prepared and loaded into the cartridge by filtering the latex through a 5 μ m filter. No agglomeration or obstruction was noted during this procedure. The print head was attached to the cartridge and a manual purge was carried out using a syringe to create positive pressure within the cartridge, expelling the liquid XSBR through the nozzles. Once the nozzles were cleaned, and a clean filter was installed in the printer, the ink was loaded onto the head attachment and a print was initiated. A cleaning cycle was also utilised for every 20 passes that the

printer made. After the single layer was printed, the substrate was removed and the area where the print was carried out was observed. Upon inspection, it was found that no material was jetted from the nozzles, which indicated a blockage. The print head was removed and cleaned before attempting the same process, albeit with no improvement. It was determined that there was an underlying problem with the material, however there was an uncertainty whether the issue lay with the viscosity, surface tension, or particle size. After extensive material analysis that determined that the values and properties of the XSBR material were within the normal printing range as specified in the Fujifilm Dimatix manual, it was determined that another problem was present. It was determined that the XSBR was drying too quickly inside the nozzles and causing blockages. One solution to prevent quick drying was to dilute the XSBR.

The XSBR was diluted to 25% solids content with 1% Triton surfactant added to the diluted XSBR to attempt to reduce the risk of any agglomeration occurring. As for the previous test, 10 layers of diluted XSBR were printed onto silicone coated paper in a 2 cm by 2 cm square. A side angle photographic image taken of the printed diluted XSBR is given in Figure 5.6. Although the printing was successful, a significant problem was that frequent cleaning cycles needed to be introduced during printing to delay nozzle clogging.



Figure 5.6 Photograph of 10 layers of diluted XSBR printed using a 2cm x 2cm square pattern onto silicone coated paper

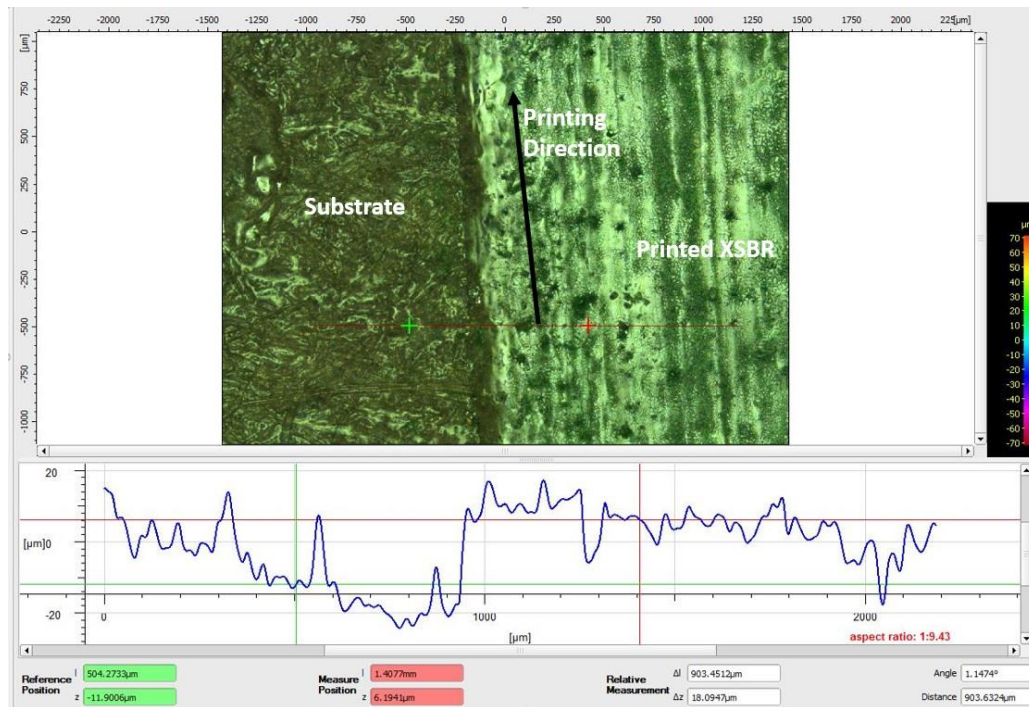


Figure 5.7 Thickness measurement and topography analysis using the Alicona white light interferometer

Once a printed sample was successfully created, it was necessary to analyse the topography and thickness of the XSBR. In order to do that, white light interferometry using the Alicona device was implemented, as illustrated in Figure 5.7. The thickness was recorded at approximately 18 μm. One of the advantages of using the Alicona is that the data can be used to present a 3D image of the sample. A 3-D representation of the printed sample is provided in Figure 5.8.

From Figure 5.8, it is apparent that the surface topography of the paper substrate is very rough. This is a concern as it can affect the topography and resolution of the 3D print. These results prompted the next printing experiments to be carried out on smoother and more uniform substrates. Towards the centre of the printed latex (the right-hand side of the image in Figure 5.8) it is possible to observe the printed lines of XSBR, which give a slight wave pattern on the surface. The profile and 3D results indicate that white light interferometry is a good method of assessing both the thickness and surface topography of the printed latex.

The first printing trial was successful in that it showed it is possible to print with an elastomer latex, however, the repeated clogging of the nozzles was a serious problem. The next section describes how the latex inks were developed to avoid this problem.

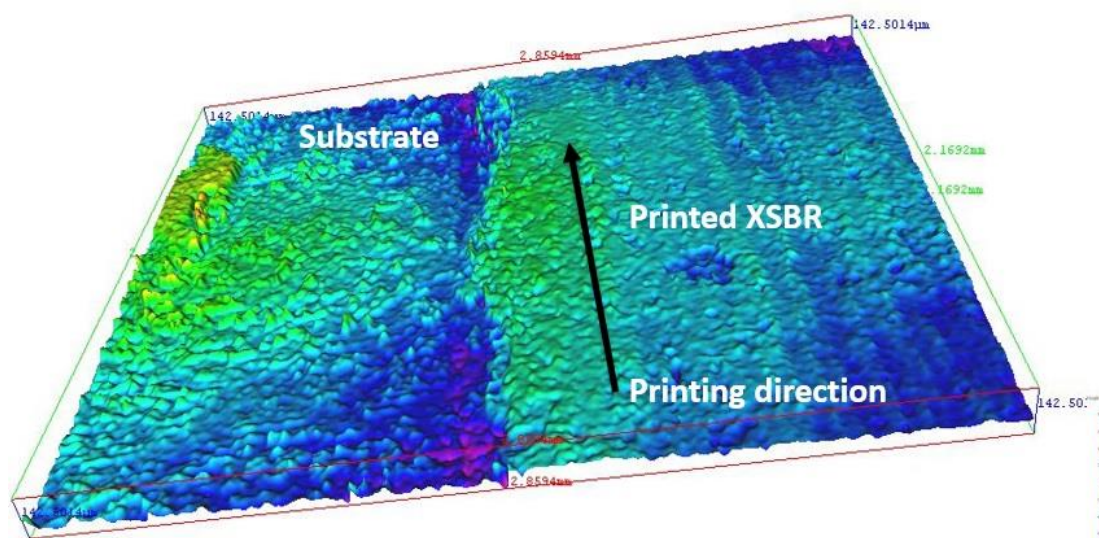


Figure 5.8 A 3-D image of the printed XSBR generated by the Alicona white light interferometer

5.3 Development of a Latex Ink

One concern that was identified early in the research was the drying time and behaviour of XSBR latex. Undiluted, the XSBR latex dried quickly to form a film first while the latex remained a liquid underneath. This caused tension on the top layer during drying that created cracks and breaks that would cause the dried sample to separate into segments. This posed an issue for ink jetting, as such small quantities of latex were used that the latex dried almost instantly inside the print head and caused blocked nozzles. Research was carried out to investigate the possibility of delaying evaporation. Initially experimentation was undertaken to dilute and reduce the solids content of the latexes with de-ionised water, as discussed in the previous section. Diluting XSBR with de-ionised water, although lowering the solids content overall and preventing latex particles from blocking the nozzles, did not delay evaporation enough to ensure repeatable printing. Therefore, humectants were given consideration, and triethylene glycol monomethyl ether (TGME) was selected as it is a humectant that is widely used in the ink jetting industry, especially with experimentation carried out for novel ink material development.

5.3.1 Effect of TGME on drying time of XSBR latex

Experiments were carried out to determine how the concentration of TGME affects the drying time of XSBR. Figure 5.9 illustrates the percentage of weight lost for undiluted XSBR containing varying amounts of TGME samples over a period of 24 hours at a temperature of

60°C. The temperature was chosen to simulate the platen temperature in the Dimatix printer. The layer of latex was relatively thick (approximately 3mm in this experiment compared to the very thin layers (3 to 6 μm) produced during printing. Consequently, a much longer drying was used in this experiment than would be used in printing. However, it is assumed that the relative effect of TGME on drying will be similar in both cases.

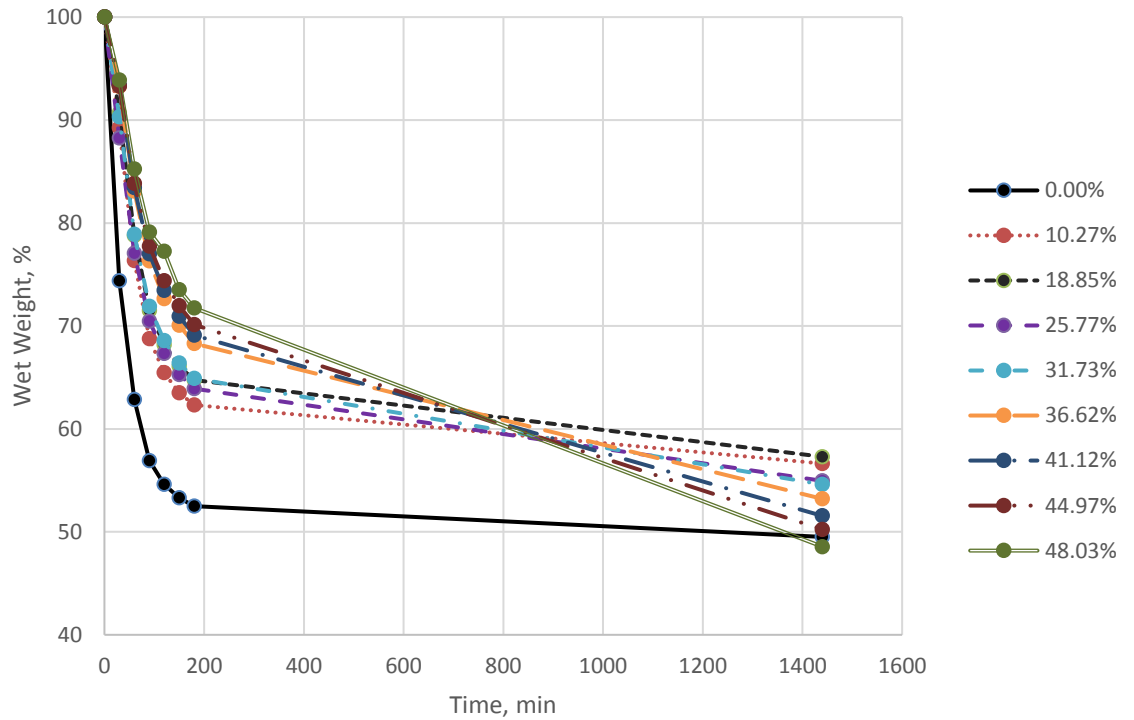


Figure 5.9 Effect of TGME on drying of XSBR latex at 60°C. The percentage rates displayed in the legend refer to the wet weight % of TGME

The graph in Figure 5.9 is a little difficult to interpret because with increasing TGME content the solids content decreases so it is difficult to see how much liquid remains. For this reason, the remaining liquid content was determined by subtracting the calculated rubber solids content from the total remaining weight. Assuming that the water evaporates first and that all the TGME remains until all the water has evaporated then the amount of water remaining after 180 min. at 60°C was calculated and is shown in Figure 5.10. The graph shows that 5 to 10% TGME results in a significant retention of water compared to the pure latex. Perhaps surprisingly, higher TGME contents did not result in more retention of water. It was noted that the higher TGME contents did show some agglomeration of the latex and this could have resulted in slightly greater drying by preventing a skin of latex forming at the surface and inhibiting drying.

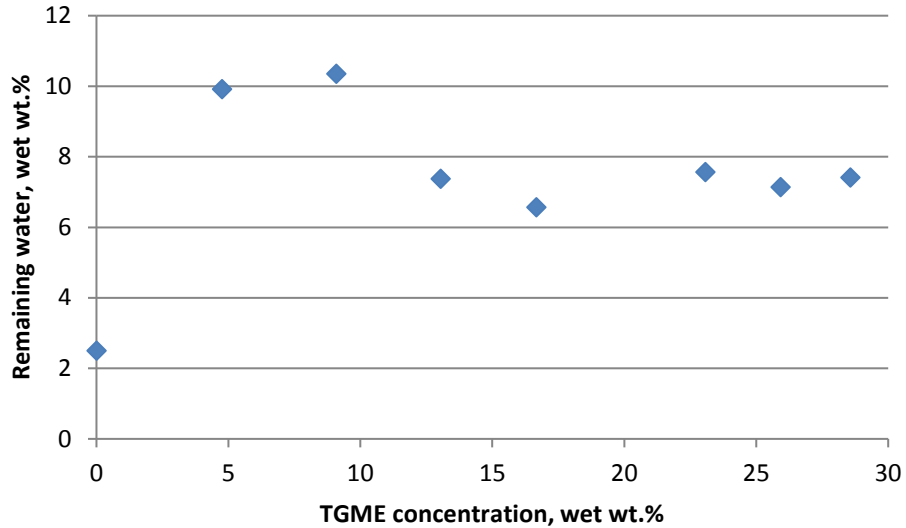


Figure 5.10 Effect of TGME on water content after drying at 60°C for 180 min.

A potential problem of adding TGME is that it could remain in the latex after drying and so affect the properties of the dried latex. To assess this, the amount of remaining liquid, after 24 hours was determined and is shown in Figure 5.10 as a percentage of the final dried weight. As in the previous example, it is assumed that all the water will dry first, followed by the TGME. The graph shows that some water still retained after 24 hours of drying for the 5 and 10% TGME contents, confirming the increased drying time. However, all samples show significant amounts of TGME remaining after drying, which is clearly undesirable. A further drying experiment was carried out at a higher temperature of 120°C for 1 hour. No water remained after this time but a small amount of TGME did remain (Figure 5.11). The result does suggest that by using a sufficiently high bed temperature during printing all the TGME could be removed from the latex material.

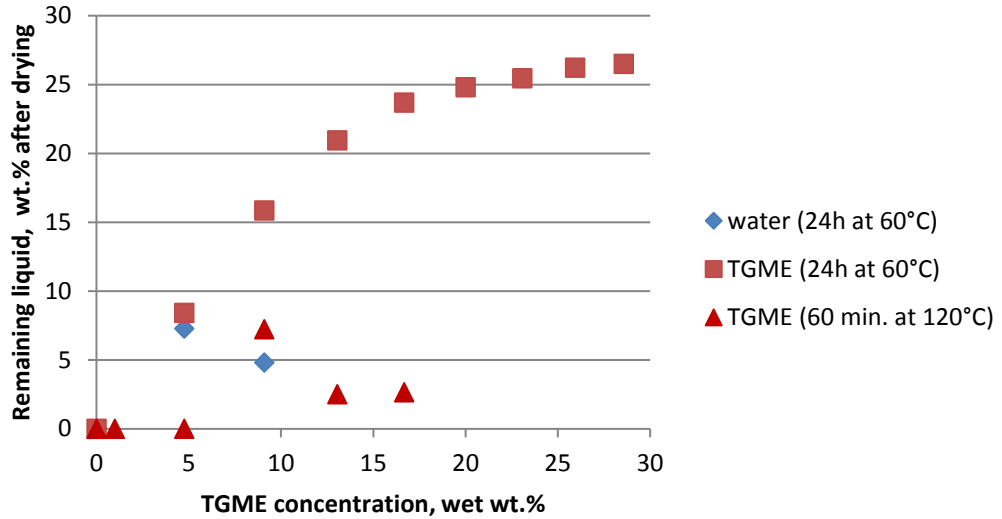


Figure 5.11 Effect of TGME concentrations on remaining liquid after drying at 60°C for 24 h

The results confirm that both dilution and the addition of TGME could have a positive effect on reducing clogging due to premature drying in the nozzle. It was then necessary to consider how dilution and TGME addition affected the properties of the latex. The diluted latexes with TGME added are referred to as “inks”.

5.3.2 Surface Tension

The surface tension of the modified latexes was tested to determine how the addition of humectants and de-ionised water affects the surface tension of each material (Tables 5.1 – 5.3).

Table 5.1 Surface tension of latexes in their original form

	Original			
	XNBR	XSBR	CR	HNBR
	31.13	48.82	35.52	30.64
	31.02	48.98	35.53	30.68
	31.06	48.87	35.5	30.83
	31.01	48.89	35.64	30.85
Average	31.055	48.89	35.5475	30.75

Table 5.2 Surface tension of latexes diluted with de-ionised water to 33 % solids content

	50% dilution			
	XNBR	XSBR	CR	HNBR
	31.11	50.82	37.26	31.02
	31.23	50.52	37.47	31.24
	31.22	50.07	37.48	31.21
	31.09	50.2	37.47	31.11
Average	31.1625	50.4025	37.42	31.145

Table 5.3 Surface tension of latex inks, diluted with deionised water and with 10 wet wt.% TGME (solid content = 33 wet. wt.%)

	Ink composition			
	XNBR	XSBR	CR	HNBR
	32.1	45.91	37.1	30.96
	32.16	45.84	37.25	30.96
	32.17	45.98	37.32	30.99
	32.17	46.03	37.22	31.05
Average	32.15	45.94	37.2225	30.99

The latexes were diluted from 50% solids content as supplied by the manufacturer to 33% solids content using de-ionised water. It might have been expected that dilution with water would cause an increase in surface tension of the diluted latexes because of water's high surface tension (72 mN/m). This is significant as high surface tension could hinder the jetting process and cause problems during the printing such as increased amount of satellite or debris droplets. Debris droplets are formed during the jetting process at the nozzle exit due to the liquid ink residue that is formed after every cleaning cycle is completed. During jetting, the main droplet is ejected but due to surface tension some residual ink is pulled with the droplet and breaks off to fall near or around the printing perimeter. However, diluting the latexes caused no significant change in surface tension for XNBR and HNBR XSBR and CR both experienced only a slight increase in surface tension by almost 2 mN/m (Table 5.2). The final measurements involved adding 10 wet wt % of triethylene glycol monomethyl ether (TGME) humectant into the already diluted samples of latex. The addition of the humectant appears to have a favourable effect on the surface tension, reducing the values from 50.4 mN/m for the diluted XSBR to 45 mN/m. The values for XNBR and CR increased,

which could be due to the interaction between the latexes and the humectant which was observed to cause particle agglomeration.

The surface tension values do not appear to increase significantly with the addition of even a substantial amount of de-ionised water, which is favourable. However, the addition of the humectant appears to reduce the surface tension of the XSBR slightly, while increasing the values for the other latexes. The addition of the TGME humectant did not cause a particle agglomeration for the XSBR latex. These results confirm the conclusion for the other experiments that the XSBR latex is the more favourable material to use for ink jetting.

5.3.3 Viscosity

During the initial viscosity measurements, it was evident that the latex materials were experiencing shear thinning as the strain rate increased (Figure 5.3). Further measurements were carried out to determine what effect diluting the latexes would have on the shear viscosity, as well as determining the effect of adding the humectant.

The samples that were diluted to 33% solids content showed generally lower viscosities than the undiluted latexes, as expected. However, the diluted latexes also experienced fluctuations in shear viscosity as is evident in Figure 5.12 it is possible that the fluctuations in viscosity may have been because the samples began to sputter around the edges of the parallel plates. Results for the diluted samples with 10 wet wt.% of TGME (referred to as ink) are shown in Figure 5.13.

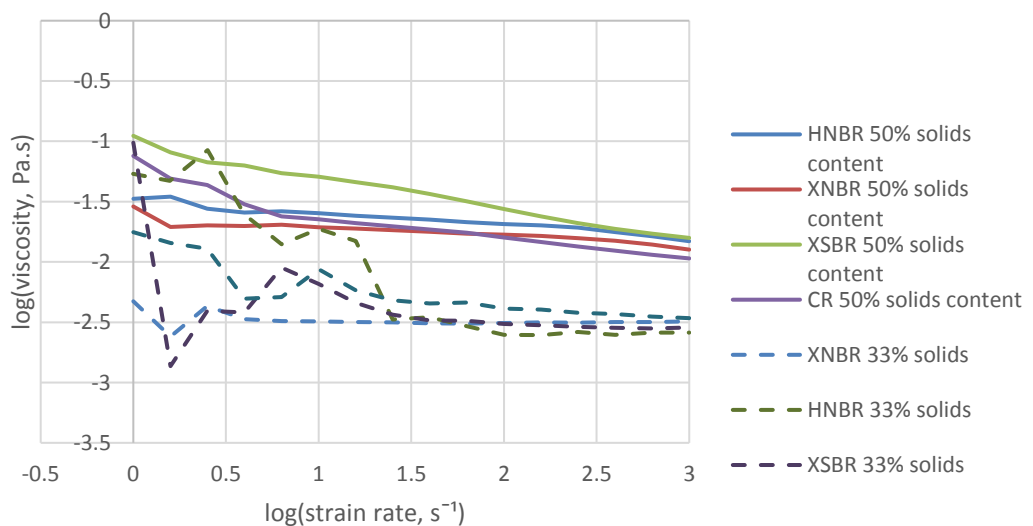


Figure 5.12 Shear viscosity measurements for original and diluted latex

When the results of the diluted and undiluted latex samples shown in Figure 5.12 are compared, it is evident that the shear viscosity of the diluted materials contains anomalies, with viscosity varying widely in the low to medium strain rate region. Despite repeating the measurements with identical measurement parameters, the results for all the diluted samples exhibit the same abnormalities. However, it is evident that the addition of de-ionised water in all the latex samples has reduced viscosities for all latex materials. Despite the decrease in the viscosity values, the latex materials would still be suitable for printing, but the performance of the diluted materials during shear viscosity measurements is a concern as any fluctuations caused inside the inkjet printer when exposing the ink to shear forces could potentially destabilise the droplets, causing ink to be jetted improperly and possibly create a significant amount of satellite droplets.

Despite the troubling effect of dilution on viscosity at relatively low strain rates, the addition of a humectant to the latexes was carried out for all materials. The results for the modified latexes, referred to as inks, are shown in Figure 5.13.

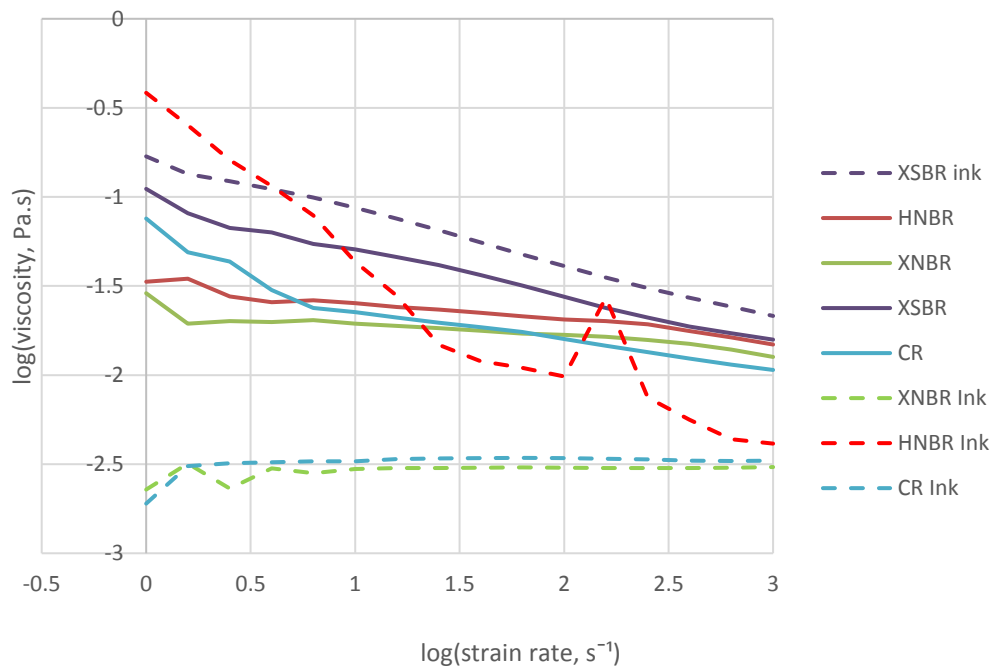


Figure 5.13 Shear viscosity measurements for original latex and latex ink

Results displayed in Figure 5.13 illustrate shear viscosity measurements obtained from unmodified latex materials and latex that was diluted to 33% solids content and the addition of 6.6 wet wt.% TGME (1 mL TGME humectant) with the same parameters used

to obtain the results. HNBR shows extreme shear thinning, unlike the other inks. Upon the completion of the measurements, it was discovered that particle agglomerates had formed in the HNBR sample after it was dispensed in the shear rheometer, which was caused by the addition of TGME. This is a likely explanation for the higher viscosity and shear thinning that was recorded during the start of the test, causing the abnormality in the results for the material. Particle agglomerates also formed for XNBR when TGME was introduced, which indicates the possibility that the addition of a humectant with glycol to latexes with nitrile rubber causes the latex particles to coalesce.

The addition of TGME appears to have increased the viscosity of the XSBR slightly, despite the material being diluted to 33% solids content. The increase in viscosity should not negatively impact the jetting ability or performance of the XSBR ink as the viscosity values fall within acceptable values for jetting with the Dimatix Inkjet Printer. After the measurements were complete the sample was examined for any particle agglomerates. None were detected; therefore, the conclusion was determined that it was the addition of the humectant that caused the slight increase. Upon analysing the shear viscosity results for XSBR, it was determined that despite the slight increase in viscosity, the material is suitable for ink jetting as the shear thinning is stable and no agglomerates were found in the sample. CR and XNBR however do not show any shear thinning but have very low viscosities, which is likely due to the agglomeration of latex particles that was discovered once the measurements were completed. This result could impact the jetting performance as low viscosity inks are more susceptible to producing unstable droplet ejection. However, a simple solution to stabilising droplet ejection for low viscosity inks is available and involves modifying the jetting voltages of the nozzles while drop jetting is being observed.

5.3.4 Particle size

Particle size measurements were carried out for latex inks prepared for printing by diluting the original latex with de-ionised water to 33% solids and adding 10 wet wt. % TGME humectant. Figure 5.14 illustrates the particle size results collated for the latex inks.

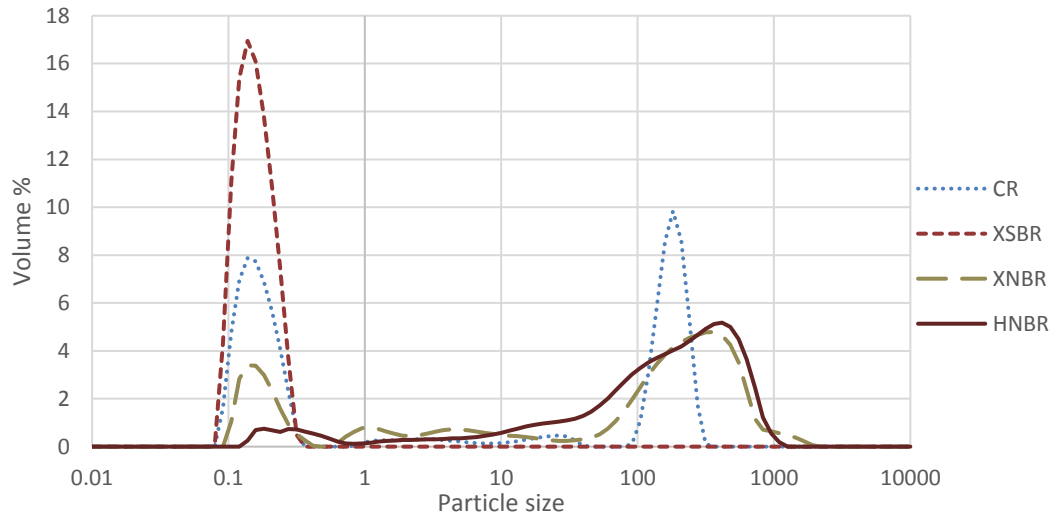


Figure 5.14 Particle size distributions for CR, XSBR, XNBR, and HNBR inks

Analysing the results presented in Figure 5.14 it is evident that the modification to the HNBR, XNBR, and CR has affected the particle size results. When compared to Figures 5.2 and 5.3, there is a drastic increase in particle sizes greater than 10 μm, showing agglomeration has occurred for these three materials. This agglomeration was observed visually after modifying the latexes. An extreme agglomeration reaction occurred with the diluted CR sample after combining TGME. A large solid cluster of agglomerated CR formed at the bottom of the glass tube container. The particle size analysis was carried out on the remaining liquid after the cluster was removed. Due to this reaction with TGME however, it was concluded that CR would not be an ideal latex for ink jetting.

The agglomeration that occurred with XNBR and HNBR was not ideal, however there was no extreme reaction as observed with CR. These results do represent a problem with regards to printing as it would be detrimental to the print head to use an ink where the latex particles can agglomerate to a great extent that clogging would occur. The XSBR ink showed no agglomeration and so is conformed as the preferred latex ink for further printing trials.

At the end of this ink development process, it was concluded that an XSBR ink based on latex diluted to 33% solids and with 10% TGME added would be the best ink to use in further ink jetting trials. This composition was found not to agglomerate, while the dilution and addition of TGME increased the drying time and so would be expected to reduce the nozzle clogging problem observed in the first printing trial.

5.3.5 Z number

After the material properties were measured and the results compiled, the Ohnesorge number was calculated for the latexes. The inverse of the Ohnesorge number, Z , is the ratio between the Reynolds number and the square root of Weber number and is used in calculations and simulations to determine whether stable droplets of ink can be generated by an inkjet printer. The results for the Z number of the latexes that have been considered in this project are detailed in Table 5.4.

Table 5.4 Properties of the inks related to their printability (Z)

<i>Materials</i>	Upper Decile particle diameter (μm)		Surface Tension (mN m^{-1})	Viscosity (Pa s)	Z
	<i>Before Sonication</i>	<i>After Sonication</i>		<i>at strain rate of</i> 10 s^{-1}	
<i>XNBR</i>	0.12	0.12	31	12.6	3.1
<i>XSBR</i>	0.138	0.138	49	15.8	3.1
<i>CR</i>	0.138	0.138	35	3.3	12.6
<i>Zeon HNBR</i>	0.12	0.12	33	14	2.8
<i>XNBR Ink</i>	363	1258	28	3	13.3
<i>XSBR Ink</i>	0.138	0.138	45	4	11.8
<i>CR Ink</i>	182	1258	37	3	14.3
<i>Zeon HNBR Ink</i>	416	416	31	4	9.8

As described in Chapter 2 section 2.2, the Z range for stable droplet formation is $10 > Z > 1$. It has also been discussed in Chapter 2 that varying Z numbers produce different droplet jetting results, as found by Jang and Kim [1] where inks with Z values that are less than 4 produce droplets with a long tail and increase the time taken for a droplet to be ejected. However, inks that have a Z number greater than 14 create minimal satellite droplets during printing due to the high surface tension and low viscosity of the inks. Therefore, the results for the Z number for the latexes that were analysed illustrate that the values are within the normal range for successful inkjet printing. The values of the particle size measurements are a concern as the approximate diameter of the Dimatix inkjet printing nozzle is $20\mu\text{m}$, which limits the number of materials that can be considered for inkjet printing. Upon studying the material properties displayed in Table 5.4, it can be determined that XNBR, CR, and HNBR are not suitable for inkjet printing due to the high variations in particle size, particularly with the addition of TGME. The observation of agglomerates that had formed during the shear viscosity measurements also present a problem for inkjet printing of XNBR and CR.

5.4 Jetting Trials

With the evaporation rate of the XSBR ink reduced, jetting trials commenced which enabled the droplets to be studied as they formed when ejected from the nozzles. Jetting trials were carried out before each pattern was selected for printing. This ensures that the most optimally performing nozzles were selected to minimize satellite and debris droplets from forming and interfering with the shape of the pattern.

Overall, the jetting of any ink is dependent on the control of the PZT system by the waveform, which includes the voltage, slew rate, and duration of the pulse. Voltage determines the amount of deformation of the PZT material and hence the volume of ink in the chamber before ejection. The slew rate and pulse duration determine the speed and duration of the deformation. These in turn affect the jetting process. The voltage and duration of the pulse determine the actuation of the piezoelectric element inside the ink chamber, which results in how quickly and with how much force the ink is ejected, which directly relates to the droplet's velocity. The duration of the pulse determines how long the transducer stays in the jetting position. The slew rate of the jetting pulse determines the speed with which the volume of the ink changes.

The waveform is split into Phases as illustrated in Figure 5.15 where the y-axis on the plot represents the applied voltage, while the x-axis represents time in microseconds. These phases dictate the sequence that is carried out to eject one droplet of ink. The start is the standby to Phase 1, which is the interim that is used during the printing process to allow ink to settle. In Phase 1 a current is passed through the PZT bimorph to create a slight deflection, which draws ink into the nozzle in preparation to be ejected. In Phase 2 the voltage reduces to zero and is used as a second break before the droplet is ejected to allow the material that has been drawn into the chamber to stabilise. In Phase 3 the formation of the droplet is initiated where the increase in voltage deflects the PZT to eject the ink out of the nozzle (Figure 5.15). After Phase 3 is complete, the last segment of the jetting process is resetting before the cycle is repeated again.

In-situ droplet analysis was carried out for several waveforms to determine what effect the different waveforms had on the jetting of the XSBR ink and to determine the ideal jetting waveforms for printing. The printer had a waveform editor that allowed segments to be added and removed and other parameters to be adjusted. Jetting performance was recorded using the Dimatix drop watching camera.

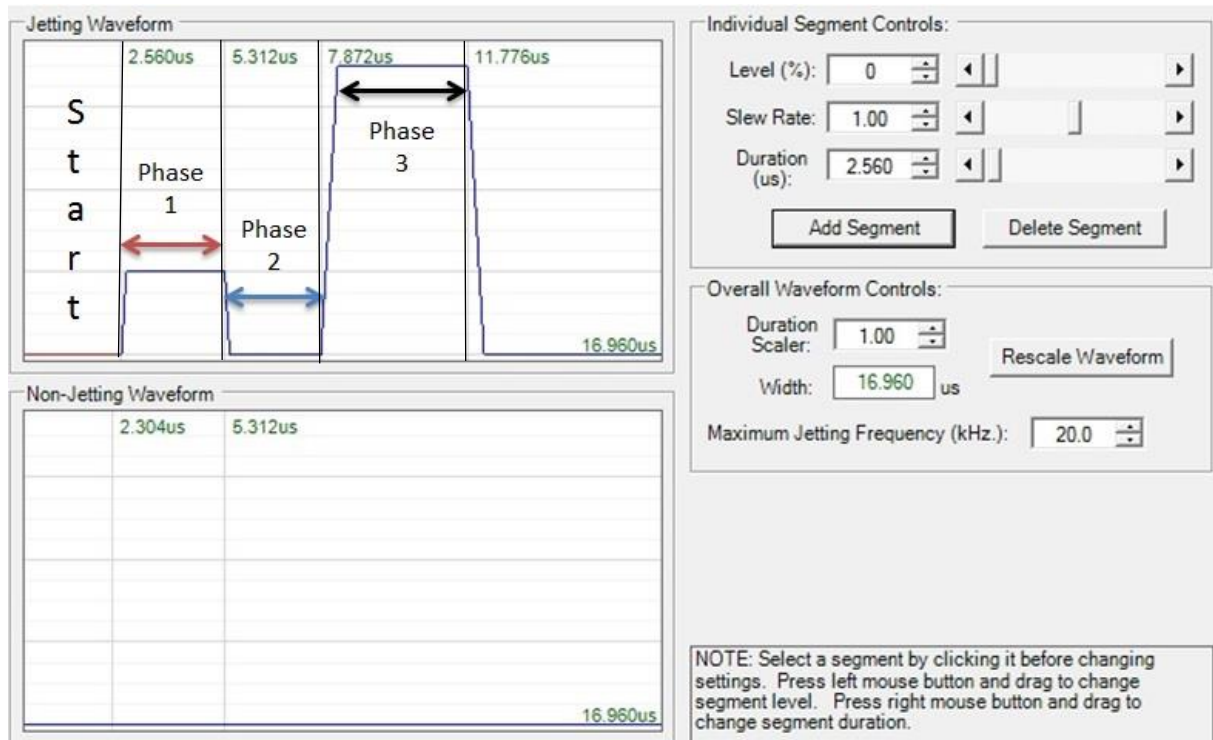


Figure 5.15 Jetting waveform split into 3 phases or stages

First Jetting trial

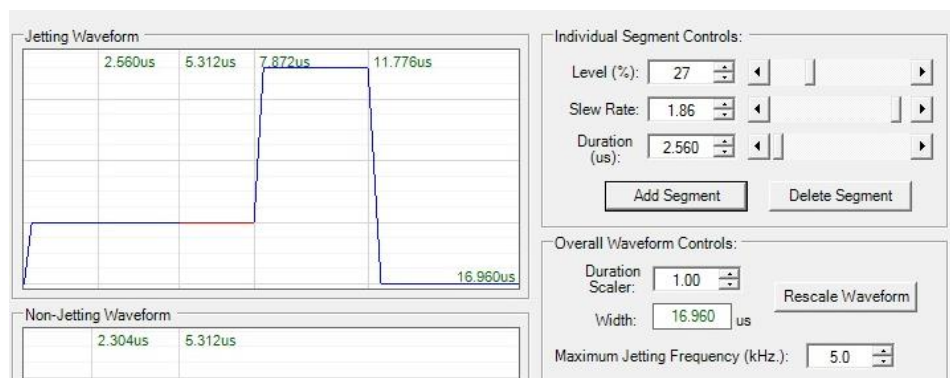


Figure 5.16 Waveform for first jetting trial

The waveform that was initially utilised for jetting trials was created considering the viscosity and surface tension properties of the XSBR latex. Figure 5.16 shows a screen shot of the waveform with Figure 5.17 illustrating the corresponding jetting performance of nozzle number 8. This waveform was utilised to test if the material properties of the XSBR ink would allow for it to be ejected as soon as liquid was drawn into the chamber. This waveform was suggested for use by a Dimatix technician for waterbased inks. Figure 5.17

shows ink was jetting an unsteady stream of droplets at a sharp angle instead of vertically downwards. This waveform was not ideal for ink jetting and had clogged the nozzle after about 30 seconds of jetting as the nozzle was continuously jetting the XSBR ink. As the surface tension, viscosity, and particle size of the latex ink was within printable parameters, it was determined that the reason for the clogging was the waveform. Figure 5.16 shows there was no Phase 2 at zero voltage (see Figure 5.15) which meant that liquid was being drawn into the nozzles directly from the cartridge and not allowed to stabilise, therefore resulting in a rapid and angled jetting stream from the nozzle. The addition of a Phase 2 where liquid could be allowed to settle for several microseconds after being drawn into the jetting chamber eliminated this problem.

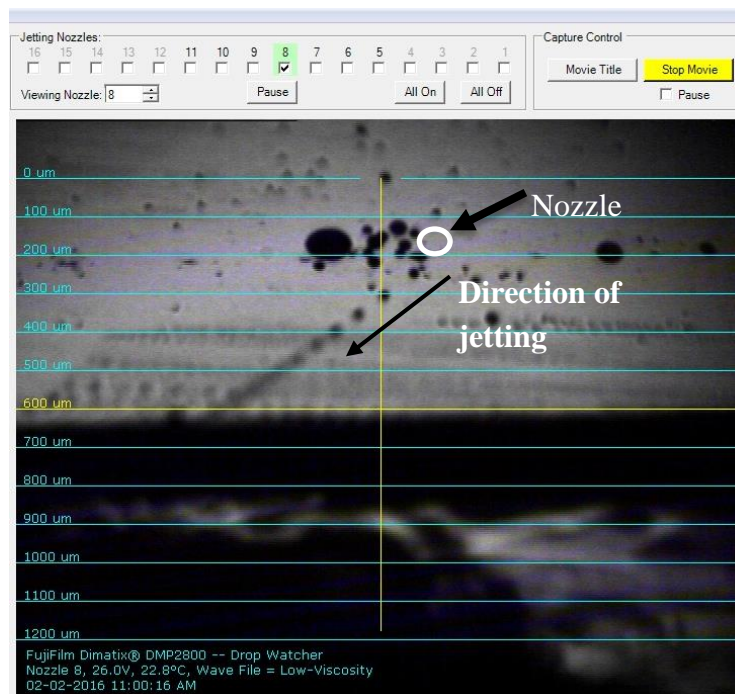


Figure 5.17 Ink jetting resulting from to the waveform as shown in Figure 5.16

Second jetting trial

After the first jetting trial did not yield ideal jetting results, another waveform shown in Figure 5.18 was selected for more viscous materials. The waveform utilised in Figure 5.18 yielded no jetting. The probable cause for this result is that Phase 3 was never completely finalised. The likely cause for this was the change in slew rate, increased duration, and the level voltage at 27%, rather than zero. After further research was conducted into waveforms used for ink jetting [3], it was determined that due to the properties of liquid inks with low

viscosities, for ideal jetting it is preferable to keep the slew rate to 1, with a duration of approximately $2.5\mu\text{s}$ and a voltage of 0.

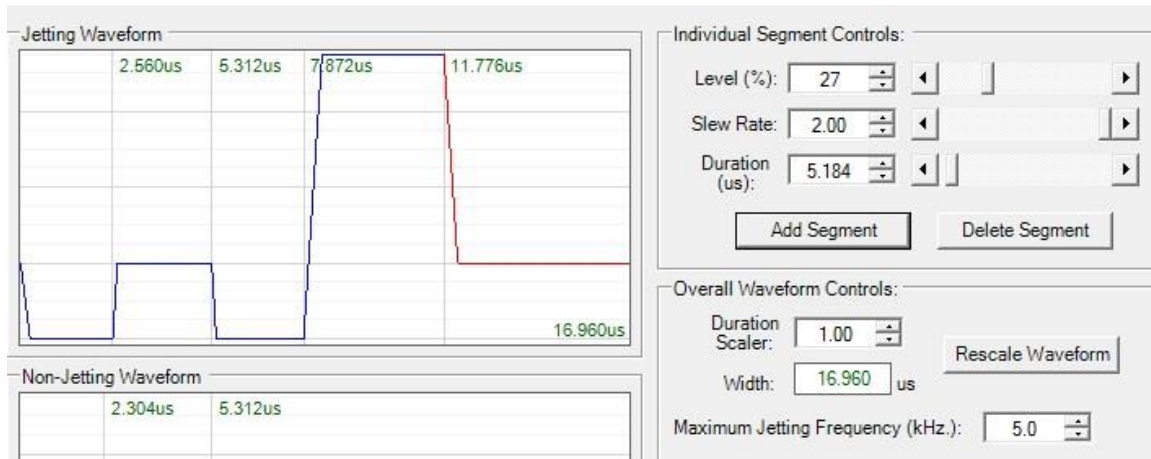


Figure 5.18 Waveform for second jetting trial

Third jetting trial

After determining that the high level (27%) was preventing jetting, the waveform was edited to include a voltage of 0%, slew rate was reduced from 2 to 1 and the duration was decreased from $5.184\mu\text{s}$ to $2.56\mu\text{s}$. This waveform is illustrated in Figure 5.19 and produced nozzle jetting illustrated in Figure 5.20. This waveform produced good droplet ejection where the main droplets did not break away from the tail (thus less chance to create satellite droplets) and the droplets themselves appeared to follow a straight downward path without deviation in various directions as happened with jetting in Figure 5.20. This waveform was one of the standard waveforms that was pre-loaded into the Dimatix computer for jetting low viscosity materials. As the viscosity properties of the XSBR ink were low, the decision was made to test an already established jetting waveform from Fujifilm and observe the effects.

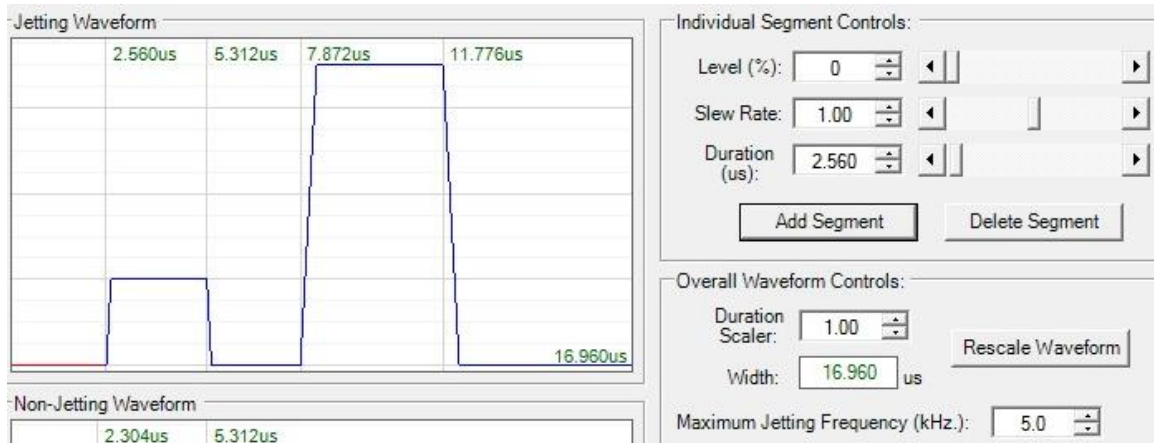


Figure 5.19 Waveform for third jetting trial

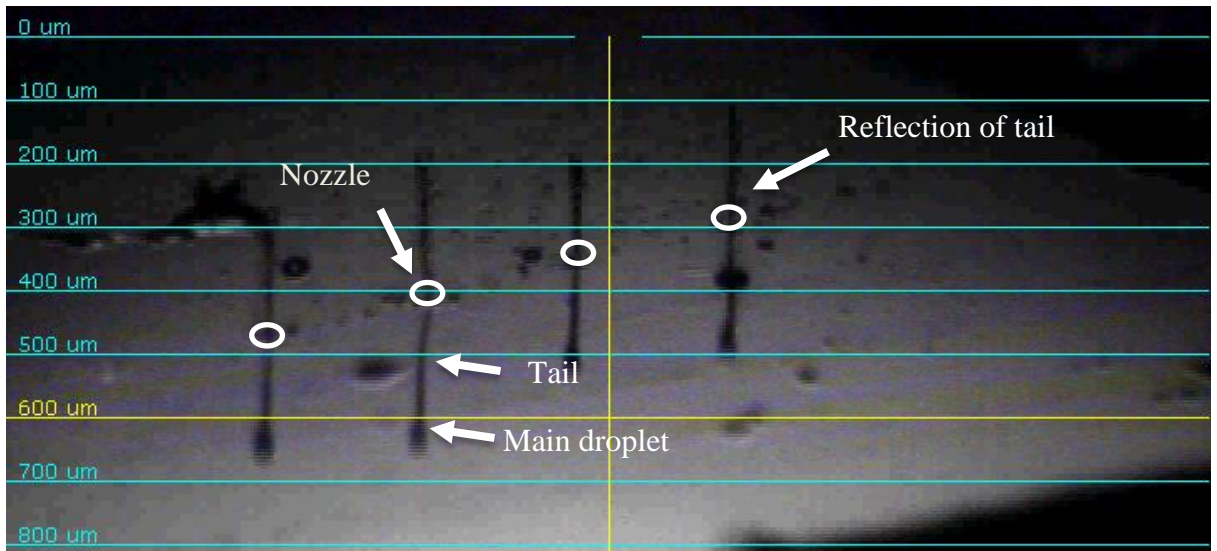


Figure 5.20 Ink jetting resulting from the third waveform shown in Figure 5.24

Fourth jetting trial

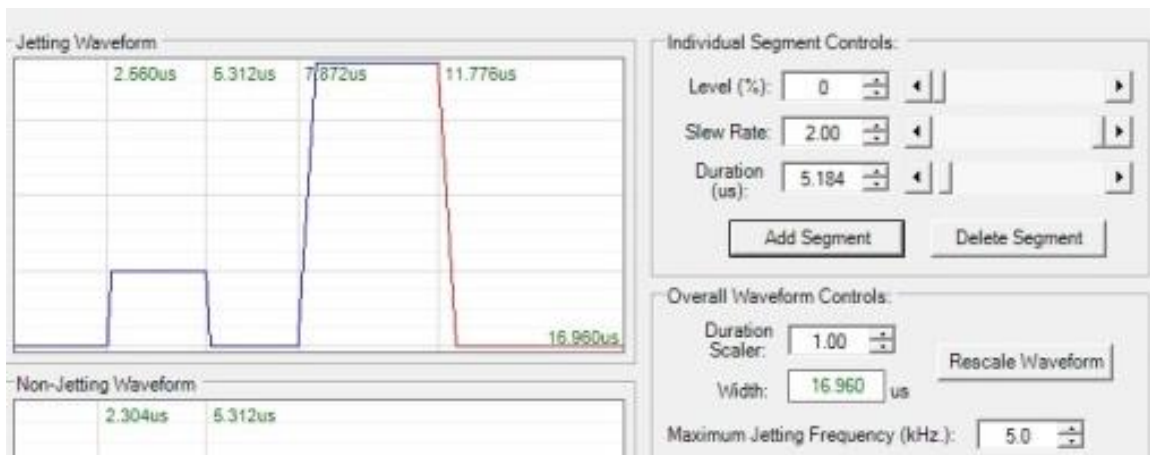


Figure 5.21 Fourth waveform used for ink jetting

A fourth jetting trial was carried out using a similar waveform to that used for jetting very low viscosity materials, such as water. The waveform displayed in Figure 5.21 provided jetting results as illustrated in Figure 5.22. The main differences between the waveform illustrated in Figure 5.19 and Figure 5.21 is the increase in duration and slew rate. These values were altered to observe the impact on jetting performance and whether that may improve droplet stability. However, after analysing the video recording of the jetting process using the waveform presented in Figure 5.24, it was apparent that the increase in slew rate and duration was causing a breakup of the main droplet from the tail, along with misfiring of Nozzle 1, which appeared to eject droplets at a slight angle [i]. Figure 5.22 shows nozzles 1 to 4, from right to left, ejecting XSBR ink using the third waveform (Figure 5.21). Nozzles 1 and 3 are not performing optimally as the droplets are not falling in a straight vertical direction. From the shape of the droplets and the tail, nozzles 2 and 4 appear to be performing well.

Two common issues can account for the two nozzles that are misdirected. The first cause is contamination of the nozzle at the plate. This is a common issue when jetting and requires performing cleaning cycles after printing, which necessitates the nozzles to make physical contact with the cleaning sponge, which contains ink residue from the previous cleaning cycles and this residue can block the nozzles. The residual debris can lodge itself inside the nozzle, which in turn forces the droplets to be ejected at an angle. Another issue could be air that has become trapped inside the nozzle descender. Microbubbles are present in the ink and get trapped inside the nozzle opening, and this affects the formation of the droplets in that nozzle.

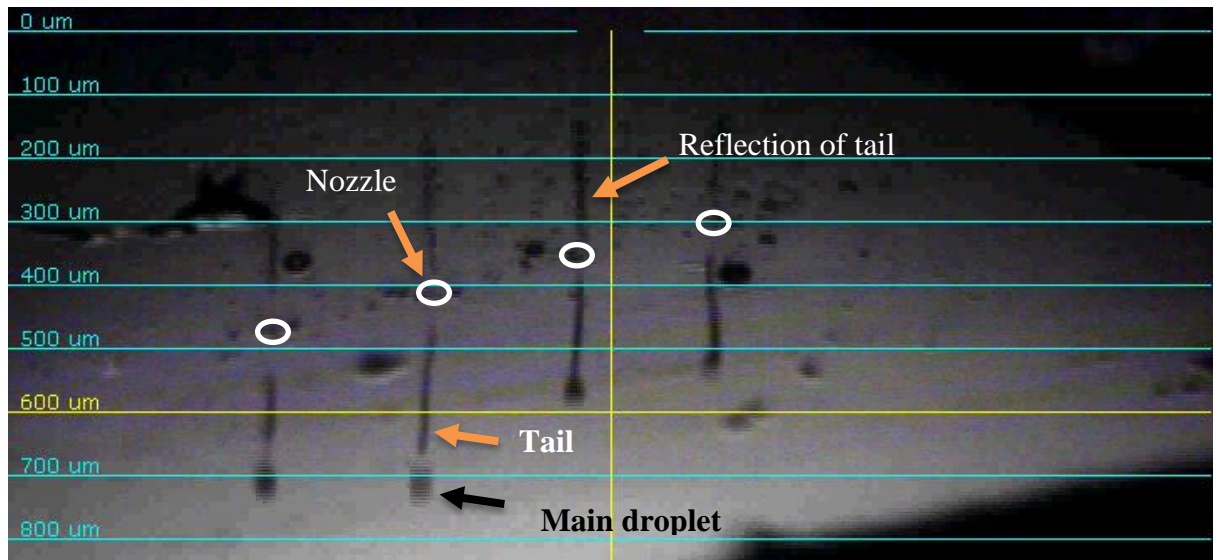


Figure 5.22 Formation of droplets from 4 nozzles as they are ejected utilising the fourth waveform

Out of all 4 of the nozzles, it appears that nozzle 1 had the poorest jetting performance due to the misdirected jetting when utilising the fourth waveform. Nozzle 2 had the best jetting performance and was used to print the droplets as illustrated in Figures 5.24 and 5.25. Once analysis of the waveforms was complete after observing the jetting trials, it was determined that the third waveform presented in Figure 5.22 yielded the most stable droplets compared to all other waveforms that were tried and modified.

The images that are displayed in Figures 5.20 and 5.22 were captured while having the print head adjusted to a 36.8° angle. This was done to carry out a droplet analysis for the ink onto various substrates.

5.5 Droplet Deposition

5.5.1 Substrate surface energy

The surface energy of substrates used for depositing ink onto can have a dramatic impact on the shape and behaviour of the ink once it is deposited. If the substrate has low surface energy, the latex will not retain the pattern as printed but will instead gather into a single spherical shape. Another issue is encountered with a substrate with high surface energy, which enables the ink to completely wet the surface and causes spreading.

The surface energies of PET, PTFE coated fabric, PTFE tape, microscope glass slides, and a cast sheet of XSBR latex were determined using contact angle measurement.

These substrates were chosen as they cover a wide range of surface energies. Cast XSBR was chosen to determine its surface energy and observe how the liquid XSBR ink would react when it is printed onto dried XSBR, as would occur in 3D printing.

Table 5.5 illustrates the different surface energies of the substrates. As was expected of hydrophobic materials, the PTFE and PTFE coated fabric have a very low surface energy. The glass microscope slides have the highest surface energy value, which indicates that it has high wetting potential.

Table 5.5 Surface energies of substrates

Substrate	Surface energy, mN/m
PTFE coated fabric	9.5
PTFE tape	19.1
Cast XSBR latex	35.5
PET	39.9
Glass slide	63.7

Comparing the results of the surface energies for the substrates, the glass slide has the highest surface energy value and the PTFE coated fabric has the lowest. Glass has high wetting potential due to the smooth surface of the material. A perfect example of how surface properties can affect wetting is a Lotus leaf. The leaf is known to have a rough and even distribution of hydrophobic fibres on its surface, which allows water to bead onto it without wetting [4]. Furthermore, glass slides created for microscopes have a higher surface energy to encourage wetting, spreading a liquid sample so that it may be imaged effectively under the microscope.

The ideal surface energy for a substrate for inkjet printing should be high enough to provide adequate wetting to allow for the droplets to spread slightly, still maintaining something of the droplet shape but allowing a continuous, well defined pattern to be printed. If the surface energy is too low it will prevent the droplets from spreading and may create a broken pattern [10].

Figure 5.23 illustrates a droplet of de-ionised water that has been deposited onto a PET substrate during surface energy measurements using the contact angle equipment. The

droplet has an ideal semi-circle shape where it has retained a droplet shape but has also wetted the substrate sufficiently.

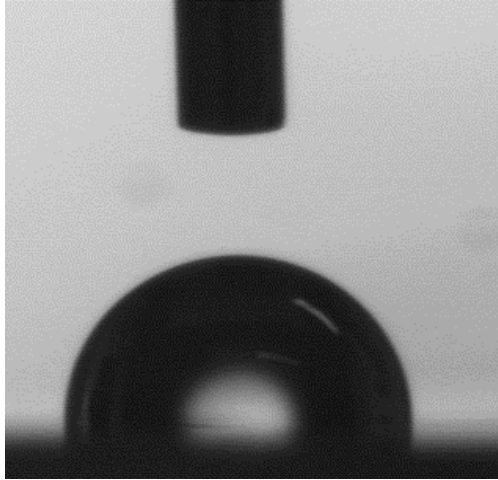


Figure 5.23 Captured image of a droplet of de-ionised water on PET substrate

5.5.2 Droplet Analysis

Droplet analysis was carried out to determine the accuracy and precision of printing, the shape and uniformity of the jetted droplets, the spreading behaviour on the substrate and to assess the extent of satellite droplet formation. XSBR ink was printed in a regular pattern of individual drops (Section 4.8) and SEM was used to analyse the droplets printed on PET and PTFE substrates.

One of the first factors that are considered when carrying out a droplet analysis is the overall shape and size of the droplets. In Figure 5.24 we can see that the size of the droplets is consistent, they are evenly spaced out, and there are no droplets that are coalescing together, which indicates that jetting is good and that the nozzle is not obstructed. On average, the droplets are about 28 μ m in diameter. However, there are persistent satellite droplets that follow the direction of the main droplet. These are caused by the tip of the tail of the main droplets that break off during the jetting process. These satellite droplets follow the printing direction and land next to the parent droplet. This does not necessarily pose a problem for the printing process and it is a common occurrence with inkjet printing technology.

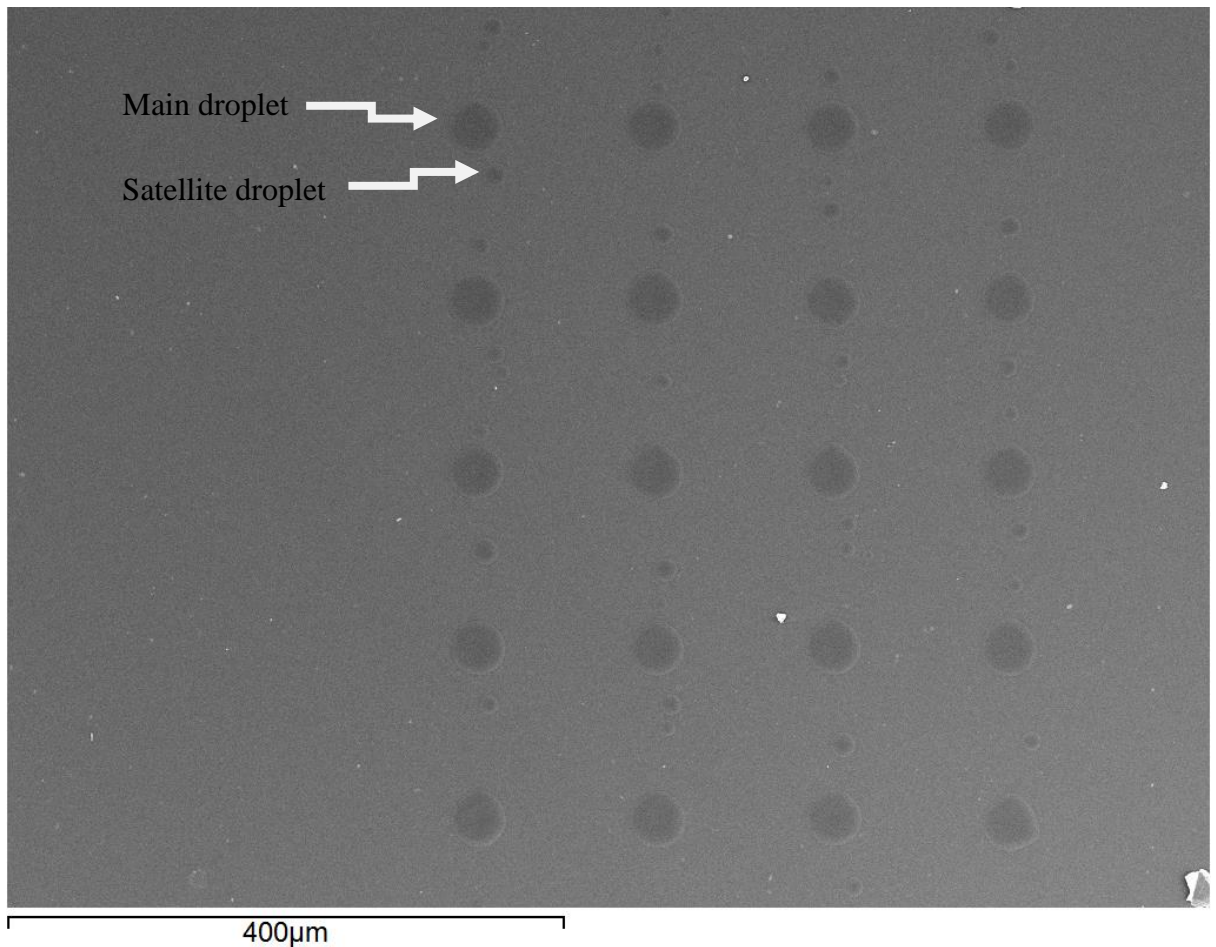


Figure 5.24 SEM image of droplets printed onto PET substrate for droplet analysis

Droplet analysis was also carried out for glass microscope slides and PTFE tape to determine how the substrate affects the morphology of the droplets (Figures 5.25 and 5.26). Figure 5.25 displays the XSBR droplets that were deposited onto a glass substrate. The bed temperature inside the printer was not heated and remained at ambient room temperature between 19°C and 20°C. It is possible to observe a slight depression in the majority of these droplets. This is due to the slow drying process of the XSBR latex because the bed temperature was low and this allowed the latex particles to be drawn to the edges of the droplets due to surface tension and a lack of convection current within the liquid that would keep the particles in motion and prevent the depression from forming. Some of the droplets that were printed had spread too much and had merged together with the tail, forming pear shaped droplets instead of the perfectly rounded and symmetrical ones that were created on PET. The average size of the droplets is about 52 μm on the glass slide, compared to 35 μm on the PET, confirming that considerable spreading has occurred. This indicates that the high surface energy of the glass substrate promotes 32.7% more wetting than the PET and

51% more than PTFE tape substrates, which is a considerable amount. This is significant since it can affect the accuracy and resolution of the print, as is shown by the results of the droplet analysis conducted on the glass slide and the PET substrate. Due to the high surface energy of the glass slide, the main droplets spread and merged with the satellite droplets that formed after the droplet's tail detached.

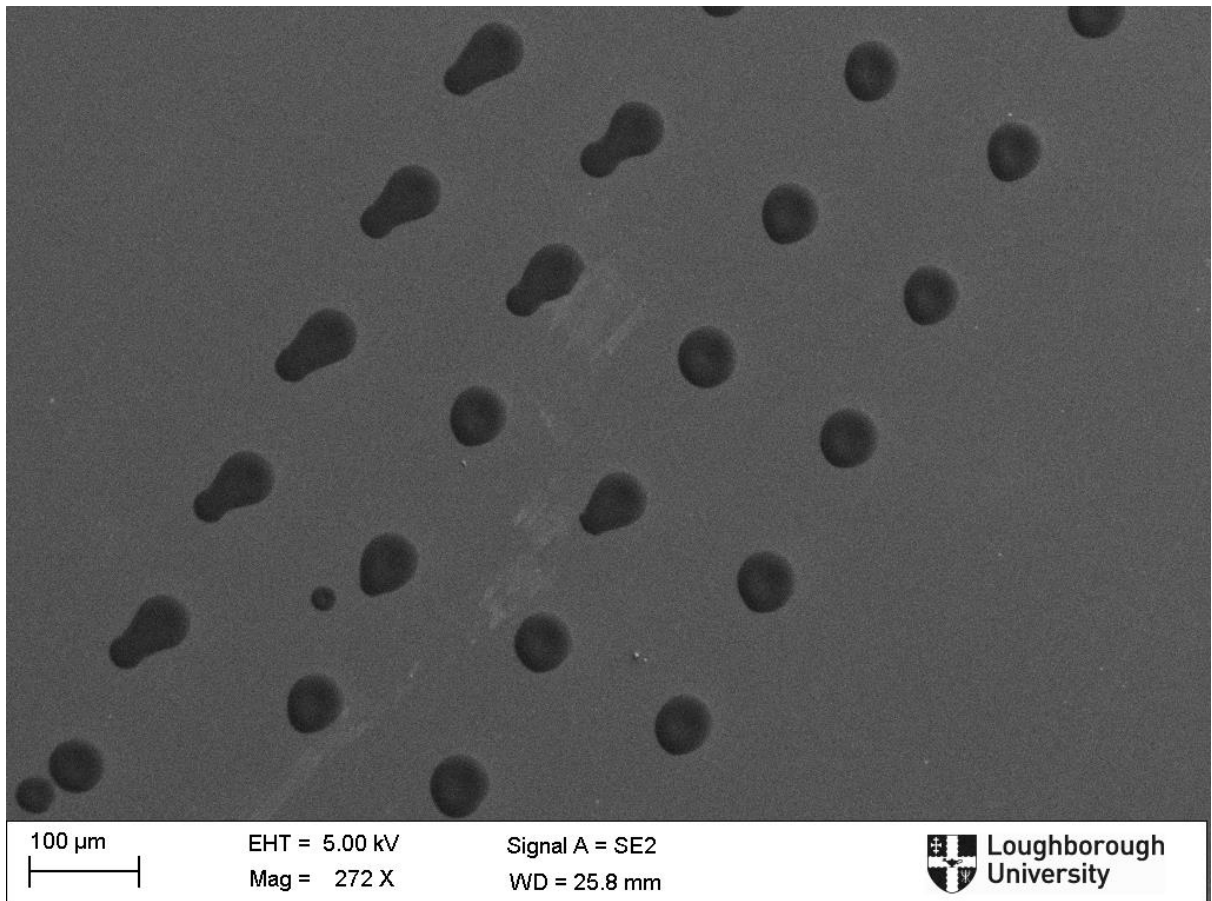


Figure 5.25 Droplet analysis of XSBR droplet printed onto a glass microscope substrate

Droplet analysis on PTFE tape involved printing on tape that was stuck onto a glass microscope slide to prevent the tape from folding and getting damaged during printing. Under SEM, the tape has an interesting pattern and structure to it (Figure 5.26). The thicker vertical lines were caused by stretching the substrate when it was placed onto the glass slide. This has not affected its hydrophobicity. Analysing the droplets, we can observe a considerable difference in droplet formation for PTFE tape compared to glass and PET. Although the temperature on the print bed remained unchanged, there is a noticeable change in the size of the droplets. The droplets have retained their shape and appear to stand up from the surface as spherical droplets. The average size of the droplets is about 25.5 μm on the

PTFE tape, compared to 35.4 μm on the PET, indicating that least wetting and spreading has occurred on the low surface energy PTFE substrate.

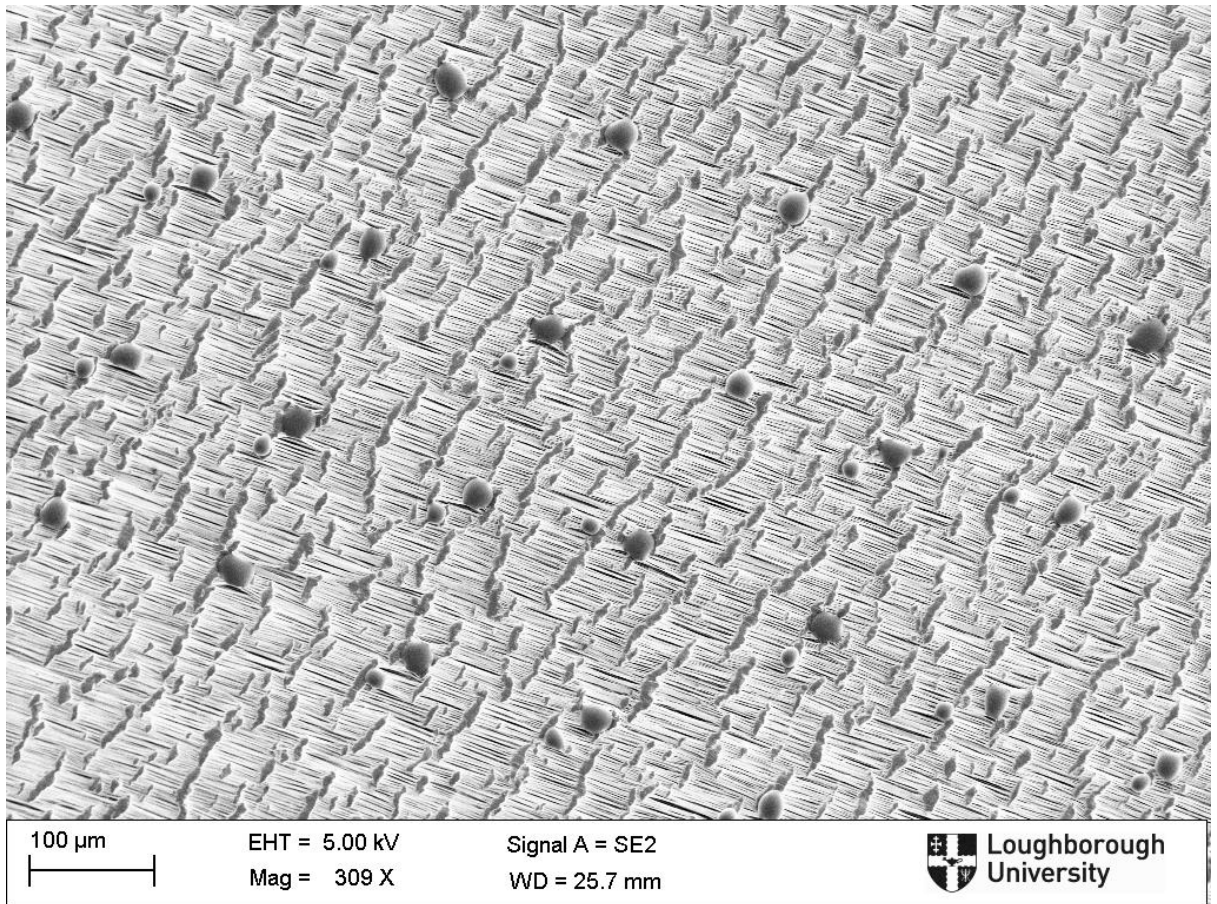


Figure 5.26 SEM image of droplets printed onto PTFE tape

A droplet analysis was attempted on PTFE coated fabric, however it was not possible to observe the droplet on the substrate. Although the ink was deposited onto the substrate, it is possible that the droplets may have passed through the gaps between the fibres or slipped off of the substrate due to its uneven surface.

The results show that droplet analysis is a useful method to determine how an ink interacts with a substrate, particularly with regard to spreading. Figure 5.27 shows how the size of the printed drops increases with the surface energy of the substrate. The even spacing and uniform size of the droplets on a particular substrate also indicate how well the print head nozzles are jetting and that the latex ink is performing well. However, a droplet analysis only considers drops in isolation and does not indicate how the ink will behave when printed

in more continuous patterns. The next section details the printing trials that were carried out to deposit single layers of XSBR ink.

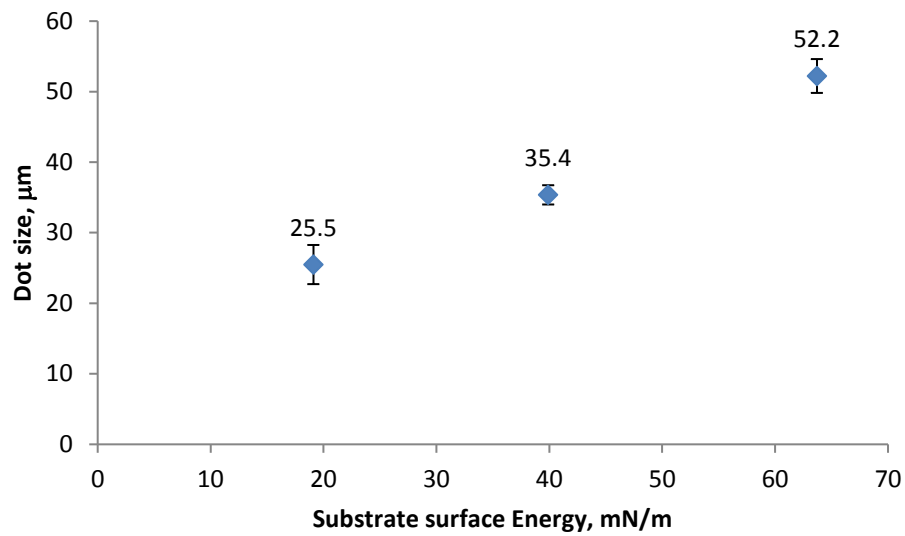


Figure 5.27 Effect of substrate surface energy on printed dot size

5.6 Single Layer Latex Ink Deposition

It is important to assess the behaviour of the ink when one layer is printed because it shows how individual dots and lines interact, for example, whether coalescence occurs and it indicates the level of accuracy and precision which can be obtained. Furthermore, the first layers that are deposited onto a substrate can affect the sample's shape as a whole. The fiducial camera that is mounted inside the Dimatix printer was used to determine the effects of single layer printing of XSBR onto PTFE coated fabric, PTFE tape, PET and a glass slide (Figures 5.28 – 5.34).

A relatively low level of wetting of the substrate may be beneficial in controlling the accuracy of printing, since high levels of wetting may lead to uncontrolled spreading. The droplet analysis shows that individual drops can be placed accurately on the very low energy substrate, PTFE tape (Figure 5.30). Another potential advantage of using a low surface energy material for the substrate is that the completed print could be easily removed from the substrate. Both PTFE tape (Figure 5.30) and PTFE coated fabric (Figures 5.28 – 5.29) were used as substrates for printing single layers of XSBR latex. The PTFE coated fabric on its own is shown in the Figure 5.28. Figure 5.29 present the results of printing a single layer of XSBR on PTFE coated fabric and PTFE tape.

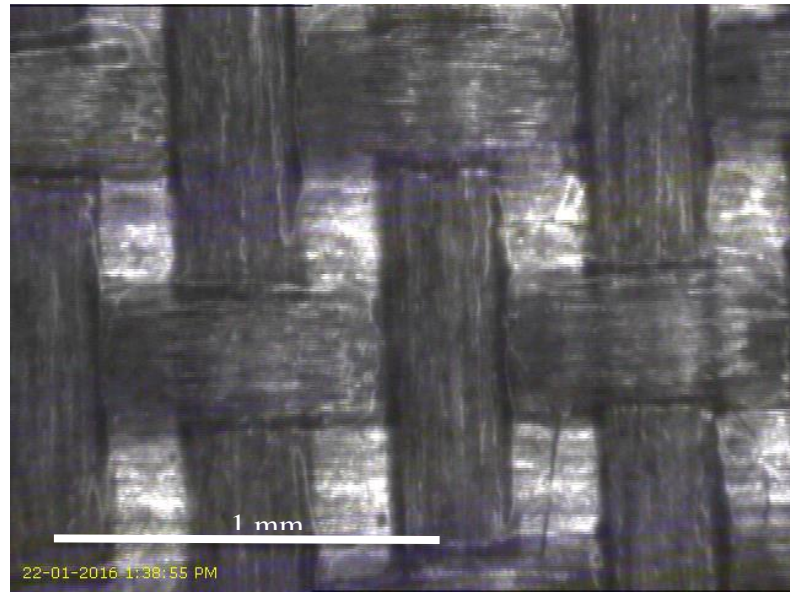


Figure 5.28 Image captured of the PTFE coated fabric using the Dimatix fiducial camera

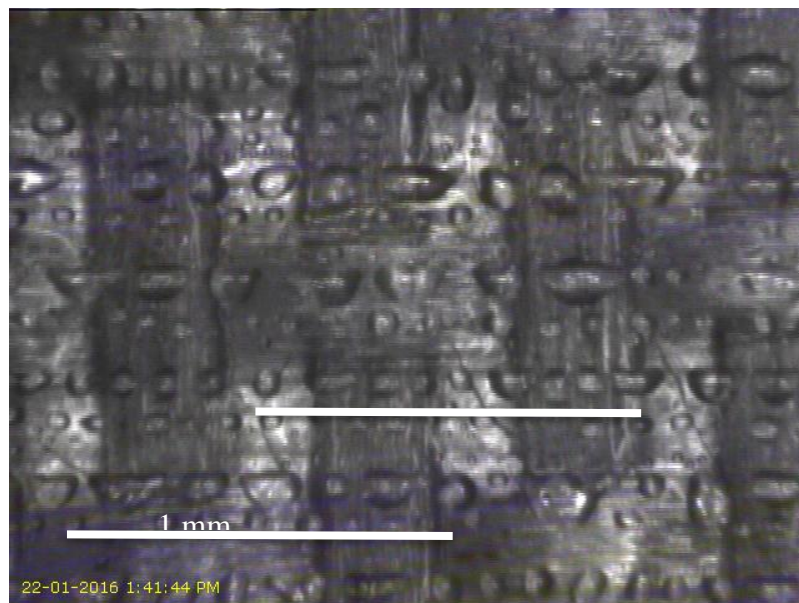


Figure 5.29 Single layer of XSBR deposited onto PTFE coated fabric

The printed layer of latex on both PTFE coated fabric and PTFE tape did not produce continuous lines once deposited. Instead the lines separated to form broken droplets. This occurs because of the low surface energy of the substrate, particularly in relation to the relatively high surface tension of the latex [5-8]. This results in coalescence of droplets which come in contact with each other and beading up of the coalesced droplets, minimising

the contact area with the substrate. The results indicate that PTFE may be too low a surface energy material for printing latex onto.

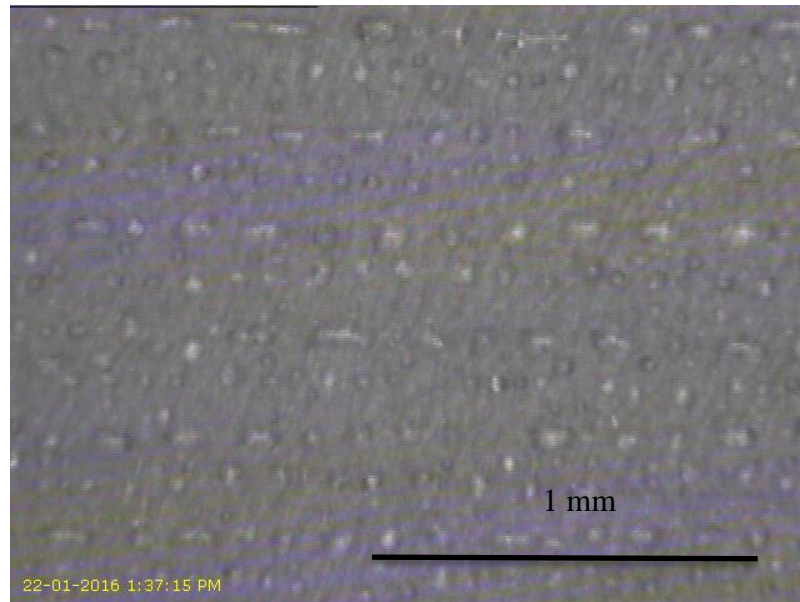


Figure 5.30 XSBR single layer deposited onto PTFE tape

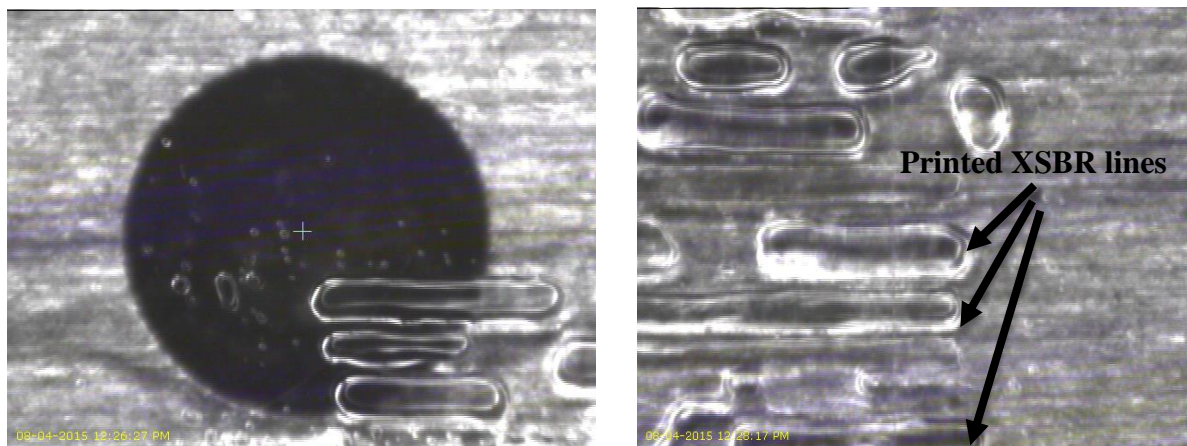


Figure 5.31 Single layer XSBR ink deposition onto PET substrate to test the wettability of the substrate

Figure 5.31 shows the results of printing a single layer of XSBR ink onto the PET substrate. The black circle on the left-hand side image is one of the many apertures in the printer's bed that are utilised to draw air in, therefore aiding in securing the substrate to the bed to ensure that it does not move during the printing process. Many consecutively printed

drops have coalesced, forming segments of line 500 to 1000 μm long and approximately 100 μm wide. The fact that distinct lines can be seen indicates a higher degree of wetting than was observed for the PET substrate than for the PTFE and a significant level in control of the printing. However, the lines are not completely continuous and lines printed side by side have not joined together.

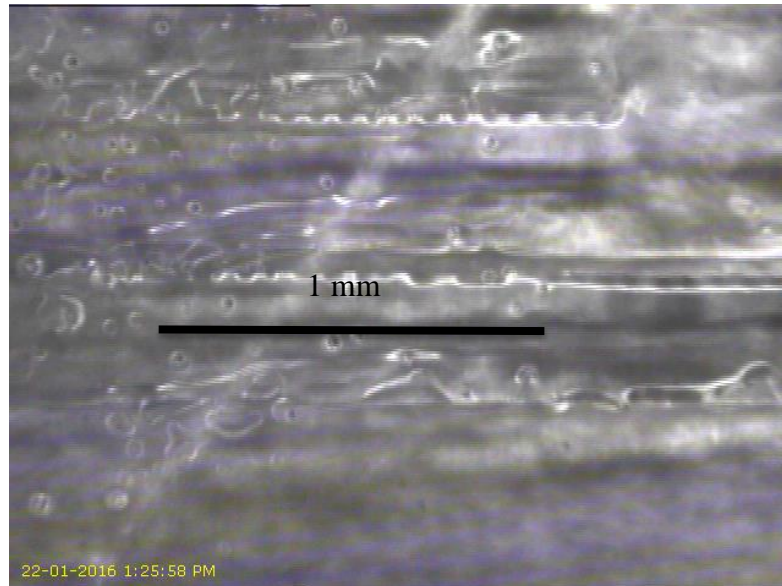


Figure 5.32 Single layer of XSBR on a glass microscope slide

Figure 5.32 shows a layer of XSBR latex printed onto a glass microscope slide. Unlike the results with printing onto PTFE, the printed lines of XSBR remained intact and are continuous over a greater length than when printed on the PET. In the highlighted sections of Figure 5.33 we can observe the remnant shape of the original droplet that was deposited. These droplets came into contact and formed a continuous line of XSBR, which demonstrates that the surface energy of the substrate is in an ideal range where a pattern can be printed and the shape maintained without either too much spreading or so little wetting that the printed material beads up on the surface in an uncontrolled manner.

Pictures from the fiducial camera were not very clear so a single layer of latex printed onto a glass slide were also examined using SEM (Figure 5.33). The image shows mostly continuous lines are printed although spaces between the lines are not even. It is probable that a nozzle blocked during printing so that a complete set of lines was not produced. This is highlighted in Figure 5.33 by a red outline.

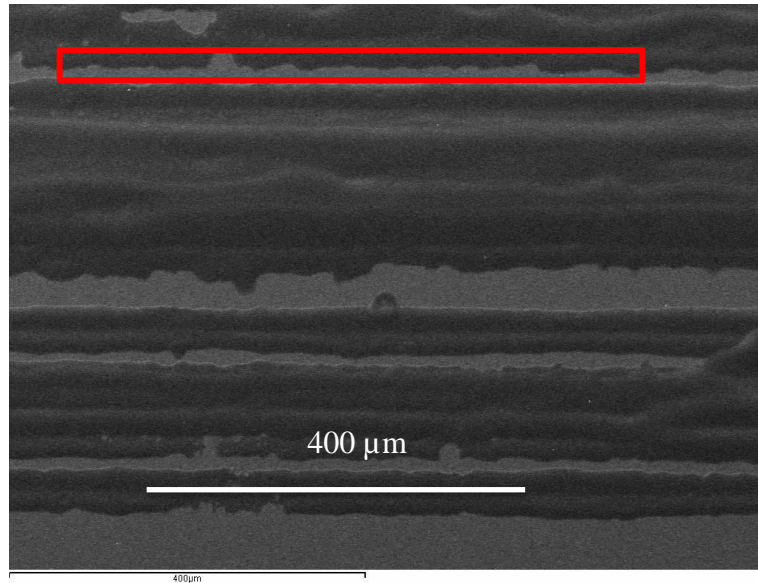


Figure 5.33 SEM image of XSBR lines printed onto glass slide

Figure 5.34 shows both a cross-section of the printed lines and a 3D image measured using white light interferometry (Zygo). The images show that the lines are approximately 70 μm wide and about 3 μm thick on average. Each printed line has a trough along the middle, an example of the “coffee ring effect”. As the sample was drying, the latex particles were spreading to the edges of the printed sample, therefore creating a concentration of latex on the edges of the lines leaving a depression down the centre [8]. This is a common occurrence with liquid materials and can be prevented by creating a convection within the liquid using heat. This is called the Bénard–Marangoni convection. However, the Bénard–Marangoni convection can cause instabilities in the surface tension of thin layer materials or liquids due to temperature variations, where one surface of the liquid is free and exposed to cooler temperatures, while another is in contact with a heated substrate.

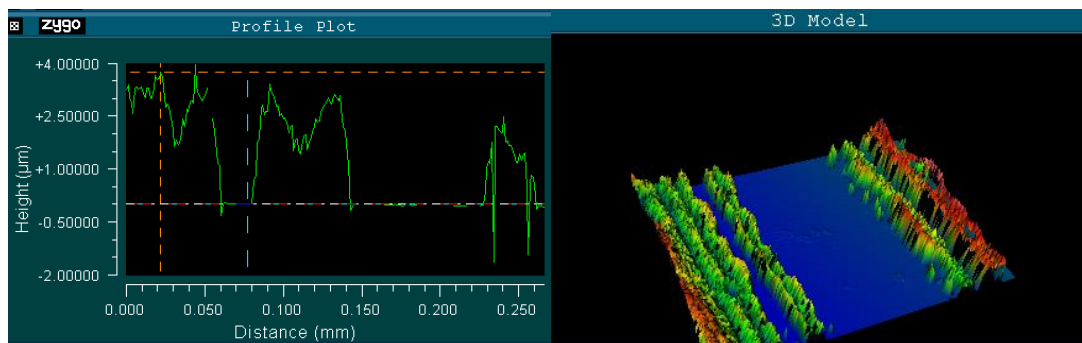


Figure 5.34 Figure 5.37 Zygo cross-sectional profile and 3D image of a section of lines printed onto glass slide

After carrying out multiple printing trials with XSBR ink onto the various substrates to determine the effects substrate surface energy has on the final printed material, PET was selected as the substrate to print onto. This material was selected as a substrate due to its versatility, flexibility, ease of use, as well as larger surface area and because it was lightweight. Although ink printed onto glass slides has demonstrated that it is a suitable substrate, and in some instances, has produced more ideal samples in terms of wetting and finer patterns, it was a rigid and relatively thick substrate. The thickness of the glass slides provided challenges during white light interferometry measurements as the substrate would not register, creating aberrations during measurements when light would pass through any gaps in the substrate to the base of the white light interferometer. This limited the pattern sizes that could be printed to 76mm x 26mm with a thickness between 1mm and 1.2mm. The other potential concern was the substrate cracking or breaking and damaging the printed material, as the samples had to be transported from Nottingham University (where they were printed using the Dimatix printer) to Loughborough University to be analysed and tested. Therefore, after all the factors were given careful consideration, it was determined that PET was a suitable enough substrate for printing XSBR ink onto and was chosen to be the principal substrate.

5.7 Multilayer printing

5.7.1 Effect of substrate on multilayer printing

After the surface energy measurements were carried out and single layers of XSBR ink were deposited on all substrates, it was determined that the PET substrate seemed to be best suited for ink jetting XSBR ink onto due to its flexibility, the surface energy, flat and even surface and texture, however further multilayer printing trials were conducted in order to firmly conclude on the optimum substrate for printing latex onto.

Multilayer printing was carried out for all substrates:

- PTFE coated fabric
- Glass microscope slide
- Sheet of PET cleaned with isopropanol and de-ionised water to remove any contaminants on the surface
- PTFE tape

Ten layers of XSBR ink were deposited onto the substrates using XSBR ink and with six nozzles. A 1x1cm square was printed in order to determine how the final print quality was affected by the surface energy of the substrates.

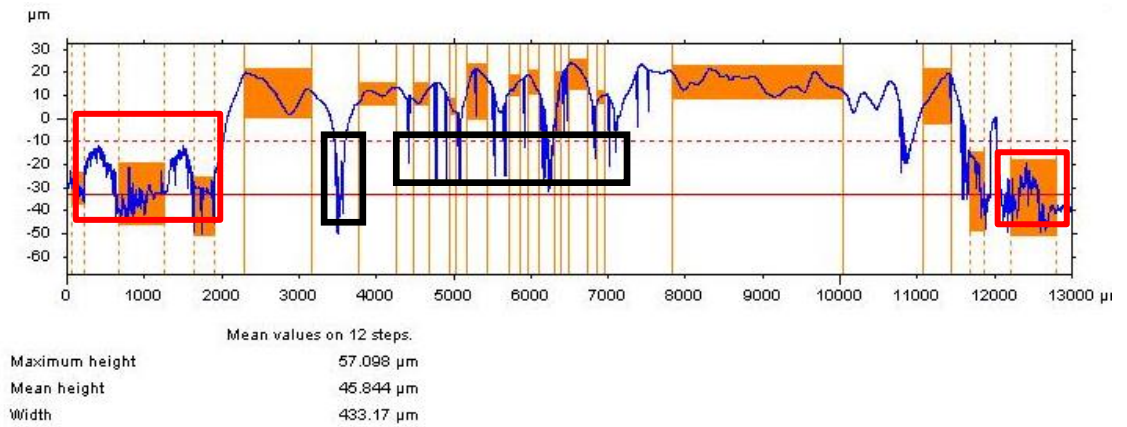


Figure 5.35 10 layers of XSBR ink printed onto PTFE coated fabric substrate

Figure 5.35 illustrates a cross-sectional profile image obtained for the sample printed onto PTFE fabric using white light interferometry. The areas highlighted in red is debris from the ink jetting process on the substrate, while areas with the sharp drops in the measurements highlighted in black are sections where the white light from the interferometer did not pick up the surface. We can observe that the substrate itself is uneven due to its woven characteristic. This unevenness was measured using the white light interferometer and is highlighted in red in Figure 5.35. The areas marked in orange were used during measurements to mark the highest and lowest points so that the white light interferometer can distinguish between substrate and the printed XSBR. A ten-layer sample printed onto the fabric had produced an XSBR sample with a rough top surface and a maximum and mean thickness of 57µm and 45µm respectively. The roughness of the surface could be due to the unevenness of the substrate. This indicates that each layer is approximately 5µm, which is a significantly high value. This can be attributed to the hydrophobic nature and uneven surface texture of the substrate, which can affect the thickness of the layers. Due to the transparent appearance of the XSBR when dry, artefacts such as a sharp drop in the measurement can appear when using white light interferometry. These drops do not represent the genuine result for thickness, but instead show where the white light passed through the XSBR down to the substrate. These artefacts are highlighted in Figure 5.35 with black rectangle outlines.

Printing results for XSBR ink onto a glass microscope slide is illustrated in Figure 5.36. As with the results shown in Figure 5.35, the sections highlighted in orange were areas of the substrate and printed XSBR after the white light interferometry measurements were completed. This was done so that maximum, mean, and width measurements could be recorded by the computer software. As with the results presented in Figure 5.36, artefacts are also present in Figure 5.36 and are outlined in red. These artefacts indicate where the white light passed through the printed material, the microscope slide, down to the base of the interferometer.

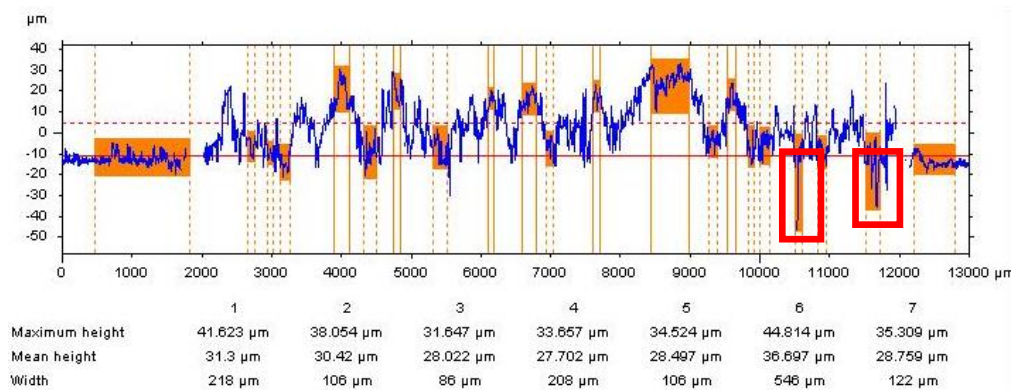


Figure 5.36 10 layers of XSBR ink printed onto a glass microscope slide

Printing XSBR ink onto a glass substrate created a sample with a jagged top surface. The printed XSBR lines could be seen with the naked eye, corresponding to the jagged peaks in Figure 5.36. Comparing the results of the glass slide in Figure 5.36 to those of the PTFE fabric in Figure 5.35, it is unmistakable that the thickness and surface topography are contrasting. Due to the higher surface energy of the glass slide, the thickness of the XSBR printed on the glass slide (approx. 30µm) is lower than the XSBR printed onto PTFE fabric (approx. 45µm). This result is expected as the surface energy of the glass slide promotes wetting and spreading, whereas the uneven texture of the PTFE fabric and the low surface energy prevents the liquid ink from spreading. However, when examining Figure 5.39 it is discernible that the surface of the printed material is rough and uneven. This is possibly due to satellite droplets formed during printing.

The third substrate that was tested was a sheet of PET, the results of which are presented in Figure 5.37. Before printing, the substrate was cleaned with isopropanol and de-ionised water to attempt to remove as much contamination as possible. However, from analysing the results in Figure 5.37, it is unmistakable that the thickness values are not

consistent across the width. The thickness of the centre of the dome is approximately 100 μm , while the thickness of the left and right shoulders is roughly 40 μm and 45 μm respectively.

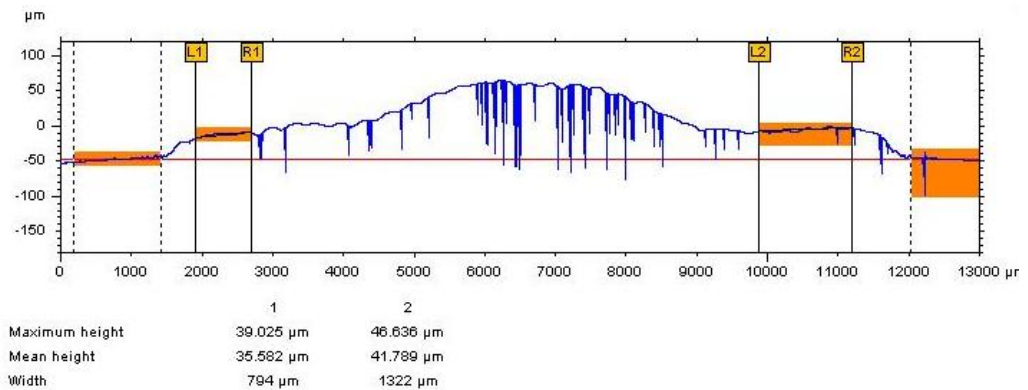


Figure 5.37 10 layers of XSBR ink printed onto PET substrate

During printing, a cloudy appearance was observed in the centre of the pattern while the edges were transparent. This suggests that the centre of the pattern still contained liquid ink while the corners and edges appeared to be dry, which caused a dome in the centre of the sample to form, due to the greater volume of the wet ink. To determine whether the effect of drying was the cause for the doming, further experimentation was carried out to speed up drying time by creating a time delay between depositing layers and increasing the print bed temperature, detailed in section 5.7.3 and 5.7.4.

Lastly it was necessary to determine the effects of printing XSBR latex ink onto hydrophobic PTFE tape. Due to its hydrophobic properties, the tape proved difficult to secure in place onto the print bed. Therefore, PTFE tape was secured to a microscope glass to prevent the substrate from moving during printing and to provide rigidity when handling. The results of the white light interferometry measurements are shown in Figure 5.38.

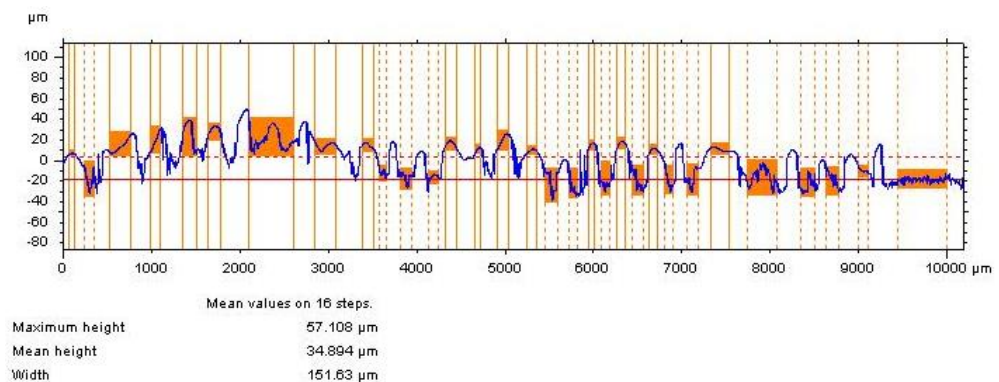


Figure 5.38 10 layers of XSBR ink printed onto PTFE tape

In comparison to the results of printing onto PET in Figure 5.37, the overall surface profile of the printed XSBR, as well as the thickness values, are significantly different. The thickness values indicate that each layer is approximately 5 μm , whereas the values of the PET are 3.5 μm . Another interesting feature that is observable in Figure 5.38 are the printed lines. The measurements were obtained by measuring perpendicular to the printing direction, therefore the peaks in the measurements indicate printed lines that did not successfully merge during deposition. This is due to the extreme hydrophobicity of the substrate, which allowed each printed line to remain intact and not spread to merge with its neighbouring line.

Depositing onto substrates with varying surface energies has provided interesting results for thickness values and surface topography analysis. It was determined that PTFE tape is not an ideal substrate for printing due to its hydrophobicity, which prevented XSBR ink from merging correctly. Printing onto the PET substrate create unexpected difficulties with doming effect in the centre of the printed area probably caused by preferential drying at the edges. Printing onto the glass slide substrate produced an XSBR sample with a slightly rough and uneven surface, as well as low single layer thickness values. This indicates probable spreading during printing, which allowed for the deposited layers to have a slightly lower thickness value. These substrates are further examined in the following sections.

5.7.2 Multilayer complex 2D Patterns

After completing several single layer deposition printing of XSBR ink onto various substrates, more complex patterns were selected for printing to observe the quality and accuracy of the completed sample. The patterns that were chosen were Loughborough University and Zeon logos. 60 layers of the Loughborough University logo was printed using XSBR ink while 120 layers Zeon was printed using an ink made with Zeon company's HNBR latex. Both patterns were deposited using 10 nozzles onto PET substrate

The printed Loughborough logo in Figure 5.39 shows some roundness to the Loughborough University shield pattern. It is probable that this can be avoided by increasing the bed temperature inside the printer to 60°C to aid drying and prevent doming, or by using a support material to contain the edges. This premise is examined in section 5.7.4.



Figure 5.39 Loughborough University logo printed with XSBR ink (approximately 5cm long and 1 cm high)



Figure 5.40 ZEON logo printed using HNBR liquid latex provided by Zeon Chemicals (approximately 4cm long and 1.5cm wide pattern)

The ZEON logo printed with the HNBR ink provided by the company was printed successfully. There were no complications during the printing process. However, the remaining HNBR ink that was stored in a small container showed indications that the particles were agglomerating. Small particles of latex were observed once the liquid was shaken, and passing the HNBR ink through the 5 μ m syringe filters was causing rapid clogging.

Due to the relative lack of stability of the HNBR latex towards agglomeration, further printing was limited to XSBR latex ink.

5.7.3 3-D Pattern Printing

Once jetting with XSBR ink was thoroughly tested and the ideal jetting parameters established, a 3D pattern was printed. This pattern included a wave-like structure as described in Chapter 5 section 5.10.2. The purpose of this printing was to determine if it would be possible to use 3D patterns for printing with an elastomeric material, and whether the ink would retain the desired shape as the pattern that was selected was normally used for testing UV curable inks. Printing was carried out onto a PET and a glass microscope slide substrate.

White light interferometry was used to determine the cross-sectional profile of these samples as well as the average thickness. Figure 5.41 displays the cross-sectional profile of the XSBR wave pattern, as illustrated in Figure 4.5 in Chapter 4 section 4.9.2 printed onto PET and Figure 5.42 shows the latex printed using the same pattern and parameters onto a glass slide.

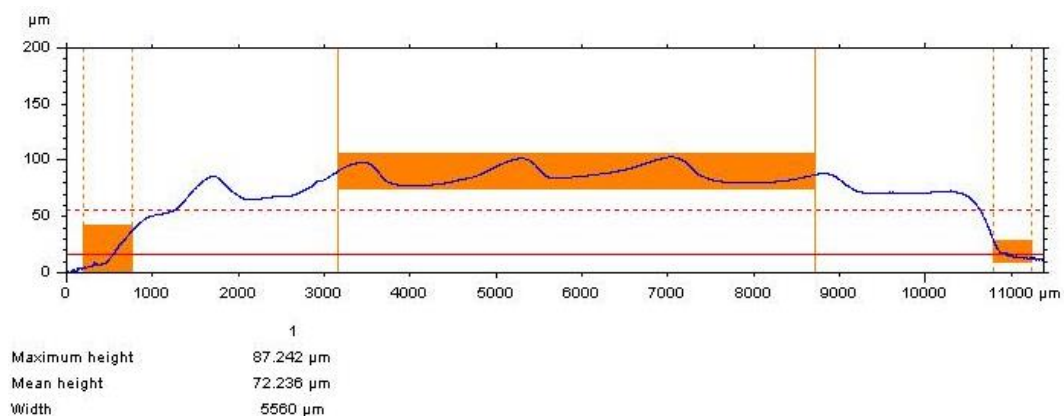


Figure 5.41 Cross sectional profile of 30 layers of XSBR ink printed using a 3D wave pattern

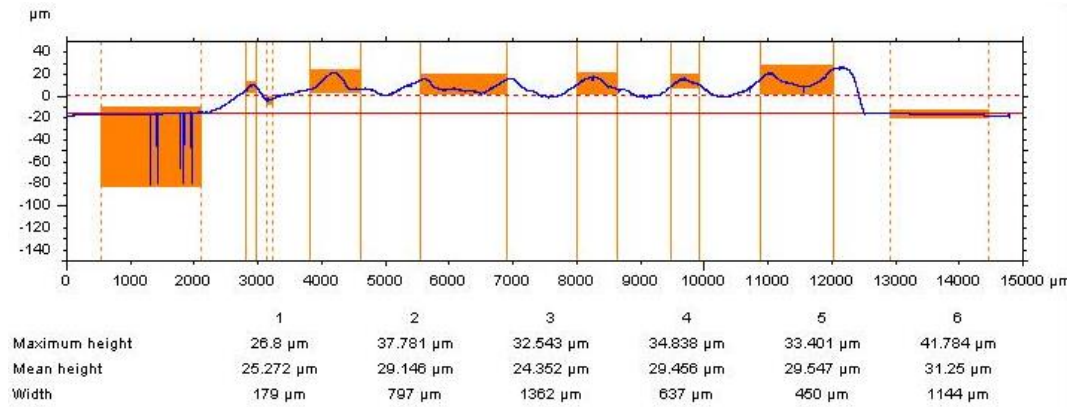


Figure 5.42 Cross sectional profile of 5 layers of XSBR ink printed using a 3D pattern of XSBR printed onto a glass microscope slide

In both instances, there is a significant impact on the general shape of the final sample. XSBR printed onto the PET substrate has a surface that curves upwards (doming); for the ink printed onto the glass, the cross-sectional profile is not curving. Instead it has remained flat as was intended. The wave pattern is more prominent on the PET substrate compared to the glass, where it appears that in some areas the ink was not distributed evenly, and could also possibly be attributed to nozzle blocking. From the pattern that was utilised, the number of waves, or peaks, should be seven. There are only five peaks in the sample printed onto PET and exactly seven for the sample deposited onto glass. This indicates that although the glass substrate promotes spreading to an extent, the pattern that was used for printing remained accurate. The PET substrate yielded a less accurate sample possibly due to spreading, which could be attributed to variations in surface energy of the substrate due to contaminants or debris. This spreading caused some of the peaks to merge, which can also explain the increased in the thickness of the sample printed onto PET. These results demonstrate how much the surface energy of the substrate can affect the pattern and the thickness of the sample during printing.

Due to these results, it was postulated that the drying behaviour of the ink may have had an impact on the doming of the sample during printing.

5.7.4 Effect of Time Delay between Layers

During printing onto PET, it was observed that most of the XSBR samples that were printed retained a domed or curved shape. The intention was to create a sample that has

almost completely straight edges and a smooth level top. It was postulated that insufficient drying was the cause for surface doming. The drying rate in the centre of the printed area may be expected to be slower than at the edge, due to the smaller exposed area and this could lead to the build-up of a thicker water-rich latex layer in the centre. It may also be that insufficient drying may result in the much softer water-rich latex slumping or spreading outwards. An increase in drying time, or the time that each layer was allowed to dry before a subsequent layer was deposited, may be expected to reduce the problem. Therefore, a series of printing trials were carried out with time delays of 0, 30, and 60 seconds between each layer and printing 10, 20, and 30 layers to determine if the delays would affect the surface shape of the printed 1cm x 1cm XSBR square, using the experimental process detailed in the experimental chapter, section 4.9.3. White light interferometry was used to determine the cross-sectional profile of the samples to detect doming.

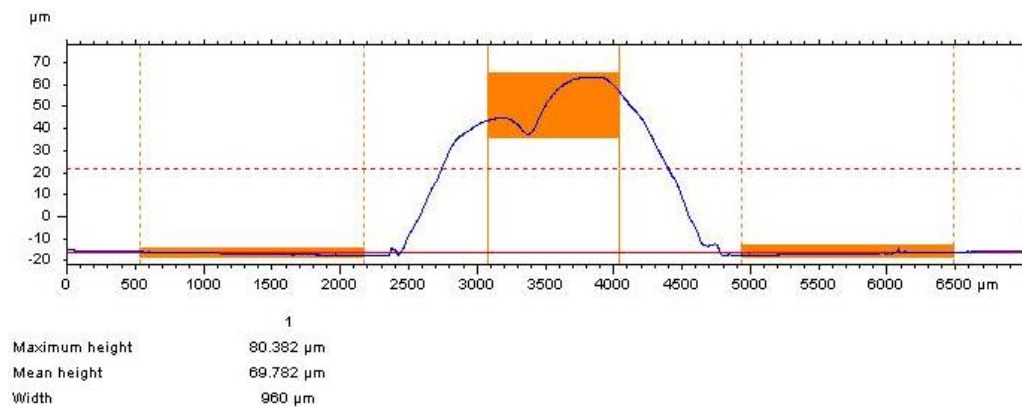


Figure 5.43 10 layers of XSBR ink printed onto PET without time delay

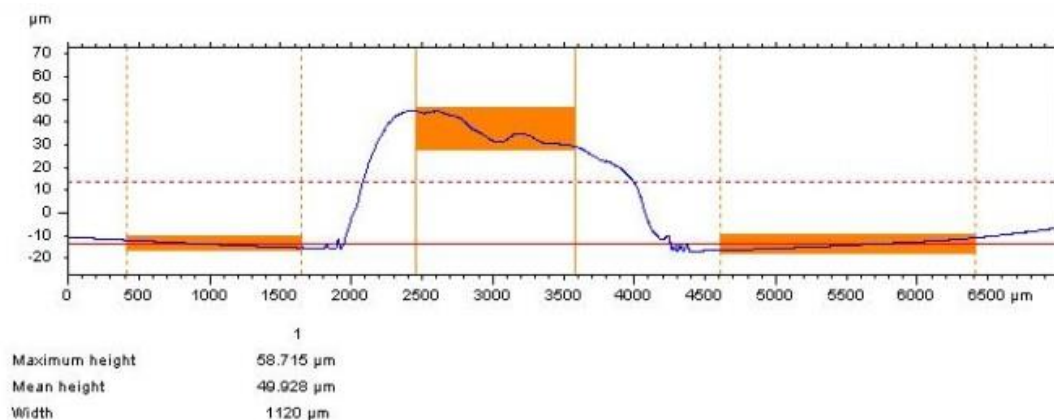


Figure 5.44 10 layers of XSBR ink printed onto PET substrate with a 30 second time delay between layers

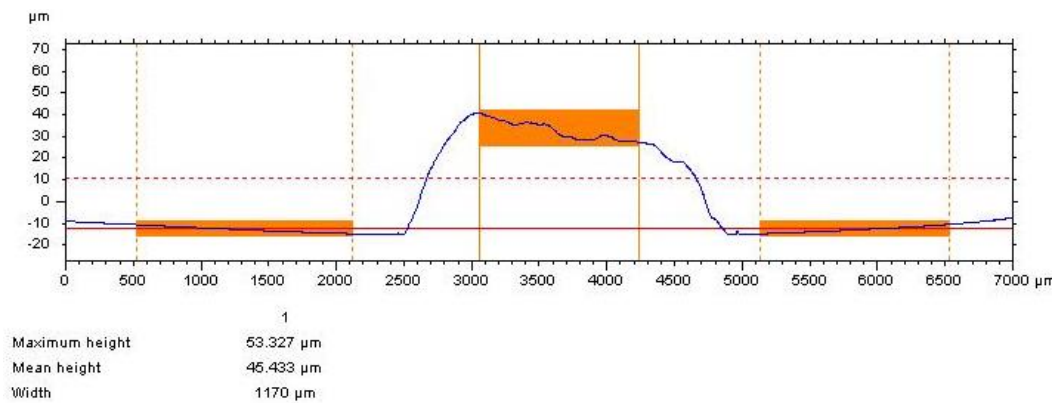


Figure 5.45 10 layers of XSBR ink printed onto PET substrate with a 60 second time delay between layers

From observing Figures 5.43 – 5.45 we can determine that the doming that was prominent with 0 second delay between layers has reduced with the introduction of a 30 second delay, and slightly more so with 60 second delay. All other printing parameters were un-altered, with the same nozzles and jetting frequencies used for each printed sample. These samples were printed side by side onto the same PET substrate. The maximum height for the 60 second delay sample reduced substantially from the 80μm observed for the sample with no delay to 53μm, suggesting that the sample has had more time to dry and the layers to spread more evenly, allowing for straighter edges to develop and for the top surface to level out.

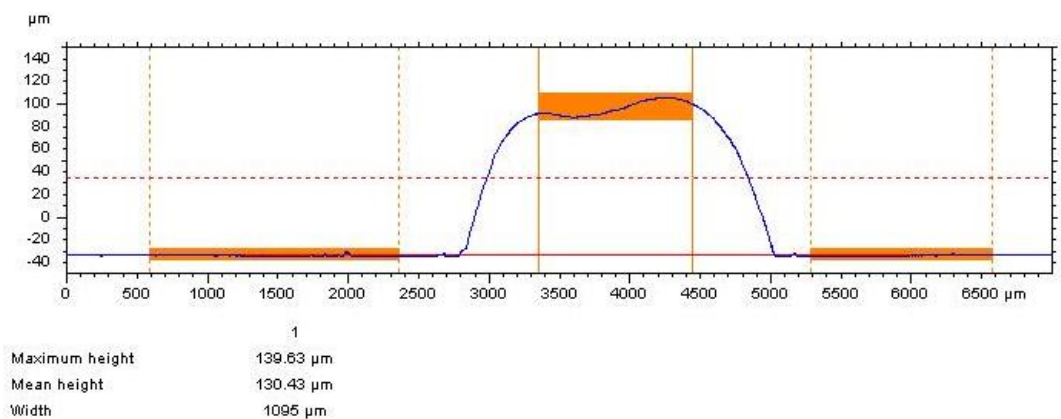


Figure 5.46 20 layers of XSBR printed without time delay

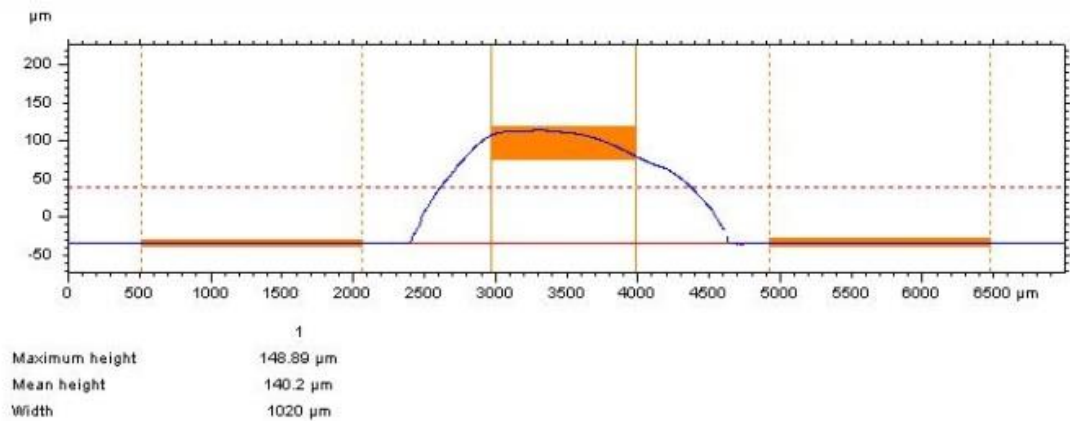


Figure 5.47 20 layer of XSBR printed with a 30 second time delay between layers

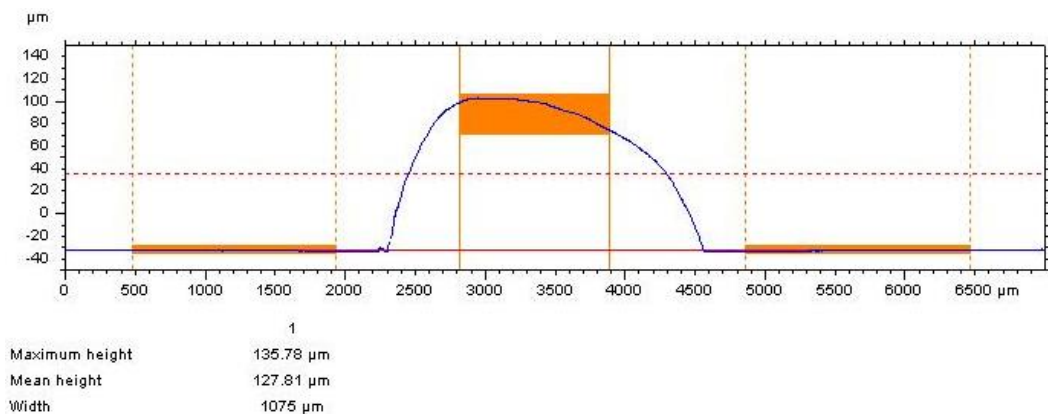


Figure 5.48 20 layers of XSBR printed with a 60 second time delay between layers

The results for 20 layers of XSBR with and without time delay differ from the 10 layers of XSBR. The doming effect increases with the added layers, and the 60 second time delay did not improve the final shape of the pattern. There was also no variation in the thickness of each sample, which indicates that even with the time delay between layers, the ink did not have enough time to dry before the next layer was deposited. The results comparing the mean thickness height of single layers for 10, 20, and 30 layer printed samples with 0, 30, and 60 second delays are shown in Table 5.6.

It is apparent that the number of layers influences the overall individual layer thickness during printing. The thickness of individual layers for the 20-layer sample is higher than the 10-layer sample, which indicates the probability that the added layers slow the drying process. This means that the volume of the material is greater, hence the increase in the layer thickness. Further experimentation and analysis was carried out by printing 30 layers using the same pattern and time delays so that a more rounded comparison could be

created. Figures 5.49 – 5.51 illustrate the results for 30 layers of XSBR printed using 0, 30, and 60 second time delays.

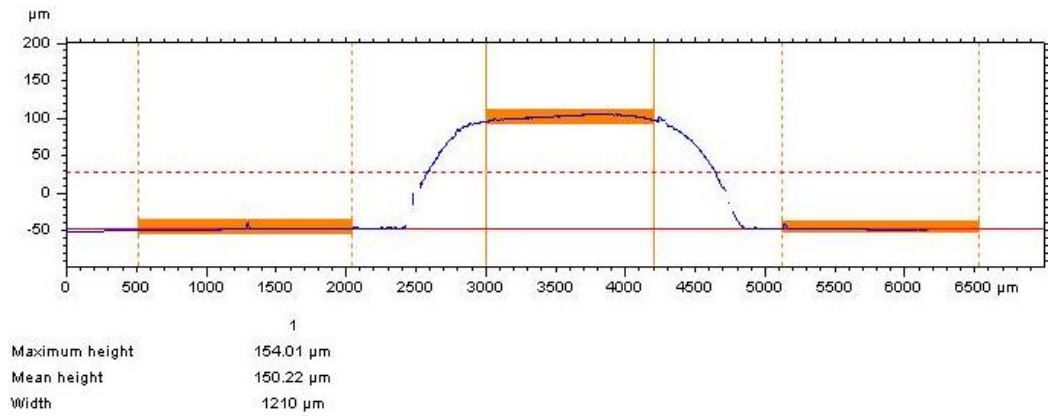


Figure 5.49 30 layers of XSBR printed without time delay

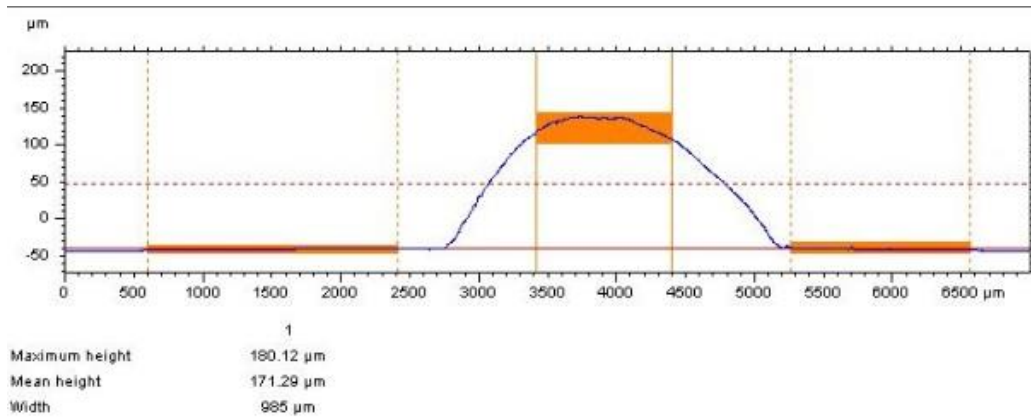


Figure 5.50 30 layers of XSBR printed with a 30-second delay

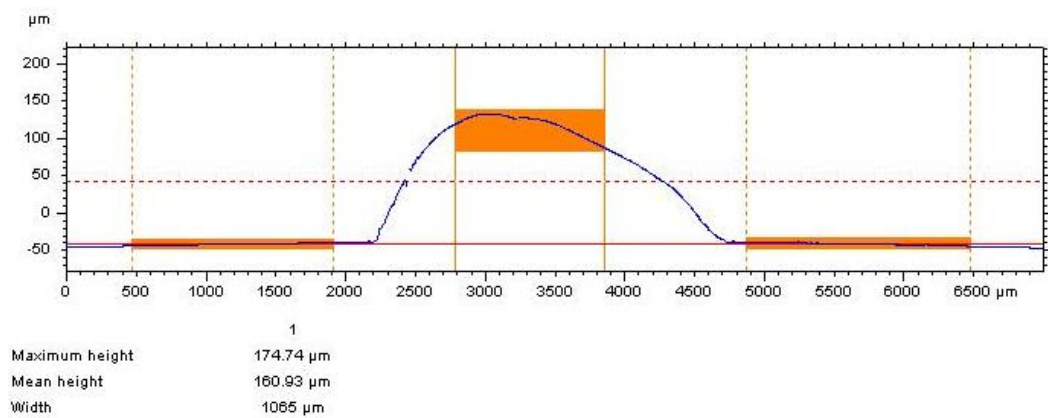


Figure 5.51 30 layers of XSBR printed with a 60 second time delay between layers

Figures 5.49 – 5.51 show the results for 30 layers. The average thickness is similar with and without the time delay indicating that the overall drying rate probably decreases as the number of layers increases. The average layer thicknesses for the 30 layer samples are less than for the 20 layer samples, suggesting there may be some spreading and compression caused by the subsequent layers of ink deposited directly onto a wet layer. Table 5.6 provides a comparison for the individual layer thickness of the 10, 20 and 30 layers printed.

Table 5.6 Comparison of individual layer thickness for 10, 20, and 30 layers of XSBR with varying time delays

	10 Layers (μm)	20 Layers (μm)	30 Layers (μm)
0 sec	6.9	6.9	5
30 sec	4.9	6.7	5.7
60 sec	4.5	7.7	5.3

The results of this set of experiments were somewhat inconclusive, however overall it does seem likely that the time delay between layers was not enough to dry the samples entirely. Hence, another set of experiments was conducted, increasing the temperature inside the Dimatix printer to aid drying.

5.7.5 Effect of Heated Bed

To understand whether the doming effect that has been noted for the XSBR ink and the variation in layer thickness noted in the previous section was due to drying, printing was carried out on heated bed. The pattern was the same one used for printing as detailed in section 5.7.3 with a 30 second time delay. The printer bed temperature was set to the highest level at 50°C and an A4 sized sheet of PET was taped down to secure it. The vacuum was also enabled to ensure that the substrate did not move or warp due to the temperature of the print bed. Table 5.7 details the thickness values for the samples printed with time delays between layers.

Table 5.7 Effect of number of layers on layer thickness with a 30 second time delay (bed temperature 50°C)

Layers	Max height (µm)	Mean height (µm)	Layer height (µm)
10	31	19	1.9
20	70	61	3
30	250	172	5.7
40	291	280	7
50	346	332	6.6
60	438	381	6.3
70	500	489	6.9
80	585	573	7.2
90	663	640	7.1
100	702	699	6.9

Figure 5.52 provides a better illustration of the results presented in Table 5.7.

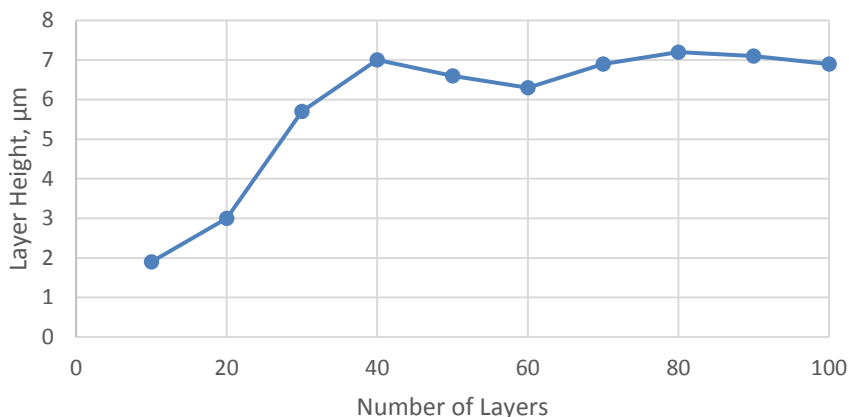


Figure 5.52 A scatter graph illustrating the effect the number of printed layers have on the individual layer height when introducing a 30 second time delay between printing of layers and a bed temperature of 60°C

These samples of XSBR ink were printed to determine what effect does printing multiple layers have on the average layer thickness. The samples with 10 and 20 layers of XSBR have the lowest average layer thickness compared to the 30 layers to 100 layers. This is due to the fast drying of the latex as there are fewer layers, therefore less material, to be dried. As the number of layers increases, so does the average layer thickness because there is more material and it requires more time for the heat of the print bed to permeate through the printed XSBR ink to dry it. However, it appears that after depositing 40 layers of XSBR ink, the thermal insulating effect of the previously deposited layers seem to level off the individual layer height. Although increasing the print bed temperature inside the printer appeared to aid in speeding up the overall drying time of the printed materials, the increase in the number of printed layers appears to counteract the effects of the heating.

5.7.6 Depositing onto Different Substrates

Various substrates were used to deposit XSBR ink onto to study the effects surface energy has on the final shape of the sample. These samples were printed onto a 60°C heated bed due to the number of layers that were deposited, to aid drying and ensure that spreading is minimised.

The first samples that were analysed using the SEM was a 2x3 mm rectangle sample of 100 layers of XSBR ink deposited onto PET, shown in Figure 5.53.

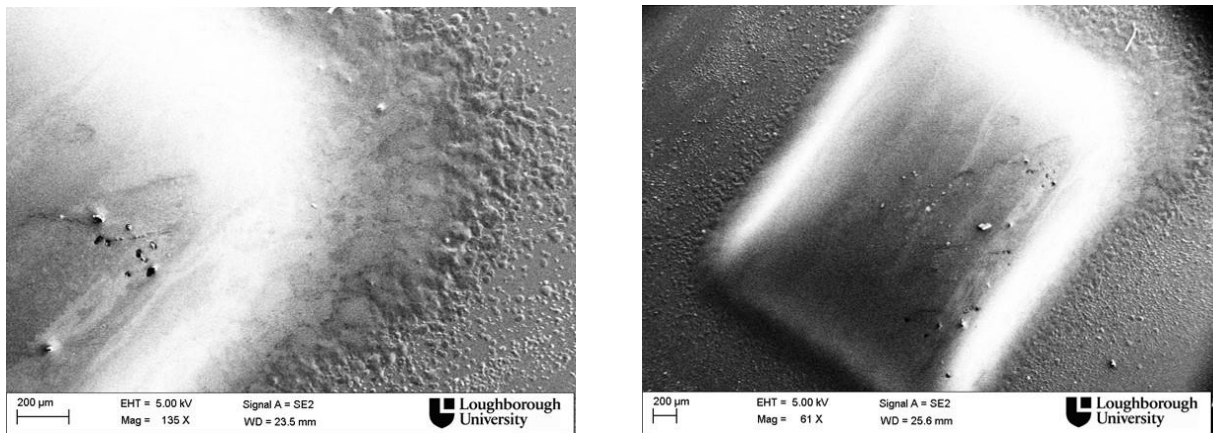


Figure 5.53 SEM image of XSBR latex ink printed onto a PET substrate

Examining the SEM images in Figure 5.53, it was evident that the sample had rounded sides and that there was some spreading. Measuring the sample determined that the spreading was not substantial. The printed sample measured 2.57 x 3.42 mm, a slight deviation from its original pattern. However, most the spreading was concentrated in the top right corner. This type of spreading occurs due to debris or a contaminant that is present on the substrate. If ink comes into contact with the contaminant it re-directs the rest of the ink and creates a new path for the liquid to spread to. This is what has occurred with the sample.

Another sample of XSBR ink was printed onto a PTFE coated fabric, shown in Figure 5.54. The pattern that was used to print this sample was slightly larger than the one for PET, measuring at 4x5mm. Printing onto a highly hydrophobic substrate created a sample that has sharply defined and steep sides as well as a smooth and even top surface. Spreading of the ink was still detected. An entire length of the sample had spread beyond the pattern size. This is likely due to an uneven distribution of PTFE coating on the area of the fabric where ink made contact, rather than an issue with debris. The latex ink had spread evenly and steadily along the path of the fabric.

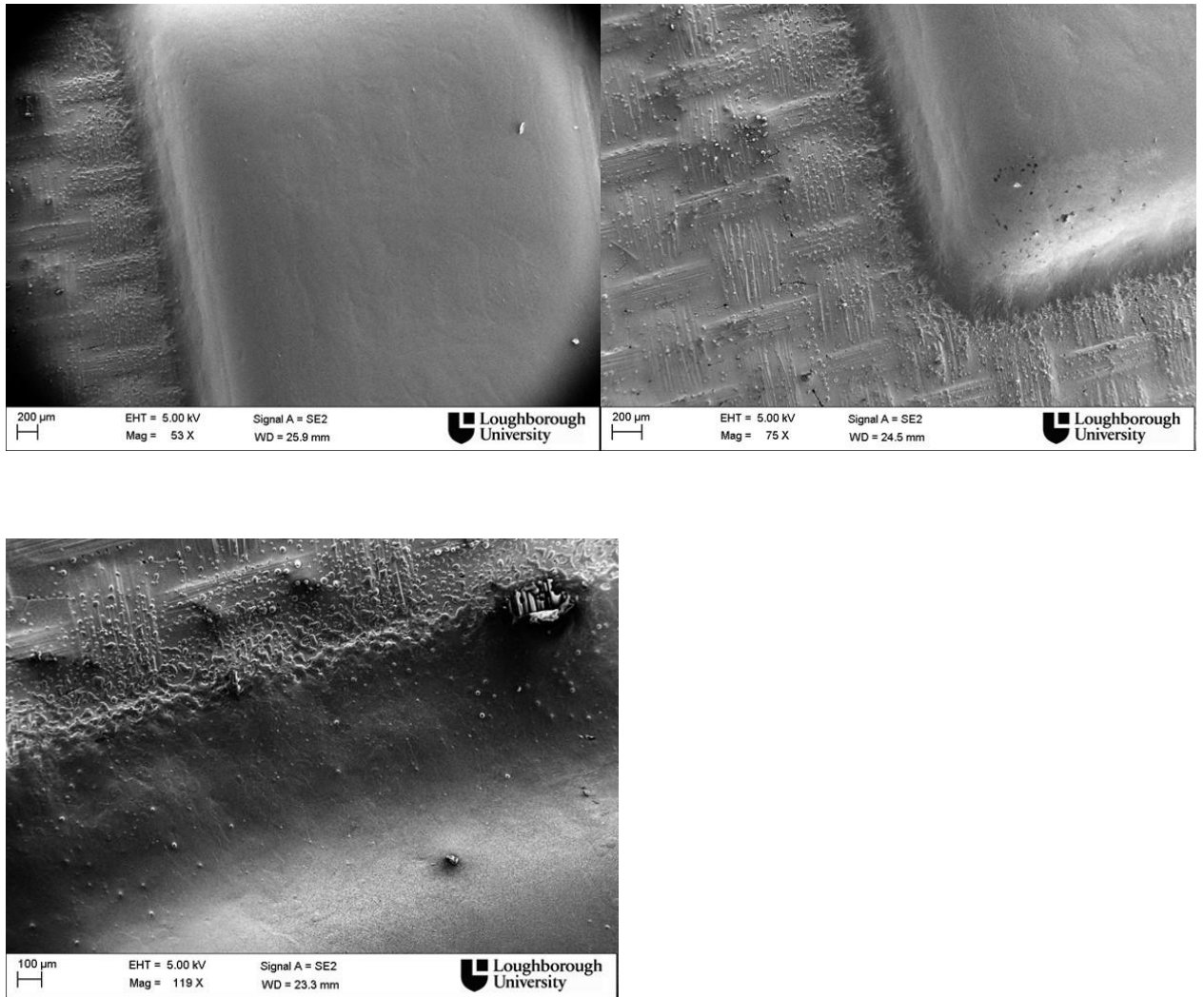


Figure 5.54 XSBR ink printed onto Teflon coated fabric

Using white light interferometry to observe the cross-sectional area, it was found that the top surface was flat and there were no issues with doming. 70 layers of XSBR printed onto the PTFE coated fabric produced a sample with a 628 μ m average thickness. Due to sputter coating the sample with silver particles, it was not possible to measure the sides due to the reflectivity of the silver interfering with the white light. There is also a possibility that the sides were too steep to be measured. The PTFE coated fabric was initially considered as a suitable substrate for printing onto, however due to the uneven surface finish and some issues which involved the XSBR ink spreading where the PTFE coating wasn't evenly distributed (or the gap between the fabric was too great and caused the ink the spread due to capillary forces), this substrate was not considered for further trials.

Finally, a 4x5mm pattern of XSBR ink was printed onto a cast sheet of XSBR latex to observe how the ink behaved once printed onto latex, as shown in Figure 5.55. The

temperature of the print bed was kept at 21°C as the latex substrate was approximately 4mm thick and the heat would not spread evenly enough to dry the ink.

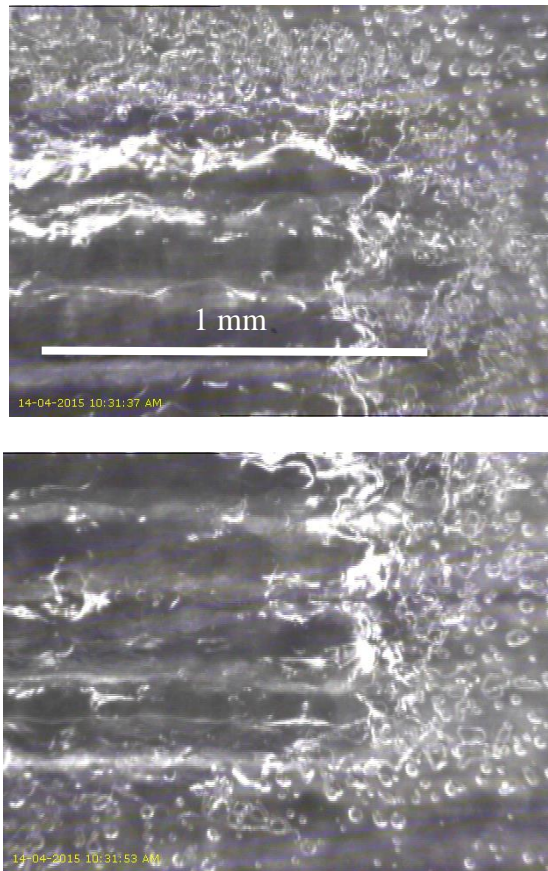


Figure 5.55 XSBR ink printed onto cast sheet of XSBR

Figure 5.55 displays the result of printing ten layers of XSBR onto a cast sheet of XSBR. A significant issue that came up was the overabundance of satellite droplets, which was potentially caused by slightly blocked nozzles. Another characteristic are the printed lines that have remained instead of melding together to form an even and flat surface. This is due to the relatively low surface energy of the XSBR once dried. A similar effect was observed when printing the Loughborough University logo onto a sheet of PET on a heated bed as detailed in section 5.7.2, where the previous layers dried before the next layer was deposited.

5.7.7 3-D Jetting to Create a Latex and Carbon Black Composite

3-D jetting of XSBR latex was carried out along with a conductive carbon black ink supplied by Methode Development Company. Jetting was carried out by printing a layer of XSBR onto a PET substrate, then removing and replacing the print head and cartridge which

contained latex ink and inserting another which contained the conductive carbon black ink to print a layer on top of the XSBR. A total of ten layers of each material were printed in this manner in order to create a final latex and carbon black composite material. The pattern that was used to create this sample was a 3mm x 2mm rectangle. After printing, the sample was sputter coated with silver particles and placed in the SEM for analysis. A key concern that was immediately realised was that the top layer of the carbon black ink was damaged. This was due to the sample flexing during handling as when the carbon ink dried it became fragile and susceptible to cracking and detaching off the surface. These results are illustrated in Figure 5.56.

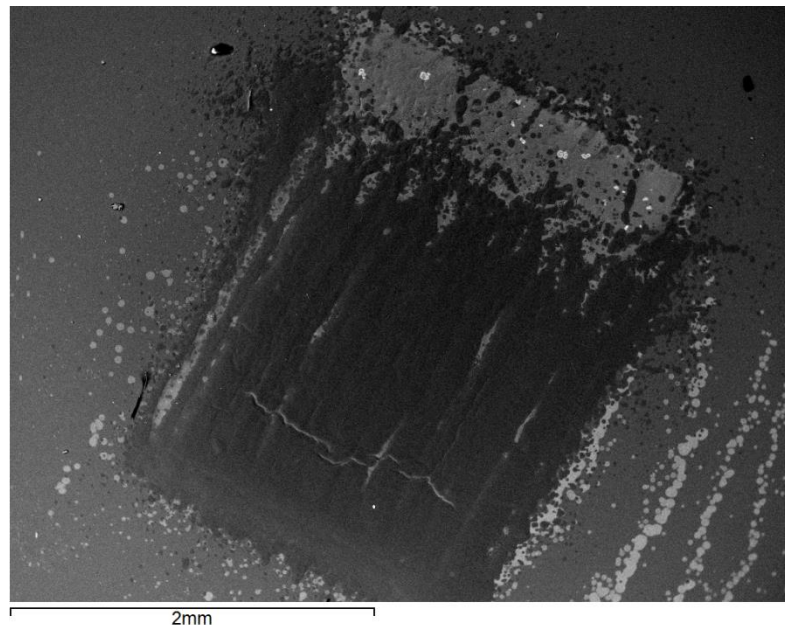


Figure 5.56 XSBR and conductive carbon black 3-D jetted composite material

It became evident that without a top layer or a coat of a protective material that the top carbon black coat would continue to deteriorate. Cracks can be observed in Figure 5.56 as the carbon black was damaged during handling and on one edge the carbon black ink had begun to flake off, revealing the layer of XSBR underneath. This result produced a problem with future considerations of printing XSBR with a carbon black layer on top.

However, another sample was created using a 4x5 mm pattern but using the same printing process, with an additional top layer of XSBR ink was introduced. This sample was then placed in the SEM for observation and illustrated in Figure 5.67.

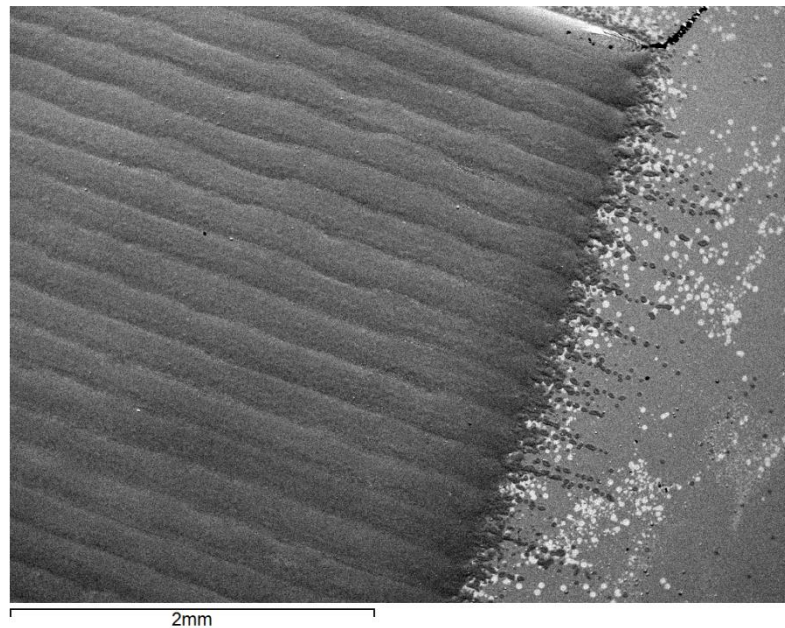


Figure 5.57 The 5x4mm XSBR carbon black composite with a top layer of XSBR latex ink

Printing an additional layer of latex on top of the carbon black ink proved to provide enough reinforcement for the carbon black and prevent it from being damaged during handling. This proved to be a simple yet effective solution.

It is noticeable that the printed lines of XSBR are prominent. This effect is not detrimental and does not hinder the sample's performance as the lines merged together during printing.

Although the current additive manufacturing process that was carried out to create this composite material has produced small samples, it is possible to create a larger sample using the Dimatix inkjet printer. Small samples were created due to the desire to limit the amount of time a print head is not jetting. As detailed in Chapter 4, it was necessary to remove a print head and cartridge once a layer of material was deposited so that a layer of conductive carbon black ink could be printed. This increases chances of the nozzles becoming clogged as there was a minimum 3-minute wait before a layer was printed before another cartridge was switched. In order to avoid clogging of the ink jet nozzles, it would be preferable to utilise a different printer that can hold up to two ink cartridges and with more nozzles that can deposit more ink.

Once the composite sample was ink jetted, several layers of carbon black were printed and their thicknesses were measured using the Talysurf white light interferometer. These samples were ink jetted for the purpose of carrying out dielectric tests to determine their shielding properties; however, it was necessary to determine their thicknesses in order to input the values into the software to use for the SPDR.

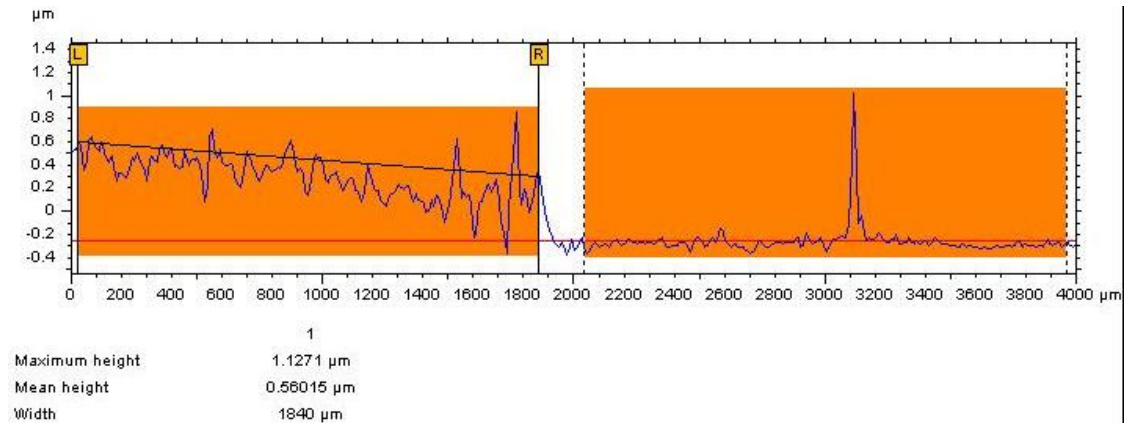


Figure 5.58 Thickness measurement of one layer of conductive carbon black ink printed onto PET substrate

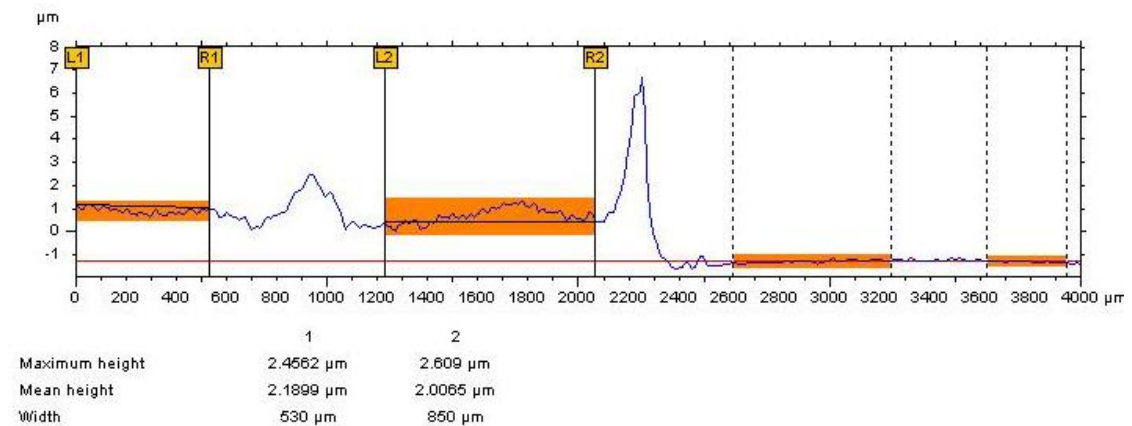


Figure 5.59 Thickness measurement for five layers of conductive carbon black printed onto PET substrate

Two samples were printed in a rectangle pattern onto PET substrate with one and five layers of carbon black in total. One layer of printed carbon black has an approximate thickness of 0.6μm while five layers produced a 2.2μm thickness.

5.7.8 3-D Jetting with XSBR Combination with Resorcinol Curing Resin

A combination ink of XSBR with Resorcinol curing resin was created to print a sample that would be possible to cure in the oven at high temperatures to achieve a cross-linked elastomer. XSBR latex does not contain any curing agents or chemicals, therefore once the latex dries the polymer chains are not crosslinked and therefore do not possess ideal mechanical properties. Some polymer inks utilise a UV curing agent to crosslink the polymer chains, however this results in a hard material and the UV curing chemical has not been tested with XSBR latex. Typically, a sulphur cure is used for curing latex as it is soluble and the chemistry is known to work with the chosen elastomer. However, this would have meant that sulphur particles would need to be introduced into the latex ink, which would increase chances of nozzle clogging; therefore, it was necessary to explore the use of resin curing option. One concern with the addition of the curing resin to the XSBR ink was the potential that the resin would clog the print head nozzles; possibly interfere with the evaporation rate due to the presence of formaldehyde in the resin, as well as the resin affecting the jetting process. However, this issue was not encountered.

Several samples of XSBR ink combined with Resorcinol resin were printed onto a PET substrate, with the print bed temperature set to 50°C to aid the drying time for the ink. Ten, fifty, and one hundred layers of XSBR Resorcinol ink were printed in a 3 mm x 2 mm pattern. These samples were printed in order to determine the cross-sectional profiles of the resin mixed XSBR with the XSBR ink and the height values.

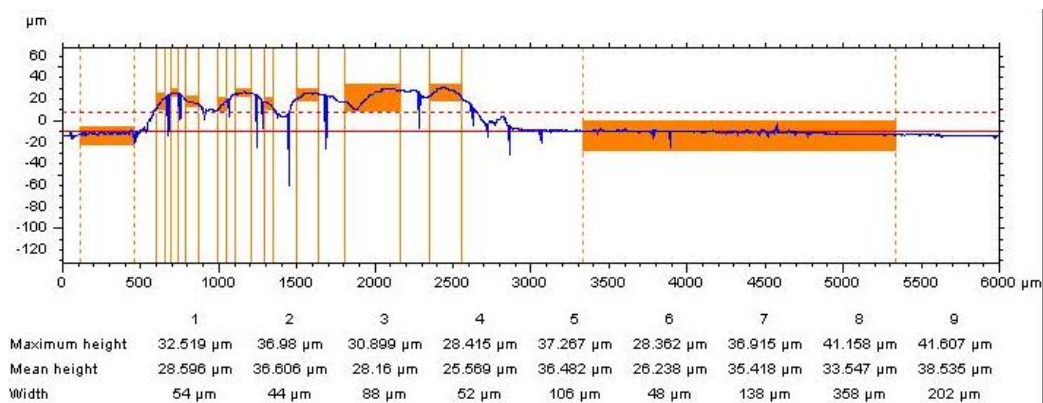


Figure 5.60 Ten layers of XSBR Resorcinol ink printed onto a PET substrate

The cross-sectional profile and maximum height results for the ten layers of ink printed onto PET are consistent with the results detailed in Table 5.7 with ten layers of XSBR ink printed onto the same substrate. The interesting characteristic between the cross-

sectional results detailed in Figure 5.60 and Figure 5.61 is that the XSBR mixed with Resorcinol has produced a sample with a similar pattern at the top of the sample, where the printed lines have merged but a wave pattern can still be seen. This is due to the lines drying fast before they have a chance to completely merge.

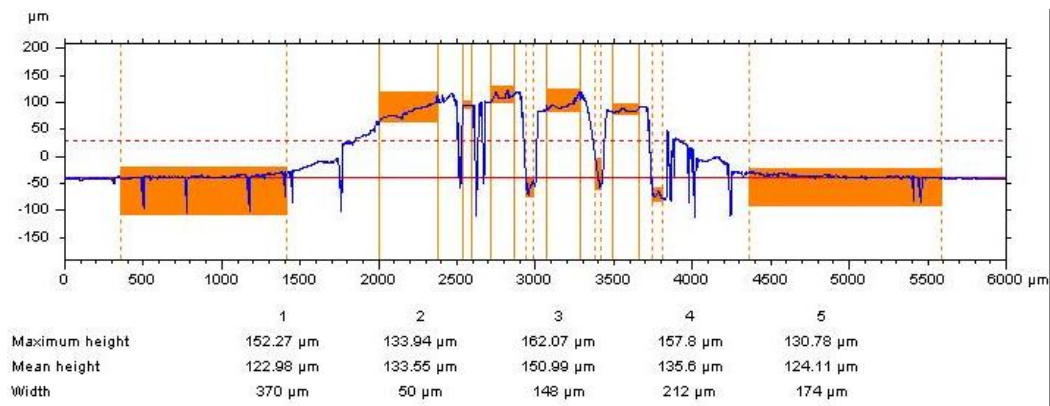


Figure 5.61 Fifty layers of XSBR ink combined with Resorcinol resin printed onto PET substrate

Printing fifty layers of XSBR ink with Resorcinol resin amounted to an average maximum height of 147µm and an average mean height of 133µm. This result means that, if the maximum height is taken into account, the height for a single layer of printed XSBR with resin is 2.94µm and 2.66µm for the average mean height.

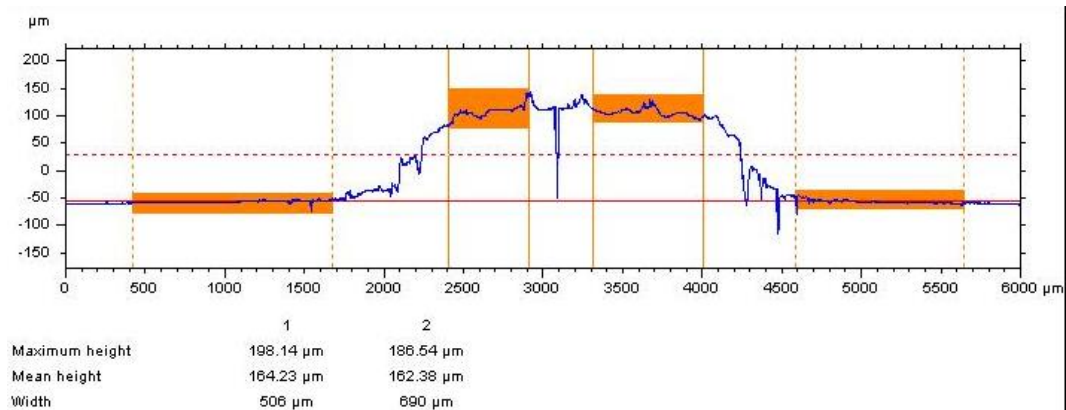


Figure 5.62 One hundred layers of XSBR ink with Resorcinol resin printed onto PET

One hundred layers of XSBR and Resorcinol resin ink printed onto PET substrate has a significantly lower thickness value than was expected. This could be due to an issue with the nozzles in the print head clogging during printing as the temperature of the print

bed was set to 50°C, and this could have caused latex in the nozzles to begin drying, leaving behind debris once it was ejected.

5.7.9 Crosslinking and Tensile Properties of XSBR latex cured with Resorcinol Resin.

This section reports and analyses the swell test and stress and strain results that were obtained on XSBR samples combined with Penacolite resorcinol resin. Figure 5.63 shows the relationship between cure temperature and degree of swelling in toluene. The purpose of the swell test was to determine which temperature values used had produced the most effectively cured samples, as well as to determine what specifically identifies a sample's effective curing process.

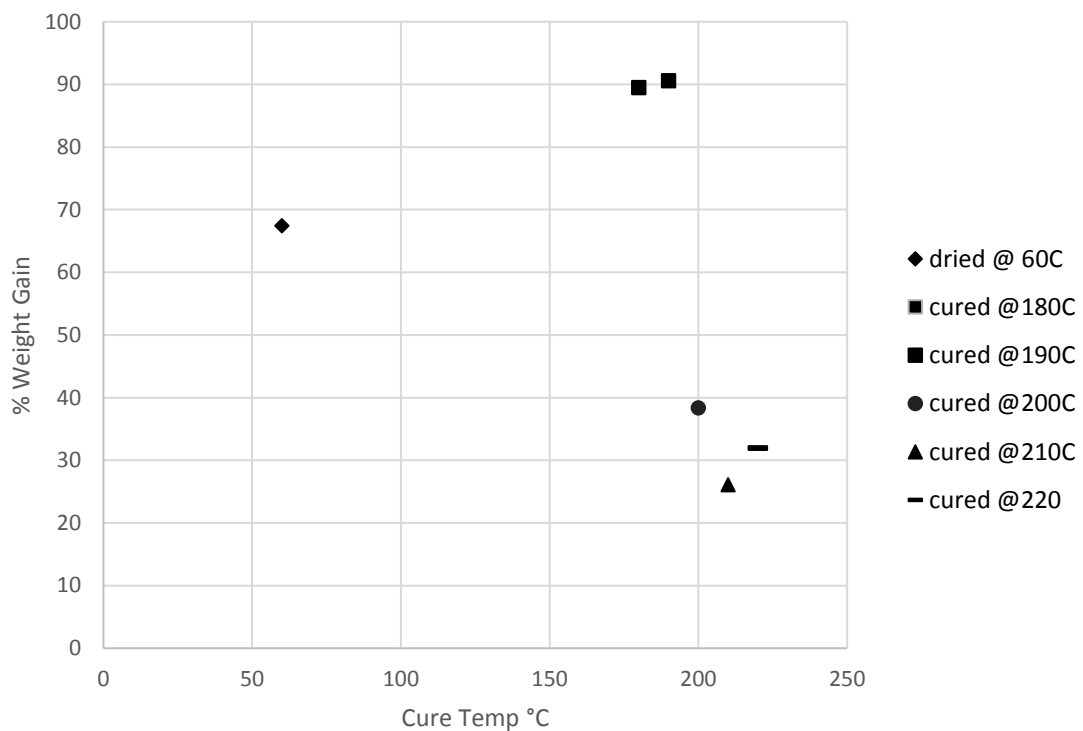


Figure 5.63 % Weight gain results for swell tests on cured XSBR samples, as well as a control test of uncured sample with resin

A control sample of XSBR combined with resin that was only dried at 60°C, but not cured at high temperatures, was used to determine how much an uncured sample of XSBR and resin would swell under normal conditions. Figure 5.63 illustrates that the samples cured at higher temperatures had experienced the least amount of swelling. This indicates that the

materials cured at high temperatures of 200°C-220°C had crosslinked more than the sample materials cured at 180°C and 190°C. The result of the % weight gain for the uncured XSBR and resin sample dried at 60°C is unexpected. The result value was expected to be highest compared to the cured materials, yet it is significantly lower. A possible explanation for this result is that some of the material dissolved in the solvent.

Exposing latex materials to high temperatures potentially degrades the material and could have a negative impact on material's mechanical properties. For this reason, tensile tests were carried out for all the cured samples. The results are illustrated in Figure 5.64.

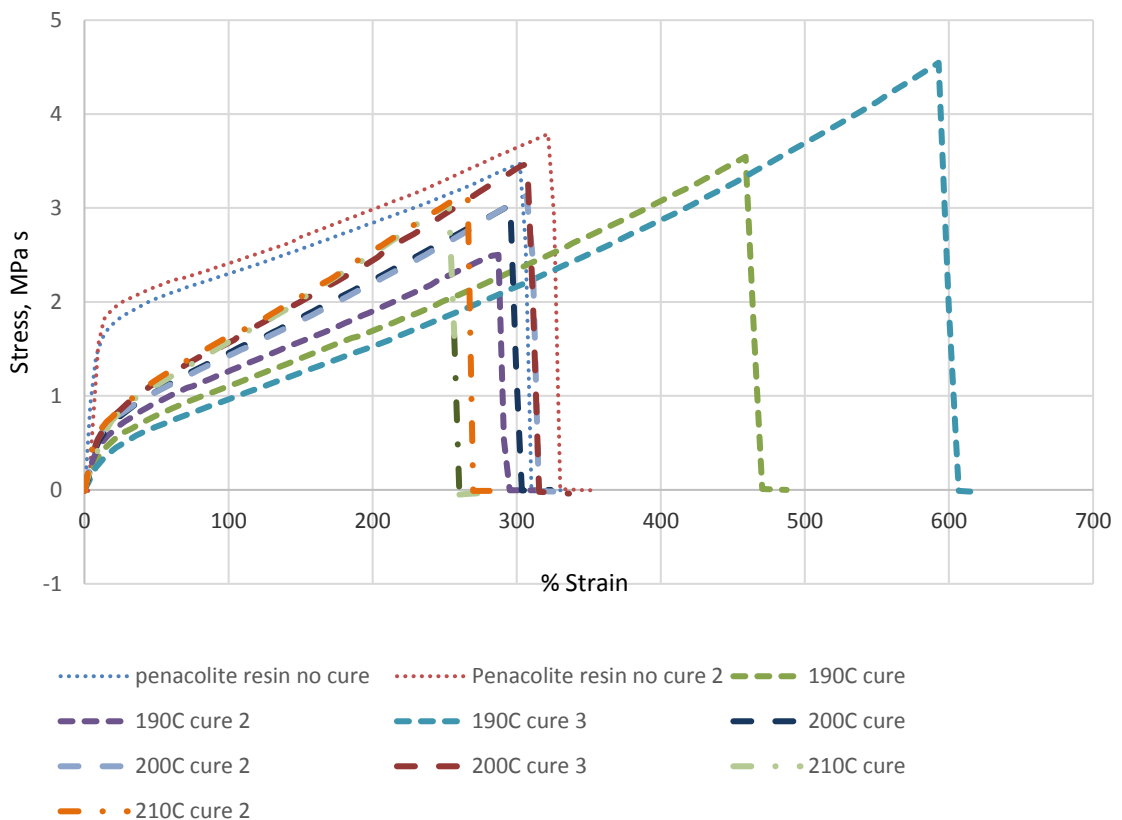


Figure 5.64 Tensile test results for cured and control XSBR samples

Analysis of the tensile test results showed some inconsistencies with the results for the cured samples. Curing the XSBR with the Penacolite Resin did have an impact on the elasticity of the material. There is a trend in Figure 5.64 that shows that the percentage strain at break decreases with the samples that are cured higher than 200°C. This can also be due to the latex material degrading under high temperature.

One physical feature was observed with the cured samples, and that was that the samples cured between 200°C-220°C developed small defects in the surface where it appeared that air cavities had formed due to trapped moisture within the material. Due to these defects, sample 210C cure 3 failed at the start of the tensile test and the result could not be recorded. Another set of samples were created under more monitored conditions to avoid the creation of cavities in the samples which can affect the tensile test results. These results are illustrated in Figure 5.65 and the tensile strength and % elongation are presented in Table 5.8.

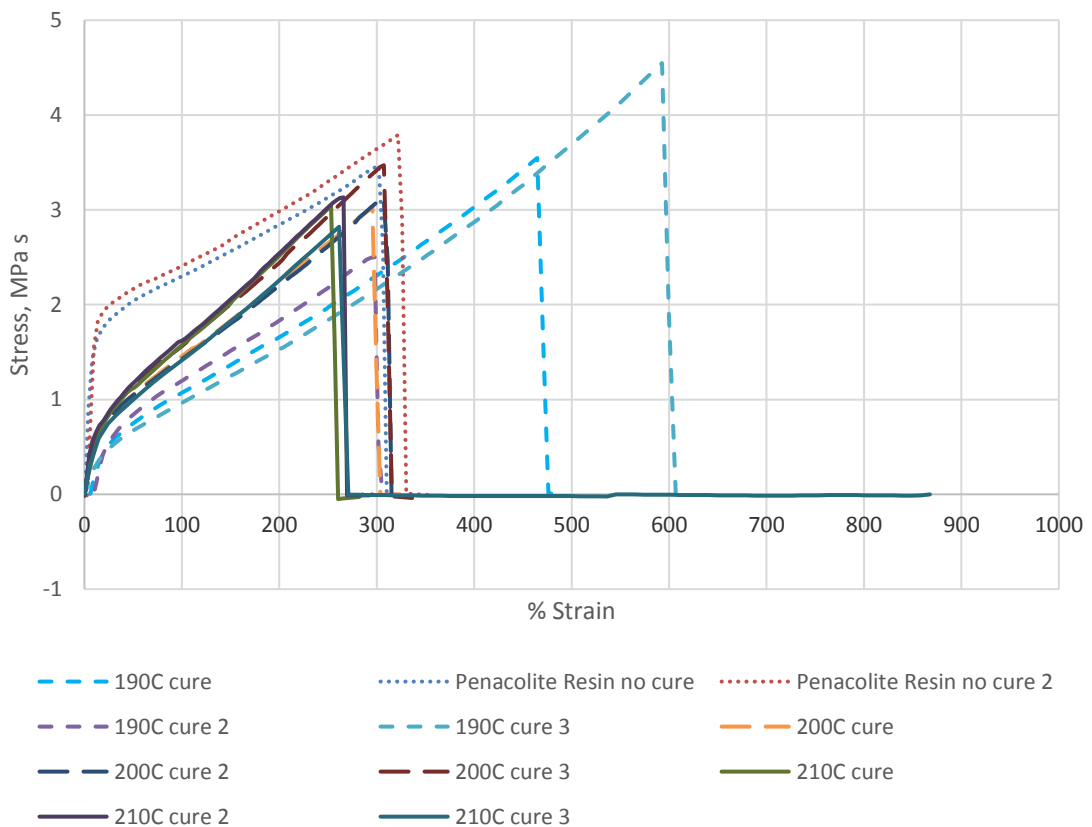


Figure 5.65 Second tensile test results for cured and control XSBR samples

Table 5.8 Recorded values of tensile strength and % elongation

Samples	Tensile strength (Mpa)	% Elongation
Penacolite Resin No Cure 1	306.2	97
Penacolite Resin No Cure 2	338.8	101.9
190C Cure 1	487.5	144.7
190C Cure 2	301.6	95.4
190C Cure 3	599.8	182.1
200C Cure 1	299.6	93.8
200C Cure 2	311.1	97.4
200C Cure 3	311.4	97.5
210C Cure 1	256.6	82.8
210C Cure 2	266	85.7
210C Cure 3	261.2	251.6

When results in Figure 5.64 and Figure 5.65 are compared, although the stress values have not increased, it is visible that the strain values in Figure 5.65 are significantly higher than the initial measurements. The second samples that were created had visibly less surface imperfections, were smoother in texture and there were fewer trapped air pockets. This explains the improved performance of the second sample batch. However, while reviewing both sets of data, a trend is noticeable. The stress and strain values for the samples cured at 190°C were higher than those sample cured at higher temperatures. This result is possibly due to temperature degradation of the polymer, as well as excessive crosslinking of the polymer chains, which resulted in samples that were stiffer than those exposed to lower temperatures. The results of the swell test illustrate that significant crosslinking was achieved for samples cured at temperatures at 200°C and above, which is a highly probable explanation for the low stress and strain values recorded.

Resorcinol resin has proven to be an effective chemical additive to initiate the polymer crosslinking process, which has visually and practically affected the swell and stress and strain measurements. Special attention to the size and thickness of the sample, as well as temperature and exposure time of any polymeric material combined with a curing resin is essential as over-crosslinking can occur at high temperatures and increased exposure

duration. To determine what constitutes an effectively cured XSBR, it is necessary to take several factors into consideration:

- Stress
- Strain
- Swell

An effectively cured polymer sample does not swell considerably after exposure to a solvent as this would mean the material has degraded beyond practical use. Based on the swell tests, the ideal samples were the ones cures between 200°C and 210°C. Samples that were exposed to 190°C were only partially cured, as evidence by the swell and stress and strain results.

5.8 Combining carbon black with latex

Many rubber materials are combined with a filler, such as carbon black, which can enhance the material properties. Carbon black has many uses and there are many variations that have their own specific qualities. Materials that can block or reflect electromagnetic interference are comprised of a conductive material, or contain a filler that has conductive properties. Therefore, to create a novel composite material which has the ability to screen or block electromagnetic frequencies, a conductive carbon black was selected to be combined with the liquid latex.

Combining the conductive carbon black powder with the XSBR latex proved to be ineffective. The powder was incompatible with the latex and agglomerated once it came into contact with the XSBR. Ultrasonic treatment and bath were ineffective at dispersing the agglomerates. Another conductive carbon black material was chosen to replace the powder from Bare Conductive. The carbon black is thinned with water that creates a nontoxic, water-soluble paste that has high resistivity. This material is mainly used to create conductive circuits and therefore an ideally conductive material to combine with latex to produce a material that could have similar shielding properties as the rubber materials that are used for electromagnetic shielding.

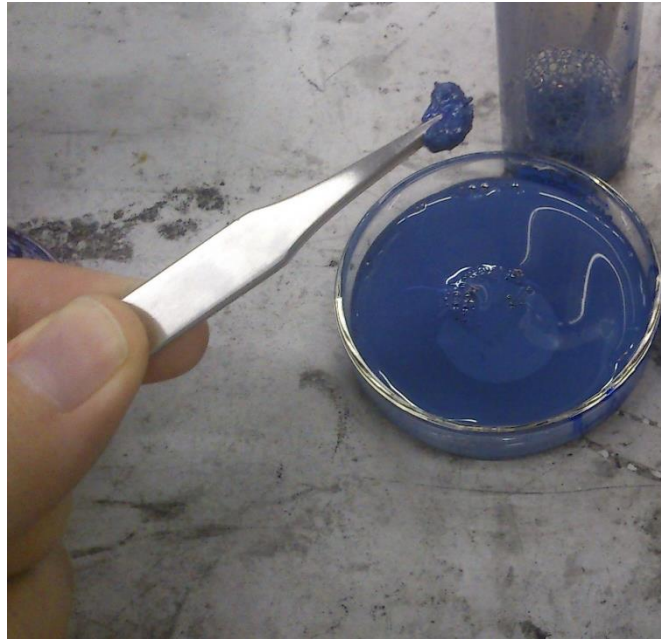


Figure 5.66 Conductive carbon black powder mixed with diluted XSBR latex

The image in Figure 5.66 illustrates the combination of the conductive carbon black powder with diluted XSBR. Once the powder was introduced into the liquid latex, it proceeded to agglomerate. The carbon black particles agglomerated into a mass that was surrounded by a thin layer of XSBR, however in the middle of the mass the carbon black remained in its powder state. The powder reacted as a hydrophobic material once it came into contact with the latex. This could be caused due to the polarity of each material, making them incompatible for mixing.

A simple test was conducted with the conductive carbon black powder and the paste from Bare Conductive to observe how both materials interact with water. The results of this test are illustrated in Figure 5.67. It is evident that after three hours of the samples being stagnant the conductive carbon black powder had separated from the water, while the paste remained in a homogeneous dispersion. This is likely due to the additives in the carbon black paste which prevent the material from drying out and settling to the bottom of the container. These results lead to the creation of cast XSBR with various concentrations of carbon black paste in order to carry out measurements of the dielectric properties.

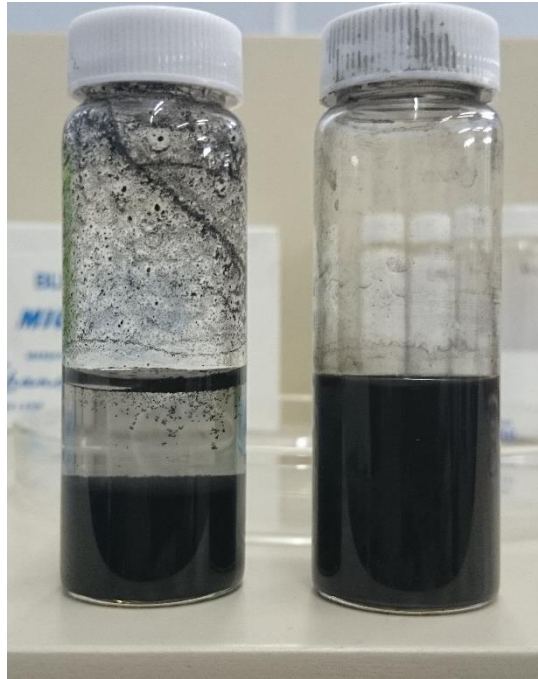


Figure 5.67 Diluted conductive carbon black powder on left and diluted conductive carbon black paste on right. Samples were left stagnant for three hours

The carbon black paste, once dispersed in de-ionised water, was then effortlessly combined with XSBR latex. Figure 5.68 illustrates the successful combination of the Bare Conductive carbon black paste with XSBR latex.



Figure 5.68 Carbon black paste combined with XSBR latex

Once the carbon black paste was combined with XSBR latex, it was placed in a 15cm diameter petri dish and placed in the oven at 60°C to dry overnight as demonstrated in Figure 5.69. Comparing the photographs of the carbon paste mixture in Figure 5.69 to the mixture

illustrated in 5.70, we can observe that although the colour is similar, there are no agglomerates in the mixture with the carbon paste.



Figure 5.69 XSBR combined with carbon black in a petri dish to be dried

After the sample was left to dry for approximately 3 hours, it was taken out of the oven to observe the drying process. The sample had started to dry and form a top film layer that was contracting as the sample was drying, leading the top surface to develop an uneven surface finish around the edges.

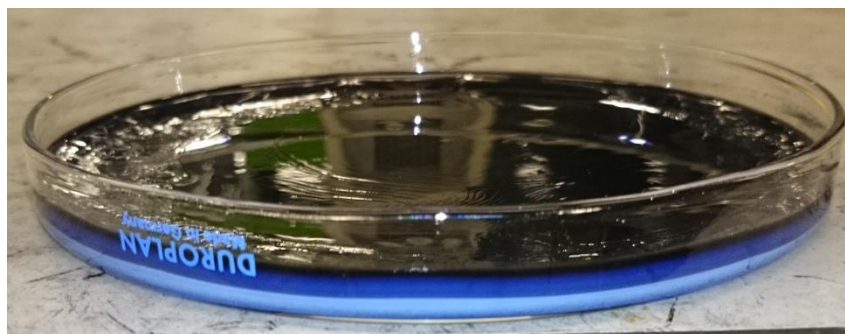


Figure 5.70 Colour changes were observed during the drying process

The top layer of the material as observed in Figure 5.70 changed colour once the drying process was initiated from a light purple colour to black. Underneath the top film layer, the XSBR and carbon black was still in a wet state, as evidence by the colour difference. The difference in colours are not due to settling, but drying.

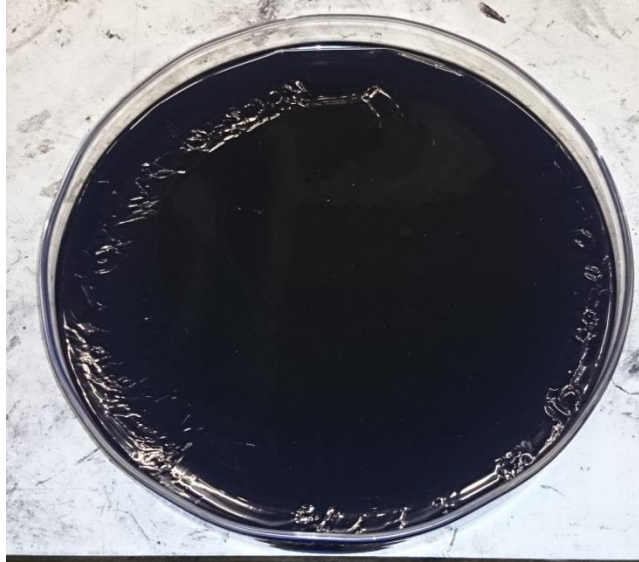


Figure 5.71 Dried sample of XSBR combined with carbon black paste produced for dielectric measurements

The final dried sample, as shown in Figure 5.71, changed colour entirely to black. There were some inconsistencies with the surface levelness; however, the material in the middle of the petri dish was smooth enough to cut into a 6x7cm rectangle to use for dielectric measurements. Similar drying results were observed for samples created using 2, 5, and 10 weight percentage of carbon black to XSBR latex.

The dielectric results for these samples are available and discussed in Chapter 6, section 6.2.1.

5.8.1 TGA Results for Carbon Black Content in XSBR

Thermogravimetric analysis (TGA) was used to determine the carbon black concentration in the printed XSBR composite materials. TGA was also used to analyse the properties of 70 layers of XSBR ink that were printed without the addition of conductive carbon black ink as a control sample. The mass of the samples that was recorded for the

TGA results ranged from 14mg to a maximum of 18mg. Figure 5.72 illustrates the TGA results for printed XSBR.

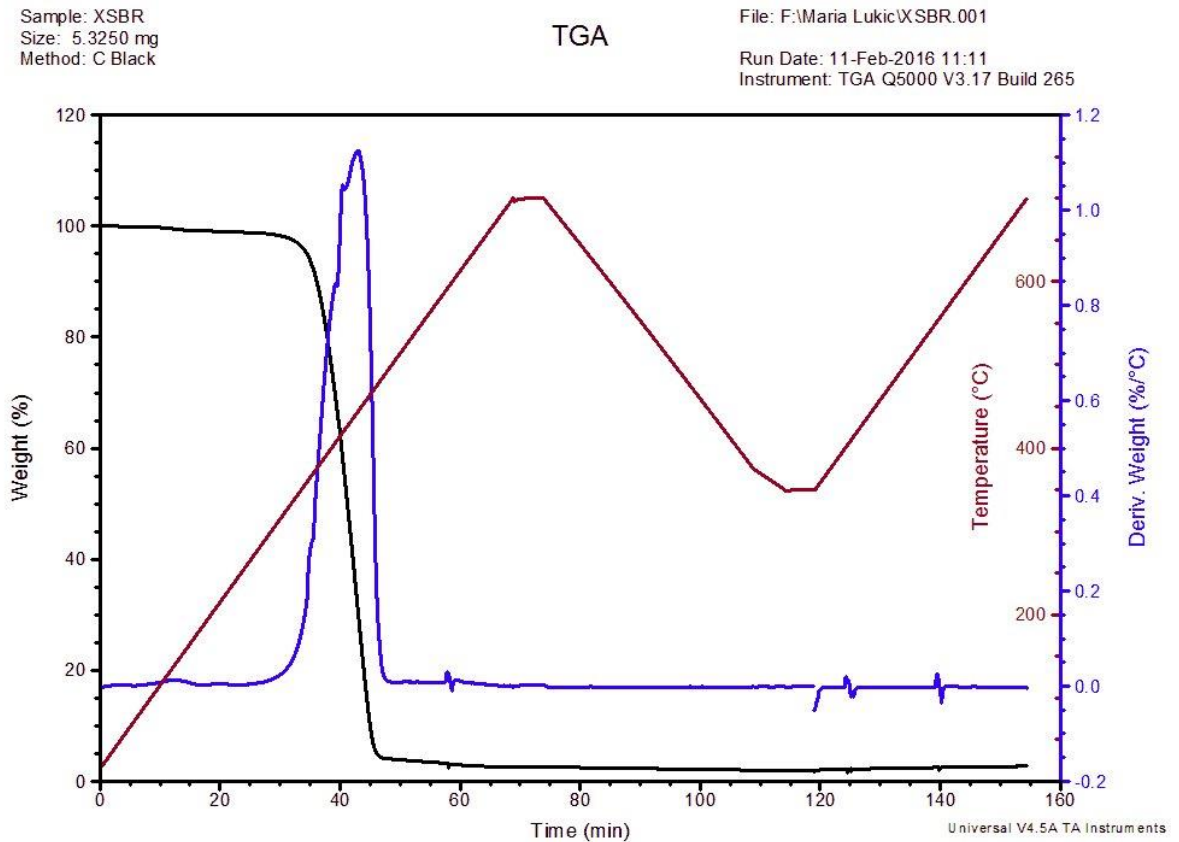


Figure 5.72 TGA results for printed XSBR ink

In Figure 5.72, we can observe the results of the XSBR latex decrease in mass as shown by the black line. The results indicate that there was some residual carbon black content in the sample. However, this could be due to a slight contamination of the sample during handling.

TGA was also carried out on samples that had conductive carbon black paste combined with the XSBR latex, with carbon black ink printed onto cast sheets of XSBR, and with carbon black ink printed onto pre-vulcanised natural rubber. TGA results for a sample of natural rubber with a high 55% phr carbon black content was also analysed to compare with the samples that were printed. The conductive carbon black printed onto PET was not analysed due to pyrolysis that PET undergoes at high temperatures. This would have led to a discrepancy in the carbon black content of the printed sample.

Results shown in Table 5.9 indicate a slight difference in the carbon black concentration of the samples. The crosshatch pattern printed onto caste XSBR had the highest concentration of carbon black, while the lowest value recorded belonged to the caste NR latex with one layer of printed conductive carbon black ink on the surface.

Table 5.9 TGA carbon content results for all samples

Samples	Weight %/°C
CB ink printed on NR	0.34
CB ink parallel lines printed on NR	0.74
XSBR w/ conductive carbon black paste painted on surface	1.50
XSBR combined w/ CB paste	1.46
XSBR w/ printed CB ink crosshatch pattern	1.54

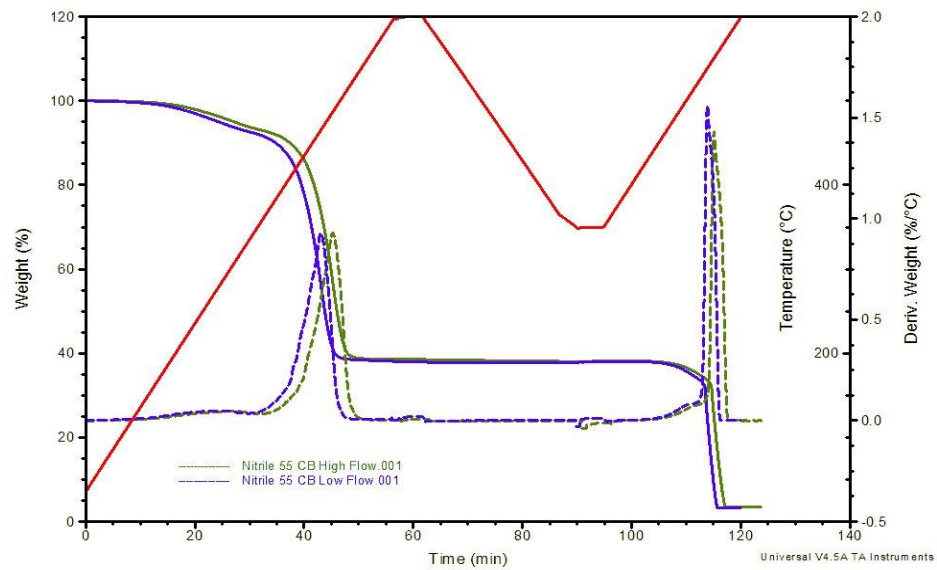


Figure 5.73 TGA results for NR with 55% phr carbon black

From the TGA results for the 55% phr natural rubber material shown in Figure 5.73, we can observe that as expected the carbon black content is high compared to the samples previously tested with printed carbon black and combined with XSBR latex.

From the results presented in this section, it is evident that the concentrations of carbon black in all measured samples is low, and that as expected the lowest carbon black content belongs to the single layer of carbon ink printed in crosshatch pattern.

5.9 Conclusion

This chapter details the findings from the experiments listed in Chapter 4. The prominent findings in this chapter determined that slight modifications to the elastomers were required to ensure successful continued printing and prevent blockages in the printhead from developing; this included diluting the latexes to reduce solids content and adding TGME to reduce the evaporation rate of the liquid. The addition of the humectant, however, had some unexpected results for CR, HNBR, and XNBR latexes where it caused the latex particles to agglomerate. Despite attempts made to reduce this effect from occurring, it was determined that even partial particle agglomeration would cause problems during ink jetting and a decision was made to select XSBR latex as the final material despite its higher surface tension values.

Inkjet printing was carried out on a variety of substrates, which included glass slides, PET, PTFE coated fabric, and PTFE tape. These materials were chosen due to their surface energy properties to test the effects of printing onto hydrophilic and hydrophobic materials. After a series of droplet and contact angle tests, where small droplets of XSBR ink were deposited on these substrates, it was determined that PET possessed the more ideal surface energy that would allow for ideal wetting without compromising resolution. Multilayer printing of XSBR proved successful and illustrated an intriguing doming effect when printing multiple layers using a small pattern size compared to larger patterns used, which can be attributed to insufficient drying between layers.

Attempts at adding conductive carbon black powder to XSBR to create a material capable of providing EMI shielding proved challenging due to the hydrophobic properties of the powder, which was difficult to disperse homogeneously in the liquid and in all attempts resulted in the powder agglomerating. Therefore, another solution was found that combined a version of conductive carbon black paste from Bare Conductive diluted with de-ionised water and then combined with XSBR was shown to be the ideal mixture.

References:

[1] Jang, D., Kim, D., Moon, J., Jang, D., Kim, D., & Moon, J. *Influence of Fluid Physical Properties on Ink-Jet Printability Influence of Fluid Physical Properties on Ink-Jet Printability*. (25 February 2009), pp. 2629–2635.

- [2] Tuladhar, T.R. and Mackley, M.R. *Filament stretching rheometry and break-up behaviour of low viscosity polymer solutions and inkjet fluids*. (2008). *Journal of Non-Newtonian Fluid Mechanics*, 148(1-3), pp. 97–108
- [3] Nahid, M. *In Quest of Printed Electrodes for Light-emitting Electrochemical Cells: A Comparative Study between Two Silver Inks*. (2012). Master Thesis in Physics, Umeå University, Linnaeus Väg 20, Umeå.
- [4] Balani, K., Batista, R.G., Lahiri, D. and Agarwal, A. *The hydrophobicity of a lotus leaf: A nanomechanical and computational approach*. (2009) *Nanotechnology*, 20(30), p. 305707
- [5] Dongliang Tian, Yanlin Song, Lei Jiang. *Patterning of controllable surface wettability for printing techniques*. (2013). *Chemical Society Reviews*, Vol. 42, no. 12, pp. 5184.
- [6] HaiJun Yang, ZhengChi Hou, Jun Hu. *Surface modification of ultra-flat polydimethylsiloxane by UV-grafted poly(acrylic acid) brushes*. (2012). *Journal of Applied Polymer Science*, Vol. 123, no. 4, pp. 2266-2271.
- [7] JaiJun Yang, HuaBin Wang, ZhengChi Hou, Peng Wang, Bin Li, JingYe Li, Jun Hu. *Fabrication and application of high quality poly(dimethylsiloxane) stamps by gamma ray irradiation*. (2011). *Journal of Materials Chemistry*, Vol. 21, no. 12, pp. 4279.
- [8] Dou, R., Wang, T., Guo, Y., & Derby, B. *Ink-jet printing of zirconia: Coffee staining and line stability*. (2011). *Journal of the American Ceramic Society*, vol. 91, no. 11, pp. 3787-3792.
- [9] D. Hoath, S., Martin, G. D., & Hutchings, I. M. *Effects of fluid viscosity on drop-on-demand ink-jet break-off*. (2010). *NIP26 and Digital Fabrication*, pp. 10–13.
- [10] Derby, B., *Inkjet Printing of Functional and Structural Materials: Fluid Property Requirements, Feature Stability, and Resolution*. *Annual Review of Materials Research*, Vol 40, 2010. **40**: p. 395-414.
- [11] Reis N, Derby B. *Ink jet deposition of ceramic suspensions: modelling and experiments of droplet formation*. (2000). *MRS Symp. Proc.* Vol. 624, pp. 65–70.

Chapter 6: EMC Results

6.1 Introduction

One of the objectives of this project was to analyse the potential of utilising 3-D printing to create a novel polymer material that would offer protection against electromagnetic interference. A common industrial method for manufacturing EMI shielding polymers is to combine conductive or metallic fillers during the manufacturing process [1-4]. These fillers help to insulate any electrical components sensitive to interference frequencies.

This chapter presents and analyses the results of the experiments that were carried out on polymer samples combined with conductive carbon black, with conductive carbon black patterns printed on the surface of polymers, as well as the measurements of only carbon black ink. The novelty of this method of EMI shielding lies in the 3-D printing method of producing shielding materials.

6.2 Electromagnetic Simulations

Prior to carrying out experiments on sample materials, it was determined that simulations of electromagnetic experiments would be useful to study the propagation of EM waves through various materials and to aid in the physical experiment. As well as providing a useful visual aid of what occurs to a material during exposure to EM waves, simulations can in some capacity help with experimentation planning and to compare simulated results with the experimental results to determine consistency in the values that have been obtained.

The EMPIRE XCcel V6 software was utilised to carry out simulations of monopole antennas. At the start of the EMI shielding experimentation plans, it was initially decided that monopole antennas would be created and utilised to measure the shielding properties of the polymer materials. A simulated 3-D representation of this experiment was modelled using the EMPIRE software and is illustrated in Figure 6.1.

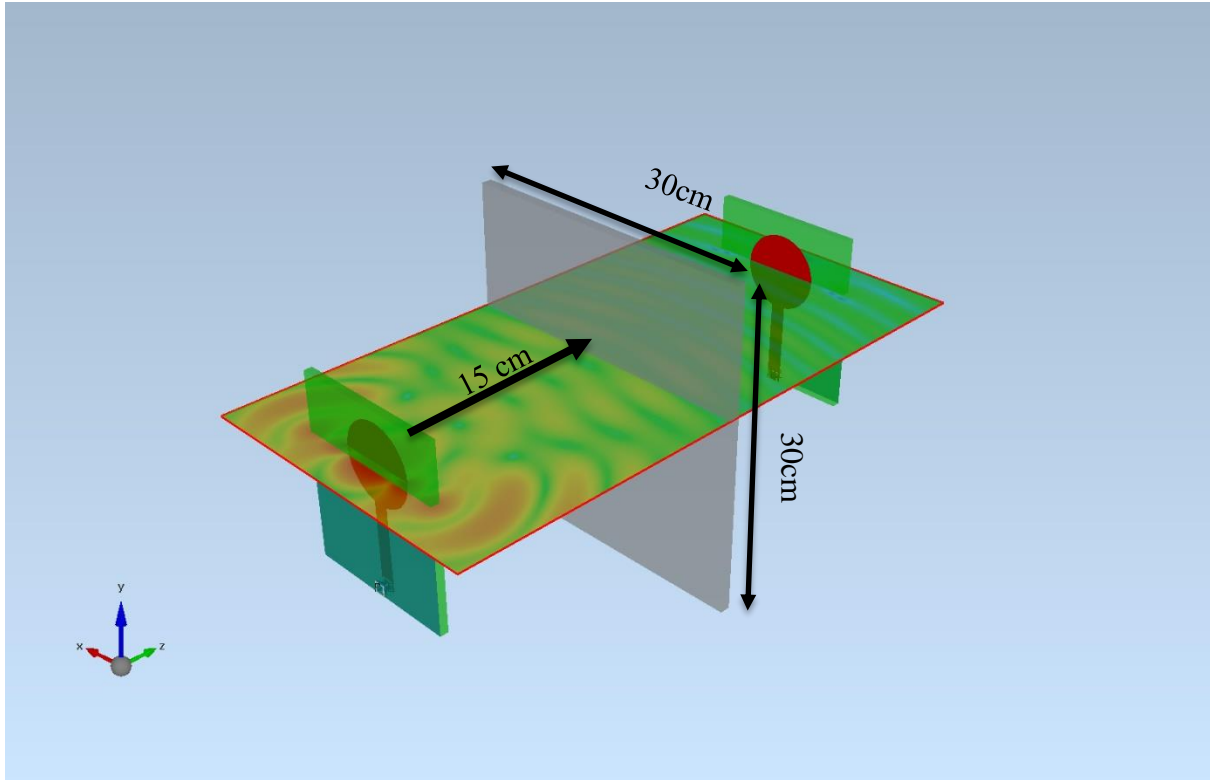


Figure 6.1 Monopole antenna simulation

The monopoles were simulated at 30cm distance apart, attached onto a RF-45-0620 (Taconic) material, which is a low loss high performance laminate. A sheet of copper with 0.8 mm thickness was positioned precisely in between the antennas, 15cm away from each antenna. This material has a loss tangent of 3.5 and a relative permittivity of 2.45 for a thickness of approximately 1.5mm, and was to be the material that would provide shielding against the EM waves that would be simulated. The dimensions of the monopole antennas are detailed in Figure 6.2.

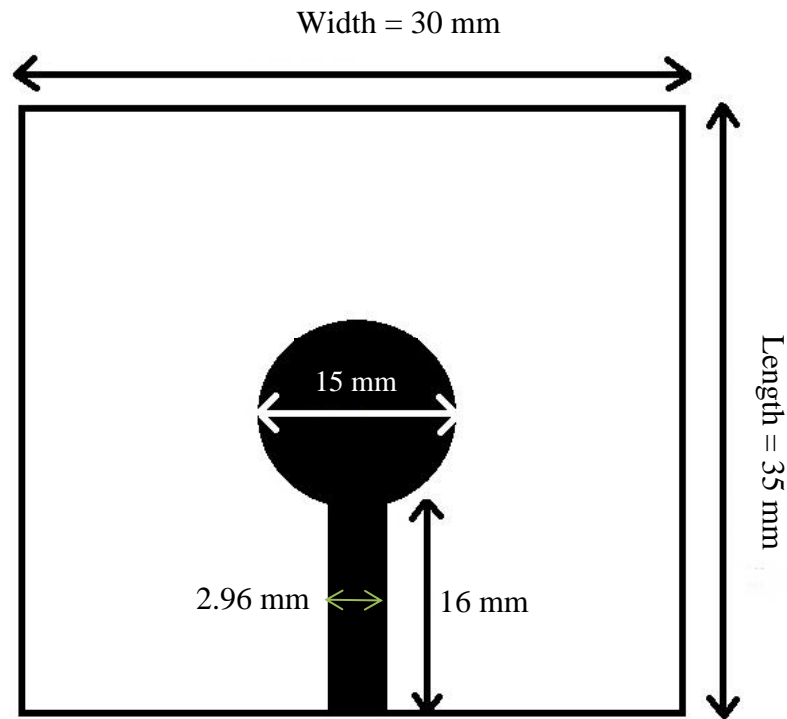


Figure 6.2 Monopole design (Figure not to scale)

The thickness of the polymer shielding material was entered as 1.6mm, which was determined based on the average thickness of samples that were produced during casting of latex samples, while relative permittivity and dielectric loss tangent values were entered as 4.5 F/m and 0.005 respectively.

For the simulations, an infinitely wide copper substrate was utilised which extended to the edges of the problem space; however, in the measurements the copper sheet was 0.83mm thick and bonded to a polystyrene material of approximately 5 mm.

Creating a simulation of the experiment was carried out to help visualise the propagation of the EM waves through the space and observe how the waves interact when a shielding material is placed between the probes. The simulations also enabled the user to observe the effects that changing the material properties, such as thickness, material type, and size, and how that would influence the overall result.

6.3 Electromagnetic Characterisation of Latex and Conductive Carbon Black Utilising Monopole Antennas

6.3.1 Latex samples with Carbon Black

Figures 6.3 to 6.5 illustrate some of the samples that were utilised during monopole antenna measurements. The latex samples included cast sheets of XSBR, NR, and XNBR. The total thicknesses of the samples (polymer with carbon printed on surface) were as follows:

- 1 layer of conductive carbon black onto XSBR: 1.471mm
- 5 layers of conductive carbon black onto XSBR: 1.382mm
- 10 layers of conductive carbon black onto XNBR: 1.613mm
- Horizontal pattern (Fig. 6.6) printed onto XSBR: 1.43mm
- Cross-hatch pattern (Fig. 6.7) printed onto NR: 2.295mm

Using white light interferometry to measure the thickness of the carbon layer on top of the polymer and PET substrates, 1 layer of conductive carbon black measured at $1\mu\text{m}$, 5 layers measured at $1.2\mu\text{m}$. The patterns were measured to determine whether they would affect the shielding properties. It is known that conductive patterns orientated in specific ways can affect the shielding properties of a material [5]. A good example of this is a Faraday cage, where conductive material can be made either in continuous, solid form, or a fine mesh can be utilised to help shield any EMI.

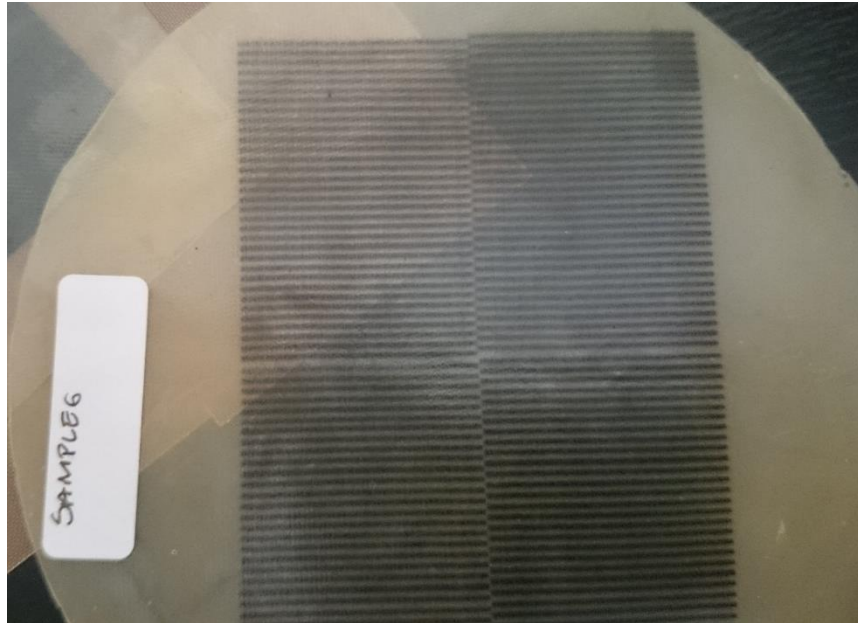


Figure 6.3 Horizontal lines of conductive carbon black printed onto cast sheet of XNBR. Lines are approximately 1mm thick with 1mm gap between lines. Thickness of printed carbon black was measured at 1.2 μ m

During these experiments, patterns utilising straight parallel lines, cross-hatch, and continuous layers of conductive carbon black were printed onto polymer substrates. Multilayer carbon black printing was carried out to determine whether the increase in conductive carbon black concentration would provide more shielding against EMI.



Figure 6.4 A crosshatch pattern (3 layers) printed onto cast sheet of XSBR latex

A benefit to utilising patterns is that less material is required to produce a shielding device that would provide similar shielding properties as a solid component. This in turn can save on production costs, weight, and the amount of waste material that is produced, as well as add physical stability and robustness.

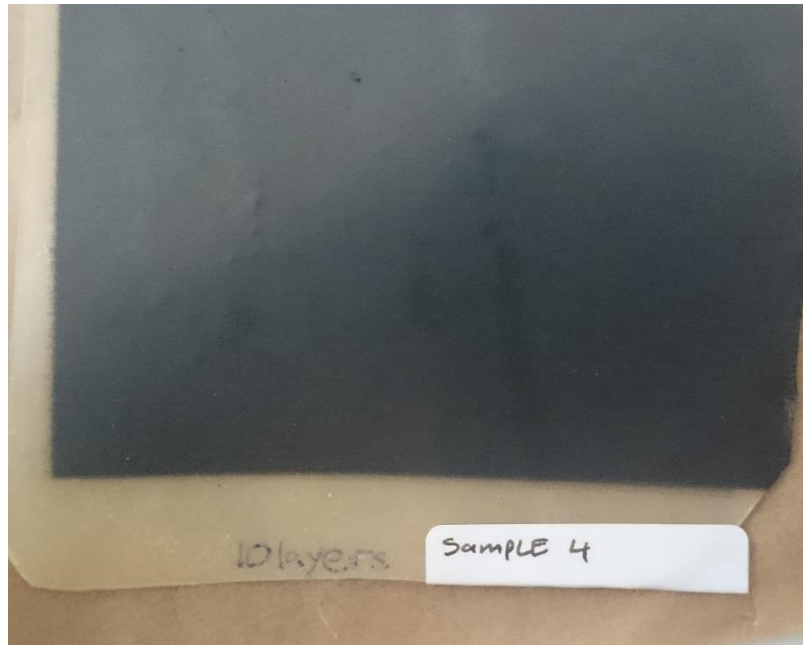


Figure 6.5 10 layers of conductive carbon black printed onto XNBR

These conductive carbon black samples were printed utilising the Fujifilm Dimatix material printer that was used to inkjet the latex inks. The same inkjet printing parameters were used for printing carbon black as with XSBR ink. In order to measure the EMI shielding properties of the latex, it was necessary to create an aperture 5x5cm in the centre of the copper and polystyrene substrate. The polystyrene was only used for physical stability. The monopole antenna equipment was set up, with each monopole facing the sample at 15cm distance from the aperture.

The results are displayed in Figure 6.6. However, during the measurements and the data collection from the equipment, it was observed that there was a high probability that the recorded results were not accurate. The introduction of the aperture and the lack of an insulated, or shielded, environment in which to carry out the measurements resulted in wave propagation through the aperture as well as around the shielding substrate. There were also environmental factors to consider, such as reflections off the floor, equipment and people. Therefore, to ensure more accurate results, as well as ensure more repeatable measurements, another method that utilised the split-post dielectric resonator equipment was selected to

measure the dielectric properties (permittivity and dielectric loss tangent) of the samples. These results are discussed in Section 6.3.2.

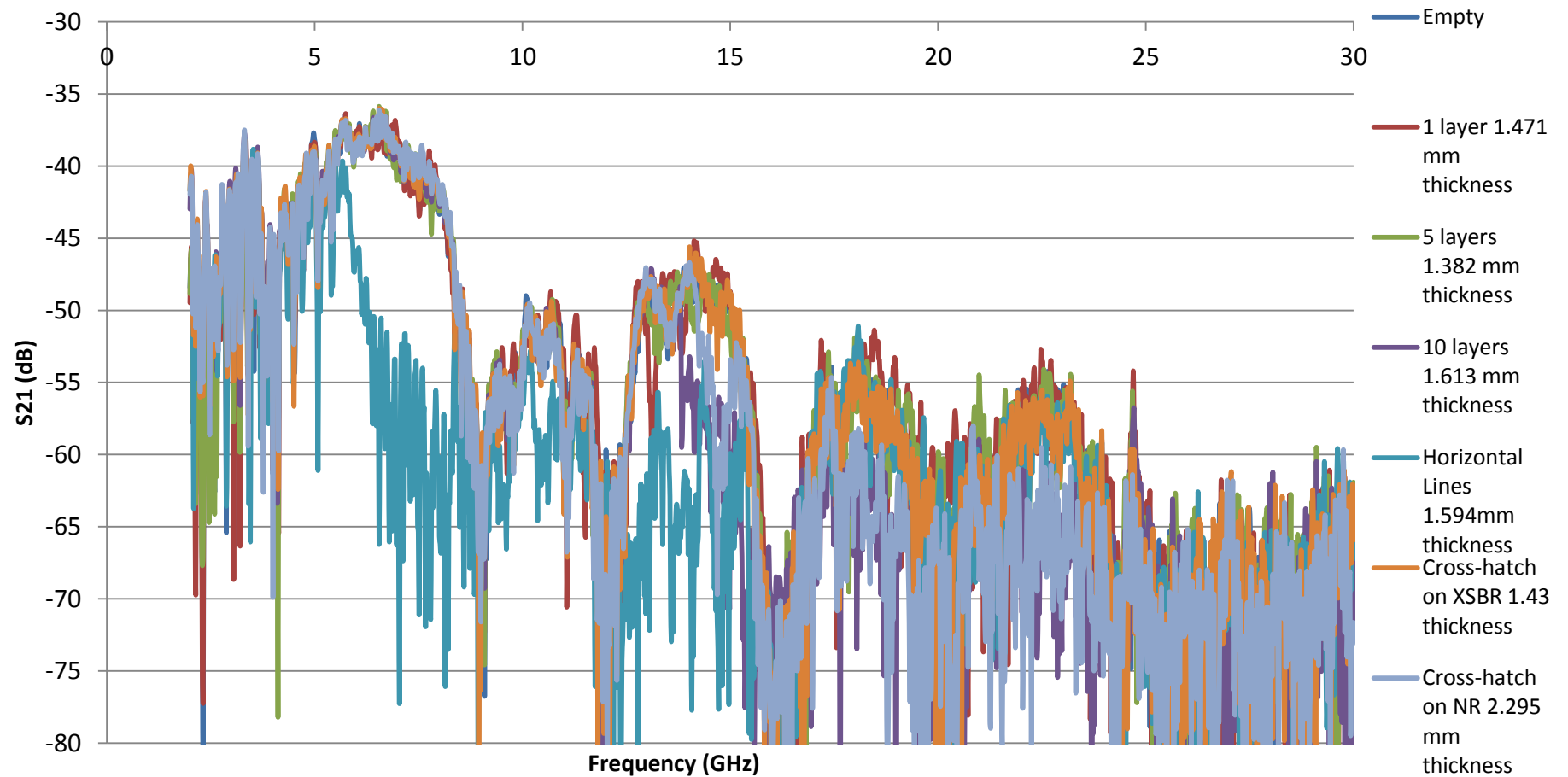


Figure 6.6 Measured results for the transmission between two monopoles with different printed shields for cast samples with printed conductive carbon black patterns. Sample thickness measurements include the combined thickness of the polymer and conductive material printed onto the surface. The results of each pattern were measured and recorded twice to minimize errors.

6.3.2 SPDR Results for Carbon Black Patterns Printed on Cast Latex and PET

This section discusses the results of the electromagnetic characterisation of cast latex materials and the conductive carbon black ink printed in various patterns to attempt to block specific electromagnetic frequencies using the split post dielectric resonator (SPDR) [8]. The objective of electromagnetic characterisation for this project was to find the optimum amount or pattern of printed conductive material to prevent a 2.4 GHz signal from penetrating the material, therefore creating a foundation onto which 3D jetting technology could be used to create a composite material that has electromagnetic shielding properties.

One of the first properties that are typically measured for a dielectric material is its relative permittivity. The property of permittivity relates to a material's ability to resist an electric field, rather than "permitting" an electric field. Materials with a high permittivity reduce any electric field that is present. Permittivity is a property that is measured in Farads per meter (F/m) and is represented as ε , where

$$\varepsilon = \varepsilon_r \varepsilon_0 = (1 + X) \varepsilon_0 \quad \text{Eq. 6.1}$$

Where ε_r = relative permittivity of material

$$\varepsilon_0 = 8.854187 \dots \times 10^{-12} \text{ F/m (permittivity of a vacuum)}$$

X = electric susceptibility

Another property that is also measured is the Q-factor, also known as the Quality factor. This is the maximum energy that has been stored in circuit relating to the dissipated energy of an oscillation cycle. The formula for Q is expressed as:

$$Q = f_r / BW \quad \text{Eq. 6.2}$$

One of the objectives of the electromagnetic aspect of this project was to perform an analysis of different concentrations of carbon black and how they impact the permittivity and dielectric loss tangent values.

Patterns ranging from small and large dots and interconnected lines, such as the octogrid, as well as a chevron pattern were all used to test the effectiveness a pattern print compared to a continuous layer of carbon black. These measurements were obtained from

carbon black printed onto PET substrates in order to determine the effectiveness of the carbon black ink without the latex.

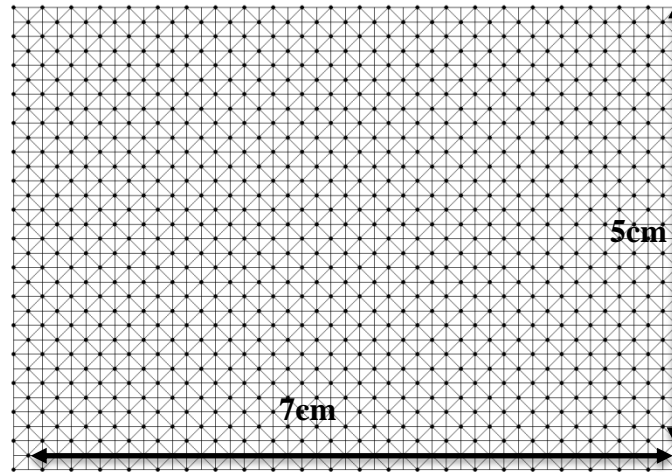


Figure 6.7 Octogrid pattern that was used to print conductive carbon black ink onto PET substrates

To measure the dielectric properties of the conductive carbon black only, a sheet of PET was placed inside the SPDR and the results for the PET were registered as “Empty” in the computer. This enabled the system to disregard the dielectric properties of the PET and to only measure the values for the carbon black.

Each sample was placed in the SPDR and ten measurements were collected for each sample. This was done to ensure the results gathered were correct and to remove errors due to changes in thickness or local variations. Results of these measurements are displayed in Table 6.1.

Table 6.1 Measured relative permittivity and dielectric loss tangent results for single and 5 layers of conductive carbon black printed onto PET sheets in various patterns

	1 Layer Chevron	5 Layers Chevron	1 Layer Octogrid	5 Layers Octogrid	1 Layer Dot Grid	5 Layers Dot Grid
Mean Permittivity	9.404	43.137	4.147	13.965	6.845	18.911
Standard deviation	0.148	0.262	0.212	0.246	0.203	0.140
Mean Dielectric Loss Tan	2.859	1.993	1.408	1.316	1.228	0.886
Standard deviation	0.035	0.014	0.070	0.010	0.022	0.004

Thickness values for 1 layer and 5 layers of conductive carbon black were measured using white light interferometry as 1 μ m and 1.2 μ m respectively. The standard deviation values were obtained in MS Excel by using the STDEV function.

The Dielectric Loss Tangent is a way to quantify a dielectric material's inherent dissipation of electromagnetic energy. It is the ratio at any particular frequency between the real and imaginary parts of the permittivity. A large loss tangent value denotes that there is a large amount of dielectric absorption. Therefore, the higher the loss tangent, the more absorption and less EM waves passing through. A higher loss tangent also increases reflections; therefore, making for a more effective EM shield.

Results for the dielectric loss tangent and permittivity properties were measured for all samples and collated into a bar graph with standard deviation, as shown in Tables 6.2 and 6.3. The measurements were made in order to observe the difference between the shielding effectiveness of each material and to study the effects of conductive patterns on the dielectric properties.

Table 6.2 Measured relative permittivity results for hot press moulded rubber and conductive carbon black printed onto PET

	25% CB	40% CB	CB mixed w xsbr	CB painted on xsbr	CB parallel lines on NR	Cross pattern on PET	Crosshatch on xsbr	Diagonal CB on NR	Large dots on PET	NR with solid CB	PET	Small dots on PET
Mean	7.60128	13.04203	2.24351	3.11564	2.36522	3.11974	2.11265	2.01287	3.31282	2.28770	2.88230	3.61265
Standard deviation	0.11616	0.06403	0.03786	0.10891	0.03284	0.03507	0.09052	0.11614	0.00289	0.11320	0.02940	0.00629

Table 6.3 Measured dielectric loss tangent results for hot press moulded rubber with 25 % and 40% carbon black concentration and conductive carbon black printed onto PET, NR, and XSBR

	25% CB	40% CB	CB mixed w xsbr	CB painted on xsbr	CB parallel lines on NR	Cross pattern on PET	Crosshatch on xsbr	Diagonal CB on NR	Large dots on PET	NR with solid CB	PET	Small dots on PET
Mean	0.12547	0.19947	0.01017	0.05778	0.02242	0.15408	0.15075	0.02472	0.26915	0.11686	0.00554	0.27763
Standard deviation	0.00361	0.00283	0.00311	0.00569	0.00077	0.00145	0.02067	0.00294	0.00498	0.01577	0.00009	0.00797

Both the 25phr and 40phr hot press moulded nitrile rubber (labelled as 25% CB and 40% CB in the results) have high permittivity values. The relative permittivity results are illustrated in Table 6.1.

Another set of samples using the dotted, chevron, octogrid, and continuous layer of carbon black patterns were printed onto PET to determine if the second set of results were repeatable. These results are presented in Table 6.4.

Table 6.4 Permittivity and dielectric loss measurements of samples

	Dots	5 layer Dots	5 layers chevron	1 layer CB	5 layers CB	1 layer Octogrid	5 layers Octogrid
Mean Permittivity	37.769	141.201	44.341	37.321	11.636	22.252	74.336
Standard Deviation	6.108	2.946	0.791	0.429	5.206	0.365	0.346
Mean Dielectric Loss Tan	1.940	0.811	5.511	7.649	82.053	3.412	2.379
Standard Deviation	0.019	0.050	0.071	0.082	21.267	0.052	0.008

From the dielectric results displayed in Table 6.4 we can observe that the number of layers of conductive carbon black has an impact on the dielectric properties. An increase in the number of layers of conductive carbon black material has the potential to increase the level of absorption shielding as there is more lossy material. However, a higher number of carbon black layers does not guarantee a significant improvement in the ability to insulate against interference, but rather improve the absorption shielding.

Analysing the permittivity results displayed in Table 6.4, the 5 layer dots and 5 layer octogrid display the two highest values. This indicates that these two patterns will have a higher level of reflecting shielding compared to other patterns. This is likely due to the pattern shapes, which indicates that variations in patterns can affect shielding capabilities. It can be observed that the number of layers for these two patterns has an effect on the absorption. More layers of conductive carbon black produced more absorptive shielding. With connected lines, the structure forms small apertures that only high wavelengths can pass through freely. Lines can provide a similar level of shielding as continuous layers for low frequencies where the wavelength is large, while dot patterns increase the loss tangent compared to non-dotted patterns.

Results shown in Table 6.2 illustrate that the 5 layers of carbon black sample printed on PET exhibited the highest loss tangent value. This indicates that a continuous pattern, with 5 layers of conductive material, possibly has the potential for more absorptive shielding.

6.3.3 SPDR Results for Cast Latexes

SPDR was used to determine the electromagnetic properties of cast XSBR combined with varying concentrations of conductive carbon black material. A control sample of unmodified cast XSBR was also used to measure the properties of plain latex in order to make a complete comparison between the materials with and without carbon black. Initially the materials produced during this research that contained a high concentration of conductive carbon black powder could not be measured inside the SPDR due to the materials being significantly lossy and the SPDR having a high sensitivity to such materials. It was determined that by increasing the S21 of the SPDR (or decreasing the gap between the plates) that it was possible to reduce the sensitivity enough to be able to measure the properties of the dielectric materials. This means that more power from the top plate was being transferred to the bottom, and that the coupling (or fraction of power received) from the top was greater. By increasing the coupling, lossier materials can be measured.

Once the adjustments were made to the SPDR, measurements of cast latex samples containing varying concentrations of conductive carbon black (percentages of carbon black based on dry weight of the latex) were carried out. As with the PET samples, ten measurements were recorded for each sample to obtain the graphs presented in Table 6.5.

Table 6.5 Permittivity and dielectric loss tangent results for XSBR with varying concentrations of conductive carbon black

Permittivity			
	<i>Unmodified XSBR</i>	<i>1% Carbon Black</i>	<i>2% Carbon Black</i>
Mean	2.682	2.562	3.210
Standard Deviation	0.017	0.014	0.016
Dielectric Loss Tangent			
Mean	0.056	0.016	0.082
Standard Deviation	0.001	0.001	0.016

Although it was possible to obtain results for the XSBR with varying concentrations of conductive carbon black paste after decreasing the sensitivity of the equipment, the results

presented in Table 6.5 do not provide conclusive values. Expected values for permittivity and dielectric loss tangent are significantly lower than those of previously recorded samples. The standard deviations for the final sample (5% carbon black) were high, indicating that there were errors during the measurements which made repeatability of measurements unreliable; therefore, these results have not been included in the table. The measured relative permittivity and the loss tangent also registered as negative values.

6.3.4 Shielding Effectiveness of 1, 5, and 10 Layers of Inkjet Printed Carbon Black

Determining shielding effectiveness is a measure of the factor by which the electromagnetic wave reduces in power when it passes through a shield, and these properties are frequency dependent. Protecting against interference involves absorption and reflection. Metal materials are good at reflecting interference, especially if the thickness is greater than 1 mm [6]. Shielding effectiveness calculations in this section have been carried out for materials with continuous layers of conductive material on the surface, as the formulas used for determining shielding rely on materials with an uninterrupted layer of conductive material.

To calculate shielding effectiveness, it is necessary to determine the skin depth in conductive carbon black. Skin depth refers to the electric current measurements of the electromagnetic wave flowing over a conductive material [9].

$$\delta_{CB} = \frac{1}{\sqrt{\pi f \mu \sigma}} \quad [10] \quad \text{Eq. 6.3}$$

Where δ_{CB} = is the skin depth of carbon black,

σ = Conductivity

$f = 2.4 \times 10^9$ (2.4 GHz, the frequency that was used during the experiments)

$\mu = 4\pi \times 10^{-7}$

Absorption loss:

$$A(dB) \approx 8.7 \left(\frac{t}{\delta}\right) \quad [10] \quad \text{Eq. 6.4}$$

Where A = absorption loss

t = thickness

δ = skin depth

Once absorption is calculated, it is necessary to determine the impedance:

$$|\eta_{CB}| = \sqrt{\frac{2\pi f \mu}{\sigma}} \quad \text{Eq. 6.5}$$

Then determining the reflection loss is necessary as a final step to calculating shielding effectiveness (S.E.):

$$R(dB) = 20 \log\left(\frac{\eta_0}{A\eta_{CB}}\right) \quad [11] \quad \text{Eq. 6.6}$$

Where η_0 = impedance of free space (377 Ω).

Figures 6.8 and 6.9 display the results for S.E. of single and five layers of conductive carbon black printed in a continuous rectangle pattern onto PET substrate. These results were obtained by using Equations 6.3 – 6.6. Shielding Effectiveness is obtained by the summation of the reflection and absorption loss. We can observe that there is not a significant difference between the two results. This is due to the reflection shielding being more dominant over the absorption shielding. According to Methode Development Co., the conductive carbon black ink only has a 10% carbon particle concentration, which is significantly lower than the XSBR ink. As the carbon black ink dries, it adopts a somewhat powdery texture, which is the possible cause for the low thickness values obtained from white light interferometry of single, five, and ten layers. This is beneficial for printing of thin film flexible circuits, as the ink was designed for. However, a significant amount would be needed for applications in EMI shielding technology.

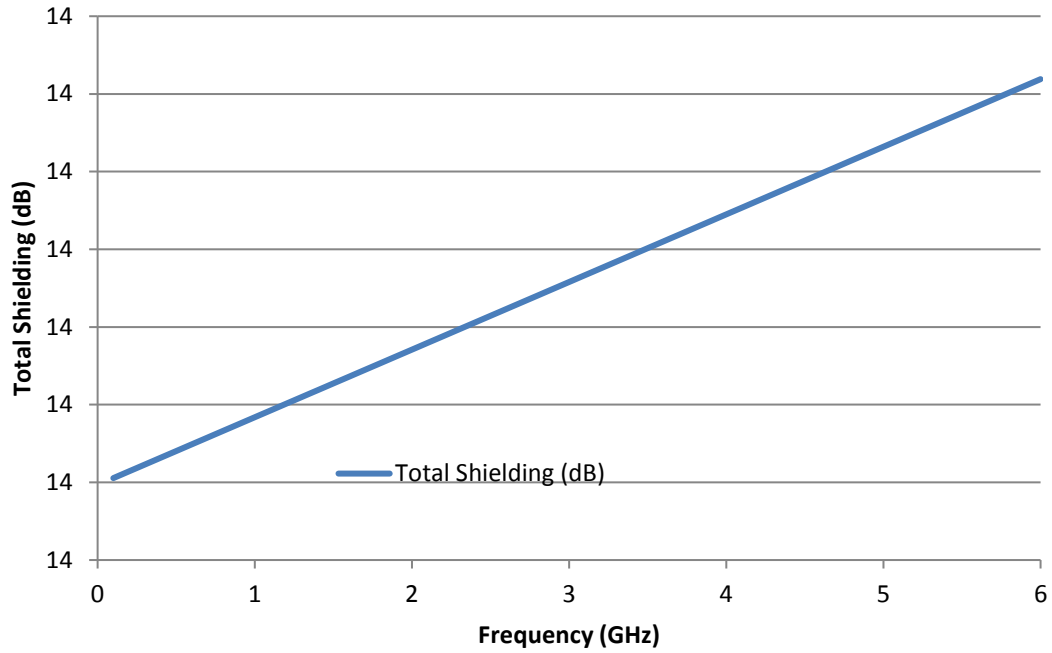


Figure 6.8 S.E. of single layer of carbon black with thickness of 1 μm

From analysing Figure 6.8, it is evident that the total shielding remains steady at 14 dB. At higher frequencies, the impedance of the shield becomes closer to the impedance of free space, hence the reflection shielding is reduced. Shielding attenuation between 90 – 120 dB is exceptional, with almost 100% S.E [1], while 10 - 30 dB is considered as poor or minimal shielding. This result does indicate that the conductive carbon black material is providing some shielding, and considering that the amount of material that was deposited on the PET was low (less than 2 ml, as a single cartridge can hold approximately that amount), it is possible that more shielding could be provided by depositing additional layers.

Figure 6.9 illustrates the results for five layers of conductive carbon black ink printed onto PET substrate, with a thickness of 1.2 μm .

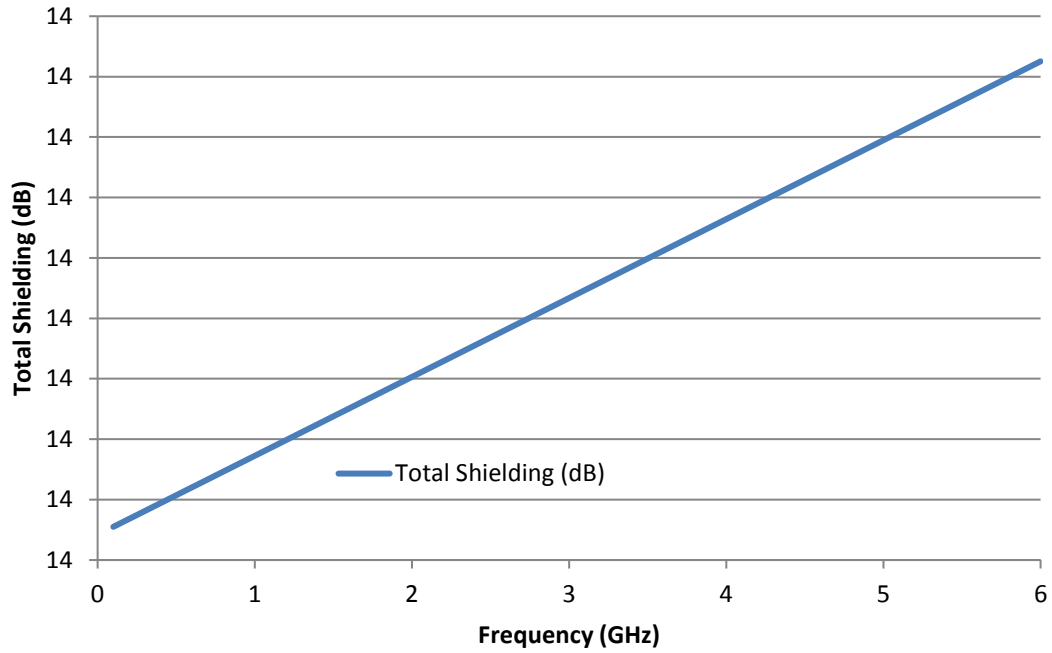


Figure 6.9 S.E. of five layers of carbon black with thickness of 1.2 μm

From the results in Figure 6.9, it can be concluded that five layers does not improve the overall S.E. values as they remain almost identical to the results obtained for the single layer. This is due to the thickness of the printed carbon black. The difference in thickness values between one and five layers is only 0.2 μm , which is possibly due to the low carbon content in the ink. As the ink was deposited, it dried to have an almost powdery surface finish, which must affect any additional layers that are deposited on the surface. Due to this and the colour of the material, it also made it difficult to obtain a clear cross-sectional profile measurement using white light interferometry. Table 6.6 details the values that were calculated from S.E. calculations for 1, 5, and 10 layers of carbon black. Thickness value of the 10-layer sample was recorded at 2 μm .

Table 6.6 S.E. (dB) comparison for 1, 5, and 10 layers of conductive carbon black printed onto PET substrate

Frequency (GHz)	Total Shielding (1 layer)	Total Shielding (5 layers)	Total Shielding (10 layers)
0.1	14	14	14
1	14	14	14
2	14	14	14
3	14	14	14.01
4	14	14.01	14.01
5	14.01	14.01	14.02
6	14.01	14.01	14.02

Despite the low S.E. values, the material does provide some shielding against EMI. The absorption shielding is small; this is due to the skin depth in the material is much larger than the thickness of the material. At much higher frequencies, this will form a better absorptive shield. Therefore, the total shielding for 1, 5 and 10 layers is 14 dB. This assumes that a plane wave where the impedance of the wave is 377 ohms. When the shield is close to an electric source where the electric fields dominate close to the source, the shielding of the material will be improved. However, if the shield is close to a loop source where the magnetic fields dominate, then the shielding is poorer.

The S.E. values for the other samples (dots, cross-hatch, lines, octogrid and chevron patterns) were not calculated due to their non-continuous pattern.

6.4 Conclusion

In conclusion, this Chapter has demonstrated that the addition of a conductive carbon black material for shielding does offer some protection via absorption. However, during measurements, it has been found that certain samples displayed significant discrepancies in the results, such as the dielectric loss tangent and relative permittivity for the 5% carbon black concentration sample. Due to the inconsistencies in the thicknesses of the measured XSBR combined with conductive carbon black paste (greater than 10%), the results of the cast latex samples cannot be effectively compared and analysed side-by-side. Likewise, pattern variation appears to influence absorption; however, its effects are not on par with some more conventional methods of EMI shielding [4-6]. Future work in this field could

focus to address the influence of different variations of conductive ink (metal and non-metal materials) to observe and compare the dielectric loss tangent, permittivity, and determine the shielding effectiveness.

References:

- [1] D.D.L. Chung. Carbon materials for structural self-sensing, electromagnetic shielding and thermal interfacing. (2012). *Carbon*, vol. 50, no. 9, pp. 3342-3353.
- [2] Dhawan SK, Ohlan A, Singh K. Designing of Nano Composites of Conducting Polymers for EMI Shielding. In: Reddy B, editor. *Advances in Nanocomposites – Synthesis, Characterization and Industrial Applications* [Internet]. InTech; 2011 [cited 2017 April 24]. Available from: <http://www.intechopen.com/books/advances-in-nanocomposites-synthesis-characterization-and-industrial-applications/designing-of-nano-composites-of-conducting-polymers-for-emi-shielding>.
- [3] S.H. Park, P. Thielemann, P. Asbeck, P.R. Bandaru. Enhanced dielectric constants and shielding effectiveness of, uniformly dispersed, functionalized carbon nanotube composites. (2009). *Appl Phys Lett*, vol. 94, no. 24, pp. 243111.
- [4] J. -M. Thomassin, D. Vuluga, M. Alexandre, C. Jerome, I. Molenberg, I. Huynen, et al. A convenient route for the dispersion of carbon nanotubes in polymers: application to the preparation of electromagnetic interference (EMI) absorbers. (2012). *Polymer*, vol. 53, no. 1, pp. 169-174.
- [5] Al-Saleh, M., H., and Sundararaj, U. Electromagnetic interference shielding mechanisms of CNT/polymer composites. (2009). *Carbon*, vol. 47, no. 7, pp. 1739-1746.
- [6] H. Ott, *Electromagnetic Compatibility Engineering*. John Wiley & Sons, New York, 2009.
- [7] *Measuring EMI Shielding Effectiveness*, 2017, ThomasNet.com., Accessed 10th June 2017, <<http://www.thomasnet.com/articles/automation-electronics/effective-emi-shielding>>
- [8] Rudnicki, J. (2017). QWED – Software for Electromagnetic Design. [online] Qwed.eu. Available at: <https://www.qwed.eu/resonators.html> [Accessed 20 Jun. 2017].
- [9] Chemandy Electronics. (2016). *Calculator for Skin Effect Depth*. [online] Available at: <http://chemandy.com/calculators/skin-effect-calculator.htm> [Accessed 10 Feb. 2018].
- [10] Hayt, W. H., Jr. *Engineering Electromagnetics*. 3rd ed. McGraw-Hill, New York, 1974.
- [11] Paul, C. R. *Introduction to Electromagnetic Compatibility*, 2nd ed. Chapter 9 (Crosstalk) New York Wiley, 2006.

7. Conclusions and Recommendations

7.1 Conclusions

This work has demonstrated that additive manufacturing of elastomer latex materials using inkjet printing is not only feasible, but repeatable when the right composition and printing conditions are used. It is particularly important that the correct concentrations are utilised to lower the solids content and an ideal humectant is added to slow the evaporation of the polymer and prevent clogging in the nozzles. The research shows that it may be possible to make 3D printed components with shielding properties if a suitable conductive material is incorporated. Measurements taken using the Split Post Dielectric Resonator indicated that the addition of a conductive carbon black ink did yield a material that was better able to reflect and/or absorb interference frequencies compared to materials measured without any conductive material additions.

Specific conclusions are listed below.

1. Factors that affect printability for elastomer latex have been identified (in order of most to least important):
 - a. Particle size (between 0.079 μm and 2 μm)
 - b. Viscosity (between 2-12cP)
 - c. Surface tension of the liquid (between 30-45 mN/m)
 - d. Evaporation rate
 - e. Z number
2. This study shows that inkjet printability with elastomer latex is possible if adjustments to the evaporation rate of the latex are made with the addition of humectants and de-ionised water to lower the overall solids content.
3. Addition of de-ionised water to XSBR, XNBR, CR, and HNBR elevated the surface tension of the latex slightly. However, the addition of TGME to diluted latexes reduces the surface tension to a value more like that of the pre-diluted latex.
4. Mastersizer measurements illustrated that the addition of TGME to HNBR, XNBR, and CR caused agglomeration. Ultrasonic treatment was implemented for the

agglomerated samples, however the agitation only exacerbated the agglomeration issue.

5. Initial jetting trials with unmodified XNBR and XSBR were not successful due to the high evaporation rate of the latex, which caused nozzle clogging. Dilution of XSBR to reduce the solids content from 50% wet weight to approximately 33% made it possible to deposit the material in a 2 x 2 cm square shape onto a silicone coated paper substrate. However, after printing the first layer of diluted XSBR was completed the nozzles clogged and the introduction of TMGE into the latex was implemented in all further study.
6. The addition of TGME to reduce evaporation of the latex proved successful and enabled successful printing trials to carry forward with XSBR. It was determined early on in the experimentation that TGME caused CR, XNBR and HNBR latex particles to agglomerate. This affected the repeatability of the inkjet printing trials, therefore all further experiments were focused on improving jettability of XSBR, ensuring printability, and determining the effects of inkjet parameter modification on jet stability, and printing resolution/accuracy.
7. Jetting trials of XSBR ink using the Dimatix Materials Printer DMP-2831 by Fujifilm showed that a jetting waveform that utilises a slew rate of 1 and duration of 2.56 μ s, with jetting voltage of 25-26V, maximum jetting frequency 20kHz, meniscus set point of 4.0 and no nozzle temperature yielded the best jetting results.
8. Deposition onto substrates with varying surface energies proved to affect the final resolution and accuracy of the print. A droplet analysis was carried out with the substrates, where droplets of XSBR ink were deposited onto PET, PTFE coated fabric, PTFE tape, and glass microscope slides to determine the interaction between ink and substrate. Droplet spreading on PET and glass slides was observed, which indicated that these substrates were more hydrophobic, while droplet spreading was suppressed with PTFE tape due to its high hydrophobicity. Droplets deposited onto PTFE coated fabric was not observed, it was possible that the droplets were displaced due to the uneven properties of the fabric. It was found that printing onto PTFE coated fabric aided in creating samples with more straight edges. This was due to the hydrophobic nature of the substrate, which prevented the latex ink from spreading.

However, the uneven surface texture of the substrate, as well as the uneven coating of PTFE, created areas, or pockets, that enabled the ink to spread. Depositing onto glass slides also yielded samples that were somewhat inconsistent in evenness in the surface topography. This was possibly caused by impurities on the surface of the glass, which would have affected the surface properties and spreading of the XSBR ink that was deposited onto it. Jetting onto PTFE tape proved to be unsuccessful due to the extremely hydrophobic nature of the material, which negatively affected the resolution of the printed pattern due to uncontrolled coalescence and pooling. PET was a substrate that allowed for improved repeatability with regards to surface topography and resolution, therefore this material was selected as the primary substrate for depositing latex ink onto. PET was also a more versatile substrate and easy to secure onto the Dimatix print bed compared to the PTFE coated fabric, PTFE tape, and microscope glass slide.

9. Multiple layers of XSBR ink were printed and thicknesses recorded. A surface doming effect was observed for multilayer samples. It was thought the doming was due to incomplete drying of the latex because it was possible to reduce this effect by increasing the bed temperature of the print bed and introducing time delays between layers during printing.
10. Attempts taken to combine conductive carbon black powder with XSBR ink did not succeed due to the hydrophobic properties of the powder, which caused complications during the mixing process, yielding non-homogeneously dispersed carbon black. Instead, a conductive carbon black ink, provided by Methode Development Co. was implemented in ink jetting of conductive patterns.
11. A conductive carbon black, provided by Methode Development Co., was used to print a variety of patterns onto PET. These patterns included dots, continuous lines running in parallel and/or perpendicular, chevron and mesh patterns; all of which were tested using the Split Post Dielectric Resonator (SPDR) to observe the effectiveness of each pattern to absorb or reflect the 2.2 GHz frequency that they were exposed to. Results indicated that some patterns, such as the crosshatch carbon black printed onto cast XSBR, large dots on PET, small dots on PET, and the crosshatch pattern on PET can absorb more of the interference frequencies, than the

parallel and diagonal lines. The diagonal lines were less effective at absorbing the EM radiation due to lack of reflection and absorption. The shape and positioning of the lines made it possible for the signal to pass through the gap between the lines.

12. SPDR measurements of single and 5-layer conductive carbon black indicated that there was no significant increase in EM absorption with an increase in the number of conductive layers printed. It is possible that the increase in the number of layers results in a pattern that is better able to reflect interference rather than absorb it; therefore an increase in the number of layers would yield a more efficient interference reflector. However, the variations in the pattern shapes was a key factor that affected its abilities to reflect or absorb interference. The variations in the patterns, such as the size and space between conductive material, as well as whether the patterns form disjointed or continuous connections between each other, can allow certain frequencies to pass through. The higher the frequency, the smaller the wavelength, which in turn means that smaller gaps in the patterns are necessary to avoid interference.
13. A resorcinol curing resin was combined with the XSBR ink and was found to be ink jettable. This was carried out to attempt to crosslink the polymer chains to improve the mechanical properties of the polymer. Samples cured at varying temperatures from 180°C to 220°C for 30 minutes, then tensile tests carried out illustrated that the samples cured at 190°C had higher tensile strength. The results show that it is possible to create a crosslinked rubber article by ink jetting elastomer latex combined with a curing agent and then curing it in a separate heating stage.

7.2 Recommendations for Future Work

Based on the research, experimentation, and results of this work, the recommendations for future work in this area include:

1. One of the main limitations of the current work was that only small samples could be created due to the limitations of the 2ml cartridge as well as the relatively small print bed area. Future work could use equipment capable of greater deposition rates and printing larger multilayer samples with a greater 3D aspect.

2. A larger composite material with XSBR ink and conductive carbon black printed together, preferably utilising a dual cartridge system, could enhance effective interlayer bonding. The resulting samples could be used to test both EMI shielding effectiveness of the novel composite material and its potential for controlled anisotropic mechanical properties.
3. The preliminary results of the tensile tests of the XSBR with resorcinol resin cured at 190°C show a sizeable improvement in the stress and strain values compared to the uncured cast XSBR. It would be ideal to carry out tensile tests on cured inkjet printed XSBR and resorcinol resin mixtures printed in appropriate dog bone shapes.
4. Further investigations should be carried out to determine the cause for particle agglomeration observed in XNBR, CR, and HNBR with the addition of TGME. Experiments should be carried out to identify a suitable humectant to be selected for combination with these latex materials so that inkjet printing can be carried out utilising these and other polymers in latex form.
5. Finally, an investigation into in situ curing of the printed elastomer latex ink should be carried out. This could be carried out by using a heat source attached inside the printer, such as a compact infrared heating light, to dry and cure the printed latex as it is deposited onto the substrate. This would also aid in reducing spreading on more hydrophilic materials, as well as reduce or prevent coffee rings from occurring.

Appendix

Conferences presented at:

- 15th May 2014: **International Rubber Conference** (PowerPoint Presentation)
- 15th May 2015: **MAST [dstl]** (poster presentation)
- 26th November 2015: **Defence and Security Doctoral Symposium** (PowerPoint Presentation)

Papers published:

- Lukic, M., Clarke, J., Tuck, C., Whittow, W., Wells, G. *Printability of elastomer latex for additive manufacturing or 3D printing*. (29 September 2015). Journal of Applied Polymer Science, Vol. 133, no. 4.